UNIVERSITY OF CALIFORNIA SAN DIEGO

Risk-targeted Performance-based Seismic Assessment and Design of Bridges

A dissertation submitted in partial satisfaction of the requirements for the degree
Doctor of Philosophy

in

Structural Engineering

by

Angshuman Deb

Committee in charge:

Professor Joel P. Conte, Chair
Professor Jose I. Restrepo
Professor Peter M. Shearer
Professor Pui-Shum Benson Shing
Professor Michel D. Todd

2021

The dissertation of Angshuman Deb is approved, and it is acceptable in quality and form for publication on microfilm and electronically.

University of California San Diego

2021

DEDICATION

To my parents,
for their endless love, support, and patience.

Also, to all my friends,
for being there, through thick and thin.

EPIGRAPH

What we observe is not nature itself, but nature exposed to our method of questioning.

Werner Heisenberg

TABLE OF CONTENTS

LIST OF FIGURES

LIST OF TABLES

ACKNOWLEDGEMENTS

The work presented in this dissertation could not have been possible without the support and nurturing of many people. First and foremost, I would like to extend my deepest gratitude to my advisor, Professor Joel P. Conte, whose excellent mentorship, brilliant insight, and unparalleled enthusiasm contributed towards making my academic journey incredibly rewarding. I am deeply indebted to him for his profound belief in my work and abilities, constructive criticism, and unwavering support.

I am also extremely grateful to Professor Jose I. Restrepo whose expertise, guidance, practical feedback, and relentless support throughout the entire duration of my graduate studies have not only made me a better engineer, but also were instrumental in formulating the work presented herein. I feel honored to have been under the tutelage of both Professor Conte and Professor Restrepo and look forward to a lifelong friendship with them.

I would like to express my sincere appreciation to other members of my doctoral committee, Professor Michael D. Todd, Professor Pui-Shum Benson Shing, and Professor Peter M. Shearer, for their valuable feedback on this research. Their knowledge and insights have truly contributed towards enriching this work.

I shall always cherish the fantastic opportunity of being mentored in the initial years of my doctoral studies by Dr. Yong Li. He contributed significantly to honing my critical-thinking and problem-solving abilities, thus shaping me as an independent researcher. I also had the opportunity to meet and learn valuable lessons from Dr. Rodrigo Astroza and Dr. Hamed Ebrahimian during these initial years for which I am genuinely grateful.

I must also thank all the students and faculty members associated with the Department of Structural Engineering at UC San Diego for fostering an atmosphere of academic excellence and

productivity, which helped me thrive during my graduate/doctoral studies. Special thanks should also go to the present and past members of the staff in the Department of Structural Engineering, especially Lindsay Walton, Yvonne Wollmann, and Julie Storing for their time, consideration, hospitality, and endless patience.

I would also like to extend my deepest gratitude to all my friends, fellow students, and co-workers at UC San Diego. I cannot begin to express my gratitude to Mukesh Ramancha and Rahul Hazra, and there is no way words can describe how much their presence meant to me during this time. My heartfelt thanks are also due (in randomized order) to Krishna Anish Adusumilli, Dr. Manuel Vega, Mohamed Elgabaly, Dr. Ahmed Ebeido, Adithyvijay Ramanitharapandian, Marion Elise Sanchez, Dr. Gloria Faraone, Saif Jassam, Athul Prabhakaran Parayancode, Rohan Raut, Nicholas Sera, Krista Seaman, Dr. Raghavendra Sivapuram, Sanjay Rachapudi, Derek Ring, Srikar Gunisetty, Sneha Raj, Donovan Andres Llanes, Dr. Mayank Chadha, Dr. Rodrigo Carreno, Lin Sun, Laksha Sharma, Muhammad Zayed, Carleen Altinok, Dr. Adel Mashayekh, Zachary Withall, Harshith Kodumuru, James Mallard, Giovanni Montefusco, Jennifer Lim, Amit Yalwar, Heryang Lee, Manasa Vijaykumar, Nishant Nemani, Kiida Lai, Torrey Bolden, Jody Cheung, Ricardo Bustamante, Elesh Lakhani, Kimberly Bowes, Amanpreet Singh, Ata Mohseni, Sachin Jagarlamudi, Alex Zha, Maitreya Kurumbhati, Sitanan Tanyasakulkit, and many others. I will always fondly remember the precious time I spent with them. The moral and emotional support they unknowingly provided helped me push through and find my footing in many difficult situations.

Especially helpful to me during my time here in UC San Diego, thousands of miles away from India, was the love and support of my friends back home, Raunak Ghosh, Shivaji Bhattacharjee, and Anirban Sengupta. I sincerely thank them for making our friendship stand the

test of time and space by picking up right where we left off every time, regardless of how long it has been since we connected or how far apart we are.

I faced a couple of physical injuries during my doctoral studies which could have significantly set back my research work if not for the extraordinary care and support I received from orthopedic surgeon, Dr. Catherine M. Robertson (and her team at UC San Diego Health Sports Medicine), and from exceptional physical therapists, Kayla Hindle and Nicolas Carrillo (at Physical Rehabilitation Network (PRN) La Jolla). I am genuinely grateful to them for "having my back" and "lending a shoulder" in every sense of these terms.

I cannot conclude this section without recognizing the contribution of my first academic mentor, Professor Aminul Islam Laskar, from the Civil Engineering Department of National Institute of Technology (NIT), Silchar, my undergraduate alma mater in India. My heartfelt appreciation and thanks go to him for sowing the seeds of independent study and research in my young mind. This brings me to also thank my high-school teacher, Biswajit Ghosh, for his unabated belief in me and helping me choose the right direction early in life.

Finally, a very special word of thanks goes to my parents, Dr. Manabendra Deb and Dr. Gouri Deb, my brother, Mriganka Shekhar Deb, and my aunt, Namita Deb, for their endless love, support, and patience. They stood by me and believed in me, even when I did not.

Portions of this dissertation have been published or are currently being considered for publication. Chapter 4, in full, is a reprint of the material as it appears in the following paper (the dissertation author is the first author of this paper):

Deb, A., Zha, A. L., Caamaño-Withall, Z. A., Conte, J. P., Restrepo, J. I. (2021). "Updated probabilistic seismic performance assessment framework for ordinary standard bridges in California." *Earthquake Engineering & Structural Dynamics*; 1–20. https://doi.org/10.1002/eqe.3459

Chapter 5, in full, has been submitted for publication of the material as it may appear in the following paper (the dissertation author is the first author of this paper):

Deb, A., Zha, A. L., Caamaño-Withall, Z. A., Conte, J. P., Restrepo, J. I. (2021). "Framework for risk-targeted performance-based seismic design of ordinary standard bridges." Submitted to *Journal of Structural Engineering*

Chapter 6, in full, is currently being prepared for submission for publication of the material as it may appear in the following paper (the dissertation author is the first author of this paper):

Deb, A., Zha, A. L., Caamaño-Withall, Z. A., Conte, J. P., Restrepo, J. I. (2021). "Simplified risk-targeted performance-based seismic design method for ordinary standard bridges." Under preparation for submission to *Journal of Bridge Engineering*.

Chapter 7, in full, is currently being prepared for submission for publication of the material as it may appear in the following paper (the dissertation author is the first author of this paper):

Deb, A., Conte, J. P., Restrepo, J. I. (2021). "Comprehensive treatment of uncertainties in risk-targeted performance-based seismic design and assessment of bridges." Under preparation for submission to *Earthquake Engineering & Structural Dynamics*.

VITA

2013	Bachelor of Technology, National Institute of Technology, Silchar, India
2015-2021	Teaching Assistant, University of California San Diego
2016-2021	Research Assistant, University of California San Diego
2017	Master of Science, University of California San Diego
2021	Doctor of Philosophy, University of California San Diego

PUBLICATIONS

Journal Papers:

Deb, A., Zha, A. L., Caamaño-Withall, Z. A., Conte, J. P., Restrepo, J. I. (2021). "Updated probabilistic seismic performance assessment framework for ordinary standard bridges in California." *Earthquake Engineering & Structural Dynamics*; 1–20. https://doi.org/10.1002/eqe.3459

Deb, A., Zha, A. L., Caamaño-Withall, Z. A., Conte, J. P., Restrepo, J. I. (2021). "Framework for risk-targeted performance-based seismic design of ordinary standard bridges." Submitted to *Journal of Structural Engineering*

Deb, A., Zha, A. L., Caamaño-Withall, Z. A., Conte, J. P., Restrepo, J. I. (2021). "Simplified risk-targeted performance-based seismic design method for ordinary standard bridges." Under preparation for submission to *Journal of Bridge Engineering*.

Deb, A., Conte, J. P., Restrepo, J. I. (2021). "Comprehensive treatment of uncertainties in risk-targeted performance-based seismic design and assessment of bridges." Under preparation for submission to *Earthquake Engineering & Structural Dynamics*.

Conference Papers

Deb, A., Zha, A. L., Caamaño-Withall, Z. A., Conte, J. P., Restrepo, J. I. (2019). "Parametric probabilistic seismic performance assessment framework for ordinary standard bridges." *In 13th International Conference on Applications of Statistics and Probability in Civil Engineering (ICASP13), Seoul, South Korea*, May 26-30. https://doi.org/10.22725/ICASP13.390

Deb, A., Zha, A. L., Caamaño-Withall, Z. A., Conte, J. P., Restrepo, J. I. (2019). "Towards a simplified and rigorous performance-based seismic design of ordinary standard bridges in California." *In 7th ECCOMAS Thematic Conference on Computational Methods in Structural Dynamics and Earthquake Engineering (COMPDYN 2019), Crete, Greece*, June 24-26.

ABSTRACT OF THE DISSERTATION

Risk-targeted Performance-based Seismic Assessment and Design of Bridges

by

Angshuman Deb

Doctor of Philosophy in Structural Engineering

University of California San Diego, 2021

Professor Joel P. Conte, Chair

Driven by the necessity to meet changing public expectations in the wake of natural disasters, such as earthquakes, the structural engineering community has been moving towards rational, risk-informed, and transparent approaches to structural design, amidst which probabilistic performance-based seismic design (PBSD) has emerged as the most scientific and promising one.

The main objective of this research is to formulate a simplified yet rigorous framework for risk-targeted PBSD of Ordinary Standard Bridges (OSBs), which, despite being simple bridges, constitute an integral part of lifeline infrastructure systems, especially in earthquake-prone regions such as California. A seismic performance assessment methodology integrating site-specific seismic hazard analysis, structural demand analysis, and damage analysis in a comprehensive and consistent probabilistic framework is computationally implemented as a modular tool unifying several state-of-the-art advancements related to the field. This tool is used for a parametric probabilistic performance assessment of four different testbed OSBs over a primary design parameter space to investigate the effects of varying key structural design parameters on targeted structural performance measures. Erratic performance levels exhibited by these real-world traditionally designed bridges, compared to expert-opinion-based target performance levels, expose the inconsistency and opacity of current (prescriptive) design principles that do not explicitly state, analyze, and design for risk-targeted performance objectives but implicitly expect them to be satisfied. A comprehensive risk-targeted simplified yet rigorous PBSD method is distilled out and proposed, and its efficacy is validated using four real-world bridges as cases in point. The framework is then enhanced by the inclusion and consistent propagation of pertinent sources of uncertainty (typically ignored in practice) to obtain a more complete picture of seismic performance, thereby leading to a more comprehensive, transparent, and reliable design of OSBs, facilitating effective and risk-informed decision-making in the face of uncertainty. It is believed that the adoption of the proposed PBSD methodology, although non-traditional in its format, will be highly beneficial in the medium to long term. This initial venture will also prove crucial in supporting and fostering future research work and innovative technological developments in bridge infrastructure engineering.

1 Introduction

1.1 Background

Traditional seismic design philosophy for earthquake resistant structures permits them to deform beyond elastic limits and thereby yield, incur damage, and dissipate energy, conditioned on the prevention of collapse. The main requirements of such a design philosophy can be summarized as:

(i) No, or unnoticeable damage to structural and non-structural elements should be incurred in the event of small earthquakes,

(ii) Minor and repairable damage to structural and non-structural elements is admissible in the event of an earthquake of moderate intensity, and

(iii) Severe structural damage is allowed for strong earthquakes if collapse is prevented.

With the above being the overarching requirement of seismic design codes till date, all design codes can be considered performance-based, although partially. The idea has always been to design structures such that a performance objective, usually that of collapse prevention, is achieved. Traditionally, this fulfilment of structural performance goals along with certain functional requirements has been carried out by means of prescriptive measures, primarily empirical. A deterministic approach to the design of structural systems, wherein loads and resistances are considered deterministically quantifiable without any uncertainty, has been in dominance until recently. According to this approach, structural members are designed so as to have their capacities exceed the demands expected to be imposed on them by a certain margin. The capacity-to-demand ratio, also known as safety factor, is considered to be a measure of

structural reliability. Experience and engineering judgment have dictated the prescription of values for structural loads/demands, capacities, and safety factors in codes of practice.

The structural engineering profession's realization of uncertainties inherent in structural loads and strengths has led to the advent of structural reliability and risk analysis in structural design. A reflection of this can be seen in the form of *Load and Resistance Factor Design* (LRFD) in newer design codes wherein partial safety factors are applied to characteristic values of uncertain loads and resistances to ensure the safety of a structural member. LRFD aims to ensure that a factored load is less than or equal to the factored strength, where the partial safety factors are derived based on calibration to desired measures of reliability obtained by probabilistic methods.

Due to the large uncertainty associated with seismic loads by virtue of random occurrence time, magnitude, source-to-site distance, seismic wave attenuation, etc., and hence the structural response under the same owing to uncertain structural capacity to withstand such loads, seismic design and evaluation of structures calls for the inclusion of methods of probability and statistics in order that these uncertainties be properly quantified, and their effects adequately considered. However, the handling of uncertain seismic loads to date has primarily been limited to the selection of design ground motion parameters based on a certain return period. Henceforth, the treatment becomes tacit by way of designing conservative structural systems to ensure that structural capacities are not exceeded by the demands. A lack of explicit consideration of the uncertainties prevalent in structural loads and resistances deem such a design to be one of questionable reliability.

Also, from experiences of severe losses and damages incurred during recent earthquakes, such as 1994 Northridge, 1995 Kobe, and 1999 Turkey and Chi-Chi earthquakes, an urgent need to amend the seismic design framework has arisen (Wen 2004). An important observation from

these recent earthquake events is that structures complying with seismic codes based on traditional design philosophy, although having performed satisfactorily as per their design objectives, did not perform equally well in terms of resiliency and public expectation, and thereby failed to serve the community (Günay and Mosalam 2013). This realization highlighted the need for refining the definition of performance goals such that they hold reliably well for the stakeholders and the society as a whole. Societal expectations of structural performance can only be met by explicit statements of performance objectives in terms of the risk associated with well-defined performance levels, rather than ambiguous and misleading statements of "collapse prevention" that is assumed, and not directly checked, to be engendered upon satisfaction of prescriptive measures. Performance objectives stated in terms of the risk associated with performance levels (e.g., exceedance of damage limit-states (*LS*s) and/or specific values of monetary loss/deaths etc.) will not only allow an active participation of the public/stakeholders in the design/decision making process thereby making it more rational, scientific, and transparent, but also lead to greater societal awareness of earthquake risk and consequences (May 2001). Consistent incorporation, quantification, and propagation of the inherent uncertainties involved in various stages of the design process is therefore inevitably called for. The necessity of having quantitative methods ensuring adequate performance of structures, i.e., satisfaction of multiple risk-targeted performance objectives within a confidence level, laid the path towards the development of performance-based earthquake engineering and design.

Identification and filling of knowledge gaps in earthquake engineering, accelerated through advancement in technology and the availability of tremendous computational power has made it possible for researchers to make substantial progress in the domain of performance-based earthquake engineering and design whereby prescriptive measures have become more and more

conceptual, rather than empirical. Fueled by the societal demands of improved life safety, economy and resiliency, the structural engineering community has made some considerable advancement in the realm of performance-based earthquake engineering over the last few decades, consistently improving over time and culminating in the fully probabilistic, rigorous and advanced assessment framework (Moehle and Deierlein 2004; Porter 2003) developed by the researchers at the Pacific Earthquake Engineering Research (PEER) Center.

The PEER performance-based earthquake engineering (PBEE) methodology has been mainly developed for analysis and assessment and not directly for design, except for some initial efforts (Cornell et al. 2002; Mackie and Stojadinović 2007), but has recently been recommended as a future alternative for bridge seismic design (NCHRP 2013). The inherent theoretical complexity of the full-fledged PEER PBEE methodology also adds to its hampered implementation in engineering and design practice. This study focuses on bridging the gap that exists between the theoretical rigor PEER PBEE framework and its practical implementation in the design of bridges, which is also a less trodden area in terms of performance-based earthquake engineering applications as compared to buildings.

1.2 Research Objectives and Scope

This work is aimed to deliver performance-based seismic design (PBSD) guidance for Ordinary Standard Bridges (OSBs) in California. OSBs, i.e., conventional, multiple-span, skewed reinforced concrete bridges, are the most common bridges in California designed in-house by the California Department of Transportation (Caltrans) and are chosen as bridge testbeds in this study to determine the possible benefits of using a performance-based design approach over the current bridge design procedure.

Rooted in the formulation of the targeted PBSD framework is the four-step PEER PBEE assessment methodology integrating site-specific seismic hazard analysis, structural demand analysis, damage analysis, and loss analysis in a comprehensive and consistent probabilistic framework. This assessment methodology involves a sequential execution of the four analytical steps (as mentioned) pieced together (integrated) using the Total Probability Theorem of probability theory to arrive at an estimate of a performance measure, e.g., the mean annual rate (MAR) at which an *LS* is exceeded, and/or the MAR at which a decision variable (e.g., monetary loss, deaths, etc.) exceeds a value of interest. Performance measures considered in this study are the MARs or equivalently the mean return periods (MRPs) of *LS* exceedances for a selected set of *LS*s. The task of probabilistically predicting the future seismic performance of a bridge is, therefore, broken down into the following three steps: Probabilistic Seismic Hazard Analysis (PSHA) in terms of a ground motion intensity measure (*IM*), Probabilistic Seismic Demand Hazard Analysis (PSDemHA) in terms of engineering demand parameters (*EDP*s), and Probabilistic Seismic Damage Hazard Analysis (PSDamHA) for various *LS*s of interest. It is noted that the fourth and the final step of the PEER PBEE assessment methodology, i.e., probabilistic seismic loss hazard analysis, is kept outside the scope of this work.

While moving towards accomplishing the central objective of a PBSD framework for OSBs, completion of the following tasks is achieved in course of this study:

(i) Selection of testbed bridges for the study based on previous Caltrans funded research projects, revisiting inherited finite element (FE) models of these testbed bridges, and incorporation of improvements in the FE modeling approach employed for these bridges.

(ii) Incorporation of improvements of several aspects in various stages of the state-of-the-art PEER PBEE assessment methodology. This includes: (1) introduction of an improved

earthquake *IM* to account for structural period elongation caused by damage during an earthquake, and the lack of certainty in identifying the time period of the predominant mode of vibration of a reinforced concrete OSB; (2) conditional mean spectrum-based hazard-consistent site-specific ground motion selection for ensemble nonlinear time-history analyses involved in the PSDemHA stage; (3) introduction of material strain-based *EDP*s which are better correlated to damage (Priestley et al. 2007) than are traditionally used displacement based *EDP*s (e.g., column drift, plastic hinge rotation); (4) identification of material strain-based *LS*s of interest, viz., concrete cover spalling, precursor stage to longitudinal rebar buckling and onset of longitudinal bar fracture, which are pertinent to the seismic evaluation of bridge structures and meaningful to practicing bridge engineers, and finally (5) development of strain-based normalized fragility functions, required in the PSDamHA stage, for the considered *LS*s through proper identification of previous experimental/numerical research programs, experimental/numerical data, and appropriate capacity prediction equations for normalization.

(iii) Documenting a comprehensive treatise on the first three steps, i.e., PSHA, PSDemHA, and PSDamHA, of the PEER PBEE assessment methodology. This exposition of the PEER PBEE assessment framework revisited and applied to a set of testbed OSBs is expected to serve in the interest of the structural engineering community and bridge any knowledge gap, whatsoever, that is holding back a full-fledged PBSD method from being implemented in bridge design practice.

(iv) A fully-automated and portable (in terms of computational platform, i.e., easily scalable from desktop computing environments to cloud-based supercomputing environments)

implementation of the improved version of the PEER PBEE assessment methodology for probabilistic performance assessment of OSBs.

(v) Numerical seismic performance-based assessment of the selected testbed bridges using the implemented improved PEER PBEE assessment methodology.

(vi) Conceptualization of a generalized workflow for a full-fledged parametric probabilistic seismic performance assessment for OSBs (i.e., probabilistic performance-based assessment of parametrically redesigned versions of the testbed OSBs) and a fully-automated and computationally portable implementation of the same making use of high-throughput computing to solve an embarrassingly parallelizable problem.

(vii) Development and formulation of a simplified, risk-targeted PBSD framework for OSBs accommodating multiple risk-based design objectives with target levels of risk to be specified based on risk tolerance of the engineering community and the society.

(viii) Enhancement of this framework to account for the following additional sources of uncertainty (typically ignored in practice): (i) the aleatory uncertainty associated with FE model parameters, and (ii) the epistemic parameter estimation uncertainty associated with using finite datasets to estimate the parameters of the probability distributions characterizing FE model parameters and *LS* fragilities.

Risk-targeted performance-based design is undoubtedly the most advanced design methodology that will shape the seismic design philosophy of future design codes (Cornell 2000; Ellingwood 2008; NCHRP 2013). PBSD also presents a novel way of approaching design and construction technologies, allowing the tailoring of structural design to meet changing public expectations in the wake of natural disasters such as earthquakes (Ellingwood 2008). The targeted PBSD framework will provide a more rational, scientific, consistent, and transparent design

process, thus resulting in more reliable estimates of bridge safety against various *LS*s of interest. It is believed that the adoption of the targeted PBSD framework will equip practicing bridge engineers with scientific and risk-informed approaches towards building economic and safe bridge structures, especially with regard to the seismic hazard. This will be extremely beneficial in the medium to long-term. This initial venture will also prove to be crucial in supporting and fostering future research work and innovative technological developments in bridge infrastructure engineering that might lead to significant financial savings in the long term.

1.3 Organization of Dissertation

Details of the current research work has been comprehensively documented in the form of this dissertation consisting of nine chapters, brief accounts of the contents of which are outlined below:

Chapter 1 serves as an introduction by posing the need to revise the traditional seismic design philosophy and solve problems of structural design in a rigorously probabilistic, risk-targeted, performance-based context. The research objectives of this work are also outlined in this chapter.

A thorough literature review on the history and development of performance-based engineering, particularly applicable to structural, and especially bridge, engineering practice is presented in **Chapter 2**. This chapter also familiarizes the reader with the PEER PBEE assessment methodology by succinctly going over each analytical step of this methodology.

Chapter 3 introduces four distinct ordinary standard bridge structures in California located in regions with disparate levels of seismicity. A brief description of these OSBs, selected as testbed structures for the remainder of the dissertation, is also presented in Chapter 3.

The multidisciplinary nature of the PEER PBEE framework allows various researchers to work on various aspects of the framework independently and come up with novelties and improvements that particularly relate to the individual steps (or modules) of the framework. The implementation of a modular computational framework that unifies (integrates) such state-of-the-art advancements is outlined in **Chapter 4**.

Chapter 5 presents the analytical and computational implementation of a parametric probabilistic seismic performance assessment framework for OSBs, thus laying the groundwork for solving a risk-targeted PBSD problem, an inverse assessment problem. A PBSD methodology involving the design of the bridge piers is proposed wherein a feasible design domain in the primary design parameter space of an OSB is identified which facilitates risk-informed design/decision making in the face of uncertainty.

A full-fledged implementation of the all-inclusive design method formulated in the Chapter 6 by retaining the inherent rigor of the underlying seismic performance assessment methodology might impose a seemingly prohibitive computational cost for the available resources in the current scenario of seismic bridge design practice. For reasons of practicability, the findings of the full-fledged design framework are inventively utilized to distill out a computationally more economical and simplified PBSD procedure in **Chapter 6**.

The PBSD framework proposed thus far explicitly considers: (1) the uncertainty in the seismic input, and (2) the uncertainty in the capacity of the various *LS*s. This framework is enhanced in **Chapter 7** to account for the following additional sources of uncertainty: (i) the aleatory uncertainty associated with FE model parameters, and (ii) the epistemic parameter estimation uncertainty associated with using finite datasets to estimate the parameters of the probability distributions characterizing FE model parameters and *LS* fragilities.

Finally, a concluding chapter, i.e., **Chapter 8**, summarizes the work performed, provides a highlight of the results obtained, and throws light on several avenues for future research work in this area.

2 Literature Review of Performance-based Design with Application to Bridge Engineering

2.1 Introduction

The Pacific Earthquake Engineering Research (PEER) Center is not the only organization that has worked towards the development of performance-based engineering, in general. The PEER performance-based earthquake engineering (PBEE) methodology is the culmination of years of research, implementation and progress made in multi-disciplinary branches of engineering by various researchers and numerous organizations. Performance-based engineering lies in the heart of all fields of engineering that entail decision making under uncertainties, risk analysis, and structural reliability. Whenever a system is to be designed or assessed in an environment where there is an uncertain hazard leading to uncertain demands on the system, which in turn has an uncertain resistance, thereby leading to uncertain levels of damage, performance-based engineering provides the most scientific and rational way towards a design and assessment process.

Being rooted in the broader area of structural reliability and quantitative risk assessment, performance-based engineering is not restricted to earthquake engineering only. It has been in practice in the nuclear industry (Cornell and Newmark 1978; Kennedy et al. 1980; Kennedy and Ravindra 1984; Shinozuka et al. 1984), and offshore/marine engineering (De 1990; Guenard 1984; Marshall 1969; Moan 1981, 1994) for quite some time now, where quantitative risk assessment plays a significant role. Earlier works in probabilistic risk assessment of civil engineering facilities (Ellingwood 2001; Ellingwood and Ang 1974) are also worth mentioning in this regard.

This Chapter provides a brief account of performance-based engineering, particularly as it relates to the history and current state-of-the-art of earthquake engineering assessment and design practice of structural systems, in general. The discussion in this Chapter is gradually narrowed down to the applicability of PBEE in the seismic design of the testbed structural systems to be considered in this research work, i.e., ordinary or conventional bridges in California.

2.2 History and Development of Performance-based Earthquake Engineering

Before being shaped by PEER in its most scientific and rigorous form, performance-based seismic engineering had evolved over a period of decades in the building industry. Advancement in seismic hazard analysis (Cornell 1968) started showing up in the evolution process of PBEE as the seismic input began to be rationally and probabilistically considered, although partially, by way of introducing the concept of a design earthquake associated with a certain return period (ATC 3-06 1978). Over the next few years, the description of seismic input became more elaborate with the introduction of a more severe hazard level, viz. the Maximum Considered Earthquake (ASCE 2005), however, the design and assessment of structures continued to be followed based on a deterministic structural behavior. The first generation PBEE, although implemented with the correct intention, thus fell short of a thorough and exhaustive quantitative implementation by disregarding the various uncertainties associated with the entire design and assessment process.

A sudden and more recent (during early 90's) spike in the advancement of PBEE occurred with the need to assess existing structures for safety. The Structural Engineering Association of California (SEAOC) came up with the Vision 2000 report (Poland et al. 1995) where structural performance objectives were defined in terms of performance levels (see Figure 2.1), viz. Fully

Operational, Operational, Life Safety, and Near Collapse at different levels of seismic hazard, for example, Frequent (43 yr. return period), Occasional (72 yr. return period), Rare (475 yr. return period) and Very Rare (970 yr. return period). Other documents like FEMA-273 (FEMA-273 1997) and FEMA-356 (FEMA-356 2000) followed a similar approach to develop a performance-based framework by associating discrete levels of performance with discrete hazard levels, the difference with Vision 2000 (Poland et al. 1995) lying in the definition of these levels. However, all throughout these stages of development of the framework, performance evaluation was primarily done deterministically by comparing element forces and deformation to prescriptive limits and acceptance criteria. These criteria were derived based on laboratory tests, simplified analytical models, or plain engineering judgment. Furthermore, element or component performance was assumed to be indicative of a global system performance which is not necessarily always true. Also, the performance measures, in terms of element forces and deformations, used in the 1st generation PBEE were not of direct interest to the stakeholders which led to a gap in the process of decision making between engineers and the public.

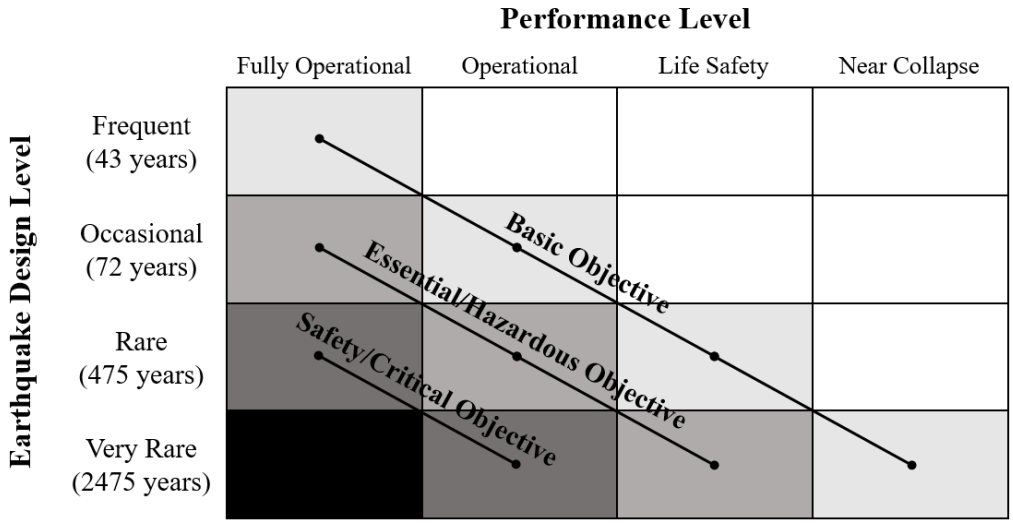

Figure 2.1 Vision 2000 (Poland et al. 1995) performance matrix

These shortcomings of the 1st generation PBEE were attempted to be resolved through the development of a more robust, and technically sound framework at PEER. The performance-based framework developed at PEER provides a more transparent process in which performance objectives are explicitly stated as measures of monetary losses, downtime, and deaths, that make more sense to stakeholders, and all pertinent sources of uncertainty are included in the analysis procedure. As the structural engineering community aims to move toward more rational, risk-informed approaches to structural design and assessment, the paradigm of performance-based engineering is expected to provide technical support for this move and a novel way to tailor structural design to meet the changing public expectation after disasters (public's risk tolerance). The placement of structural performance classification based on acceptable risk is the key feature of this methodology developed at PEER.

The PEER PBEE methodology has been used extensively by the United States Federal Emergency Management Agency (FEMA) and the Applied Technology Council (ATC) to develop a new generation of performance-based seismic design (PBSD) guidelines (FEMA-445 2006) for structural engineering practice. In recent years, PBEE has been followed in designing the seismic force resisting system of a number of tall buildings in the western U.S. (Ellingwood 2008). PBEE will continue to shape the core of future seismic design codes. Design methodologies for port structures are moving towards performance-based (PIANC 2001). This trend has also been followed by port owners and code developers who have issued design guidelines for seafront structures (Johnson et al. 2013; POLA 2010; POLB 2009) and has now reached a national level with the publication of the *Seismic Design of Piers and Wharves* Code (ASCE/COPRI 2014). This code incorporates elements of PBSD and, in prescriptive language, states performance objectives as well as damage limit-states (*LS*s).

The PEER PBEE formulation has also been extended to other engineering fields such as blast engineering (Whittaker et al. 2003), fire engineering (Rini and Lamont 2008), tsunami engineering (Keon et al. 2016; Riggs et al. 2008), wind engineering (Augusti and Ciampoli 2008; Ciampoli et al. 2011; Ciampoli and Petrini 2012; van de Lindt and Dao 2009), hurricane engineering (Barbato et al. 2013; Masters et al. 2010), offshore engineering (Nezamian and Morgan 2014), and aerospace engineering (Gobbato et al. 2012, 2014).

2.3 PEER PBEE Assessment Framework

This section aims to present the PEER PBEE framework in detail elucidating all the steps included therein (Moehle and Deierlein 2004; Porter 2003). The PEER PBEE methodology breaks down the task of predicting probabilistically the future seismic performance of a structure into four analytical steps pieced together (integrated) using the Total Probability Theorem (TPT) as shown in Figure 2.2. These steps are: (1) probabilistic seismic hazard analysis in terms of a ground motion intensity measure (*IM*), (2) probabilistic seismic demand analysis given *IM*, in terms of engineering demand parameters (*EDP*s), (3) probabilistic capacity analysis (or fragility analysis) and probabilistic damage analysis for various *LS*s associated with the critical potential failure modes of the structure in concern, and (4) probabilistic loss analysis for decision variables (*DV*s), that are of great interest to stakeholders.

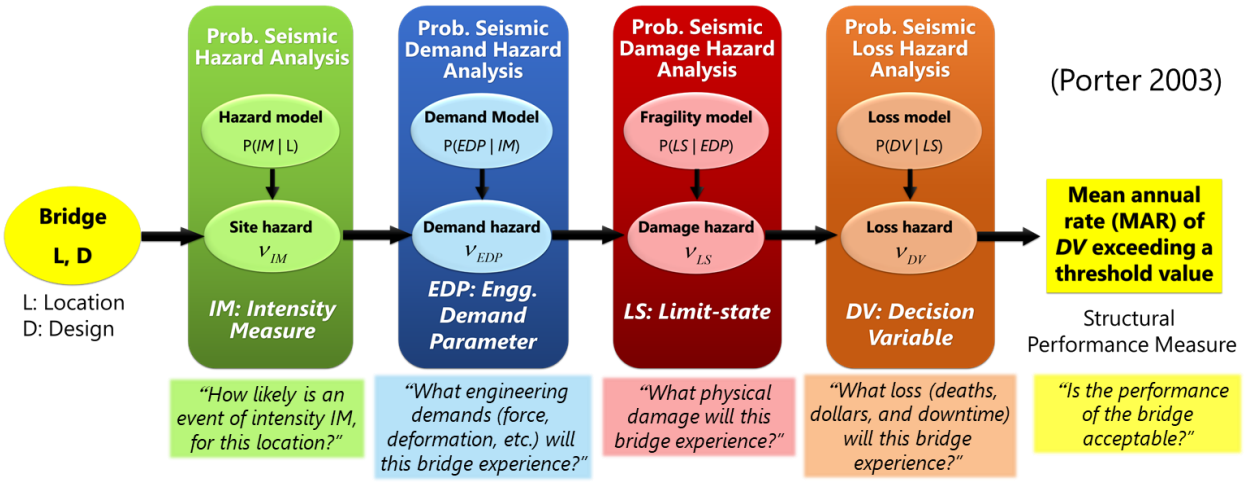

Figure 2.2 PEER performance-based earthquake engineering methodology (Porter 2003)

2.3.1 Probabilistic Seismic Hazard Analysis (PSHA)

The objective of PSHA is to compute for the site of the considered structure, the mean annual rate (MAR) $\nu_{IM}(x)$ (or annual probability) of exceeding any specified value x of a specified ground motion *IM*. The latter is usually taken as a structure-independent ground motion parameter (e.g., peak ground acceleration (PGA), peak ground velocity (PGV), Arias intensity, Housner's spectrum intensity) or more often as a structure-dependent ground motion parameter such as the first-mode pseudo-spectral acceleration, $S_a(T_1,\xi)$, or the spectral displacement $S_d(T_1,\xi)$ at the expected predominant period. For a given site, PSHA integrates the contribution of all possible seismic sources to calculate the MAR of random events $\{IM > x\}$ according to the TPT as

$$\nu_{IM}(x) = \sum_{i=1}^{N_{\text{flt}}} \nu_i \int_{R_i} \int_{M_i} P\left[IM > x \mid M_i = m, R_i = r\right] \cdot f_{M_i}(m) \cdot f_{R_i}(r) \cdot dm \cdot dr \qquad (2.1)$$

where N_{flt} = number of causative faults; ν_i = MAR of occurrence of earthquakes on fault (or seismic source) i. The functions $f_{M_i}(m)$ and $f_{R_i}(r)$ denote the probability density functions (PDFs) of the magnitude (M_i) and source-to-site distance (R_i), respectively, given the occurrence

of an earthquake on fault *i*. The conditional probability $P\left[IM > x \mid M_i = m, R_i = r\right]$ in Eq. (2.1) is referred to as attenuation relationship (predictive relationship of *IM* given seismological variables *M* and *R*), is typically developed by applying statistical regression analyses to recorded earthquake ground motion data. The seismic hazard curve at a given site accounts for the uncertainty of *IM* due to the randomness of the time and spatial occurrences of future earthquakes affecting the site, as well as the uncertainties related to the seismic wave propagation path and the local site conditions. The random occurrence of earthquake in time is commonly modeled using the Poisson model. For small values of $\nu_{IM}(x)$, typical of large earthquakes of interest to structural engineers, the value of the MAR and the corresponding annual probability of occurrence almost coincide.

2.3.2 Probabilistic Seismic Demand Hazard Analysis (PSDemHA)

The next step in the PEER PBEE methodology is to estimate in probabilistic terms the seismic demand that future possible earthquake ground motions will impose on the structure. The objective of PSDemHA is to compute the MAR, $\nu_{EDP}(\delta)$, that a given structural response parameter (i.e., an *EDP*) exceeds any specified value δ as (Zhang 2006)

$$\nu_{EDP}\left(\delta\right) = \int_{IM} P\left[EDP\left(\bar{\mathbf{y}}, IM, \varepsilon_I\right) > \delta \mid IM = x\right] \cdot \left|d\nu_{IM}\left(x\right)\right| \tag{2.2}$$

where $EDP(\bar{\mathbf{y}}, IM, \varepsilon_I)$ denotes the dependence of *EDP* on the best estimates (expected values) $\bar{\mathbf{y}}$ of the system properties $\mathbf{Y}$, the ground motion intensity measure *IM*, and the record-to-record variability ε_I. Thus, according to Eq. (2.2), the demand hazard curve $\nu_{EDP}(\delta)$ is obtained as the convolution of the conditional complementary CDF (CCDF) of the *EDP* given *IM*, $P\left[EDP > \delta \mid IM = x\right]$, with the seismic hazard curve $\nu_{IM}\left(x\right)$. The conditional CCDF

$P[EDP > \delta \mid IM = x]$ is obtained through subjecting the FE model of the considered structure through ensembles of scaled earthquake records.

2.3.3 Probabilistic Seismic Damage Hazard Analysis (PSDamHA)

The objective of the third step of the PEER PBEE methodology is to compute the MAR of exceedance of a specified *LS*, ν_{LS}. Although in reality, there is a continuous progression of physical damage in a structure subjected to a damaging load, we typically focus on discretely observed (Veletzos et al. 2008) or prescribed (ASCE 2013) damage-states. For example, discrete damage-states for reinforced concrete bridge piers include the onset of concrete cracking, concrete spalling, bar buckling, fracture of transverse and longitudinal reinforcement. The MAR of exceedance of a specified *LS* can be obtained as (Conte and Zhang 2007; Zhang 2006):

$$\nu_{LS} = \int_{EDP} P[LS \mid EDP = \delta] \cdot \left| d\nu_{EDP}(\delta) \right| \tag{2.3}$$

where $P[LS \mid EDP = \delta]$ denotes the probability that the *LS* is reached or exceeded given that the associated *EDP* is equal to the specific value δ. This probability quantity, $P[LS \mid EDP = \delta]$, viewed as a function of δ is referred to as a *fragility function* or *fragility curve* in the literature. Thus, according to Eq. (2.3), the MAR of exceedance of a specified *LS*, ν_{LS}, is obtained mathematically as the convolution of the corresponding fragility curve, $P[LS \mid EDP = \delta]$, and the seismic demand hazard curve $\nu_{EDP}(\delta)$ of the associated *EDP*. A fragility curve is typically developed based on the joint use of a simplified (design code type) analytical, semi-analytical or empirical predictive capacity model for this *LS* and experimental data collected from an ensemble of specimens for this *LS* (Berry and Eberhard 2004, 2005). In the absence of experimental data for

a given *LS* (e.g., structural system *LS*s), fragility curves are obtained through numerical simulation of the structural response behavior using reliable (e.g., validated at the component level) FE structural models (Mackie and Stojadinovic 2004; Nielson 2005).

2.3.4 Probabilistic Seismic Loss Hazard Analysis (PSLHA)

In the PEER PBEE methodology, the probabilistic performance assessment results reviewed above can be propagated further to decision variables (*DV*s) that relate to loss of life, cost (direct and indirect), and downtime and are of great interest to property owners. The objective of probabilistic seismic loss analysis is to assess *DV*s probabilistically (e.g., compute the MAR that the total repair/replacement cost due to seismic damage exceeds any specified dollar amount) for a given structure at a given location. The probabilistic assessment of these *DV*s, which are random variables, accounts for the uncertainties in the seismic hazard at the site or in *IM*, in the seismic demand (*EDP*s), in the structural capacity and damage *LS*s, and in the cost associated with the repair of individual structural components or replacement of the entire structure. The outcome of a probabilistic loss analysis is the seismic loss hazard curve $\nu_{DV}(v)$, which expresses the MAR of the *DV* (e.g., total repair/replacement cost) exceeding any specified threshold value v.

In the case of global failure of the structure, a new structure will be constructed, and the total repair cost is defined by the construction cost of the new structure. In the case of "no global collapse", it is assumed that all damage occurs at the component level and the total repair cost L_T of the structure (in a year) is equal to the summation of the repair costs of all components damaged during that year, i.e.,

$$L_T = \sum_{j=1}^{n} L_j \tag{2.4}$$

where L_j is the repair cost of the j^{th} damaged component, and *n* is the number of damaged components in the structure. The repair cost of a damaged component is generally associated with a specified repair scheme, which is associated with the damage state of the component. Basic ingredients to probabilistic loss assessment are repair actions and probability distributions of their costs given the component damage state. A multi-layer Monte Carlo simulation approach can be used to compute very efficiently the seismic loss hazard curve related to L_T (Conte and Zhang 2007; Zhang 2006).

The loss hazard curve incorporates the effects of the uncertainties related to earthquake occurrences in space and time, ground motion intensity, ground motion time history (record-to-record variability), structural capacity, damage *LS*s, and repair costs. The relative importance of these various sources of uncertainty in regard to the loss hazard results can be investigated through parametric studies.

2.4 Current Bridge Design Practice

Current practices of seismic design for ordinary or conventional bridges primarily includes two design methodologies. The first is a force-based approach incorporated into the AASHTO LRFD Bridge Design Specifications (AASHTO 2012), while the second one is a displacement-based approach, originating partly from the Caltrans Seismic Design Criteria (SDC) version 1.4 (Caltrans 1999), and on which the AASHTO Guide Specifications for Seismic Bridge Design (AASHTO 2011) is predicated. Ordinary or conventional bridges are subjects of concern in this proposed research because these are the most common bridges designed in-house by Caltrans and it is aimed to determine whether the reported benefits of using a design approach corresponding to the PEER PBEE framework over the current design procedure used by Caltrans are significant.

This section briefly discusses both methodologies with an aim to primarily highlight the weak points of the current seismic bridge design practice and how PBSD can serve to bolster it.

2.4.1 Force-based Approach

The force-based approach, with capacity design as its underlying philosophy, relies on providing adequate resistance to structural elements of the bridge that are selected to dissipate energy by way of yielding when subjected to an earthquake. This is done by selecting a design ground motion (with a probability of exceedance of 5% in 50 years or 1000-year return period) and subjecting a linear elastic model of the bridge to the same. The forces generated in the critical locations of the energy-dissipating (yielding) elements are obtained and these regions are designed to resist only a fraction (called design forces) of the originally calculated forces by multiplying response modification factors (called *R*-factors) to them. These *R*-factors are selected primarily based on structure geometry, and anticipated ductility. Adequate detailing is provided at the locations of yielding to get desired inelastic action through ductility. Having designed for ductility, all other members are then protected against overstrength forces so as to make sure that they remain linear elastic.

Apart from the usual problem of incomplete incorporation of uncertainty by only considering it in determining the seismic hazard, that too for a single hazard level, this approach has the added disadvantage of assuming that prescriptive requirements of detailing will do their job of ensuring bridge performance without any firsthand scrutiny been made.

2.4.2 Displacement-based Approach

The displacement-based approach differs from its force-based counterpart in that a direct check of the displacement capacity of the system is made. The Caltrans SDC v1.7 (Caltrans 2013) uses this approach for the design of bridge systems. Still rooted in capacity design philosophy, this approach involves the selection of a trial design that is detailed for suitable inelastic action and ductility, followed by checking for the displacement capacity directly. The system displacement capacity is controlled by prescribing material strain limit states which can be related to global system displacements through element curvature and rotations. The inelastic displacement capacity is then compared to the elastic displacement demand generated due to the action of the design earthquake (with a probability of exceedance of 5% in 50 years or 1000-year return period).

This approach has the merit of a firsthand quantitative check of displacement capacity being made. Additionally, it is welcoming of the complete PBSD framework, because it already follows a partial 1st generation performance-based procedure by allowing prescriptive strain limits (related to various damage states and hence performance levels) to control the system displacement capacity. However, it has the drawbacks, similar to that of the 1st generation PBEE procedures mentioned earlier, of having inadequately accounted for uncertainty only in the seismic input, that too for a single hazard level. Element performance evaluation is considered to be void of uncertainties and prescriptive strain limits, based on laboratory tests, simplified analytical models, and engineering judgment are assumed to be representative of system behavior. Also, metrics of structural performance being based on element forces and deformation, does not allow the public and/or owners to participate in risk-informed decision making, unlike what is promised by the PEER PBEE framework.

Prescriptive design methodologies form the heart of current seismic bridge design practice in the US. With a latent objective of collapse prevention and life safety under a design earthquake event, these prescriptive measures do the job of evaluating the seismic performance of bridges only to a limited extent as there is no direct control over the seismic performance of bridges in the hands of the designer. Although this has proved to be a satisfactory design methodology for the bridge engineering profession to date (NCHRP 2013), the application of PBSD in bridge design, nonetheless, does not become less promising in this regard. With a significantly better comprehension and quantification of seismic demand and response of bridges due to the incorporation of all the sources of inherent uncertainties, PBSD will allow designers and the owners/public to make collective and risk-informed decisions regarding the performance of bridges during a seismic event, thereby leading to a more efficient and rational design practice.

2.5 Recent Performance-based Design Developments in Bridge Engineering

The fully probabilistic PBSD is the most advanced design methodology and is expected to provide the foundation for future design codes (Cornell 2000; Ellingwood 2008; NCHRP 2013). Although not in its all-inclusive form, PBSD has already started to be implemented in practice (ASCE 2010; Buckle et al. 2006; FEMA-445 2006; NCHRP 2013) by the structural engineering profession and several design and retrofit projects have also been undertaken by various organizations. Significant work has been done and progress is being made in both spheres of building and bridge engineering, albeit the latter has seen relatively less advancement as compared to the former (NCHRP 2013).

A recent investigation led by the Transportation Research Board of the National Academies under the National Cooperative Highway Research Program (NCHRP) (NCHRP 2013) regarding the current state of seismic design practice in the area of bridge engineering, made the necessity and significance of the implementation of PBSD in bridge design quite evident. This synthesis brings out the fact that the current bridge design practice considers safety and risk associated with seismic performance of bridges as mere ramifications of the fulfillment of prescriptive measures. May's argument (May 2001) of explicit consideration of safety and risk, in order that public and engineers participate in the decision-making process in tandem, is emphasized. This process of collective decision-making, however, will require an unambiguous definition of performance objectives that will facilitate its smooth working and will also help to keep post-hazard, performance-related, political and/or legal issues at bay.

The synthesis also covers the 4 analytical stages of PEER PBEE framework discussed before highlighting the areas where special attention is the need of the hour as per the current state of practice in the bridge engineering profession. With the current tools of seismic hazard analyses and nonlinear structural analyses, the implementation of the first two steps of the framework seems to be a little less demanding and more feasible than the last two steps, via a probabilistic treatment of the seismic hazard and structural response. A noteworthy highlight of the synthesis is that the field of damage and loss prediction, in a rigorous probabilistic manner, has yet to see significant advancement. The complexity of predicting the highly uncertain phenomenon of damage has so far been underestimated by its treatment based on deterministic strain-limits. A complete probabilistic treatment of damage requires extensive laboratory testing and analytical investigations (Berry and Eberhard 2004; Mackie and Stojadinovic 2004), thereby leading to development of fragility functions which relate an engineering demand parameter or a response

quantity to the probability of exceedance of a specific damage state. The final and the most important step, novel to the PEER PBEE framework, is the explicit probabilistic consideration of loss metrics, which are of interest to owners and stakeholders. Loss prediction, till date, has largely been qualitative and has lacked objectivity. Thus, the need to explicitly consider this, in a probabilistic manner, whereby the risk of incurring losses pertaining to decision variables, viz., deaths, dollars, downtime, etc., can be accurately evaluated is expressed. For this purpose, loss models (Baker and Cornell 2003; Mander et al. 2012; Miranda et al. 2004; Moehle and Deierlein 2004) relating damage to the probability of exceeding various levels of losses are required. Once equipped with all the tools required for a rigorous implementation of the framework, wherein all sources of uncertainty are accounted for, it can be applied to the design (inverse assessment problem) of new bridges. As mentioned earlier, the works of Cornell and coworkers (Cornell et al. 2002) and Mackie and Stojadinović (Mackie and Stojadinović 2007) can be cited as premises to such an effort.

More recently, research conducted at the University of Nevada, Reno, led to the development of the Probabilistic Damage Control Approach (PDCA) (Saini and Saiidi 2014) for seismic design of bridge columns. This research, funded by Caltrans, is a significant step forward toward the implementation of a probabilistic PBSD in the bridge engineering industry. In this approach, the uncertainties in seismic demand and structural response are taken into account explicitly. A displacement-based representative parameter of bridge-column response, called Damage Index (DI), defined as the ratio of plastic deformation demand to the plastic deformation capacity, is used to measure the seismic performance of columns. Fragility functions correlating Damage States (DSs) to DIs were used from a previous experimental study (Vosooghi and Saiidi 2012) at University of Nevada, Reno to come up with a probabilistic resistance/capacity model.

The probabilistic load/demand model was developed using extensive analytical modeling of columns designed to have a desired probability of exceedance of a certain DS, and nonlinear time history analyses of the same subjected to a suite of ground motions conducted thereafter. In order to have a realistic load/demand model, uncertainties in seismic demand were incorporated through the inclusion of different site classes, ground motion parameters, bent properties and earthquake return period. Structural performance was evaluated based on the reliability indices (βs) associated with different DSs. Finally, a non-iterative, approximate, yet direct design method is forwarded so as to design a column bent for a target DI in order that a desired reliability index is achieved for a specific damage state.

Research studies and implementations of PBSD, as such, have served to expose the difficulties and challenges it entails, thereby helping to fill the knowledge gaps and move forward towards the goal of a convenient implementation of the framework in its most rigorous form.

3 Testbed Bridges

3.1 Introduction

For this study, four as built bridges located in California were selected for analysis and are described in this chapter. The selected bridges conform to the definition of ordinary standard bridges as described in Caltrans SDC v1.7 (Caltrans 2013). Multiple testbed bridges are required to cover a spectrum of design characteristics of ordinary bridges in California to ensure the overall methodology utilized in this project can be reproduced for a variety of design scenarios.

Each testbed bridge will be used to generate a corresponding design matrix where multiple key design parameters can be varied from the as-designed case. Practical combinations of design parameters encountered in the field and its effects on the performance of each bridge are analyzed using this design matrix. The utilization of these testbed bridges and subsequent findings are investigated and described more comprehensively later in this report.

The testbed bridges selected for this study are based on bridges studied in recent research projects funded by Caltrans and PEER (Beckwith et al. 2015; Kaviani et al. 2012, 2014; Omrani et al. 2015). The selected set of testbed bridges comprises of representative modern Ordinary Standard Bridges (OSBs) in California constructed after year 2000, viz., Bridge A, Bridge B, Bridge C and Bridge MAOC. A comprehensive explanation behind the recommendation of these bridges are described in their respective reports.

Bridge A is the Jack Tone Road Overcrossing in Ripon, California consisting of two spans with a single column bent. Bridge B is the La Veta Avenue Overcrossing in Tustin, California also consisting of two spans but supported on a two-column bent. Bridge C is the Jack Tone Road Overhead in Ripon, California (located adjacent to Bridge A) consisting of three spans on three-

column bents. The last bridge is the Massachusetts Avenue Overcrossing, Bridge MAOC, located in San Bernardino, California consisting of five spans on four-column bents. Selected characteristics of each of these bridges obtained from the National Bridge Inventory (NBI) database are listed in Table 3.1. A detailed description of the geometrical characteristics and structural properties of each bridge can be found in Section 3.2.

Table 3.1 Selected characteristics of testbed bridges in accordance with the 2017 archived National Bridge Inventory (NBI) database

NBI Item Name	Bridge A	Bridge B	Bridge C	Bridge MAOC
Structure number	29 0320	55 0938	29 0318	54 1265
Features intersected	STATE ROUTE 99	STATE ROUTE 55	UPRR, SB99 ONRP, KAMPS WY	INTERSTATE 215 & BNSF RY
Facility carried by structure	Jack Tone Road	La Veta Avenue	Jack Tone Road	Massachusetts Avenue
Location	10-SJ-099-2.34-RIP	12-ORA-055-13.20-TUS	10-SJ-099-2.32-RIP	08-SBD-215-9.03-SBD
Latitude	37450851	33465032	37450217	34075676
Longitude	121083108	117495371	121083077	117183123
Year built	2001	2001	2001	2012
Lanes on structure	1	4	4	2
Lanes under structure	7	14	3	10
Average daily traffic	20000	10000	5000	9000
Skew	33	0	36	8
Type of service	11 (highway on bridge, highway w/wo pedestrian)	51 (highway-pedestrian on bridge, highway w/wo pedestrian under bridge)	18 (highway on bridge, highway-waterway-railroad under bridge)	54 (highway-pedestrian on bridge, highway-railroad under bridge)
Number of spans in main unit	2	2	3	5
Structure type, main	606 (prestressed concrete continuous, box beam or girders - single or spread)	605 (prestressed concrete continuous, box beam or girders - multiple)	606 (prestressed concrete continuous, box beam or girders - single or spread)	205 (concrete continuous, box beam or girders - multiple)
Deck (physical condition)	5 (fair condition, minor section loss)	8 (very good condition)	5 (fair condition, minor section loss)	7 (good condition, minor problems)
Superstructure (physical condition)	7 (good condition, minor problems)	8 (very good condition)	7 (good condition, minor problems)	7 (good condition, minor problems)
Substructure (physical condition)	5 (fair condition, minor section loss)	7 (good condition, minor problems)	5 (fair condition, minor section loss)	7 (good condition, minor problems)
Inspection date	1016 (October 2016)	0616 (June 2016)	1016 (October 2016)	1016 (October 2016)

3.2 Description of Selected Bridges

Although specific requirements must be met for bridges to be classified as Ordinary Standard Bridges, as defined in Caltrans SDC v1.7 (Caltrans 2013), nevertheless considerable variations and combinations of designs are still possible. The selected testbed bridges, therefore, should attempt to cover a spectrum of design parameters commonly found in practice such that a range of possible designs can be accounted for to increase the robustness of the developed methodology. Such variations include the number of spans, columns per supporting bent, diameter of columns, height of columns, cap beam, skew, deck width and geometry, number of bearing pads shear key type etc. A detailed description of each bridge is given below focusing on the above-mentioned properties as well as derived geometrical and structural parameters pertinent for the construction of finite element models of these bridges (discussed in the next chapter).

3.2.1 Definition of an Ordinary Standard Bridge

A structure meeting all the following requirements below, where applicable, is classified as an Ordinary Standard Bridge (taken directly from Caltrans SDC, Version 1.7, April 2013):

(i) Each span length is less than 300 feet.

(ii) Bridges with single superstructures on either a horizontally curved, vertically curved, or straight alignment.

(iii) Constructed with precast or cast-in-place concrete girder, concrete slab superstructure on pile extensions, column or pier walls, and structural steel girders composite with concrete slab superstructure which are supported on reinforced concrete substructure elements.

(iv) Horizontal members either rigidly connected, pin connected, or supported on conventional bearings.

(v) Bridges with dropped bent caps or integral bent caps.

(vi) Columns and pier walls supported on spread footings, pile caps with piles or shafts.

(vii) Bridges supported on soils which may or may not be susceptible to liquefaction and/or scour.

(viii) Spliced precast concrete bridge system emulating a cast-in-place continuous structure • Fundamental period of the bridge system is greater than or equal to 0.7 seconds in the transverse and longitudinal directions of the bridge.

3.2.2 Jack Tone Road Overcrossing (Bridge A)

The Jack Tone Road Overcrossing is located in Ripon, California (south of Sacramento), spanning over California State Route 99. The bridge was constructed in 2001 and consists of a single lane serving as an onramp to the main Jack Tone Road. The bridge consists of two spans at 108.58 ft and 111.82 ft for a total length of 220.4 ft and is supported on a single column bent. Each column is supported on 25 HP 305x79 steel piles. The column has a diameter of 5.51 ft and a longitudinal reinforcement ratio of 2.0%. The deck of the bridge is a three-cell continuous prestressed reinforced-concrete box girder with a total width of 27.13 ft. The bridge abutment is at a skew of 33° and supported vertically on elastomeric bearings and restrained horizontally by monolithic shear keys. A detailed description of the Jack Tone Road Overcrossing can be found in Table 3.2

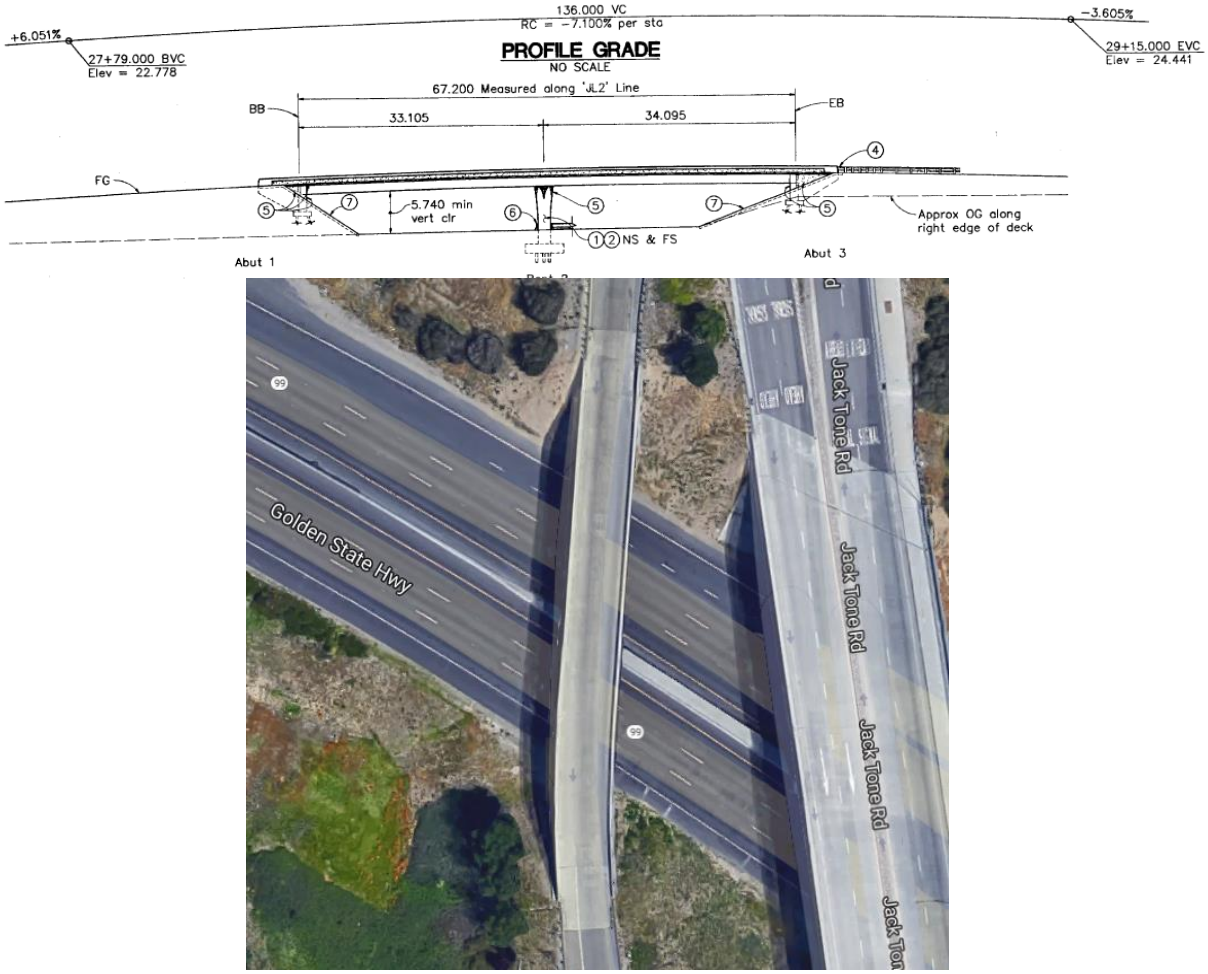

Figure 3.1 Profile and aerial overview of Bridge A on left (adjacent to main Jack Tone Road)

Table 3.2 Geometrical and structural properties of Bridge A

Parameter/Feature	**Value/Description**
Number of spans	2
Length of spans	108.58 ft (33.10 m) and 111.82 ft (34.08 m)
Total length of bridge (L_{tot})	220.4 ft (67.18 m)
Total width of deck (w_d)	27.13 ft (8.27 m)
Depth of deck (d_d)	4.64 ft (1.14 m)
Deck cross-sectional properties (Area, Torsional constant, Second moments of area)	A = 97.55 ft^2 (9.06 m^2); J = 341 ft^4 (2.94 m^4); I_y = 180.33 ft^4 (1.56 m^4); I_z = 3, 797.9 ft^4 (32.78 m^4)
Height of each bent	28.0 ft (8.5 m)
Number of columns in each bent	1
Column cross-sectional properties (Diameter, Area, Torsional constant, Second moments of area)	D_{col} = 5.51 ft (1.68 m); A_{col} = 23.84 ft^2 (2.21 m^2); J_{col} = 90.49 ft^4 (0.78 m^4); $I_{y,col}$ = 45.24 ft^4 (0.39 m^4); $I_{z,col}$ = 45.24 ft^4 (0.39 m^4)
Column reinforcement details	Longitudinal reinforcement (2.0%): 22×2#11 Transverse reinforcement: Spiral, #6 @ 3.34 in c/c
Column base hinge diameter	No base hinge
Concrete material properties of elastic superstructure (nominal) (Compressive strength, Elastic modulus)	f_c' = 5 ksi (34.5 MPa) E_c = 4, 030.5 ksi (27, 789.3 MPa)
Concrete material properties of columns (nominal) (Compressive strength, Elastic modulus)	f_c' = 5 ksi (34.5 MPa) E_c = 4, 030.5 ksi (27, 789.3 MPa)
Steel reinforcement material properties	Grade 60, ASTM A706
Bridge skew angle	33^o
Shear key type	Non-isolated (monolithic) shear keys
Number of bearing pads per abutment	4 elastomeric bearings
Bearing pad dimensions (Height, Area)	h_{bp} = 2.56 in (.065 m); A_{bp} = 139.5 in^2 (0.09 m^2)

3.2.3 La Veta Avenue Overcrossing (Bridge B)

The La Veta Avenue Overcrossing is located in Tustin, California (south of Los Angeles), spanning over California State Route 55. The bridge was constructed in 2001 and consists of two lanes in each direction running east-west. The bridge consists of two spans at 154.82 ft and 144.98 ft for a total length of 299.8 ft and is supported on a two-column bent. Each column is supported by 20 23.6 in diameter cast-in-drilled hole (CIDH) piles. The columns have a diameter of 5.58 ft and a longitudinal reinforcement ratio of 1.95%. The deck of the bridge is a six-cell continuous reinforced-concrete box girder with a total width of 75.5 ft. The bridge abutment is supported vertically on elastomeric bearings and restrained horizontally by monolithic shear keys. There is no skew in the bridge abutment. A detailed description of the La Veta Avenue Overcrossing can be found in Table 3.3

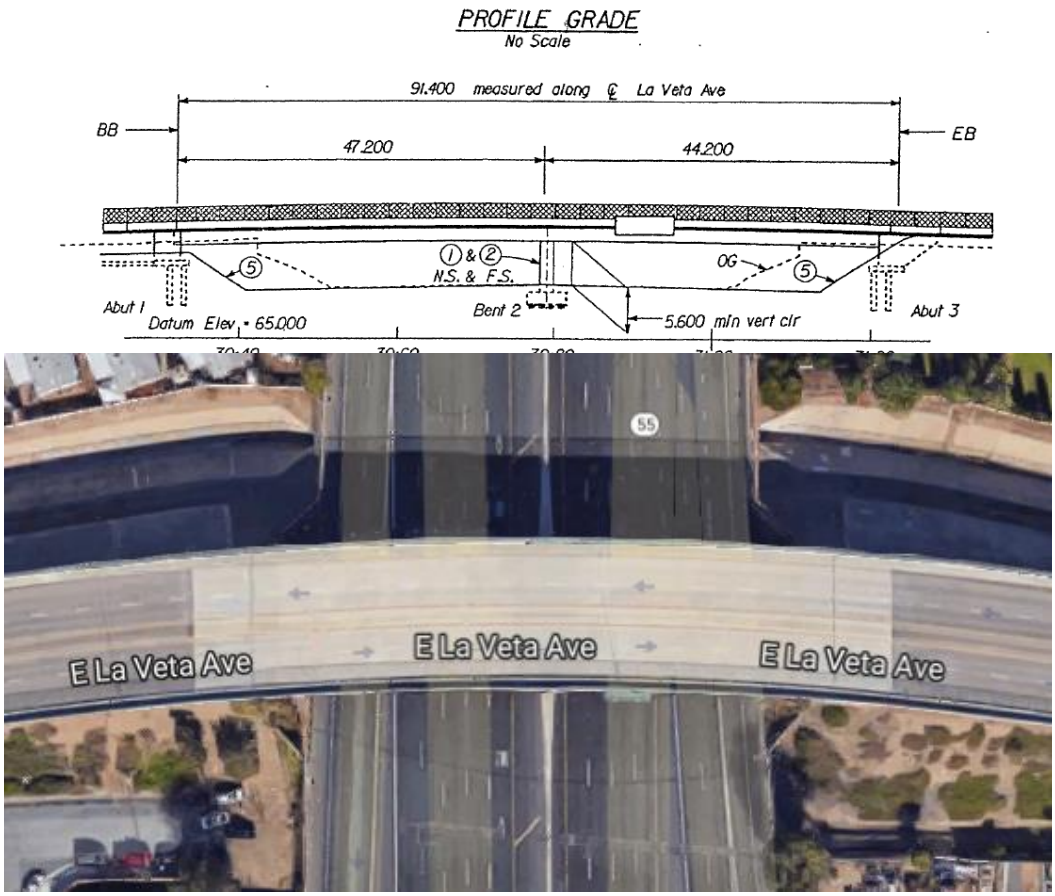

Figure 3.2 Profile and aerial overview of Bridge B

Table 3.3 Geometrical and structural properties of Bridge B

Parameter/Feature	**Value/Description**
Number of spans	2
Length of spans	154.82 ft (47.19 m) and 144.98 ft (44.19 m)
Total length of bridge (L_{tot})	299.8 ft (91.38 m)
Total width of deck (w_d)	75.5 ft (23.01 m)
Depth of deck (d_d)	6.23 ft (1.9 m)
Deck cross-sectional properties (Area, Torsional constant, Second moments of area)	A = 129.13 ft^2 (12.0 m^2); J = 2532 ft^4 (21.85 m^4); I_y = 791.76 ft^4 (6.83 m^4); I_z = 58, 352 ft^4 (503.64 m^4)
Height of each bent	22 ft (6.71 m)
Number of columns in each bent	2
Column cross-sectional properties (Diameter, Area, Torsional constant, Second moments of area)	D_{col} = 5.58 ft (1.70 m); A_{col} = 23.84 ft^2 (2.21 m^2); J_{col} = 90.49 ft^4 (0.78 m^4); $I_{y,col}$ = 45.25 ft^4 (0.39 m^4); $I_{z,col}$ = 45.25 ft^4 (0.39 m^4)
Column reinforcement details	Longitudinal reinforcement (1.95%): 22×2#11 Transverse reinforcement: Spiral, #4 @ 6 in c/c
Column base hinge diameter	3.94 ft (1.2 m)
Concrete material properties of elastic superstructure (nominal) (Compressive strength, Elastic modulus)	f_c' = 5 ksi (34.5 MPa) E_c = 4, 030.5 ksi (27, 789.3 MPa)
Concrete material properties of columns (nominal) (Compressive strength, Elastic modulus)	f_c' = 5 ksi (34.5 MPa) E_c = 4, 030.5 ksi (27, 789.3 MPa)
Steel reinforcement material properties	Grade 60, ASTM A706
Bridge skew angle	0^o
Shear key type	Non-isolated (monolithic) shear keys
Number of bearing pads per abutment	7 elastomeric bearings
Bearing pad dimensions (Height, Area)	h_{bp} = 3.74 in (.095 m); A_{bp} = 558.0 in^2 (0.36 m^2)

3.2.4 Jack Tone Road Overhead (Bridge C)

The Jack Tone Road Overhead is located in Ripon, California (south of Sacramento), spanning over California State Route 99. The bridge was constructed in 2001 and consists of two lanes in each direction running north-south and is located adjacent to Bridge A. The bridge consists of three spans at 156.12 ft, 144 ft and 118.08 ft for a total length of 418.2 ft and is supported on three-column bents. The columns have a diameter of 5.51 ft and a longitudinal reinforcement ratio of 2.20%. Each column is supported on 24 HP 305x79 steel piles. The deck of the bridge is a seven-cell continuous reinforced-concrete box girder with a total width of 77 ft. The bridge abutment is at a skew of 36° and supported vertically on elastomeric bearings and restrained horizontally by monolithic shear keys. A detailed description of the Jack Tone Road Overhead can be found in Table 3.4

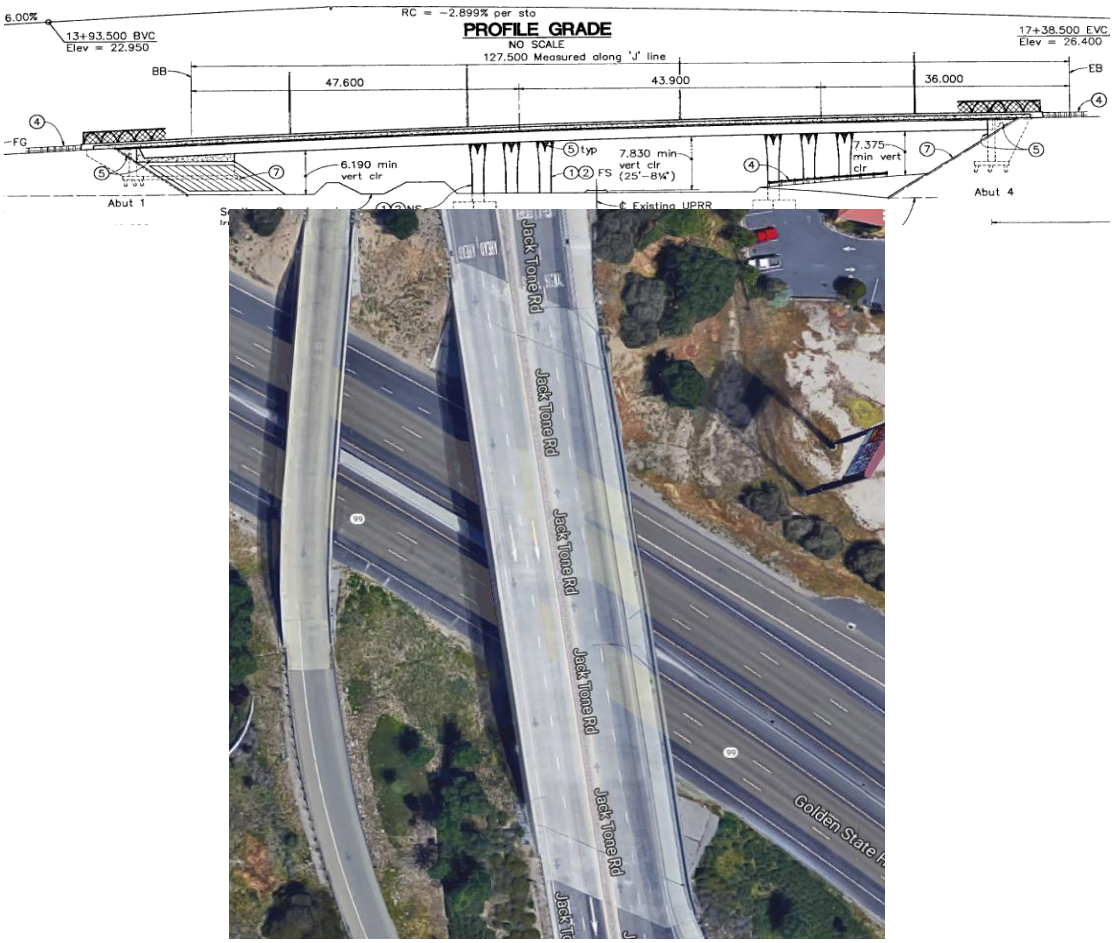

Figure 3.3 Profile and aerial overview of Bridge C (right)

Table 3.4 Geometrical and structural properties of Bridge C

Parameter/Feature	**Value/Description**
Number of spans	3
Length of spans	156.12 ft (47.59 m), 144 ft (43.89 m), and 118.08 ft (36.0 m)
Total length of bridge (L_{tot})	418.2 ft (127.47 m)
Total width of deck (w_d)	77 ft (23.47 m)
Depth of deck (d_d)	6.3 ft (1.92 m)
Deck cross-sectional properties (Area, Torsional constant, Second moments of area)	A = 131.65 ft^2 (12.0 m^2); J = 2563 ft^4 (22.12 m^4); I_y = 788.90 ft^4 (6.81 m^4); I_z = 59, 761 ft^4 (515.80 m^4)
Height of each bent	24.6 ft (7.5 m)
Number of columns in each bent	3
Column cross-sectional properties (Diameter, Area, Torsional constant, Second moments of area)	D_{col} = 5.51 ft (1.68 m); A_{col} = 23.84 ft^2 (2.21 m^2); J_{col} = 90.49 ft^4 (0.78 m^4); $I_{y,col}$ = 45.25 ft^4 (0.39 m^4); $I_{z,col}$ = 45.25 ft^4 (0.39 m^4)
Column reinforcement details	Longitudinal reinforcement (2.2%): 17×2#14 Transverse reinforcement: Spiral, #6 @ 3.34 in c/c
Column base hinge diameter	3.41 ft (1.04 m)
Concrete material properties of elastic superstructure (nominal) (Compressive strength, Elastic modulus)	f_c' = 5 ksi (34.5 MPa) E_c = 4, 030.5 ksi (27, 789.3 MPa)
Concrete material properties of columns (nominal) (Compressive strength, Elastic modulus)	f_c' = 5 ksi (34.5 MPa) E_c = 4, 030.5 ksi (27, 789.3 MPa)
Steel reinforcement material properties	Grade 60, ASTM A706
Bridge skew angle	36^o
Shear key type	Non-isolated (monolithic) shear keys
Number of bearing pads per abutment	9 elastomeric bearings
Bearing pad dimensions (Height, Area)	h_{bp} = 4.53 in (.115 m); A_{bp} = 327.98 in^2 (0.212 m^2)

3.2.5 Massachusetts Avenue Overcrossing (Bridge MAOC)

The Massachusetts Avenue Overcrossing is located in San Bernandino, California (east of Los Angeles), spanning over Interstate 215. The bridge was constructed in 2012 and consists of two lanes running in the northeast-southwest direction. The bridge consists of five spans at 49.21 ft, 94.49 ft, 91.86 ft, 99.74 and 78.08 ft for a total length of 413.39 ft and is supported on four-column bents. Each bent is supported on either 8 or 4 HP 360×132 steel piles. The columns have a diameter of 4.00 ft and a longitudinal reinforcement ratio of 1.90%. The deck of the bridge is a five-cell continuous reinforced-concrete box girder with a total width of 48.72 ft. The bridge abutment is at a skew of 8.1° and supported vertically on elastomeric bearings and restrained horizontally by isolated shear keys. A detailed description of Massachusetts Avenue Overcrossing can be found in Table 3.5.

Figure 3.4 Profile and aerial overview of Bridge MAOC

Table 3.5 Geometric and structural properties of Bridge MAOC

Parameter/Feature	**Value/Description**
Number of spans	5
Length of spans	49.21 ft (15.0 m), 94.49 ft (28.8 m), 91.86 ft (28.0 m), 99.74 ft (30.4 m), and 78.08 ft (23.8 m)
Total length of bridge (L_{tot})	413.39 ft (126.0 m)
Total width of deck (w_d)	48.72 ft (14.8 m)
Depth of deck (d_d)	4.49 ft (1.37 m)
Deck cross-sectional properties (Area, Torsional constant, Second moments of area)	A = 72.44 ft^2 (6.73 m^2); J = 724 ft^4 (6.25 m^4); I_y = 210.87 ft^4 (1.82 m^4); I_z = 12, 698 ft^4 (109.60 m^4)
Height of each bent	29.53 ft (9.0 m), 31.50 ft (9.6 m), 30.71 ft (9.4 m), and 27.43 ft (8.4 m)
Number of columns in each bent	4
Column cross-sectional properties (Diameter, Area, Torsional constant, Second moments of area)	D_{col} = 4.00 ft (1.22 m); A_{col} = 12.57 ft^2 (1.17 m^2); J_{col} = 22.34 ft^4 (0.19 m^4); $I_{y,col}$ = 11.17 ft^4 (0.096 m^4); $I_{z,col}$ = 11.17 ft^4 (0.096 m^4)
Column reinforcement details	Longitudinal reinforcement (1.9%): 22×#11 Transverse reinforcement: Circular, #7 @ 5.91 in c/c
Column base hinge diameter	2.13 ft (0.65 m)
Concrete material properties of elastic superstructure (nominal) (Compressive strength, Elastic modulus)	f_c' = 5 ksi (34.5 MPa) E_c = 4, 030.5 ksi (27, 789.3 MPa)
Concrete material properties of columns (nominal) (Compressive strength, Elastic modulus)	f_c' = 5 ksi (34.5 MPa) E_c = 4, 030.5 ksi (27, 789.3 MPa)
Steel reinforcement material properties	Grade 60, ASTM A706
Bridge skew angle	8.1^o
Shear key type	Isolated shear keys
Number of bearing pads per abutment	6 elastomeric bearings
Bearing pad dimensions (Height, Area)	h_{bp} = 3.54 in (.09 m); A_{bp} = 144.19 in^2 (0.093 m^2)

3.3 Preview to Chapter 4

The multidisciplinary nature of the PEER PBEE framework allows various researchers to work on various aspects of the framework independently and come up with novelties and improvements that particularly relate to the individual steps (or modules) of the framework. The implementation of a modular computational framework that unifies (integrates) such state-of-the-art advancements is outlined in the next chapter.

4 Updated Probabilistic Seismic Performance Assessment Framework for Ordinary Standard Bridges in California

4.1 Abstract

With the recent advent of performance-based earthquake engineering (PBEE) in seismic design practice of buildings serving as an impetus for this work, initial steps towards a fully probabilistic performance-based seismic design (PBSD) method for bridges, a less trodden area in terms of PBEE applications, are taken herein by assembling an updated probabilistic seismic performance assessment framework for Ordinary Standard Bridges (OSBs) in California. The framework stems from the comprehensive PBEE methodology developed under the auspices of the Pacific Earthquake Engineering Research (PEER) Center. With performance measures defined as the risk associated with the exceedance of a set of damage limit-states (*LS*s), improvements from the state-of-the-art literature on the PEER PBEE methodology are incorporated, including: (1) introduction of an improved intensity measure, i.e., average spectral acceleration over a period range, (2) conditional mean spectrum-based hazard-consistent and site-specific ground motion selection, (3) introduction of material strain-based engineering demand parameters, (4) use of practical *LS*s pertinent to seismic damage evaluation of bridges, and (5) development of strain-based normalized fragility functions for the considered *LS*s. The updated framework, assembled herein using a specific testbed California OSB as a case in point, is general within its scope and is applicable to the gamut of design situations representative of the population of OSBs in California. With the PEER PBEE framework implemented for OSBs in an updated and rigorous form, the groundwork for utilizing this framework in the context of PBSD of such bridges is laid.

4.2 Introduction

The performance-based earthquake engineering (PBEE) methodology (Porter 2003) developed under the auspices of the Pacific Earthquake Engineering Research (PEER) Center integrates site-specific seismic hazard analysis, structural demand analysis, damage analysis, and loss analysis, in a comprehensive and consistent probabilistic framework. The paradigm of PBEE provides technical support for moving towards more rational and risk-informed approaches to structural performance assessment and performance-based seismic design (PBSD). This methodology has recently been recommended as an innovative assessment tool to be used in bridge seismic design in a recent study under the National Cooperative Highway Research Program (NCHRP) (NCHRP 2013). The NCHRP study brings out the fact that the current bridge design practice considers safety and risk associated with the seismic performance of bridges as mere ramifications of the fulfillment of prescriptive measures and emphasizes the need for the explicit consideration of seismic risk, so that public and engineers participate in the decision-making process in tandem. The NCHRP investigation also highlights the areas where special attention is the need of the hour as per the current state of practice in the bridge engineering profession. With the current tools of seismic hazard analyses and nonlinear structural analyses, a practical implementation of the first two steps of the PBEE methodology, i.e., seismic hazard and demand analysis, is viable. However, the field of damage and loss prediction, in a rigorous probabilistic setting, has yet to see significant advancement. The complexity of predicting the highly uncertain phenomenon of damage, especially, has so far been underestimated by a subjective and rudimentary treatment primarily based on empirically derived prescriptive measures. It is only when fully equipped with all the tools required for a rigorous implementation of the PEER PBEE

framework, that this framework can be truly applied to the design (an inverse assessment problem) of new bridges.

The multidisciplinary nature of the PEER PBEE framework allows various researchers to work on various aspects of the framework independently and come up with novelties and improvements that particularly relate to the individual steps (or modules) of the framework, e.g., advanced ground motion selection approaches (Marasco and Cimellaro 2018; Shi and Stafford 2018), new probabilistic models for finite element (FE) model parameters (Xie et al. 2019), innovative interface variables (intensity measures (*IM*s), engineering demand parameters (*EDP*s), limit-states (*LS*s)) (Duck et al. 2018; Eads et al. 2015; Rezaei et al. 2020), novel methods for probabilistic loss assessment (Ghosh and Padgett 2011; Mander et al. 2012), etc. It is therefore essential to implement a modular computational framework that unifies (integrates) such state-of-the-art advancements and is flexible enough (scalable) to incorporate readily future improvements made in the field. Such an analytical tool will facilitate comprehensive seismic performance assessment of bridges, parametric performance assessment studies, evaluation of the efficacy of current (prescriptive) design methods, and calibration and validation of simplified, yet rigorous, PBSD methods. With an overarching goal of addressing, without any compromise in rigor, the somewhat hindered implementation of the PEER PBEE framework in bridge engineering practice, the PEER PBEE framework is comprehensively revisited and several improvements related to its various stages are incorporated and presented in this paper particularly as these relate to bridge structures. Currently incorporated improvements are chosen to strike a balance between rigor and practicability of the proposed framework. The modular nature of this framework, however, allows practicing engineers to replace its different components as they see fit.

The type of bridge structures considered in this study are Ordinary Standard Bridges (OSBs), which are conventional, multiple-span, skewed reinforced concrete (RC) bridges, and are the most common bridges in California designed in-house by the California Department of Transportation (Caltrans). Structural performance measures considered in this study are defined as the mean annual rates (MARs), or equivalently the mean return periods (MRPs), of exceedances of a selected set of practical *LS*s, specifically spalling of cover concrete , the onset of longitudinal bar buckling, the precursor stage to bar fracture after buckling, and the failure of monolithic shear keys. The proposed PBEE framework is applied to a testbed California OSB, chosen as a case in point, up to the third step of the PEER PBEE methodology, namely probabilistic damage analysis, and keeping probabilistic loss analysis outside the scope of this study.

4.3 Description of Testbed Bridge System and Site Conditions

The updated PEER PBEE framework was applied to a set of four testbed OSBs in California (Deb et al. 2018). For the sake of succinctness, only one of them is used as application example in this paper, namely the La Veta Avenue Overcrossing (Figure 4.1) located at the intersection of California State Route 55 and La Veta Avenue in the city of Tustin in California. This bridge, constructed in 2001, conforms to the definition of OSBs as described in Caltrans Seismic Design Criteria (SDC) v1.7 (Caltrans 2013). The bridge has no skew and spans over a total length of 91.4 m with two individual span lengths of 47.2 m and 44.2 m. The deck/superstructure of the testbed OSB is a six-cell continuous RC box girder with a total width of 23.0 m. The bridge deck is centrally supported on a single two-column bent with the bent cap-beam monolithically constructed with the deck. Each column in the bent is a circular RC column with a diameter of 1.70 m and a longitudinal reinforcement ratio of 1.95%. The columns of the

bent are supported by twenty (per column) 0.58 m diameter cast-in-drilled-hole piles. Each end of the bridge deck is supported by a seat-type abutment on pile foundation. Seven steel-reinforced elastomeric bearing pads evenly laid on top of an abutment stemwall are used to support each end of the bridge deck. The deck is restrained at each abutment in the transverse direction by two monolithic non-isolated shear keys, and in the longitudinal direction by a backwall.

The soil stratum primarily consists of layers of sandy gravel and cobbles overlaid on a layer of dense gravel. According to the average shear wave velocity (V_{S30}) in the top 30 m of 307 m/s, this site is categorized as stiff soil (class D) based on the NEHRP site classification (FEMA-368 2001).

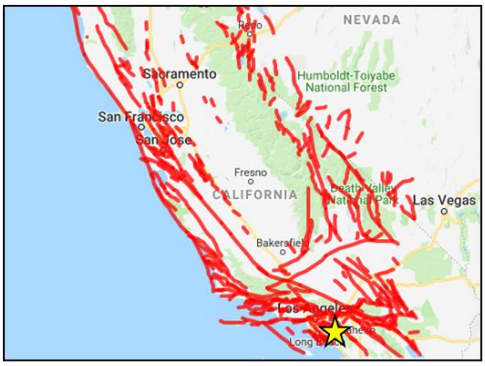

(a)

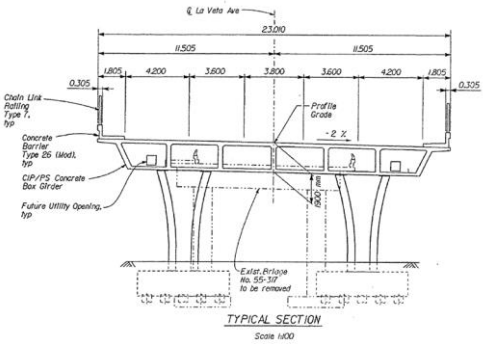

(c) (dimensions in mm)

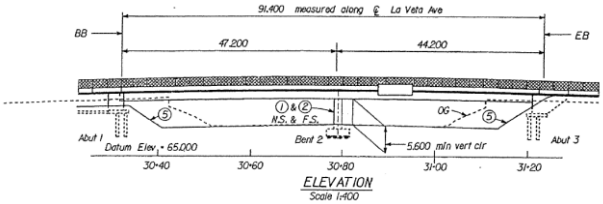

(b) (dimensions in mm)

(d)

Figure 4.1 La Veta Avenue Overcrossing: (a) Site on fault map, (b) elevation (from design drawing) and (c) column bent section (from design drawing), and (d) perspective view (from Google maps)

4.4 Computational Model of Bridge System

A three-dimensional nonlinear finite element (FE) model of the considered testbed OSB was constructed using OpenSees (McKenna 2011), the open-source software framework for creating finite element applications in structural and geotechnical engineering. OpenSees models of this bridge and corresponding Tcl input files inherited from previous Caltrans/PEER funded projects (Kaviani et al. 2014; Omrani et al. 2015) were revisited, parameterized, and improved (Deb et al. 2018) based on some experimental validation of the modeling of the bridge piers and literature review while adhering to the recommendations of the Caltrans SDC v1.7 (Caltrans 2013). A schematic representation of the computational model of the testbed OSB considered herein is shown in Figure 4.2. A brief account of the modeling techniques employed for the various components of OSBs is presented next.

4.4.1 Superstructure Modeling

Bridge decks are typically capacity-protected elements that are not meant to undergo inelastic behavior and dissipate energy under earthquake excitation. As such, the deck of the testbed OSB is modeled using elastic beam-column elements (10 per span). Section properties as per the original design drawings of the testbed OSB and expected material properties characteristic of normal-weight concrete are assigned to the deck elements.

4.4.2 Column-bent Modeling

Euler-Bernoulli fiber-section force-based beam-column elements with distributed plasticity and incorporating a numerically consistent regularized plastic hinge integration scheme (Scott and Hamutçuoğlu 2008) are used to model the clear length of RC columns of the considered

testbed OSB. These elements allow detailed fiber-section definitions for RC column sections with cover (unconfined) concrete, core (confined) concrete, and steel reinforcing bars modeled as individual fibers (Figure 4.3(a)). The Kent-Scott-Park (Kent and Park 1971; Scott et al. 1982) concrete material stress-strain law (*Concrete01* in OpenSees) (Figure 4.3(b)) with degraded linear unloading/reloading stiffness and no tensile strength is used to model the hysteretic stress-strain response of the unconfined and confined (Mander et al. 1988) concrete fibers of a column section. The uniaxial stress-strain law first proposed by Menegotto and Pinto (Menegotto and Pinto 1973) and extended by Filippou and co-workers (Filippou et al. 1983) (*SteelMPF* in OpenSees) (Figure 4.3(c)) is assigned to the reinforcing steel fibers of a column section. The column base hinge, which is a short reduced-diameter section between the base of a column and the top of the pile-cap is explicitly modeled using a single Euler-Bernoulli fiber-section displacement-based beam-column element. Fixed connections emulating rigid foundations are used to model the boundary conditions at the base of the columns.

In California, columns of OSBs are generally built monolithically with the deck. Hence, each column in the bent is attached to the deck using a rigid beam-column element to geometrically capture the vertical and horizontal offsets from the centroid of the deck cross-section to the top of each column (see Figure 4.2).

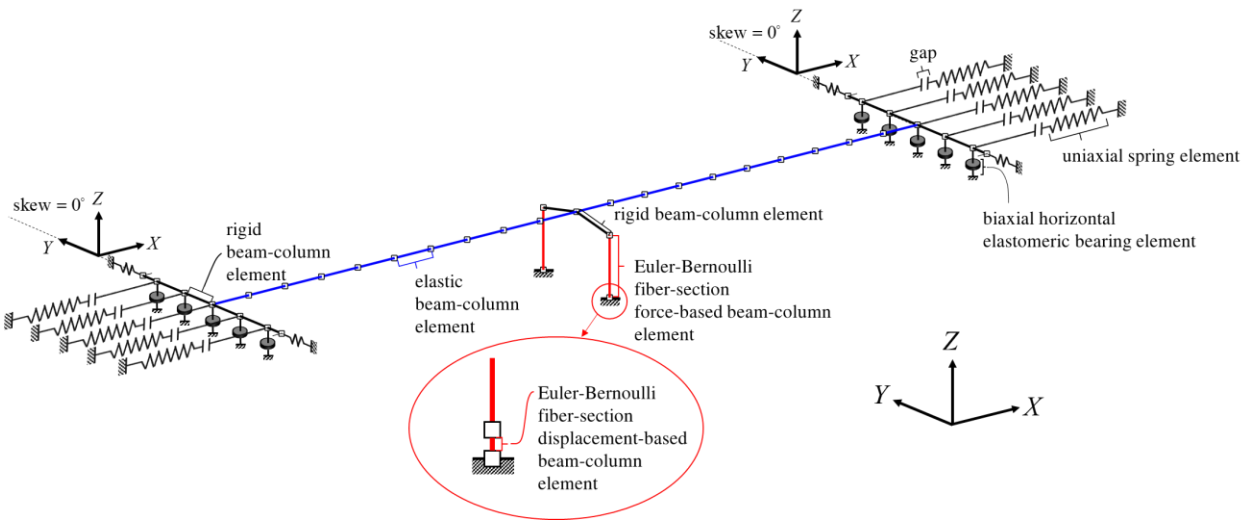

Figure 4.2 Schematic representation of the FE model of the testbed OSB considered herein

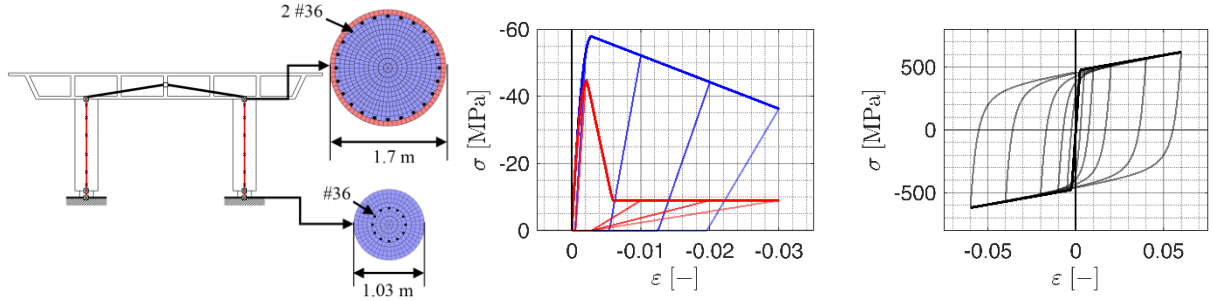

(a) (b) (c)

Figure 4.3 Bridge bent and column modeling details: (a) Fiber-section definition; Material hysteretic stress-strain laws for (b) unconfined (red) and confined (blue) concrete fibers, and (c) reinforcing steel (black) fibers

4.4.3 Abutment Modeling

Despite being constructed (as per design drawings) monolithically with the stemwall, the abutment backwall in the longitudinal direction is assumed, consistent with Caltrans' design philosophy (Caltrans 2013), to transmit horizontal forces generated by small to moderate intensity earthquakes and service loads and easily break-off (i.e., the shear force required to induce a shear failure along the perimeter of the connection between the backwall and the stem wall is assumed to be small as compared to the force required to displace/mobilize the backfill soil wedge) during

a design-basis earthquake in order to protect the stem wall and the foundation of the abutment substructure from inelastic action. Soil-structure interaction between the bridge deck and the embankment backfill is modeled using five translational compressive gap springs placed along the width of the abutment at each end of the bridge. A nonlinear hysteretic force-deformation relationship with a hyperbolic backbone curve (Caltrans 2019) (*HyperbolicGapMaterial* in OpenSees) (Figure 4.4(a)) is used to model the passive resistance of each backfill spring activated upon closure of the expansion joint gap. The effect of the abutment skew angle (in case there is a non-zero skew angle) on the passive resistance of the abutment backfill is accounted for by varying the initial stiffness and the ultimate strength of the backfill springs over the skewed length of the backwall (Shamsabadi et al. 2020). This variation is hypothesized to phenomenologically account for the increase in the available volume of engineered backfill soil, from the acute to the obtuse corner of the skewed abutment, that can be mobilized per unit length of the skewed backwall.

The longitudinal and transverse resistance of the bearing pads at the abutments are modeled using specialized zero-length 2D plasticity-based elements (*elastomericBearingPlasticity* in OpenSees) to represent the coupled bidirectional nonlinear (assumed bilinear) shear force-deformation response (Figure 4.4(b)) of such pads. Each bearing pad is supported vertically on the essentially rigid stemwall represented by a fixed connection at the base of the bearing element.

The transverse resistance of an exterior shear key (at the abutment) is modeled using a translational compressive spring. A semi-empirical mechanics-based force-deformation hysteretic macro-model (Megally et al. 2002) (Figure 4.4(c)) is used to model (using *Concrete01* material in OpenSees) the response of the (non-isolated) shear keys of the considered testbed OSB.

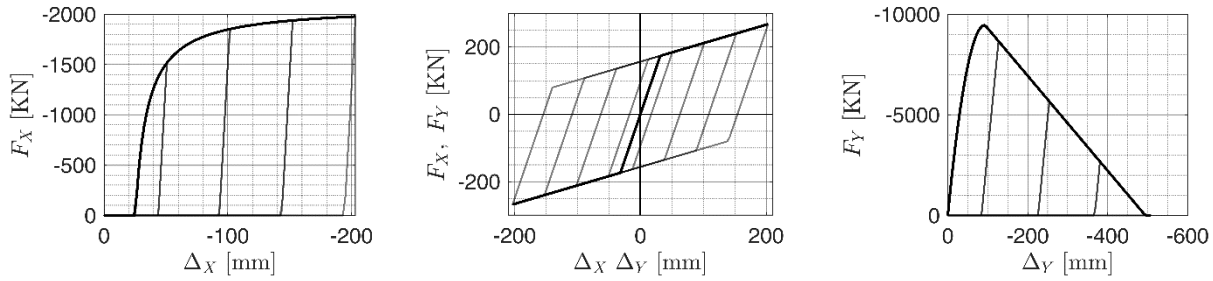

(a) *(b)* *(c)*

Figure 4.4 Bridge abutment modeling details; nonlinear hysteretic force-deformation relationship assigned to each: (a) backfill spring (since the considered OSB is non-skewed), (b) bearing pad element, and (c) exterior shear key spring

4.5 PEER PBEE Assessment Framework Revisited and Updated

This section aims to present the PEER PBEE framework, with special emphasis on the improvements proposed herein, which integrates the steps of site-specific seismic hazard analysis, structural demand analysis, damage analysis, and loss analysis using the Total Probability Theorem (TPT) of probability theory to arrive at an estimate of a performance measure, e.g., the MAR or MRP of exceedance of an *LS*, and/or the MAR or MRP at which a decision variable (e.g., down time, monetary loss, deaths) exceeds a specific threshold. Performance measures considered in this study are the MAR or equivalently the MRP of LS exceedances for a selected set of *LS*s. The task of probabilistically predicting the future seismic performance of a bridge is therefore broken down into the following three steps: Probabilistic Seismic Hazard Analysis (PSHA) in terms of a ground motion *IM*, Probabilistic Seismic Demand Hazard Analysis (PSDemHA) in terms of *EDP*s, and Probabilistic Seismic Damage Hazard Analysis (PSDamHA) for various *LS*s of interest.

The proposed PBEE assessment framework is computationally implemented as a Python library, named PyPBEE (PBEE for Python). PyPBEE admits modular class definitions of analysis steps (i.e., PSHA, ground motion selection (GMS), nonlinear time-history analysis (NLTHA),

PSDemHA, and PSDamHA) and the interface variables (i.e., *IM*s, *EDP*s, and *LS*s). PyPBEE is designed to readily accommodate alternative and more refined/effective definitions of its components reflecting future improvements made in the various steps of the multidisciplinary PBEE methodology. Figure 4.5 shows a schematic Unified Modeling Language (UML) diagram describing the relationships between objects of the classes involved in PyPBEE.

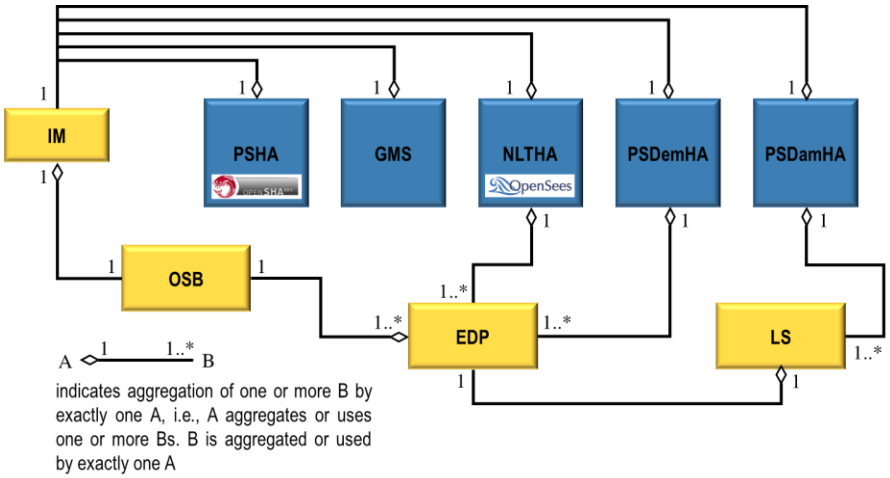

Figure 4.5 Schematic UML diagram of PyPBEE

4.5.1 Probabilistic Seismic Hazard Analysis (PSHA)

The essence of PSHA is to identify and aggregate the contributions of all possible seismic events (characterized by pairs of earthquake magnitude (*M*) and source-to-site distance (*R*)) that could potentially affect the considered structure to arrive at an estimate of the MARs at which specific values of a ground motion *IM* are exceeded. For a given site, PSHA integrates the contributions of all possible seismic sources to the MAR of *IM* exceedance as

$$\nu_{IM}(x) = \sum_{i=1}^{N_{flt}} \nu_i \int_{R_i} \int_{M_i} P\left[IM > x \mid M_i = m, R_i = r\right] \cdot f_{M_i}(m) \cdot f_{R_i}(r) \cdot dm \cdot dr \qquad (4.1)$$

where N_{flt} = number of causative faults or seismic sources; ν_i = MAR of occurrence of earthquakes on fault (or seismic source) i. The functions $f_{M_i}(m)$ and $f_{R_i}(r)$ denote the probability density functions (PDFs) of the magnitude (M_i) and source-to-site distance (R_i), respectively, given the occurrence of an earthquake on fault i. The conditional probability . $P\left[IM > x \mid M_i = m, R_i = r\right]$. in Eq. (4.1), referred to as attenuation relationship or ground motion prediction equation (GMPE) (Boore and Atkinson 2008) which is a predictive relationship of *IM* given seismological variables *M* and *R*, is typically developed by applying statistical regression analyses to recorded earthquake ground motion data.

4.5.1.1 Improved IM: Average Spectral Acceleration Over a Period Range

Depending on the results of PSHA, earthquake ground motion records producing desired levels of the chosen *IM* are selected for response assessment of structures subjected to seismic loading. Thus, an *IM* connects seismological characteristics of earthquakes (magnitude, source-to-site distance, regional seismic wave attenuation, local site-effects, etc.) to structural response. A proper choice of *IM* is therefore crucial to have a true picture of structural performance against earthquakes. To this end, an improved *IM* (in terms of "efficiency" and "sufficiency" in the prediction of displacement-based nonlinear structural response[6]), namely the average spectral acceleration over a specified period range (Baker and Cornell 2006) $(S_{a,\text{avg}})$, is used to particularly account for the following factors deemed important for OSBs and typically not captured by the traditionally used *IM*, i.e., elastic 5% damped spectral acceleration $(S_a(T_p))$ at the expected predominant period of the structure: (i) uncertainty in predicting the period of the predominant mode of vibration for RC structures such as OSBs; (ii) change in natural periods of RC structures

from pristine conditions to cracked states under service loads; (iii) lengthening of the predominant structural periods due to accumulation of damage during an earthquake which leads to higher correlation of structural response with spectral accelerations at longer periods; and (iv) difference in periods of the fundamental modes of vibration in the two orthogonal directions (i.e., longitudinal and transverse) of the bridge.

$S_{a,\,\text{avg}}$ is defined as the geometric mean of spectral accelerations at different periods over a period range, i.e.,

$$S_{a,\,\text{avg}}\left(T_1,\ldots,T_n\right)=\left[\prod_{p=1}^{n}S_a\left(T_p\right)\right]^{1/n} \tag{4.2}$$

where $[T_1, T_n]$ is the averaging period range. The range of periods used in the definition of $S_{a,\,\text{avg}}$ for the considered OSB spans from the first transverse mode of vibration, i.e., $T_{1,\,\text{trans}}$, to $2.5\,T_{1,\,\text{trans}}$ because the response of the OSB in the transverse direction is believed to be more critical than in the longitudinal direction in which the bridge response is eventually going to be stabilized by the backfill. Ten periods uniformly spaced in log scale between $T_{1,\,\text{trans}}$ and $2.5\,T_{1,\,\text{trans}}$ are used in the computation of $S_{a,\,\text{avg}}$. The selected period range also includes the first mode period of the OSB in the longitudinal direction.

The multivariate normal distribution is found to appropriately model the variability of a random vector of the natural logarithm of correlated spectral accelerations at single periods given an earthquake scenario (i.e., an *M*-*R* pair or *M*-*R* bin) (Jayaram and Baker 2008). Owing to the property of closure of the multivariate normal distribution under a linear transformation, normality of the random variable $\ln S_{a,\,\text{avg}}$, given an earthquake scenario ($S = s$), is ensued and therefore

$\ln S_{a,\,\mathrm{avg}}$, given *S*, is completely characterized by two statistical parameters, namely its mean (μ) and standard deviation (σ) defined as

$$\mu_{\ln S_{a,\,\mathrm{avg}}\,|\,S=s} = \left(\frac{1}{n}\right)\cdot\sum_{p=1}^{n}\mu_{\ln S_a(T_p)\,|\,S=s} \tag{4.3}$$

$$\sigma_{\ln S_{a,\,\mathrm{avg}}\,|\,S=s} = \left(\frac{1}{n}\right)\cdot\sqrt{\sum_{p=1}^{n}\sum_{q=1}^{n}\rho_{\ln S_a(T_p)\ln S_a(T_q)}\cdot\sigma_{\ln S_a(T_p)\,|\,S=s}\cdot\sigma_{\ln S_a(T_q)\,|\,S=s}} \tag{4.4}$$

The conditional mean and standard deviation $\mu_{\ln S_a(T_p)\,|\,S=s}$ and $\sigma_{\ln S_a(T_p)\,|\,S=s}$ in Eqs. (4.3) and (4.4), respectively, can be obtained from existing GMPEs (Boore and Atkinson 2008) for spectral accelerations at single periods. Predictive models (Baker and Jayaram 2008) of the correlation structure between spectral acceleration values at multiple periods can be used to obtain the correlation coefficient $\rho_{\ln S_a(T_p)\ln S_a(T_q)}$, which was found to be independent of the earthquake scenario (Baker and Jayaram 2008). Eqs. (4.3) and (4.4) define the GMPE for $S_{a,\,\mathrm{avg}}$, given a scenario ($S = s$), which can then be used as building blocks in the computation of the seismic hazard at the site. Details of the PSHA in terms of $S_{a,\,\mathrm{avg}}$, an improved measure of seismic intensity, are provided in the next section.

4.5.1.2 Seismic Hazard Analysis

Seismic hazard analysis involves a numerical evaluation of the seismic hazard integral defined in Eq. (4.1). Standard open-source software tools (e.g., OpenSHA (Field et al. 2003)) readily provide results of PSHA given a site and a choice of *IM*. However, owing to the novelty of the chosen *IM*, standard PSHA tools do not include seismic hazard assessments in terms of this *IM*. Hence, a convenient, yet rigorous, workaround is adopted based on the results of PSHA for spectral accelerations at single periods such that the seismic hazard in terms of $S_{a,\,\mathrm{avg}}$ can be

reasonably approximated while avoiding the esoteric step of seismic source probabilistic characterization and related calculations. This firstly involves writing the continuous seismic hazard integral in Eq. (4.1) in a discrete and simplified form as

$$\begin{aligned}\nu_{S_{a,\text{avg}}}(x) &= \sum_{i=1}^{N_{\text{flt}}} \nu_i \underbrace{\sum_{j=1}^{N_M}\sum_{k=1}^{N_R}}_{\sum_{q=1}^{N_S(=N_M\times N_R)}} P\left[S_{a,\text{avg}} > x \,|\, \underbrace{M_i = m_j^i, R_i = r_k^i}_{S_i = s_q^i} \right] \cdot \underbrace{P\left[M_i = m_j^i\right] \cdot P\left[R_i = r_k^i\right]}_{P\left[S_i = s_q^i\right]} \\ &= \sum_{q=1}^{N_S} \underbrace{\sum_{i=1}^{N_{\text{flt}}} \nu_i \cdot P\left[S_i = s_q^i\right]}_{\nu_{s_q}} \cdot P\left[S_{a,\text{avg}} > x \,|\, S = s_q\right] \\ &= \sum_{q=1}^{N_S} \nu_{s_q} \cdot \left(1 - \Phi\left(\frac{\ln x - \mu_{\ln S_{a,\text{avg}} \,|\, S=s_q}}{\sigma_{\ln S_{a,\text{avg}} \,|\, S=s_q}}\right)\right)\end{aligned} \tag{4.5}$$

where $P\left[m_j^i\right]$ and $P\left[r_k^i\right]$ are the probabilities of, now assumed, discrete random variables M_i and R_i, related to seismic source i, taking the values m_j^i and r_k^i, respectively, out of a number N_M and N_R of possible and not equally likely discrete values, respectively. The above simplification holds only if an attenuation relationship independent of the characteristics of the seismic sources/faults (Boore and Atkinson 2008) is used such that the seismic source (*i*) dependence of the term $P\left[S_{a,\text{avg}} > x \,|\, S_i = s_q^i\right]$ can be dropped. Note that $\Phi(\cdots)$ denotes the standard normal cumulative distribution function. Eq. (4.5) provides a more tractable form of the seismic hazard integral in terms of $S_{a,\text{avg}}$. The evaluation of ν_{s_q}, defined as the MAR of occurrence of scenario $(S = s_q)$ from any seismic source affecting the considered site, is discussed next.

The seismic hazard curves (SHCs), for the considered testbed OSB, in terms of $S_a(T)$ for each of the ten discrete periods used in the averaging period range are shown in Figure 4.6(a). These SHCs were obtained from OpenSHA (Field et al. 2003) using the GMPE by Boore and

Atkinson (2008). An important observation from Figure 4.6(a), that facilitates the determination of ν_{s_q} to be used in Eq. (4.5), is that all SHCs for spectral accelerations at single periods, irrespective of the period, converge to a single value (indicated by the red marker) of MAR of exceedance at very small spectral acceleration values (e.g., at 10^{-4} g). Very small values of $S_a(T)$, e.g., 10^{-4} g, are almost certainly exceeded, irrespective of the period *T*, given any earthquake scenario (i.e., $P[S_a(T) > 10^{-4} g \mid S = s_q] \approx 1.0$). Hence, the MAR of exceeding this value of $S_a(T)$ is equal to the sum of the rates of all possible scenarios contributing to the seismic hazard at the site, i.e., $\sum_{q=1}^{N_s} \nu_{s_q}$. To obtain $\nu_{s_q}(q = 1, ..., N_S)$ for a specific site, the *M*-*R* deaggregation results, a routinely available output from PSHA software tools providing the relative contribution to a specific value of seismic hazard, from each earthquake scenario resulting from any seismic source affecting the considered site, come to aid. From the value of the seismic hazard corresponding to $S_a(T) = 10^{-4} g$ for any arbitrary period *T*, $\nu_{s_q}(q = 1, ..., N_S)$ (shown in Figure 4.6(b)) is calculated as

$$\nu_{s_q} = \frac{\left(\%\text{ contribution of } S = s_q\right) \times \nu_{S_a(T)}\left(x = 10^{-4} g\right)}{\underbrace{P\left[S_a\left(T\right) > 10^{-4} g \mid S = s_q\right]}_{\approx 1.0} \times 100}, \quad (q = 1, ..., N_S) \tag{4.6}$$

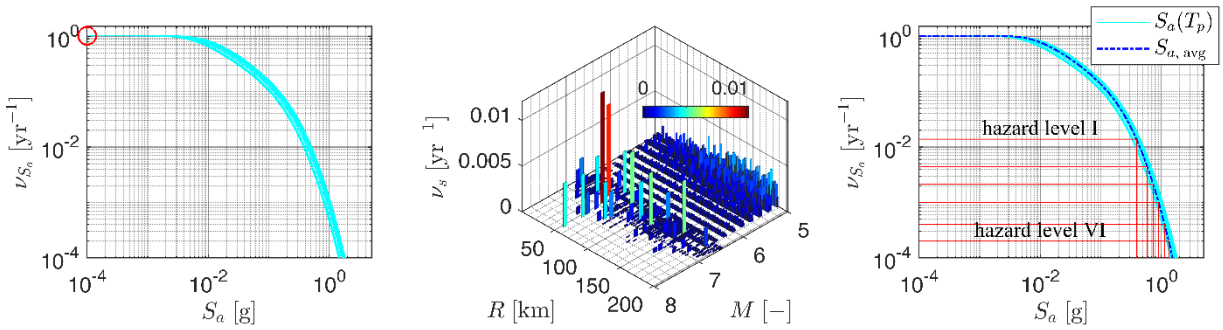

(a) (b) (c)

Figure 4.6 (a) SHCs in terms of $S_a(T)$ for each of the ten discrete periods used in the averaging period range, (b) MARs of occurrences of all *M*-*R* scenarios, and (c) SHC in terms of $S_{a,\,\mathrm{avg}}$

With $\nu_{s_q}(q=1,...,N_S)$ given by Eq. (4.6), and the GMPE for $S_{a,\,\mathrm{avg}}$ given by Eqs. (4.3) and (4.4) in hand, obtaining the seismic hazard curve in terms of $S_{a,\,\mathrm{avg}}$ for the considered OSB merely reduces to a straightforward evaluation of Eq. (4.5). Figure 4.6(c) shows the seismic hazard curve in terms of $S_{a,\,\mathrm{avg}}$, and how it compares to the SHC in terms of $S_a(T)$ for each of the ten periods in the averaging period range. The seismic hazard curve in terms of $S_{a,\,\mathrm{avg}}$ is used to define seismic hazard levels corresponding to different MARs or MRPs of *IM* exceedance (shown in Figure 4.6(c)), which are of interest to practicing engineers. Six seismic hazard levels corresponding to MRPs of 72 years (or 50 percent probability of exceedance in 50 years), 224 years (or 20 percent probability of exceedance in 50 years), 475 years (or 10 percent probability of exceedance in 50 years), 975 years (or 5 percent probability of exceedance in 50 years), 2475 years (or 2 percent probability of exceedance in 50 years), and 4975 years (or 1 percent probability of exceedance in 50 years) are chosen for the purpose of this study. These hazard levels are numbered I through VI, respectively. Ensembles of earthquake ground motion records matching these hazard levels of seismic intensity are selected next to perform ensemble nonlinear time history analyses to characterize the seismic demand on the considered OSB probabilistically.

4.5.1.3 Risk-consistent Site-specific Ground Motion Record Selection

Ground motion record selection serves as the link between PSHA and subsequent probabilistic seismic response assessment, thereby imposing a need for hazard- or risk-consistency of earthquake ground motion records to be used for ensemble nonlinear response history analyses of the considered bridge. The "exact" conditional mean spectrum (CMS) (Baker and Cornell 2006; Lin et al. 2013a), representing the expected spectral shape given a specific value of the considered *IM* and incorporating all causative scenarios (Lin et al. 2013b) (see Appendix), is used as the target spectrum for ground motion record selection in this study.

A novel ground motion selection algorithm (Jayaram et al. 2011; Kohrangi et al. 2017) is implemented for the selection of site-specific risk-consistent ensembles of ground motion records representative of the six seismic hazard levels considered. Given a seismic hazard level and the corresponding value of *IM*, the conditional multivariate probability structure of correlated spectral accelerations at different periods is first determined. The algorithm then employs a greedy optimization-based technique (Jayaram et al. 2011) to pick scaled (within bounds) earthquake records from a strong motion database (Chiou et al. 2008) that individually match Monte-Carlo simulated realizations of the target conditional spectrum and as an ensemble follow the complete probability structure of the target conditional spectrum defined for that hazard level. With the CMS chosen as the target mean spectrum over the uniform hazard spectrum (UHS), which is a more commonly used, excessively conservative, spectral envelope-based target spectrum, the natural spectral shapes of the selected ensemble of earthquake ground motion records are preserved. Ensembles of 100 bi-axial horizontal ground motion records per hazard level (Figure 4.7) are selected for the seismic response assessment of the testbed OSB considered herein.

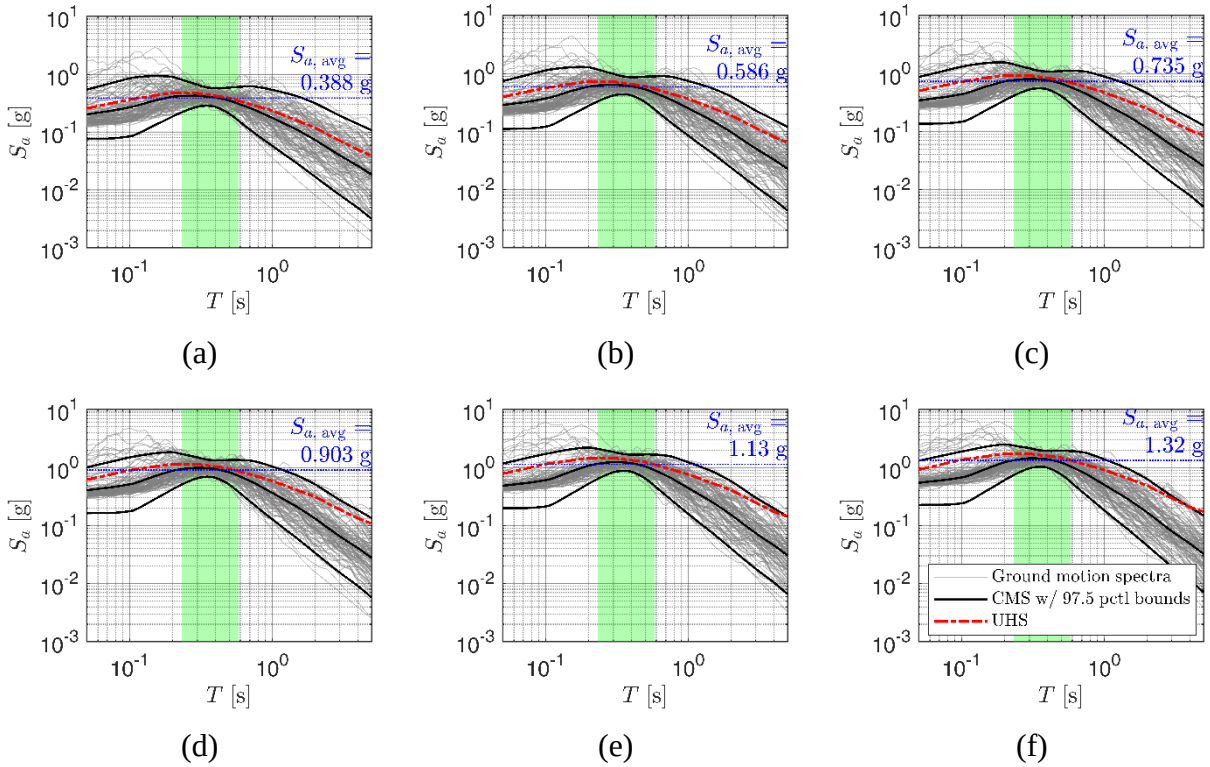

(a) (b) (c)

(d) (e) (f)

Figure 4.7 Site-specific risk-consistent ground motion ensembles at (a) hazard level I, (b) hazard level II, (c) hazard level III, (d) hazard level IV, (e) hazard level V, (f) hazard level VI

4.5.2 Probabilistic Seismic Demand Hazard Analysis (PSDemHA)

The objective of PSDemHA is to characterize probabilistically the seismic demand imposed on the considered OSB, in terms of the MARs at which specific values (say δ) of meaningful bridge seismic response parameters, called engineering demand parameters (*EDP*s), are exceeded at the bridge site. This is achieved via a convolution of the conditional probability of *EDP* exceedance, given *IM*, with the site-specific SHC as

$$\nu_{EDP}(\delta) = \int_{IM} P\left[EDP > \delta \mid IM = x\right] \cdot \left| d\nu_{IM}(x) \right| \tag{4.7}$$

where $\left| d\nu_{IM}(x) \right|$ is the absolute differential of the SHC, which corresponds to the MAR of occurrence, and not exceedance, of a specific value *x* of *IM*.

A set of *EDP*s, each associated with a discrete damage state in the bridge structure, is identified for PSDemHA. The set of considered *LS*s, pertinent to the seismic evaluation of RC OSBs and meaningful to practicing bridge engineers, and their associated *EDP*s are discussed in the next section.

4.5.2.1 Damage *LS*s and Associated Material Strain-based *EDP*s

Flexural plastic hinge regions in RC columns of an OSB are meant to act as structural fuses in a seismic event and thereby dissipate energy through controlled inelastic material behavior. Three damage *LS*s related to the desirable (targeted) damage/failure mode/mechanism concerning RC bridge columns (i.e., flexural hinging of columns) are considered in this study. These *LS*s are: (1) concrete cover spalling, (2) onset of longitudinal bar buckling, and (3) a precursor stage to longitudinal bar fracture after bar buckling occurs. The first *LS* represents superficial damage to a bridge column and requires cosmetic repair work primarily to prevent corrosion of the bars. The other two *LS*s represent ultimate *LS*s, exceedances of which lead to significant compromise of structural integrity and imminent structural collapse. A fourth *LS* corresponding to an abutment exterior shear key reaching its capacity is also considered. Note that although the exceedances of *LS*s 1 through 3 are of increasing severity and therefore increasing mean return period (i.e., *LS* 1 cannot occur after *LS*s 2 and/or 3, and *LS* 2 cannot occur after *LS* 3), the mean return period of exceedance of *LS* 4 is unrelated to those of the exceedances of the first three *LS*s.

Displacement-based *EDP*s have been found to correlate better to structural damage as compared to force-based *EDP*s (Priestley et al. 2007). Traditionally, measures of deformation such as displacements, drift ratios, curvatures, etc. have been used as *EDP*s. However, for RC flexural members, such as columns, deformations can be directly and most reliably related to structural

damage through material strains (Priestley et al. 2007). Table 4.1 lists the strain-based *EDP*s associated with the selected set of *LS*s. Definition of these strain-based *EDP*s are based on deterministic predictive capacity models (discussed later in Section 4.5.3.1) for the chosen set of *LS*s. A conventional displacement-based *EDP* is defined for the fourth *LS* and is also listed in Table 4.1. Figure 4.8 schematically describes the chosen *EDP*s for the considered OSB.

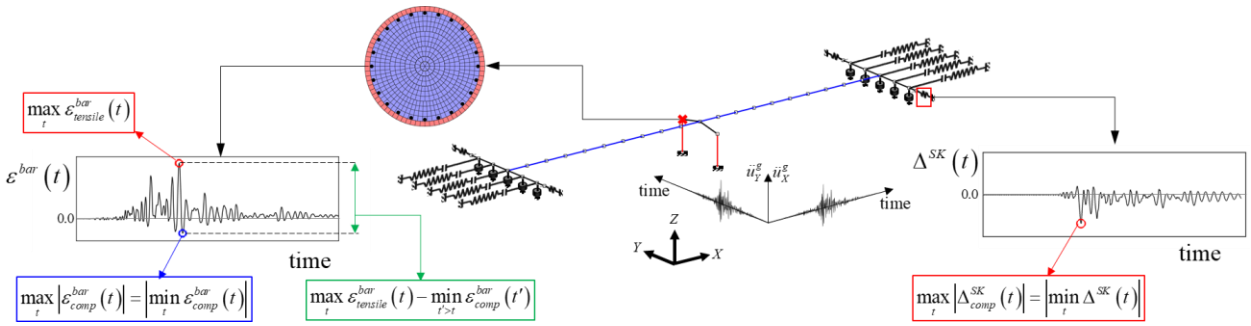

Figure 4.8 Schematic representation of *EDP*s considered herein

Table 4.1 Definition of *LS*s and associated *EDP*s

LS #	***Associated Engineering Demand Parameter (EDP)***	
1	Maximum absolute compressive strain of any longitudinal bar in any column.	$\max_{col}\left(\max_{bar}\left(\max_{t}\left\|\varepsilon^{bar}_{comp}(t)\right\|\right)\right)$
2	Maximum tensile strain of any longitudinal bar in any column.	$\max_{col}\left(\max_{bar}\left(\max_{t}\varepsilon^{bar}_{tensile}(t)\right)\right)$
3	Maximum strain range/excursion (i.e., difference of maximum tensile and minimum compressive strain, the latter following the former) of any longitudinal bar in any column	$\max_{col}\left(\max_{bar}\left(\max_{t}\varepsilon^{bar}_{tensile}(t) - \min_{t'>t}\varepsilon^{bar}_{comp}(t')\right)\right)$
4	Maximum relative shear key-abutment horizontal displacement of any shear key	$\max_{SK}\left(\max_{t}\left\|\Delta^{SK}_{comp}(t)\right\|\right)$

4.5.2.2 Demand Hazard Analysis

For the $.k^{th}.$ *LS* and its associated engineering demand parameter, EDP_k, the conditional probability of EDP_k exceeding any threshold level *x* given a specified level of *IM* is evaluated by first subjecting the nonlinear FE model of the considered OSB to ensembles of site-specific risk-consistent ground motion records selected according to the six seismic hazard levels defined earlier. All non-collapse (or non-physical failure) related numerical convergence issues encountered in this step are resolved in an automated fashion via adaptive switching between iterative solution algorithms (e.g., Newton, Newton line-search, modified-Newton, BFGS, Newton-Krylov), types of convergence tests, and the tolerance criteria used to check for convergence. At each seismic hazard level, response histories of relevant strain/deformation measures resulting from nonlinear time-history analyses of the considered OSB are recorded, and the values of the *EDP*s associated with the considered set of *LS*s are determined. A statistical demand model is constructed by fitting a probability distribution to the simulated EDP_k data, conditional on each seismic hazard level. The two-parameter ($\lambda_{EDP_k \mid IM} = \mu_{\ln EDP_k \mid IM}$, $\zeta_{EDP_k \mid IM} = \sigma_{\ln EDP_k \mid IM}$) lognormal distribution is found to appropriately model the scatter in the values of EDP_k conditional on *IM*.

PSDemHA, requiring the convolution of the conditional probability of EDP_k exceedance with the site-specific SHC, calls for a continuous regression or interpolation/extrapolation against *IM* of the parameters of the probability distribution functions fitted to EDP_k at discrete *IM* levels. Functional fits traditionally used for this purpose have often been of a power-law form (Cornell et al. 2002) for the conditional lognormal median, $\eta_{EDP_k \mid IM}$ $\left(\text{i.e., } e^{\mu_{\ln EDP_k \mid IM}}\right)$, and a constant form

(Cornell et al. 2002) for the conditional lognormal dispersion parameter, $\zeta_{EDP_k|IM}$. Improved versions of these fits, namely (i) a power-law form for piecewise interpolation of $\eta_{EDP_k|IM}$ versus *IM* with the interpolation functions for the first and last piecewise segments simply extended for extrapolation and (ii) a piecewise linear variation of $\zeta_{EDP_k|IM}$ for interpolation between *IM* levels in logarithmic space with the value of dispersion extrapolated as a constant outside the range of *IM* levels considered, are used in this study after Bradley (Bradley 2013a). These interpolation models are given by

$$\begin{aligned} &\ln \eta_{EDP_k|IM}(x) = \ln a_i + b_i \ln x \qquad x_i \le x \le x_{i+1} \\ &b_i = \frac{\ln \eta_{i+i} - \ln \eta_i}{\ln x_{i+i} - \ln x_i},\ a_i = \exp\left(\ln \eta_i - b_i \ln x_i\right) \end{aligned} \tag{4.8}$$

$$\begin{aligned} &\zeta_{EDP_k|IM}(x) = c_i + d_i \ln x, \qquad x_i \le x \le x_{i+1} \\ &d_i = \frac{\zeta_{i+1} - \zeta_i}{\ln x_{i+1} - \ln x_i},\ c_i = \zeta_i - d_i \ln x_i \end{aligned} \tag{4.9}$$

in which η_i and ζ_i are shorthand notations for $\eta_{EDP_k|IM}(x_i)$ and $\zeta_{EDP_k|IM}(x_i)$, respectively, where x_i represent the *IM* levels at which ensemble nonlinear response history analyses have been performed and the lognormal median and dispersion of EDP_k given *IM* computed. As illustration, Figure 4.9 shows the results of the ensemble nonlinear response history analyses of the considered OSB and the probabilistic characterization of the seismic demand in terms of EDP_2 conditional on *IM*. The demand hazard curves (DHCs) in terms of all considered *EDP*s and obtained upon numerical convolution of the conditional probability of *EDP* exceedance with the site-specific SHC for the testbed OSB are displayed in Figure 4.10.

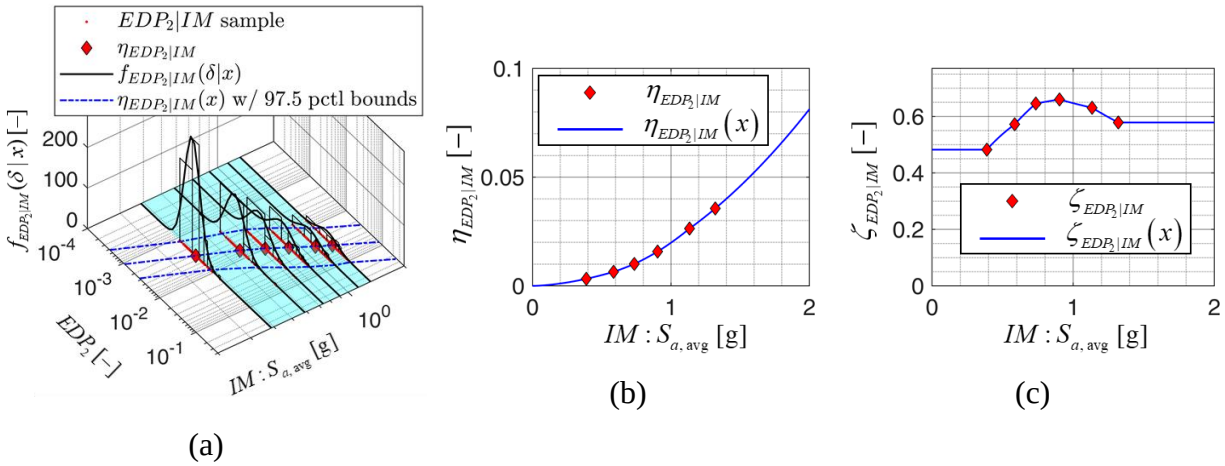

(a) (b) (c)

Figure 4.9 (a) Conditional probability distributions of EDP_2 given *IM*, Interpolation/extrapolation model for (b) $\eta_{EDP_2|IM}$ versus *IM*, and (c) $\zeta_{EDP_2|IM}$ versus *IM*.

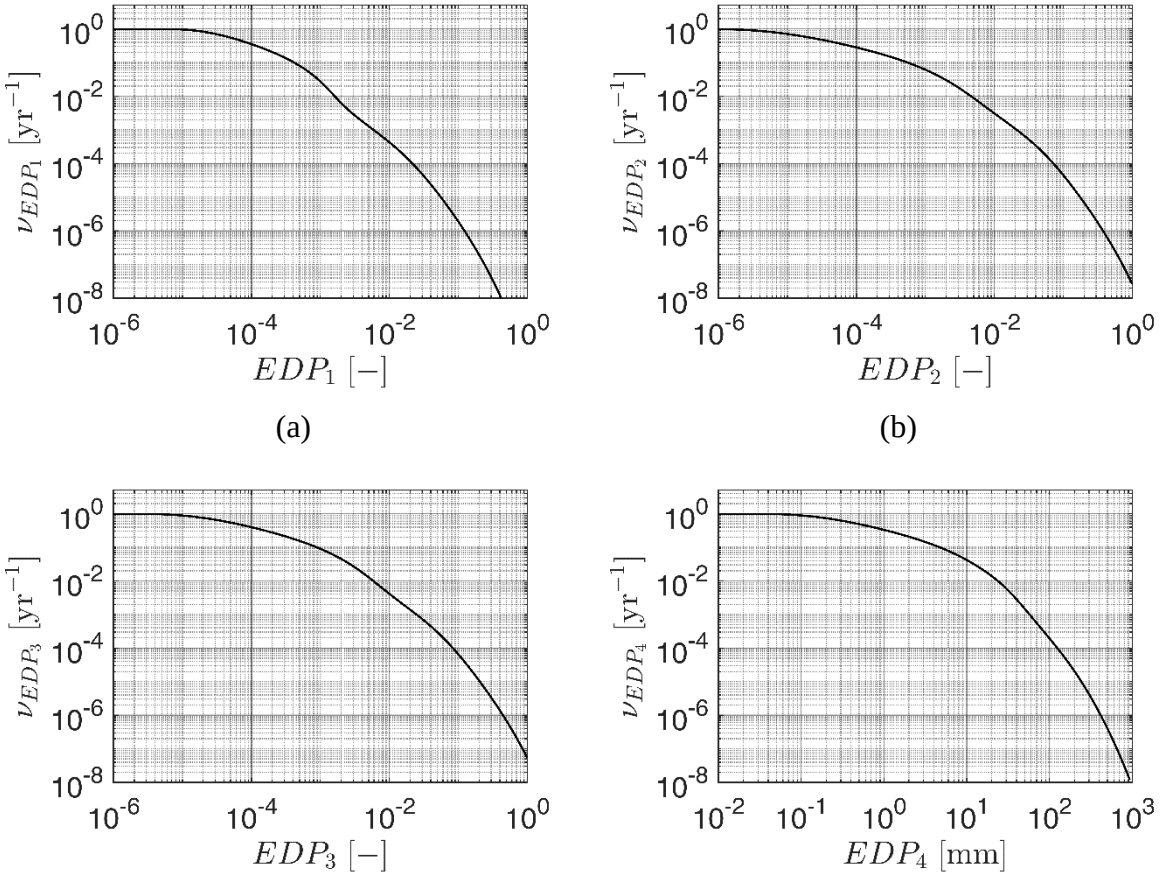

(a) (b) (c) (d)

Figure 4.10 Demand hazard curves in terms of: (a) EDP_1, (b) EDP_2, (c) EDP_3, and (d) EDP_4

4.5.3 Probabilistic Seismic Damage Hazard Analysis (PSDamHA)

PSDamHA aims at making probabilistic predictions of structural *LS* exceedances in terms of MARs or MRPs associated with these events. For a set of discrete *LS*s, a limit-state function, also known as a performance function, is mathematically expressed as

$$Z_k = C_k - EDP_k \tag{4.10}$$

where C_k and EDP_k represent the random variables corresponding to the capacity and the *EDP* associated with the k^{th} *LS*. The MAR of exceedance of the k^{th} *LS* is expressed as the convolution of the probability of *LS* exceedance conditional on the associated *EDP* with the DHC of the *EDP* as

$$\nu_{LS_k} = \int_{EDP_k} P\left[Z_k < 0 \mid EDP_k = \delta\right] \cdot \left| d\nu_{EDP_k}(\delta) \right| \tag{4.11}$$

Conditional on EDP_k, the uncertainty in Z_k is solely due to C_k, the structural capacity associated with the k^{th} *LS*. Uncertainty quantification of conditional *LS* exceedance, given a specific value of the associated demand, is typically performed using a predictive capacity model for the specific *LS* and comparing predictions from this capacity model with reliable experimental and/or numerical data. The probabilistic analysis involved in computing the conditional probability of exceeding the k^{th} *LS* conditioned on the value of the associated *EDP* is called fragility analysis. Strain-based fragility functions for the *LS*s pertaining to the flexural hinging of RC columns (most critical *LS*s for California OSBs), and a traditional displacement/deformation-based fragility function for the *LS* of a shear key reaching its shear strength capacity are developed and used in this study.

4.5.3.1 Deterministic Capacity Models

A capacity model attempts to relate a combination of structural properties, such as geometric properties, mechanical and material properties (e.g., material strength, yield strain), and structural demand, such as displacement/deformation (e.g., drift ratio) and material strain, to the reaching/crossing of a specific state of damage. The models are typically empirical or semi-empirical and derived from experimental data and/or engineering judgement and/or mechanics, but can also be purely mechanics-based (i.e., analytical/numerical). Consequently, capacity models are often found in the form of equations with variables that are deemed pertinent to the *LS*s of interest. The predictive capacity model for the k^{th} *LS* establishes the threshold value ($EDP_{C_k}^{\text{PRED}}$) of the associated *EDP*, which, upon being exceeded, deterministically predicts the exceedance of the k^{th} *LS*.

Goodnight et al. (2016), in a comprehensive experimental study on RC bridge columns, suggested the use of the peak absolute value of the compressive strain of the longitudinal bar as a predictor for the *LS* of concrete cover spalling. This same study also concludes that the capacity of a column against bar buckling can be related to the peak tensile strain of the longitudinal reinforcement which, upon exceedance of a threshold value, leads to severe instability in the bar upon subsequent reversal of load. In a recent study by Duck et al.[8], a semi-empirical, mechanics-based predictive criterion based on the maximum strain range/excursion (difference between maximum tensile and minimum compressive strain with the latter following the former, see Figure 4.8 and Table 4.1) experienced by a longitudinal bar during a complete loading history is formulated for the prediction of Plastic Buckling Straightening Fatigue (PBSF), an *LS* characterized by the initiation of incipient cracks at the root of bar deformations in the compressed concave side of a buckled bar which, upon straightening of the bar in a subsequent load cycle,

leads to fracture of the bar. A displacement/deformation-based predictive capacity model for the abutment exterior shear key reaching its shear strength capacity (i.e., full development of shear key failure mechanism) is adopted from the experimental work by Megally et al. (2002). Table 4.2 lists the deterministic predictive capacity models considered for the selected set of *LS*s.

Table 4.2 Deterministic predictive capacity models for the considered *LS*s

LS #	***Predictive Capacity Model***	
1	$EDP_{C_1}^{\text{PRED}} = 0.004$	(4.12)
2	$EDP_{C_2}^{\text{PRED}} = 0.03 + 700\rho_s \frac{f_{yhe}}{E_s} - 0.1\frac{P}{f'_{ce}A_g}$	(4.13)
3	$EPD_{C_3}^{\text{PRED}} = 0.11 + \min(0.054, 0.032\rho_s(\%)) - 0.0175\left\lvert\left(\sqrt[3]{n_{bar}} - 2.93\right)\right\rvert - 0.054\frac{T}{Y}$	(4.14)
4	$EDP_{C_4}^{\text{PRED}} = \sqrt{2}\varepsilon_y(L_d + b)\frac{(h+d)}{s}$	(4.15)

In Eq. (4.13), ρ_s is the volumetric transverse reinforcement ratio, f_{yhe} is the expected yield stress of the transverse reinforcement, E_s is the elastic modulus of the transverse reinforcement, P is the axial load on the column (taken as the axial load due to gravity loads), f'_{ce} is the expected compressive yield stress of the unconfined concrete, and A_g is the gross cross-sectional area of the column. In Eq. (4.14), $\rho_s(\%)$ is the volumetric transverse reinforcement ratio expressed in percent, n_{bar} is the number of bundles of longitudinal bars in a column, and $\frac{T}{Y}$ is the ratio of the ultimate stress to the yield stress of the longitudinal steel reinforcement (taken as 1.4[8]). In Eq. (4.15), ε_y is the yield strain of the horizontal steel reinforcement in the stemwall, *s* is the larger of the horizontal and vertical bar spacings in the stemwall, d is the height of the shear key above the

stemwall, *b* is the thickness of the stemwall, *h* is the height of the stemwall, and L_d represents the bar development length of the horizontal reinforcement at the shear key stemwall interface.

4.5.3.2 Fragility Analysis and Experimental/Numerical Data Sources

The predictive capacity models described in Eqs. (4.12) through (4.15) are deterministic and therefore do not take into account any uncertainty related to the capacity of the structural components. The uncertainty associated with capacity predictions stems from the path/history-dependence of the cyclic inelastic structural response, uncertainties in material and/or geometric properties, differences in geometric properties, test setup, loading protocols, and boundary conditions between experimental specimens, the use of idealized and imperfect predictive methods/models with missing explanatory variables, the use of a single predictive demand parameter to predict the exceedance of an *LS*, etc. To quantify the uncertainty related to an *LS* capacity, fragility functions are used. Fragility functions are obtained by making use of the deterministic capacity models and comparing their predictions of *LS* exceedances with reliable experimental data from tests conducted in the laboratory and/or numerical results obtained from high-fidelity finite element analyses.

The fragility function for the k^{th} *LS* is defined in the form of the two-parameter lognormal cumulative distribution function as

$$P\left[Z_k < 0 \mid EDP_k = \delta\right] = \Phi\left(\frac{\ln(\delta) - \lambda_k}{\zeta_k}\right) \tag{4.16}$$

where λ_k and ζ_k are the parameters of the fitted lognormal distribution representing the mean and standard deviation of the natural logarithm of experimentally and/or numerically measured values of EDP_k as the k^{th} *LS* is reached or exceeded.

Fragility functions, typically constructed using experimental and/or numerical data pertaining to specimens or models with different geometric, material, and mechanical characteristics, need to be normalized such that they can be used for structural components of any specified characteristics. To create a normalized fragility function or curve for the k^{th} *LS*, experimentally/numerically measured values of the associated *EDP* (i.e., EDP_k) at which the *LS* of interest is reached or exceeded, referred to as EDP_k^{MEAS}, are recorded for each specimen/model tested/analyzed and divided by the predicted capacity, $EDP_{C_k}^{\text{PRED}}$, obtained using the appropriate predictive capacity model (see Table 4.2) and the expected values (or best estimates) of the variables defining it. The normalized fragility function for the k^{th} *LS* is therefore defined as

$$P\left[Z_k < 0 \,|\, EDP_k^{\text{NORM}} = \frac{EDP_k^{\text{MEAS}}}{EDP_{C_k}^{\text{PRED}}} = \delta \right] = \Phi\left(\frac{\ln(\delta) - \lambda_k'}{\zeta_k'} \right) \tag{4.17}$$

where λ_k' and ζ_k' are the parameters of the fitted lognormal distribution representing the mean and standard deviation of the natural logarithm of the ratios of experimentally/numerically measured to predicted value of EDP_k for which the k^{th} *LS* is reached or exceeded.

The normalized fragility functions/curves for *LS*s 1 through 4 are shown in Figure 4.11. It is noted from Figure 4.11 that all experimental/numerical data points, except in the case of *LS* 4, lie close to the fitted cumulative lognormal distribution function with only small deviations at the upper and lower tails of the CDF. The values of the measured-to-predicted capacity ratios for *LS*s 1 through 4 at 50% probability of exceedance are 1.02, 1.05, 0.99, and 1.14, respectively, indicating minimal to moderate biases. The experimental/numerical sources selected in this study for the construction of the fragility curves are reported in Table 4.3.

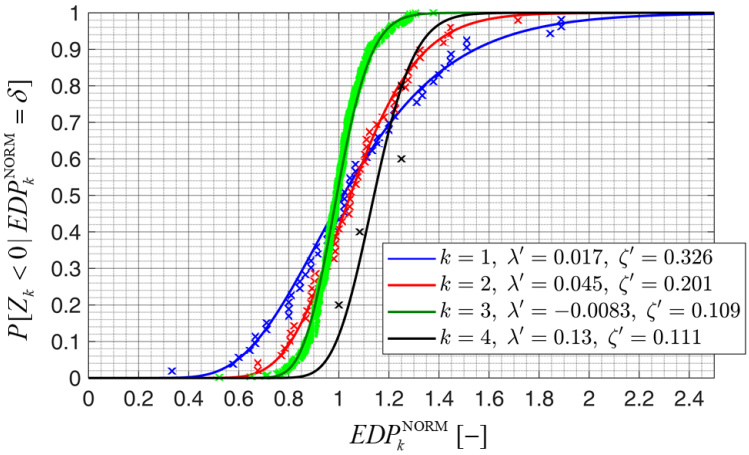

Figure 4.11 Normalized fragility curves (fitted experimental/numerical data shown as crosses)

The parameters of the denormalized fragility functions corresponding to *LS*s 1 through 4, to be used in Eq. (4.11) in computation of the MARs of exceedance for the selected set of *LS*s, are obtained using the respective values of the capacity predictors, $EDP_{C_k}^{\mathrm{PRED}}$, for the specific design of the considered testbed OSB as

$$\lambda_k = \lambda_k' + \log EDP_{C_k}^{\mathrm{PRED}}, \qquad \zeta_k = \zeta_k' \tag{4.18}$$

Table 4.3 Experimental/Numerical sources for the fragility analyses

Source	***Type***	***No. of specimens/models***	***LS #***
Schoettler et al. (2015)	full scale specimen	1	2
Trejo et al. (2014)	half scale specimen	6	1
Goodnight et al. (2015)	half scale specimen	23	1, 2
Murcia-Delso et al. (2013)	full scale specimen	4	1, 2
Duck et al. (2018)	FE model	593	3
Megally et al. (2002)	half scale specimen	4	4

4.5.3.3 Damage Hazard Analysis and Discussion of Results

For the considered testbed OSB, the MAR of *LS* exceedance for the k^{th} *LS* is obtained by numerically convolving the fragility function corresponding to LS_k with the DHC of the

associated EDP (i.e., EDP_k), as per Eq. (4.11). Results of PSDamHA conducted for the considered testbed OSB are shown in Table 4.4, where the MRP (= 1/MAR) of exceedance of each *LS* considered is reported. As expected, these results show that exceedances of increasingly severe *LS*s, i.e., *LS*s 1 through 3, concerning the RC bridge columns have increasing values of MRPs. The testbed OSB, which has monolithic non-isolated type abutment shear keys, shows a high MRP of exceeding *LS* 4 that is even higher than the MRP of exceeding the critical *LS* of bar fracture. The design of non-isolated type abutments shear keys, which are expected to transmit lateral shear forces generated by small to moderate earthquakes and service loads, is found to be overly conservative (in the present case) in terms of the risk associated with the exceedance of their limit-state capacity. The influence of such overdesigned abutment shear keys for short (2-3 span) OSBs (like the one considered in this paper) on the MRPs of exceeding the more critical column related *LS*s should be investigated as part of future research.

Table 4.4 MRPs of *LS* exceedances

LS #	***MRP of exceedance (yr)***	***Target MRP of exceedance (yr)***
1	466	250
2	2719	1000
3	5658	2500
4	5844	-

Target MRPs of exceedance for *LS*s 1-3, which are the *LS*s related to the desirable (targeted) damage/failure mode concerning RC bridge columns (i.e., flexural hinging of columns), are selected based on discussions with and feedback from expert Caltrans engineers and are listed in Table 4.4. The as-designed (following a traditional prescriptive seismic design philosophy) version of the testbed OSB is found to perform well with regard to all three column related *LS*s of interest. The MRPs of exceeding the selected set of *LS*s are higher than their respective specified

targets by factors of 1.9, 2.7, and 2.3, respectively, for *LS*s 1-3 thus very conservatively ensuring, with a high margin, the desired (target) safety against the exceedances of *LS*s 1-3.

The MAR or MRP of an *LS* exceedance, according to the PEER PBEE framework, is computed by aggregating or accounting for the contributions from all seismic hazard levels and can, therefore, be deaggregated into the contributions from different levels of *IM* (i.e., deaggregated with respect to *IM*). This deaggregation provides additional insight into the distribution of causative *IM* values leading to a specific level of damage hazard. Figure 4.12 presents the results of the *IM* disaggregation of the damage hazard corresponding to *LS*s 1-4.

The ordinate on the right-hand-side of each deaggregation plot in Figure 4.12 shows the conditional probability distribution of *IM*, given $Z_k < 0$ $(k = 1, 2, 3, 4)$. The ordinate along the left-hand-side of the same plots shows the site-specific seismic hazard curve (SHC). Also marked in each of these plots is the value *im* of *IM* with the same MAR of exceedance as the k^{th} *LS*, i.e., $\nu_{IM}(im) = \nu_{LS_k}$ $(k = 1, 2, 3, 4)$. It is noted from Figure 4.12 that contribution to the MAR of exceedance of a specific *LS* comes not only from the *IM* value with the same MAR as the limit-state (ν_{LS_k}), but from a wide continuum range of *IM* values with MAR of exceedance both below and above ν_{LS_k}. This provides a scientific basis to challenge any incomplete PBSD method according to which, for the sake of computational, theoretical and/or conceptual convenience, one chooses to design a bridge such that specified *LS*s are not exceeded (with specified confidence levels) at specified discrete seismic hazard levels (e.g., earthquake ground motions with an MRP of *IM* exceedance of 475 years, 975 years, 2,475 years, etc.). It is noted that although an appreciable part of the *IM* contributions to the seismic damage hazard associated with an *LS* of interest does come from the range of *IM* spanned by the six seismic hazard levels (indicated by the

light blue patch in Figure 4.12) selected for the ensemble nonlinear response history analyses (see Figure 4.9(a)), a significant part of the *IM* contributions, especially for the more critical *LS*s, comes from the range of *IM* above the highest seismic hazard level considered. In other words, the results of PSDamHA depend not only on the interpolation of the structural response statistics between the discrete seismic hazard levels selected for response analyses, but also on their extrapolation beyond the *IM* range considered. This emphasizes the importance of choosing an appropriate *IM* range for performing ensemble nonlinear response history analyses and suitable interpolation/extrapolation or regression models for the probabilistic prediction of *EDP* given *IM*.

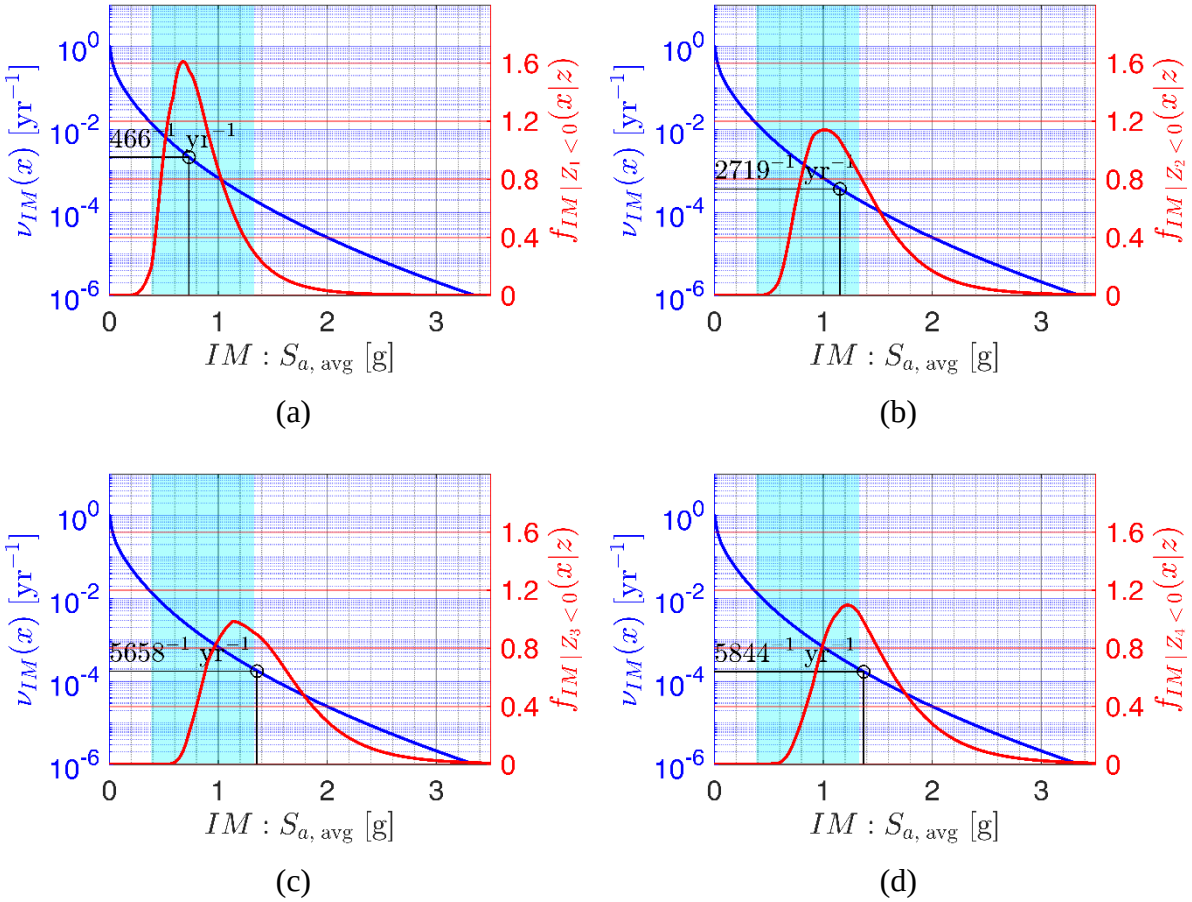

Figure 4.12 *IM* deaggregation of damage hazard: (a) *LS* 1, (b) *LS* 2, (c) *LS* 3, (d) *LS* 4

4.6 Conclusions

Different ingredients of the multidisciplinary PEER PBEE framework, developed or improved in various independent studies by past researchers, are integrated in this study, thus presenting an updated, and hence improved, framework to assess the seismic performance of bridge structures. The PBEE methodology is revisited, presented in terms of the improved interface variables considered (e.g., average spectral acceleration as *IM*, strain-based *EDP*s, and strain-based *LS*s), and applied to a real-world testbed California Ordinary Standard Bridge (OSB). The updated framework is implemented as a Python library, which allows for fully automated structural performance assessments. The modular nature of this computational framework allows for rapid implementation of future advancements made in the various steps of the PBEE methodology.

The set of *LS*s considered in this paper for the evaluation of seismic performance of OSBs is neither exhaustive nor definitive. The proposed framework is readily able to accommodate more refined (e.g., more mechanics-based) definitions of *LS*s and/or a larger number of *LS*s. Moreover, the influence of the exceedances of other *LS*s (e.g., full development of the shear key damage mechanism considered herein) on the exceedances of critical *LS*s related to column damage/failure should be investigated.

Overarchingly aiming towards a rigorous framework for PBSD of bridges, in general, and OSBs, in particular, the PEER PBEE framework is revisited, and improvements of several aspects in various stages of the state-of-the-art assessment framework are incorporated. With the PEER PBEE framework put into practice in its most updated and rigorous form, the groundwork for utilizing this framework in the context of performance-based design is laid. The implementation of the present updated version of the PEER PBEE framework, developed with painstaking details, will ensure that a PBSD method based on or distilled out of this rigorous assessment framework

will be fittingly risk-informed, rational, and scientific. Such a PBSD method for OSBs will be the subject of an upcoming paper.

The updated version of the PEER PBEE framework can be utilized to assess the seismic performance of other testbed OSBs located in regions with disparate levels of seismicity in California. The seismic performance of a wide range of design situations representative of the population of OSBs in California can be compared with respect to benchmark levels of performance reflecting the risk tolerance of the engineering community and society as a whole. Such a comparative study will expose irregularities and inconsistencies, if any, in seismic performance of OSBs designed following a more traditional (prescriptive) seismic design philosophy, rather than an explicitly performance-based one, thus promoting the need for a PBSD framework for OSBs such that explicitly stated risk-based performance objectives are consistently and uniformly satisfied.

The performance assessment framework presented in this paper is currently being enhanced via the incorporation of finite element model parameter uncertainty, probability distribution parameter estimation uncertainty, and structural model form uncertainty (i.e., model discrepancy), as pertinent sources of aleatoric and epistemic uncertainty. This will enable a comprehensive evaluation of the significance of these commonly neglected sources of uncertainty in the seismic performance assessment of OSBs.

4.7 Preview to Chapter 5

The next chapter presents the analytical and computational implementation of a parametric probabilistic seismic performance assessment framework for OSBs, thus laying the groundwork for solving a risk-targeted PBSD problem, an inverse assessment problem. A PBSD methodology

involving the design of the bridge piers is proposed wherein a feasible design domain in the primary design parameter space of an OSB is identified which facilitates risk-informed design/decision making in the face of uncertainty.

4.8 Acknowledgements

Support of this research by the California Department of Transportation under Grant No. 65A0594, Task No. 2880 is gratefully acknowledged. The authors wish to thank the following individuals for their help in insightful discussions related to the work presented in this paper: Tom Shantz, Dr. Charles Sikorsky, and Dr. Anoosh Shamsabadi from the Engineering Division of the California Department of Transportation. Opinions and findings in this study are those of the authors and do not necessarily reflect the views of the sponsor. Chapter 4, in full, is a reprint of the material as it appears in the following paper (the dissertation author is the first author of this paper):

Deb, A., Zha, A. L., Caamaño-Withall, Z. A., Conte, J. P., Restrepo, J. I. (2021). "Updated probabilistic seismic performance assessment framework for ordinary standard bridges in California." *Earthquake Engineering & Structural Dynamics*; 1–20. https://doi.org/10.1002/eqe.3459

Appendix: "Exact" Conditional Mean Spectrum Incorporating All Causative Scenarios

Baker and Cornell (Baker and Cornell 2006) defined the CMS, given a seismic hazard level, as the expected response spectrum conditioned on a specific value of *IM* (defined by the seismic hazard level considered) and the associated mean causal earthquake scenario (*M*-*R* pair), $S = \bar{s}$. Based on: (i) the multivariate normality of a vector of the natural logarithm of spectral

accelerations (Jayaram and Baker 2008) at different spectral periods, and (ii) the definition of $S_{a,\,\text{avg}}$ that ensures the multivariate normality of $\ln S_{a,\,\text{avg}}$ with the vector of jointly normal log spectral accelerations, the conditional mean and standard deviation of the log spectral acceleration at any period, T_i, given $S_{a,\,\text{avg}} = x$, are given by

$$\mu_{\ln S_a(T_i)\,|\,\ln S_{a,\,\text{avg}} = \ln x,\, S=\bar{s}} = \mu_{\ln S_a(T_i)\,|\,S=\bar{s}} + \rho_{\ln S_a(T_i),\ln S_{a,\,\text{avg}}\,|\,S=\bar{s}} \cdot \frac{\left(\ln x - \mu_{\ln S_{a,\,\text{avg}}\,|\,S=\bar{s}}\right)}{\sigma_{\ln S_{a,\,\text{avg}}\,|\,S=\bar{s}}} \cdot \sigma_{\ln S_a(T_i)\,|\,S=\bar{s}} \tag{4.19}$$

$$\sigma_{\ln S_a(T_i)\,|\,\ln S_{a,\,\text{avg}} = \ln x,\, S=\bar{s}} = \sigma_{\ln S_a(T_i)\,|\,S=\bar{s}} \sqrt{1 - \rho^2_{\ln S_a(T_i),\ln S_{a,\,\text{avg}}\,|\,S=\bar{s}}} \tag{4.20}$$

where $\mu_{\ln S_a(T_i)|S=\bar{s}}$ and $\sigma_{\ln S_a(T_i)|S=\bar{s}}$ are obtained from a standard GMPE (Boore and Atkinson 2008), and the correlation coefficient between $\ln S_a(T_i)$ and $\ln S_{a,\,\text{avg}}(T_1,\ldots,T_n)$, $\rho_{\ln S_a(T_i),\ln S_{a,\,\text{avg}}\,|\,S=\bar{s}}$, is given by (Baker and Cornell 2006)

$$\rho_{\ln S_a(T_i),\,\ln S_{a,\,\text{avg}}\,|\,S=\bar{s}} = \frac{\sum_{p=1}^{n} \rho_{\ln S_a(T_i),\ln S_a(T_p)} \cdot \sigma_{\ln S_a(T_p)\,|\,S=\bar{s}}}{\sqrt{\sum_{p=1}^{n}\sum_{q=1}^{n} \rho_{\ln S_a(T_p),\ln S_a(T_q)} \cdot \sigma_{\ln S_a(T_p)\,|\,S=\bar{s}} \cdot \sigma_{\ln S_a(T_q)\,|\,S=\bar{s}}}} \tag{4.21}$$

where the correlation coefficient between any two spectral periods, $\rho_{\ln S_a(T_i),\ln S_a(T_p)}$, is assumed to be independent of the earthquake scenario (Baker and Jayaram 2008).

The probability normalized deaggregation of the contribution of *M* and *R* to the MAR at which the *IM* $S_{a,\,\text{avg}}$ exceeds the threshold value *x* can be viewed as a bivariate probability mass function (PMF) of discretized random variables *M* and *R*, or equivalently a univariate PMF of the random variable *S* representing possible (*M*, *R*) scenarios, given the specific MAR of *IM* exceedance. The mean causal scenario, $\bar{s}$, the center of gravity of this conditional PMF of *S*, may

correspond to an unrealistic causative earthquake scenario at the site in case there are widely varying contributing scenarios leading to a multimodal PMF of *S*.

To address this issue, a more complete version of the CMS, called the "exact" CMS, incorporating all causative earthquake scenarios was introduced (Lin et al. 2013a). The formulation of the "exact" CMS relies on deriving the unconditional (with respect to *S*) PDF of the log spectral acceleration at any period, T_i, as

$$f_{\ln S_a(T_i)}(a) = \sum_{q=1}^{N_S} f_{\ln S_a(T_i)|S=s}\left(a \mid S = s_q\right) \cdot P\left[S = s_q\right] \tag{4.22}$$

where *a* is a specific value of $\ln S_a(T_i)$. The exact mean and standard deviation of the unconditional log spectral acceleration at any period, T_i, are obtained as

$$\mu_{\ln S_a(T_i)} = E_S\left[E_{\ln S_a(T_i)|S}\left[\ln S_a\left(T_i\right) \mid S = s\right]\right] = \sum_{q=1}^{N_S} \mu_{\ln S_a(T_i)|S=s_q} \cdot P\left[S = s_q\right] \tag{4.23}$$

and

$$\begin{aligned}\sigma_{\ln S_a(T_i)} &= \sqrt{E_S\left[Var_{\ln S_a(T_i)|S}\left[\ln S_a\left(T_i\right) \mid S = s\right]\right] + Var_S\left[E_{\ln S_a(T_i)|S}\left[\ln S_a\left(T_i\right) \mid S = s\right]\right]} \\ &= \sqrt{\sum_{q=1}^{N_S} \sigma^2_{\ln S_a(T_i)|S=s_q} \cdot P\left[S = s_q\right] + \sum_{q=1}^{N_S}\left(\mu_{\ln S_a(T_i)|S=s_q} - \mu_{\ln S_a(T_i)}\right)^2 \cdot P\left[S = s_q\right]}\end{aligned} \tag{4.24}$$

respectively. Note that $E_S[\cdots]$ and $Var_S[\cdots]$ refer to the expectation and variance, respectively, of the operand with respect to *S*, and $P[S = s_q]$ is the deaggregation weight, or the fractional contribution of the (*M*, *R*) scenario s_q to the considered level of seismic hazard.

The normality of the conditional distribution $f_{\ln S_a(T_i)|S=s}\left(a \mid S = s_q\right)$ is lost upon "unconditioning" with respect to *S* as per Eq. (4.22). The unconditional random variable $\ln S_a(T_i)$ distributed according to a mixture of normal distributions is, therefore, no longer necessarily

normally distributed. A rigorous treatment of this case is possible by assuming the vector of unconditional log spectral accelerations to follow some non-unique multivariate distribution (e.g., NATAF model) such that the marginal mixture distributions of $\ln S_a(T_i)$'s as per Eq. (4.22) and the correlation structure of $\ln S_a(T_i)$'s are preserved. However, for practical purposes and usability in ground motion record selection procedures, the vector of unconditional log spectral accelerations at different periods can be assumed to follow a multivariate normal distribution (Lin et al. 2013b). This is necessarily true if, and only if there is only one contributing scenario to a specific level of seismic hazard, or in other words the PMF of *S*, given a seismic hazard level, is a dirac-delta function. The exact mean and standard deviation of $\ln S_a(T_i)$ (Eqs. (4.23) and (4.24)) can therefore be used to rewrite Eqs. (4.19) through (4.21), now incorporating all causative (*M*, *R*) scenarios and thereby defining the "exact" CMS as

$$\mu_{\ln S_a(T_i)|\ln S_{a,\text{avg}}=\ln x} = \mu_{\ln S_a(T_i)} + \rho_{\ln S_a(T_i),\ln S_{a,\text{avg}}} \cdot \frac{\left(\ln x - \mu_{\ln S_{a,\text{avg}}}\right)}{\sigma_{\ln S_{a,\text{avg}}}} \cdot \sigma_{\ln S_a(T_i)} \tag{4.25}$$

$$\sigma_{\ln S_a(T_i)|\ln S_{a,\text{avg}}=\ln x} = \sigma_{\ln S_a(T_i)} \sqrt{1-\rho^2_{\ln S_a(T_i),\ln S_{a,\text{avg}}}} \tag{4.26}$$

$$\rho_{\ln S_a(T_i),\ln S_{a,\text{avg}}} = \frac{\sum_{p=1}^{n} \rho_{\ln S_a(T_i),\ln S_a(T_p)} \cdot \sigma_{\ln S_a(T_p)}}{\sqrt{\sum_{p=1}^{n}\sum_{q=1}^{n} \rho_{\ln S_a(T_p),\ln S_a(T_q)} \cdot \sigma_{\ln S_a(T_p)} \cdot \sigma_{\ln S_a(T_q)}}} \tag{4.27}$$

where $\mu_{\ln S_{a,\text{avg}}}$ and $\sigma_{\ln S_{a,\text{avg}}}$ are the mean and standard deviation of the unconditional (with respect to *S*) average spectral acceleration $S_{a,avg}$, which are obtained as

$$\cdot \mu_{\ln S_{a,\text{avg}}} = \left(\frac{1}{n}\right) \cdot \sum_{p=1}^{n} \mu_{\ln S_a(T_p)} \cdot \tag{4.28}$$

$$\sigma_{\ln S_{a,\,\mathrm{avg}}} = \left(\frac{1}{n}\right) \cdot \sqrt{\sum_{p=1}^{n}\sum_{q=1}^{n} \rho_{\ln S_a(T_p)\ln S_a(T_q)} \cdot \sigma_{\ln S_a(T_p)} \cdot \sigma_{\ln S_a(T_q)}} \tag{4.29}$$

5 Framework for Risk-targeted Performance-based Seismic Design of Ordinary Standard Bridges

5.1 Abstract

This paper presents the analytical formulation and computational implementation of a parametric probabilistic seismic performance assessment framework for ordinary standard bridge (OSB) structures, thus laying the groundwork for solving a risk-targeted performance-based seismic design (PBSD) problem, an inverse assessment problem. An updated probabilistic performance-based earthquake engineering (PBEE) assessment methodology is used for a parametric performance assessment of four distinct OSBs in California to investigate the effects of varying key structural design parameters over a primary design parameter space on risk-based structural performance measures. The dire need for a systematic PBSD framework for OSBs is illustrated given the significant variability in risk-based performance levels exhibited by these traditionally designed testbed OSBs. A PBSD methodology involving the design of the bridge piers is proposed wherein a risk-based feasible design domain in the primary design parameter space is identified which facilitates the risk-informed design/decision making process in the face of uncertainty. Sensitivities of risk-based feasible design domains to other (secondary) design variables and to the method employed for damage hazard assessment are investigated.

5.2 Introduction

Risk-targeted performance-based seismic design (PBSD) has emerged as the most scientific and promising design methodology as it involves designing a structure in the face of

uncertainty to meet performance objectives explicitly stated in terms of the risk (or the probability in a specified exposure time) associated with the exceedance of critical limit-states (*LS*s) or certain tolerable thresholds of monetary loss, downtime, etc. Performance objectives stated as such will not only allow an active participation of the public and stakeholders in the design and decision-making process thereby making it more rational, scientific, and transparent, but also lead to greater societal awareness of earthquake risk and consequences (May 2001). In order to design structures to meet risk-targeted statements of performance objectives, a rigorous treatment and propagation of pertinent uncertainties involved at various stages of structural performance assessment is inevitably called for. The paradigm of probabilistic performance-based earthquake engineering (PBEE) is expected to provide, not only technical support for this shift of design philosophy (or paradigm), but also a novel way to tailor structural design to meet the societal risk tolerance. This has paved the way for the profession to work towards identification and filling of knowledge gaps and make considerable advancement in the realm of probabilistic PBEE over the last few decades. Bolstered by the ever increasing computational power, this quest has consistently improved over time and culminated in the fully probabilistic, rigorous and advanced assessment framework (Moehle and Deierlein 2004; Porter 2003) developed under the auspices of the Pacific Earthquake Engineering Research (PEER) Center.

The PEER PBEE assessment framework integrates site-specific seismic hazard analysis, structural demand analysis, damage analysis, and loss analysis, in a comprehensive and consistent probabilistic framework. This comprehensive framework has been recommended as a future alternative for bridge seismic design in a recent study under the National Cooperative Highway Research Program (NCHRP) (NCHRP 2013). The NCHRP study also brings out the fact that the current bridge design practice considers safety and risk associated with seismic performance of

bridges as mere ramifications of the fulfillment of prescriptive measures and emphasizes on the explicit considerations of seismic risk, in order that the public and engineers participate in the decision-making process in tandem. Several studies (Cornell et al. 2002; Ellingwood 2008; Franchin et al. 2018; Hamburger 2006; Mackie and Stojadinović 2007; Saini and Saiidi 2014) have focused on the applicability of the PEER PBEE framework in the PBSD of structures. Notwithstanding, seismic design of bridge structures remains a relatively less trodden area as compared to that of building structures in terms of PBEE applications, and the rigor/completeness thereof. The PBSD procedure proposed by Mackie and Stojadinović (2007) uses closed-form solutions (Cornell et al. 2002) for the estimation of the damage/loss hazard. The accuracy of these closed-form solutions under simplifying assumptions has been previously questioned (Aslani and Miranda 2005; Bradley and Dhakal 2008) and is further investigated in this paper. Saini and Saiidi (2014) implemented a probabilistic design method wherein bridge columns are designed to satisfy target probabilities of exceedance of damage LSs conditional on different seismic hazard levels (e.g., 225 years, 975 years, and 2475 years mean return periods (MRPs) of exceedance of the considered seismic intensity measure (IM)), without aggregating the contributions of different seismic hazard levels to the total probability of LS exceedance. However, as noted in Deb et al. (2021), contribution to a specific MRP of LS exceedance comes not only from the IM value with the same MRP of exceedance, but from a wide continuum range of IM values with MRPs of exceedance both below and above the MRP of LS exceedance.

At the crux of structural design lies the selection of optimal values of critical design parameters/variables such that predetermined target specifications of certain performance measures are met. Overarchingly aiming towards a rigorous framework for PBSD of bridges, this paper presents the conceptualization and implementation of a generalized workflow for full-

fledged parametric probabilistic seismic performance assessment of Ordinary Standard Bridges (OSBs), thus laying the groundwork for performing a design through solving an inverse assessment problem. Structural performance measures considered in this study are defined as the mean annual rates (MARs), or reciprocally the mean return periods (MRPs), of exceedances for a selected set of practical *LS*s that are pertinent to the seismic evaluation of bridge structures and physically meaningful to practicing bridge engineers. To this end, the PEER PBEE methodology is revisited up to its third step, namely probabilistic damage analysis, simultaneously incorporating several novelties and improvements from the state-of-the-art literature related to the individual steps of the methodology. The final step of the PEER PBEE methodology, probabilistic loss analysis, is kept outside the scope of this study.

As the main contribution of this paper, a comprehensive PBSD framework involving the design of the bridge columns, the primary lateral load resisting components of OSBs, is proposed. This framework is applied to and validated with four actual testbed OSBs. A primary design space is defined for an OSB in terms of column design parameters to which the exceedances of the selected set of *LS*s are most sensitive. Probabilistic performance-based assessments of the as-designed and parametrically re-designed versions of the four testbed OSBs are then carried out to investigate the effect of varying these key structural design parameters on targeted structural performance measures. The end-product of this design framework are regions of safety and/or feasibility, referred to as feasible design domains, delineated over a two-dimensional design space of primary design variables pertaining to bridge columns that facilitate risk-informed design/decision making in the face of uncertainty.

5.3 Testbed bridges and Computational Models

In California, OSBs are conventional, multiple-span, short (span length less than 91.4 m or 300 ft) and, in general, skewed reinforced concrete (RC) bridges with monolithic or monolithic-equivalent superstructure supported on soils which may or may not be susceptible to liquefaction and/or scour (Caltrans 2013). These are the most common bridges in California; they are designed in-house by the California Department of Transportation (Caltrans). Several testbed OSBs located in regions of California with disparate levels of seismicity are selected for this study to cover a range of realistic design situations for OSBs and to ensure that the parametric probabilistic performance-based assessment framework formulated herein is general within its scope and is applicable to the gamut of design situations representative of the population of OSBs in California. Four existing California OSBs (Figure 5.1), namely Bridge A, Bridge B, Bridge C and Bridge MAOC, are chosen for this purpose. These OSBs have been studied extensively in past research projects (Kaviani et al. 2012; Omrani et al. 2015) and are representative of modern OSBs in California constructed between the late 1990's and early 2000s.

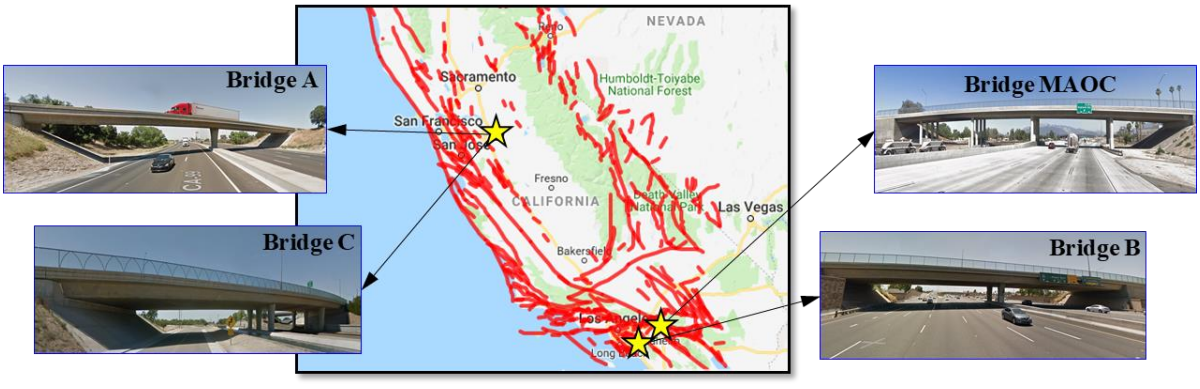

Figure 5.1 Locations of testbed OSBs

Bridge A is the Jack Tone Road Overcrossing in Ripon, California, consisting of two spans with a single column bent. Bridge B is the La Veta Avenue Overcrossing in Tustin, California, also consisting of two spans but supported on a two-column bent. Bridge C is the Jack Tone Road Overhead in Ripon, California (located adjacent to Bridge A), consisting of three spans supported on two bents with three columns each. Bridge MAOC, the Massachusetts Avenue Overcrossing located in San Bernardino, California, has five spans supported on four bents with four columns each. These bridges primarily consist of prestressed concrete box-girder decks supported by column-bent(s) on pile foundations and seat-type abutments also on pile foundations.

Three-dimensional nonlinear finite element (FE) models (consisting of nonlinear fiber-section beam-column elements and nonlinear springs) of these bridges are constructed in OpenSees (Mazzoni et al. 2006), the open-source FE analysis software framework developed at PEER. Initially inherited Tcl input files of the OpenSees models of these bridges from previous Caltrans/PEER funded projects were revisited, parameterized, and improved (Deb et al. 2018). A schematic representation of the computational model of one of the four testbed OSBs (Bridge C) is shown in Figure 5.2.

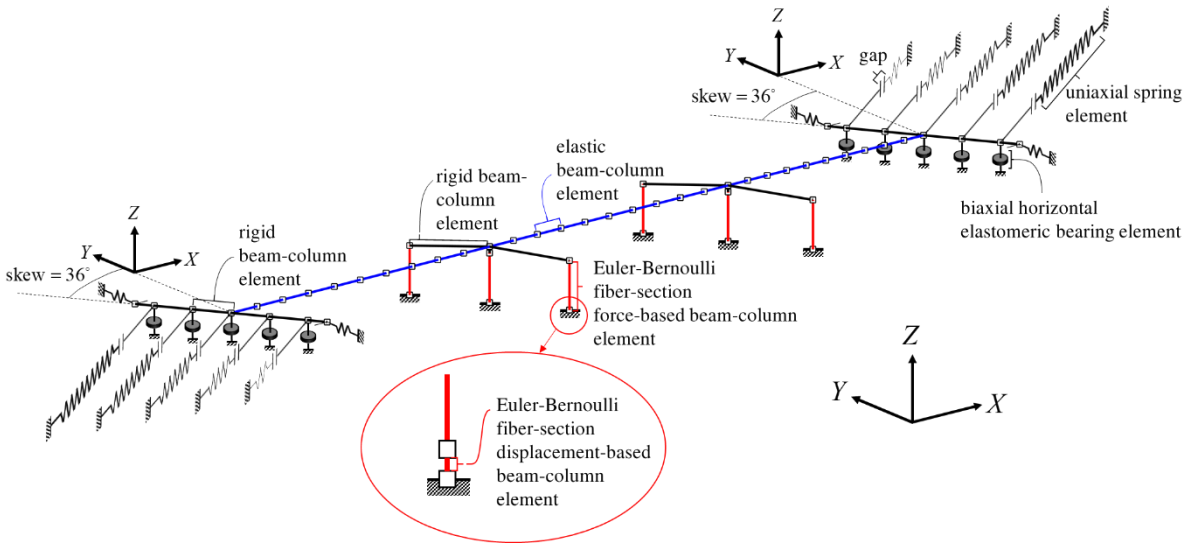

Figure 5.2 Schematic representation of the nonlinear FE model of Bridge C

Additional modeling details are shown in Figure 5.3 (a) through (f) for Bridge C, namely the (i) nonlinear fiber section definition of bridge column modeled using a single Euler-Bernoulli force-based beam-column element and of column base hinge, which is a short reduced-diameter section between the base of a column and the top of the pile cap, modeled using a single Euler-Bernoulli displacement-based beam-column element, (ii) material hysteretic stress-strain relations for concrete and steel fibers, (iii) hysteretic hyperbolic force-deformation curves of the distributed spring model with varying initial stiffnesses and ultimate strengths used to model the soil-structure interaction between the soil backfill and a skew-angled abutment (Shamsabadi et al. 2020), (iv) plasticity-based coupled bi-directional nonlinear (assumed bilinear) model of the shear force-deformation response of the bearing pads at the abutments, and (v) semi-empirical mechanics-based force-deformation hysteretic macro-model (Megally et al. 2002) used to represent the transverse resistance of the abutment exterior shear keys. The parameters of the Rayleigh linear viscous damping model pertaining to these OSBs are determined based on the following rationale. First, to prevent "double-counting" of the damping in a nonlinear FE model wherein nonlinear material hysteresis is explicitly accounted for, a low damping ratio of 1% is assigned to the first mode of the bridge in the transverse (more critical) direction. Second, to damp out any spurious participation of the higher modes, a high damping ratio of 5% is assigned to a sufficiently high frequency (about 20 Hz for the bridges considered in this paper). For a detailed description of the modeling techniques employed for the various components of the OSBs, the reader is referred to the technical report accompanying this study (Deb et al. 2018) as well as Deb et al. (2021a).

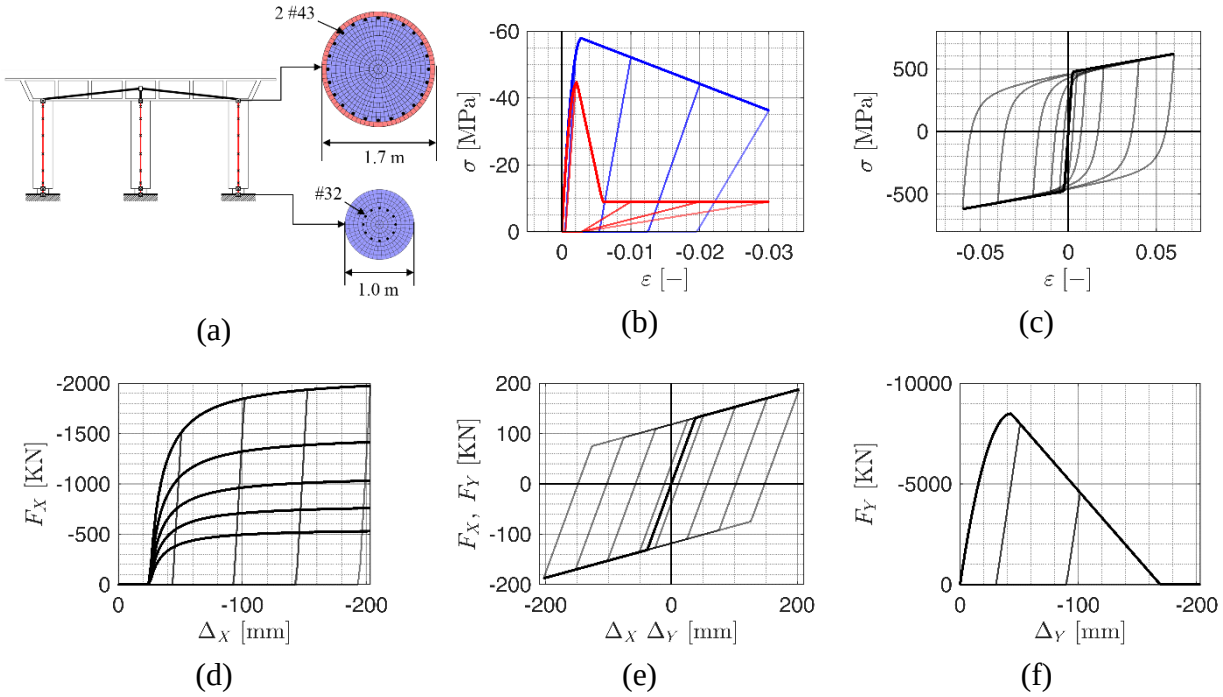

Figure 5.3 FE modeling details for Bridge C: (a) Column and base-hinge fiber-section definition; Material hysteretic stress-strain relations for (b) unconfined (red) and confined (blue) concrete fibers, and (c) reinforcing steel (black) fibers; Nonlinear hysteretic force-deformation curves assigned to: (d) backfill distributed spring model, (e) each bearing pad element, and (f) each exterior shear key spring

5.4 Updated Probabilistic Performance Assessment Framework

5.4.1 PEER PBEE Framework Integral

The formulation of the proposed PBSD framework is rooted in the four-step PEER PBEE assessment methodology integrating (i) site-specific seismic hazard analysis, (ii) structural demand analysis, (iii) damage analysis, and (iv) loss analysis in a comprehensive and consistent probabilistic framework using the Total Probability Theorem (TPT) of probability theory to arrive at an estimate of a performance measure, e.g., the MAR or MRP of exceedance of an *LS*, and/or the MAR or MRP at which a decision variable (e.g., down time, monetary loss, deaths) exceeds a specific threshold. Performance measures considered in this study are the MAR or equivalently

the MRP of *LS* exceedances for a selected set of *LS*s. The task of probabilistically predicting the future seismic performance of a bridge is therefore broken down into the following three steps (see Figure 5.4): Probabilistic Seismic Hazard Analysis (PSHA) in terms of a ground motion intensity measure (*IM*), Probabilistic Seismic Demand Hazard Analysis (PSDemHA) in terms of engineering demand parameters (*EDP*s), and Probabilistic Seismic Damage Hazard Analysis (PSDamHA) for the various *LS*s of interest. These steps are pieced together using the TPT as shown in Eq. (5.1).

$$\nu_{LS_k} = \int_{IM} \int_{EDP_k} P\left[Z_k < 0 \,|\, EDP_k = \delta\right] \cdot f_{EDP_k|IM}\left(\delta \,|\, x\right) \cdot d\delta \cdot \left|d\nu_{IM}(x)\right| \tag{5.1}$$

where $P[Z_k < 0 \,|\, EDP_k = \delta]$ is the conditional probability of exceedance of LS_k (i.e., safety margin $Z_k = C_k - EDP_k < 0$ where C_k denotes the structural capacity associated with LS_k) given a specific value δ of the associated *EDP* (i.e., EDP_k), $f_{EDP_k|IM}(\delta \,|\, x)$ is the conditional probability distribution of EDP_k given a specific value *x* of the *IM*, and $\nu_{IM}(x)$ is the MAR of *IM* exceeding the specific value *x*.

Novelties and improvements from the state-of-the-art literature related to the individual steps of the PEER PBEE assessment methodology are incorporated in this study (Deb et al. 2021a). Brief accounts of such enhancements are presented next.

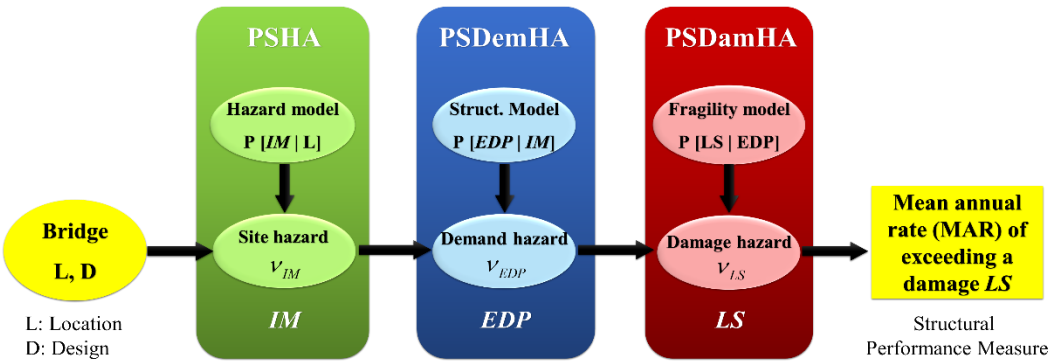

Figure 5.4 PEER PBEE Assessment Methodology (Porter 2003)

5.4.2 Improved Seismic Intensity Measure

The spectral acceleration averaged over a period range ($S_{a,\text{avg}}$), originally proposed by Baker and Cornell (2006), is selected as the ground motion *IM* in this study. Defined as the geometric mean of spectral accelerations at different periods, $S_{a,\text{avg}}$ is mathematically given by

$$S_{a,\text{avg}}(T_1,\ldots T_n)=\left[\prod_{p=1}^{n} S_a(T_p)\right]^{1/n} \tag{5.2}$$

where $[T_1,T_n]$ is the averaging period range. This *IM* has been demonstrated to perform better in terms of "efficiency" and "sufficiency" in the prediction of displacement-based nonlinear structural response (Eads et al. 2015) as compared to the traditionally used *IM*, $S_a(T_p)$, the spectral acceleration at a single predominant period of the structure. Furthermore, the period range over which the spectral acceleration is averaged specifically accounts for the following phenomena not captured by $IM = S_a(T_p)$: (i) uncertainty in predicting the period of the predominant mode of vibration for RC structures such as OSBs; (ii) change in natural periods of RC structures from pristine conditions to cracked states under service loads; (iii) lengthening of the predominant structural periods due to accumulation of damage during an earthquake which leads to higher correlation of the structural response with spectral accelerations at longer periods; and (iv) difference in periods of the fundamental modes of vibration in the two orthogonal directions (i.e., longitudinal and transverse) of the bridge. The range of periods used in the definition of $S_{a,\text{avg}}$ for the considered OSBs spans from the period of the first transverse mode of vibration, i.e., $T_{1,\text{trans}}$, to $2.5\,T_{1,\text{trans}}$ since the response of an OSB in the transverse direction is believed to be more critical than in the longitudinal direction in which the seismic bridge response is eventually stabilized

(limited) by the backfill at the abutments. Ten periods uniformly spaced in log scale between $T_{1,\text{trans}}$ and $2.5\,T_{1,\text{trans}}$ are used in the computation of $S_{a,\text{avg}}$. The selected period range also includes the period of the first mode of the OSB in the longitudinal direction.

Closed-form probabilistic characterization of $S_{a,\text{avg}}$ given an earthquake scenario (i.e., a magnitude and source-to-site distance pair), required in PSHA calculations, is obtained using existing attenuation relationships (e.g., Boore and Atkinson (2008)) for spectral accelerations at single periods. Seismic hazard analyses results for spectral accelerations at single periods along with the corresponding scenario deaggregation information, which are routinely available from standard PSHA software tools such as OpenSHA (Field et al. 2003), are inventively utilized (Deb et al. 2021a) to evaluate the MARs of exceedance of any specified value of the chosen novel *IM*. Figure 5.5 shows the seismic hazard curves for the testbed OSBs in terms of $S_{a,\text{avg}}$, and how they compare with the seismic hazard curves at single periods $S_a(T_p), \forall T_p \in \left[T_{1,\text{trans}}, \cdots, 2.5T_{1,\text{trans}}\right]$.

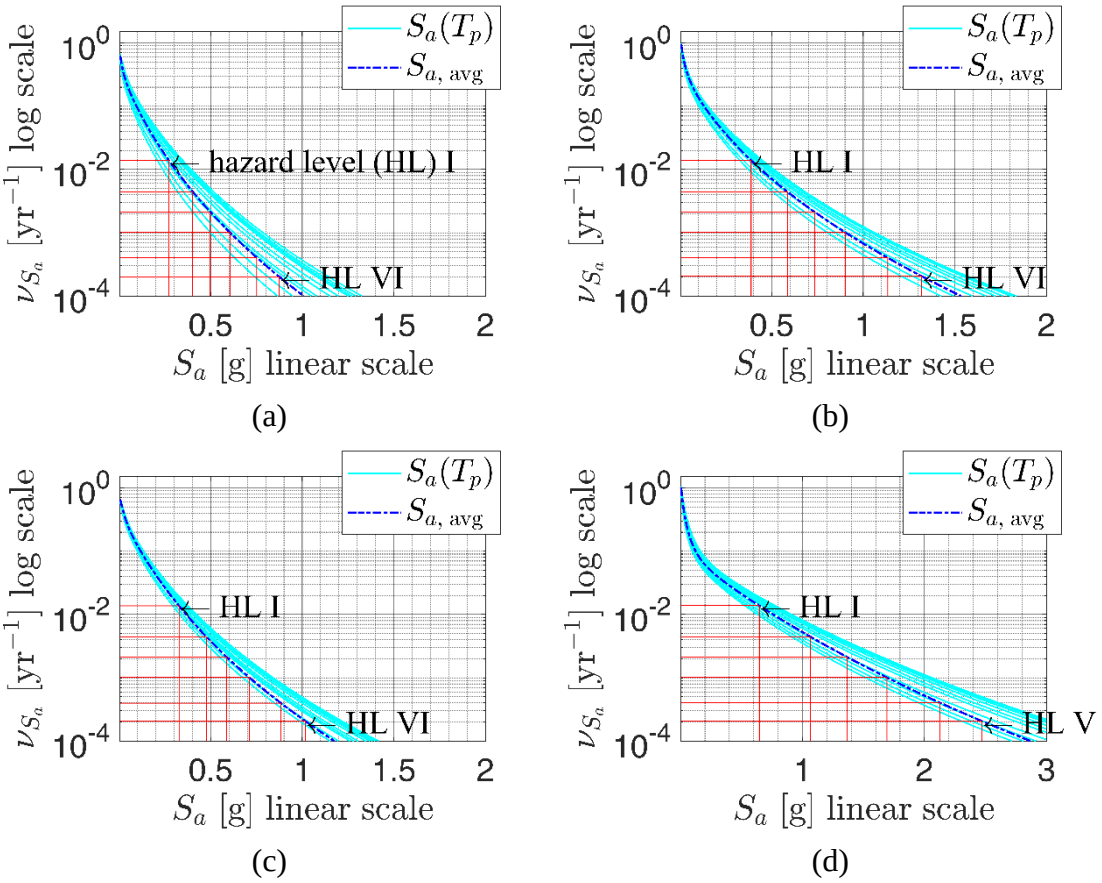

Figure 5.5 Seismic hazard curves in terms of $S_{a,\,\mathrm{avg}}$ for (a) Bridge A, (b) Bridge B, (c) Bridge C, and (d) Bridge MAOC

5.4.3 Risk-consistent Site-specific Ground Motion Record Selection

The conditional mean spectrum (CMS) (Baker and Cornell 2006; Lin et al. 2013a), representing the expected spectral shape given a specific value of the considered *IM*, is used as the target spectrum for ground motion record selection in this study. Six different seismic hazard levels corresponding to MRPs of *IM* exceedances equal to 72, 224, 475, 975, 2475, and 4975 years (numbered I through VI, respectively) are chosen and ensembles of 100 scaled bi-axial horizontal ground motions per hazard level are selected for the seismic response assessment of each (as-designed or re-designed) testbed OSB considered.

A ground motion selection algorithm, originally developed by Jayaram et al. (2011) and recently modified by Kohrangi et al. (2017) to include $S_{a,\text{avg}}$ as the conditioning *IM*, is implemented for the selection of site-specific risk-consistent ensembles of ground motion records representative of the six seismic hazard levels considered. Given a seismic hazard level and the corresponding value of *IM*, the conditional joint probability structure of correlated spectral accelerations at different periods is first determined. The algorithm then picks earthquake records from a ground motion database (Chiou et al. 2008) that, as an ensemble, follow the complete probability structure of the target conditional spectrum defined for that hazard level. As illustration, Figure 5.6 shows the set of six ensembles (corresponding to the six seismic hazard levels) of 100 records each, selected for the as-designed version of Bridge B. With the CMS chosen as the target spectrum over the uniform hazard spectrum (UHS), which is a more commonly used, excessively conservative, spectral envelope-based target spectrum, the natural spectral shapes and variability of the selected ensemble of earthquake ground motion records are preserved.

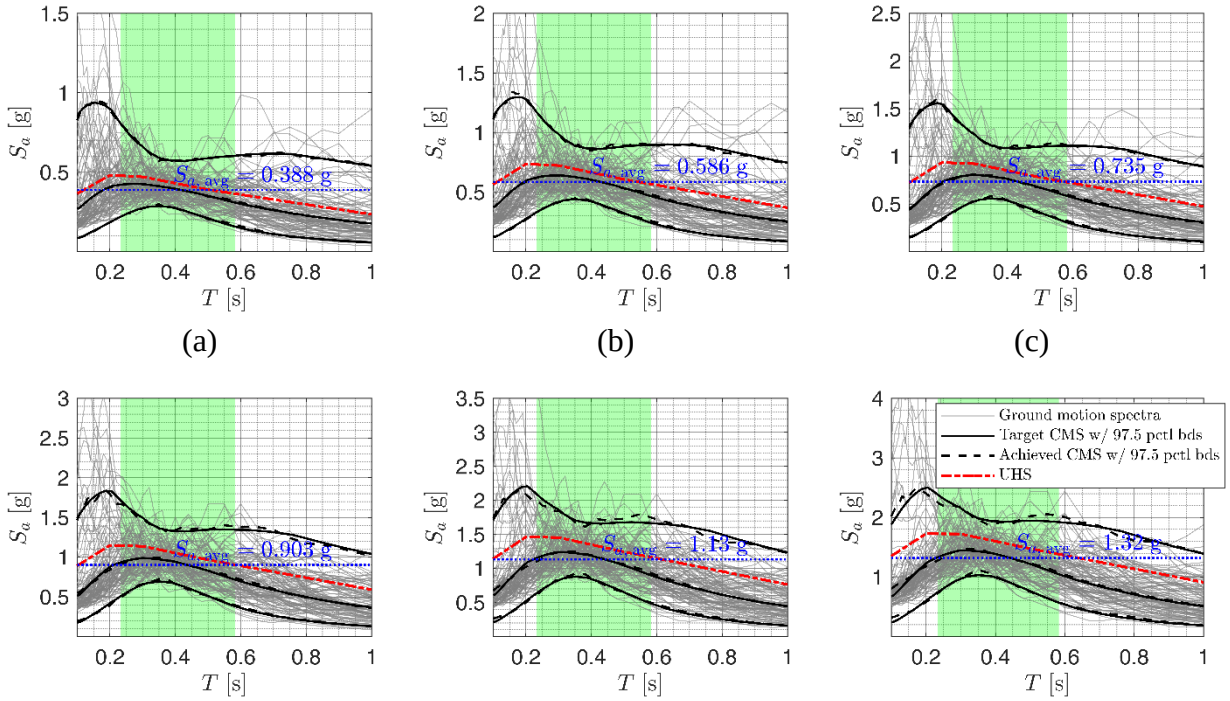

Figure 5.6 Ground motion ensembles selected for Bridge B at (a) hazard level I, (b) hazard level II, (c) hazard level III, (d) hazard level IV, (e) hazard level V, and (f) hazard level VI; green shaded region represents the averaging period range.

5.4.4 Damage *LS*s and Associated Material Strain-based *EDP*s

Three damage *LS*s related to the targeted failure mode of RC bridge columns (i.e., flexural hinging of columns), which are pertinent to the seismic evaluation of bridge structures and physically meaningful to bridge engineers, are considered in this study. These *LS*s are: (1) concrete cover crushing/spalling, (2) initiation (onset) of longitudinal bar buckling, and (3) precursor stage to longitudinal bar fracture post-buckling. The first *LS* represents superficial damage to a bridge column and requires cosmetic repair work primarily to prevent corrosion of rebars. The other two *LS*s represent ultimate *LS*s, exceedances of which lead to significant compromise of structural integrity and imminent structural collapse.

Traditionally, measures of deformation such as displacements, drift ratios, curvatures, etc. have been used as *EDP*s. However, for RC flexural members, such as columns, deformations can be directly and most reliably related to structural damage through material strains (Priestley et al. 2007). Table 5.1 lists the strain-based *EDP*s associated with the selected set of *LS*s. Definition of these *EDP*s are based on deterministic predictive capacity models (discussed in the next section) for the chosen set of *LS*s. Figure 5.7 schematically describes the chosen *EDP*s.

Table 5.1 *LS*s and associated strain-based *EDP*s

LS #	***Associated Engineering Demand Parameter (EDP)***	
1	Maximum absolute compressive strain in any longitudinal bar of any column.	$\max_{col}\left(\max_{bar}\left(\max_{t}\left\lvert\varepsilon_{comp}^{bar}(t)\right\rvert\right)\right)$
2	Maximum tensile strain in any longitudinal bar of any column.	$\max_{col}\left(\max_{bar}\left(\max_{t}\varepsilon_{tensile}^{bar}(t)\right)\right)$
3	Maximum strain range/excursion (i.e., difference of maximum tensile and minimum compressive strain, the latter following the former) in any longitudinal bar of any column	$\max_{col}\left(\max_{bar}\left(\max_{t}\varepsilon_{tensile}^{bar}(t)-\min_{t'>t}\varepsilon_{comp}^{bar}(t')\right)\right)$

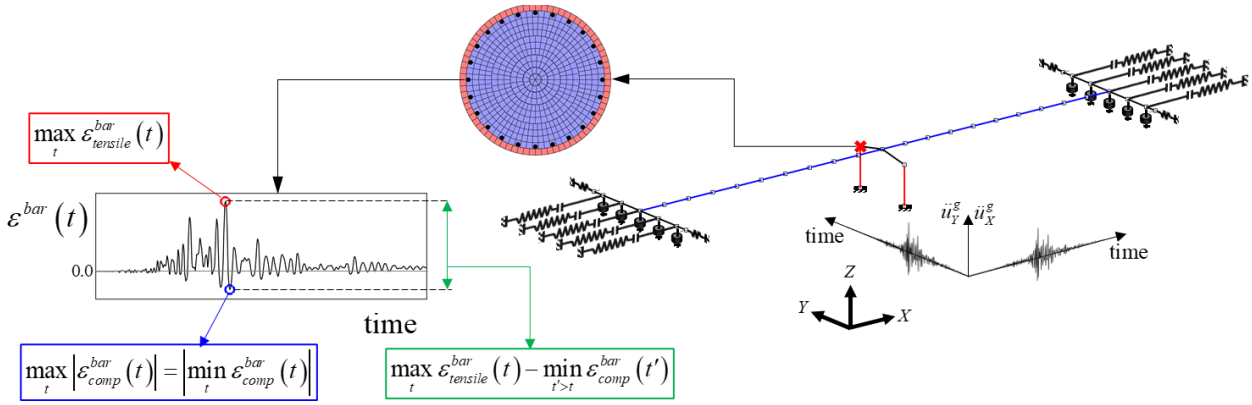

Figure 5.7 Schematic representation of material strain-based *EDP*s

5.4.5 Strain-based Fragility Functions

A fragility function expresses the probability of exceeding a system- or component-based *LS* given a specific value of a predictive demand parameter associated with this *LS*. The fragility function for the k^{th} *LS* is defined in the form of the two-parameter lognormal cumulative distribution function as

$$P\left[Z_k < 0 \,|\, EDP_k = \delta\right] = \Phi\left(\frac{\ln(\delta) - \lambda_k}{\zeta_k}\right) \tag{5.3}$$

where λ_k and ζ_k are the mean and standard deviation of the normal distribution fitted to the natural logarithm of experimentally and/or numerically measured values of EDP_k at which the k^{th} *LS* is reached or exceeded. Strain-based fragility functions developed using reliable experimental data or high-fidelity numerical data are constructed for the *LS*s considered in this study through proper identification of relevant test and research programs previously conducted (Duck et al. 2018; Goodnight et al. 2015; Murcia-Delso et al. 2013; Schoettler et al. 2015; Trejo et al. 2014). Fragility functions, typically constructed using experimental or numerical data pertaining to specimens or models with different geometric, material and mechanical characteristics, need to be

normalized such that they can be used for structural components of any specified characteristics. The normalized fragility function for the k^{th} *LS* has the form

$$P\left[Z_k < 0 \,|\, EDP_k^{\text{NORM}} = \frac{EDP_k^{\text{MEAS}}}{EDP_{C_k}^{\text{PRED}}} = \delta \right] = \Phi\left(\frac{\ln(\delta) - \lambda_k'}{\zeta_k'} \right) \tag{5.4}$$

where λ_k' and ζ_k' are the mean and standard deviation of the normal distribution fitted to the natural logarithm of EDP_k^{NORM} at which the k^{th} *LS* is reached or exceeded. EDP_k^{NORM} is defined as the ratio of experimentally or numerically measured values of EDP_k at which the LS_k is reached or exceeded, referred to as EDP_k^{MEAS}, to the corresponding predicted capacity, $EDP_{C_k}^{\text{PRED}}$, obtained using a predictive capacity model. Appropriate models for the capacity predictor, $EDP_{C_k}^{\text{PRED}}$, (Goodnight et al. (2016) for *LS*s 1 and 2, and Duck et al. (2018) for *LS* 3), are identified and listed in Table 5.2.

Table 5.2 Deterministic predictive capacity models for the considered *LS*s

LS #	***Predictive Capacity Model***
1	$EDP_{C_1}^{\text{PRED}} = 0.004$ (5.5)
2	$EDP_{C_2}^{\text{PRED}} = 0.03 + 700\rho_{trans}\frac{f_{yhe}}{E_s} - 0.1\frac{P}{f_{ce}' A_g}$ (5.6)
3	$EPD_{C_3}^{\text{PRED}} = 0.11 + \min(0.054,\, 3.2\rho_{trans}) - 0.0175\left\lvert\left(\sqrt[3]{n_{bar}} - 2.93\right)\right\rvert - 0.054\frac{T}{Y}$ (5.7)

In Eq.s (4.13) and (4.14), ρ_{trans} is the volumetric transverse reinforcement ratio, f_{yhe} is the expected yield stress of the transverse reinforcement, E_s is the elastic modulus of the transverse

reinforcement, P is the axial load on the column (taken as the axial load due to gravity loads), f'_{ce} is the expected compressive yield stress of the unconfined concrete, A_g is the gross cross-sectional area of the column, n_{bar} is the number of bundles of longitudinal bars in a column, and $\frac{T}{Y}$, taken as 1.4 (Duck et al. 2018), is the ratio of the ultimate stress to the yield stress of the longitudinal steel reinforcement.

The normalized fragility functions for *LS*s 1 through 3 are shown in Figure 5.8. These fragility functions are denormalized by the respective values of the capacity predictors for the specific designs of the considered testbed OSBs and used in Eq. (5.1) to compute the MARs of exceedances for the selected set of *LS*s.

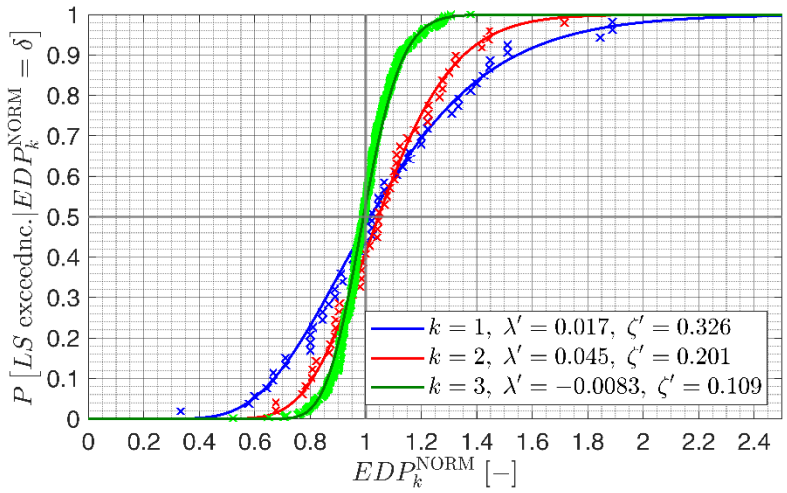

Figure 5.8 Normalized fragility curves (fitted experimental/numerical data are shown as crosses)

5.5 Framework for Risk-targeted Performance-based Seismic Design

At the crux of structural design lies the selection of optimal values of critical design parameters/variables such that predetermined target specifications of certain performance

measures are met. Hence, carrying out a parametric full-fledged probabilistic seismic performance assessment of the testbed bridges is a rational first step towards a rigorous framework for PBSD of OSBs so that the effects of varying key structural design parameters on the sought performance measures can be investigated. To design complex structural systems such as bridges in a rigorous manner such that multiple risk-targeted performance objectives are consistently satisfied, computationally expensive forward assessments of design iterations are unavoidable. To ensure computational feasibility and practicability of the parametric study, it is therefore essential to identify primary (key) design variables to which the sought performance measures are sensitive and perform the parametric study in terms of these variables.

5.5.1 Primary and Secondary Design Variables

*LS*s pertaining to RC bridge columns are considered in this study because columns constitute the primary lateral load resisting structural components of OSBs. Design variables/parameters selected for the parametric seismic performance assessment study, referred to as primary design variables, are structural parameters to which the exceedances of the selected set of *LS*s are most sensitive. Two such key parameters, revolving around the design of RC bridge columns and with readily alterable values from a design perspective, are (i) the column diameter, D_{col}, and (ii) the column longitudinal reinforcement ratio, ρ_{long}. A high-dimensional inverse problem of PBSD is therefore reduced to a two-dimensional search over the primary design space of an OSB.

In defining an OSB's primary design space, practical constraints applicable to the values of the chosen primary design variables are considered. According to engineers at Caltrans, admissible values of the diameter of a bridge column, with regard to the availability of existing prefabricated formwork used in bridge construction, range from 1.2 m (4 ft) to 2.4 m (8 ft) in

increments of 152 mm (6 in) depending on the bridge span and/or number of columns per bent in an OSB. Practical values of the longitudinal steel reinforcement ratio, although a continuous variable, range from 0.01 (1.0 %) to 0.03 (3.0 %) in increments of 0.005 (0.5 %). The primary design space of each testbed OSB considered is hence defined as a two-dimensional regular grid of possible design points (see Figure 5.9). It is noted that in defining the primary design space for each testbed OSB, the minimum value of D_{col} is selected such that localization or softening behavior (leading to loss of objectivity in strain prediction (Coleman and Spacone 2001)) is not observed for RC column sections with low expected axial load ratios (typically less than 15% under combined gravity and earthquake loading) which are characteristic of OSBs in California.

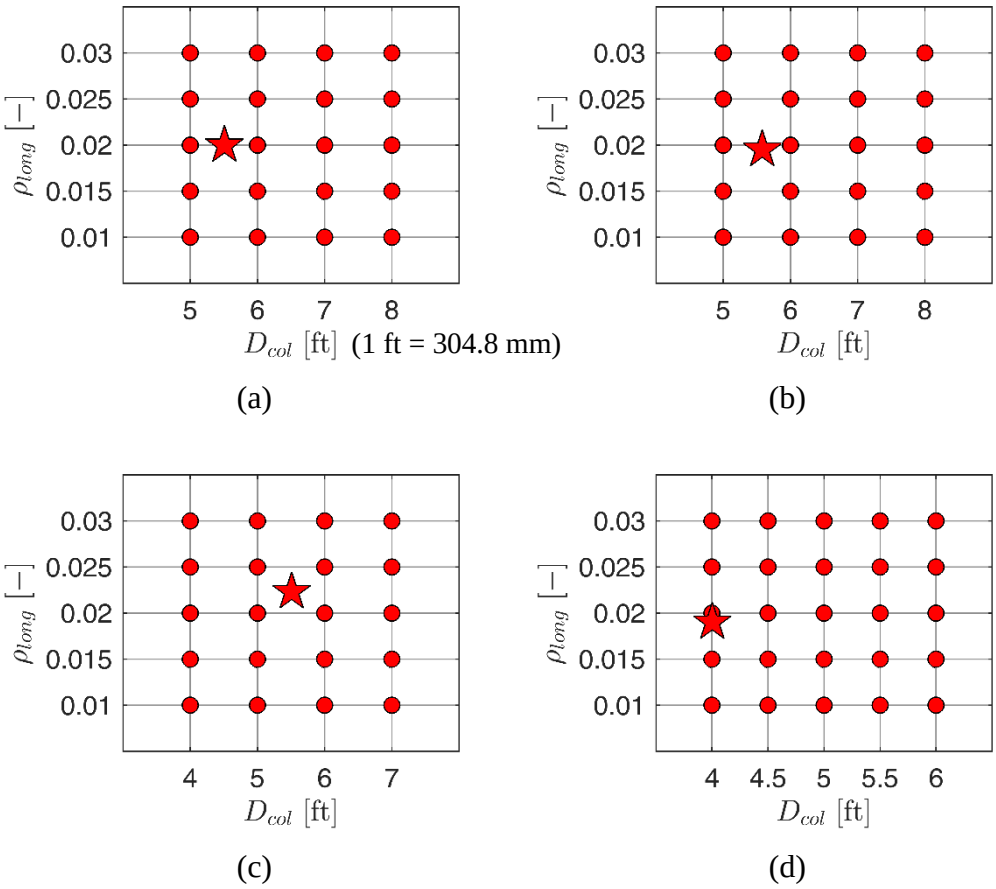

Figure 5.9 Primary design space for (a) Bridge A, (b) Bridge B, (c) Bridge C, and (d) Bridge MAOC (red stars indicate the as-designed testbed OSBs, red circles indicate considered re-designs of the testbed OSBs); (1 ft = 304.8 mm)

All other bridge design parameters, i.e., (i) parameters whose values are obtained after determining the values of the primary design variables, to meet the requirements of capacity design, minimum ductility capacity, code-based reinforcement ratio restrictions, etc., and (ii) those restricted by the geometry of the bridge, available real estate, traffic requirements, etc., are grouped into the category of secondary design variables. A non-exhaustive list of such variables includes the column transverse reinforcement ratio (ρ_{trans}), spacing of transverse hoops in a column, diameter and distribution of longitudinal bars in a column, height of a column, number of columns in a bent, skew of column bent(s), number of bents, variables involving the design of the bridge

deck, bent caps, abutments, abutment shear keys, backwall, foundations, etc. In the parametric study of the four testbed OSBs, values of the respective secondary design variables are taken as per the original designs of the testbed OSBs, except for ρ_{trans}. The value of ρ_{trans} is expressed as a practical fraction of ρ_{long}, i.e., $\rho_{trans} = 0.5\rho_{long}$, which has been found to ensure stable post-peak response of longitudinal reinforcement bars (Duck et al. 2018).

5.5.2 Overall Workflow and Computational Framework

For each design point in the primary design space of an OSB, a full-fledged seismic performance assessment, involving PSHA, ground motion selection (GMS), ensembles of nonlinear time-history analyses (NLTHA), PSDemHA, and PSDamHA, is carried out using the updated version of the PEER PBEE framework (see Figure 5.10) to arrive at estimates of the MRP of exceedances of the selected set of *LS*s. The mean RPs of exceedances for the considered *LS*s computed for all the re-designs of an OSB are then used to construct three (one for each *LS*) piecewise linearly interpolated surfaces for MRPs over a triangulation of the regular grid of design points (see Figure 5.10) defining the OSB's primary design space.

To seamlessly execute the above mentioned analytical steps of PSHA, GMS, NLTHA, PSDemHA, and PSDamHA for the given choice of *IM*, the considered set of *LS*s and their associated *EDP*s pertaining to a testbed OSB, a fully-automated, open-source, object-oriented, cross-platform compatible Python package, named PyPBEE (PBEE for Python) was developed (Deb et al. 2021a). The above-mentioned analytical steps are prototyped as analysis classes in the form of Python modules in PyPBEE. Moreover, PyPBEE admits modular class definitions of the key variables (i.e., *IM*, *EDP*s, and *LS*s) involved in the different analytical steps and of the type of structure (e.g., the OSB) to be analyzed. Figure 5.11 shows a schematic Unified Modeling

Language (UML) diagram describing the relationship between the objects of the classes involved in PyPBEE. It is noted that, although integrally composed of the analysis classes (shown in blue in Figure 5.11), PyPBEE is designed to readily accommodate alternative and more refined definitions of modules for an OSB (or any structure), an *IM*, and the set of *LS*s and their associated *EDP*s which are intended to be placeholder classes (shown in yellow in Figure 5.11).

A full-fledged seismic performance evaluation of an OSB over its primary design parameter space involves sequential execution of the different analysis modules. However, each module consists of several mutually independent embarrassingly parallelizable jobs (e.g., PSHA for each design point, GMS for each seismic hazard level at each design point, NLTHA for each ground motion in an ensemble selected for each hazard level at each design point, etc.). Parallelization of such tasks is achieved using multiprocessing in Python. It is noteworthy to mention here that for the sizable number of NLTHAs carried out for the performance assessment of each of the re-designs of the considered testbed OSBs, all non-collapse related numerical convergence issues encountered are resolved in an automated fashion (using built-in functionalities of the NLTHA module in PyPBEE) via adaptive switching between iterative methods (e.g., Newton line search, modified-Newton, BFGS, Newton-Krylov), convergence test types, and the convergence tolerance used to incrementally solve the nonlinear equations of motion. The exceedingly large number of NLTHAs to be performed necessitates the extensive use of high-performance computing (HPC) resources made available through Stampede2, the flagship supercomputer at the University of Texas at Austin's Texas Advanced Computing Center (TACC). This is easily achieved using the cross-platform capabilities of PyPBEE which allows for an equally efficient execution of the workflow in both desktop computing and supercomputing environments.

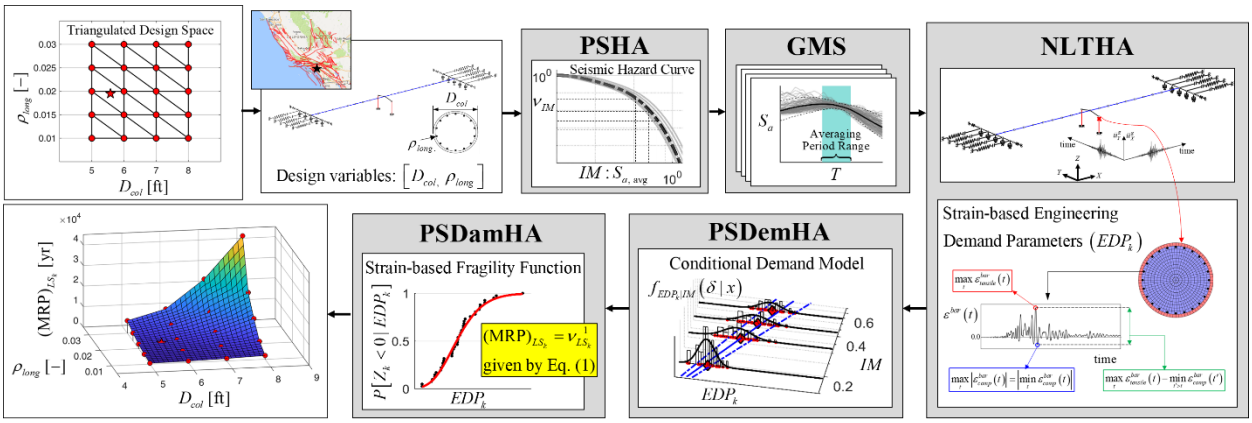

Figure 5.10 Overall workflow for parametric probabilistic seismic performance assessment

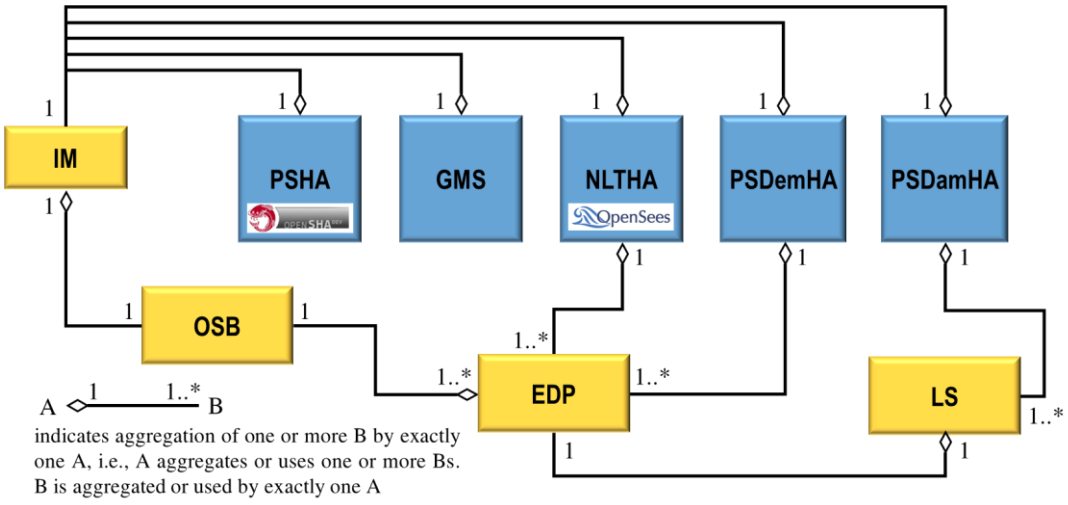

Figure 5.11 Schematic Unified Modeling Language (UML) diagram of PyPBEE

5.5.3 Feasible Design Domains

For each *LS* considered, a piecewise linearly interpolated surface for the MRP of exceedance is constructed using the computed MRPs over a triangulated regular grid representing the primary design space of an OSB (see Figure 5.12). Although the overall topologies of the MRP surfaces over the primary design parameter space are accurate, some topology details are by-products of the type of interpolation performed (here piecewise linear). It is important to notice that the MRP of *LS* exceedance results obtained for the as-designed bridges, in each case, are in

excellent agreement with the topology of the piecewise linearly interpolated MRP surfaces despite being excluded from the data used for constructing these surfaces. It is also observed that increasing the values of the two primary design variables result in stronger and safer designs characterized by lower MARs or higher MRPs of *LS* exceedances. From the topologies of the MRP surfaces, the MRPs of exceeding the considered set of *LS*s, pertaining to the seismic design of OSBs, are found to be indeed sensitive to the chosen primary design variables thereby justifying their choice.

The MRP surfaces for the considered set of *LS*s are intersected by horizontal planes (see Figure 5.12) corresponding to respective specified target MRPs listed in Table 5.3. The target values of MRPs of *LS* exceedances are based on discussions with and feedback from Caltrans expert bridge engineers, thereby reflecting the current risk tolerance of the bridge engineering community in general. An *LS*-specific feasible design domain, i.e., a collection of design points in the two-dimensional primary design parameter space of an OSB with MRPs of exceeding the considered *LS* higher than or equal to the specified target MRP, is computed through the full-fledged parametric probabilistic seismic performance assessment framework. Such domains corresponding to each *LS* are superimposed in the primary design parameter space of a bridge to delineate the overall feasible design domain (see Figure 5.12). This also helps identify the governing *LS*s along the boundary of the feasible design domain.

Table 5.3 Target MRPs of LS exceedance

Limit-state	***Target MRP of exceedance (years)***
1. Concrete cover spalling	225
2. Longitudinal bar buckling	1000
3. Longitudinal bar fracture	2500

The seismic performance of the as-designed version of a testbed bridge is gauged by the location of the corresponding design point in the design parameter space relative to the overall feasible design domain of the bridge (i.e., does the as-designed bridge belong to the feasible design domain and how close is it from its boundary?). The seismic performance of the as-designed testbed bridges is found to show considerable variability. These bridges originally designed following a more traditional (prescriptive) seismic design philosophy, rather than an explicitly performance-based one, are found to exhibit erratic levels of conservativeness. While some of the as-designed testbed bridges are found to be conservative (Bridges B and C), sometimes too much (e.g., Bridge C), with respect to the selected *LS*s and corresponding target MRPs, others are found to lie near the borderline of safety (e.g., Bridge A), or clearly in the unsafe domain (e.g., Bridge MAOC).

The concept of a feasible design domain in the design parameter space can be utilized to make risk-informed design decisions while trying to satisfy multiple risk-targeted objectives. Values of primary design variables are first selected such that multiple risk-targeted performance objectives are met. This involves selection of a physically realizable design point (i.e., satisfying practical constraints reflecting design/construction practice) in the primary design parameter space either lying on the boundary of, or inside and in the vicinity of the boundary of, the feasible design

domain. Upon selection of the primary design variables, the secondary design variables are to be determined and adjusted to meet requirements of capacity design, code-based minimum ductility capacity and minimum reinforcement, etc., and/or other restrictions imposed by the real estate available, traffic flow, etc. In this regard, knowledge of the feasible design domain of an OSB in its design space emerges as an extremely valuable resource in the context of a design process to be carried out in stages as it can be utilized to make risk-informed adjustments, if required, of the primary design variables. After all primary and secondary design variables have been determined, a final check of structural performance is required to ensure that the final design still satisfies the specified risk-targeted performance objectives.

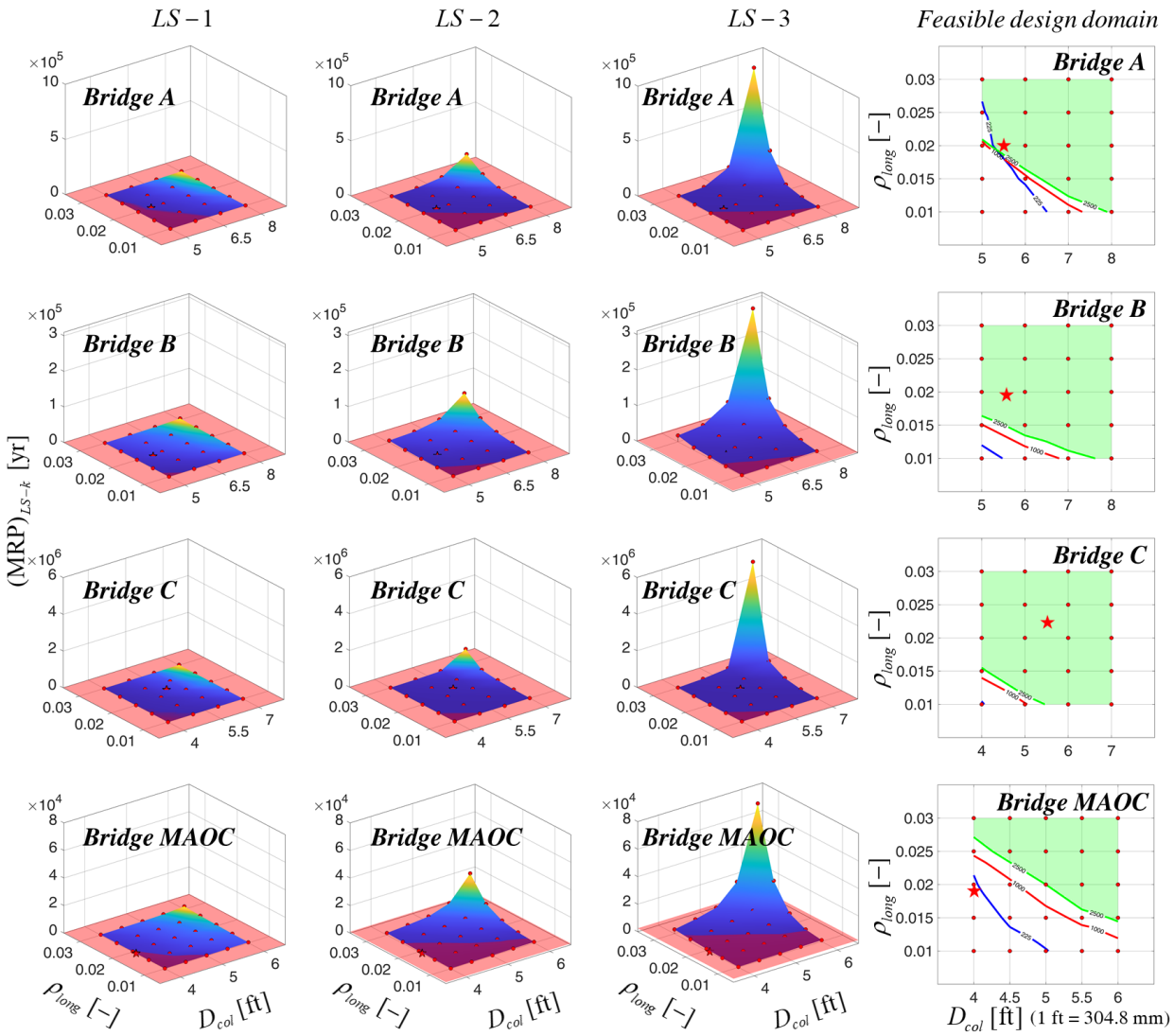

Figure 5.12 Piecewise linearly interpolated MRP surfaces and feasible design domains (green shaded region) for the considered testbed OSBs. The target MRP contour lines for *LSs* 1, 2, and 3 are shown in blue, red, and green, respectively. The as-designed testbed OSB is shown as a red star; (1 ft = 304.8 mm).

5.5.4 Sensitivity of Feasible Design Domains to Column Transverse Reinforcement Ratio

The categorization of an important column design parameter, the transverse reinforcement ratio (ρ_{trans}), for columns with low expected axial load ratios (say less than 15% under combined gravity and earthquake loading) which is typical of OSBs, as a secondary design variable is

investigated next. A sensitivity analysis is conducted by repeating the performance evaluations over the primary design parameter space of a bridge for two additional values of ρ_{trans}, with the three levels of ρ_{trans} considered, i.e., Case I: $\rho_{trans} = 0.5\rho_{long}$, Case II: $\rho_{trans} = 0.01$, and Case III: $\rho_{trans} = 0.75\rho_{long}$, spanning a practical range of column transverse reinforcement ratio in bridge seismic design practice.

To facilitate a simple, yet reasonably accurate, comparative study of Cases I through III, the analytical steps of the PBEE framework up to PSDemHA already carried out with $\rho_{trans} = 0.5\rho_{long}$ are not repeated for the other two values of ρ_{trans}. The rationale behind this being that for columns with low expected axial load ratios, and for the type of nonlinear FE modeling technique employed in this study (i.e., the use of Euler-Bernoulli beam-column elements with nonlinear fiber-sections to model bridge columns), the value of ρ_{trans} minimally affects the compressive strength of the core concrete fibers, thereby only marginally impacting the seismic demand hazard assessment of OSBs. However, because ρ_{trans} effects the prediction of the capacity of bridge columns corresponding to *LS*s 2 and 3 (i.e., incipient bar buckling and precursor stage of bar fracture, see Eq.s (4.13) and (4.14)), the sensitivity analysis performed with respect to ρ_{trans} involves recomputing the final step, i.e., PSDamHA, wherein Eq.s (4.13) and (4.14) are used to denormalize the respective fragility functions needed in the computation of the MRP of exceedance for *LS*s 2 and 3.

The feasible design domains obtained for the two additional values of ρ_{trans} for each testbed OSB are shown in Figure 5.13. It is noted that the extent to which these new feasible design domains for an OSB differ from the corresponding originally obtained feasible design domain (for $\rho_{trans} = 0.5\rho_{long}$) is noticeable. However, the overall shape of the feasible design domains and the

feasibility of the re-design points remain comparable. The observed level of sensitivity of the performance evaluation results with respect to ρ_{trans} does bring out the importance of ρ_{trans} in the context of seismic design of bridge columns. Hence, a smart and practical initial choice of this rather critical secondary design variable (like the one chosen in this study, i.e., $\rho_{trans} = 0.5\rho_{long}$) is essential as the primary design variables are being determined. As far as ductility requirements impacted by ρ_{trans} are concerned, the designer can check whether these requirements are met after the primary design variables have been determined and adjust accordingly the value of ρ_{trans} to meet these criteria.

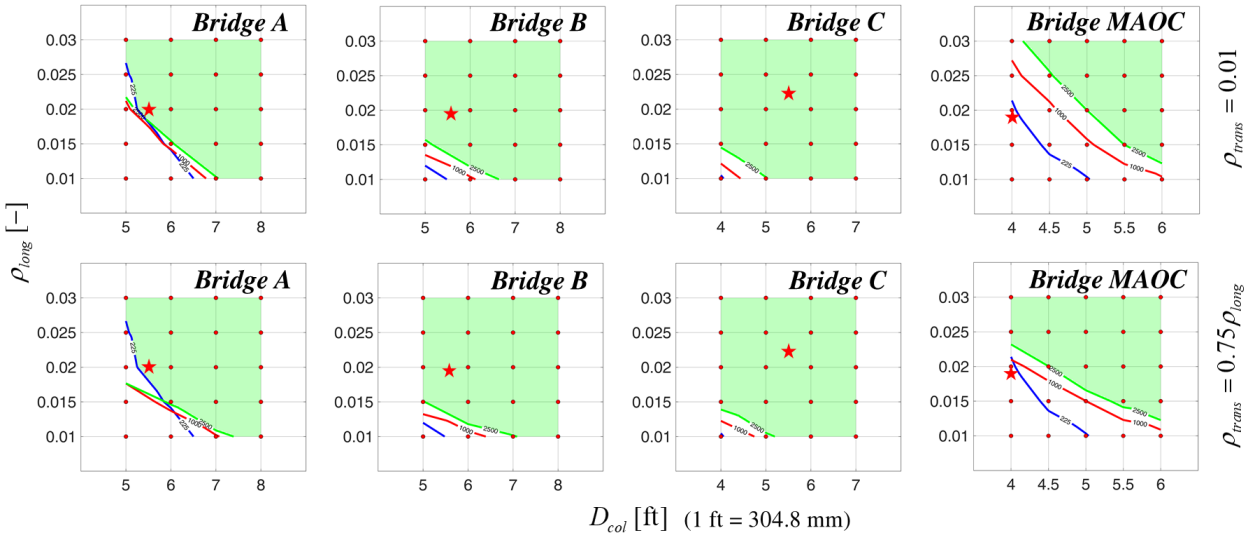

Figure 5.13 Feasible design domains for $\rho_{trans} = 0.01$ (1st row) and $\rho_{trans} = 0.75\rho_{long}$ (2nd row)

5.5.5 Accuracy of Closed-form Solutions to Damage Hazard

In an attempt to provide a PBSD format similar to that of Load and Resistance Factor Design (LRFD), closed-form solutions (CFSs) have been derived for the MAR (or the MRP) of exceedance of an *LS*. A comparative study is conducted between feasible design domains obtained using CFSs to the MRP of *LS* exceedances, available in the literature, and the one obtained

numerically via the full-fledged probabilistic performance assessment method used herein. This is done to assess the potential viability of LRFD-like design formats based on such CFSs to be used as the sought PBSD methodology. Two such CFSs proposed by Cornell et al. (2002) and Vamvatsikos (2013), referred to as CFS-1 and CFS-2, respectively, are used for this purpose. These CFSs hold under a set of restrictive (idealized) assumptions, i.e., (1) the seismic hazard curve is assumed to be either linear (Cornell et al. 2002) or quadratic (Vamvatsikos 2013) in logarithmic space, (2) the *EDP*s are assumed to be lognormally distributed when conditioned on *IM*, (3) the median of an *EDP* conditional on *IM* is assumed to have a power-law form, (4) the dispersion (standard deviation in logarithmic space) of an *EDP* conditional on *IM* is assumed to be constant, and (5) the structural capacity associated with an *LS* is assumed to follow a lognormal distribution. The feasible design domains obtained using CFS-1 and CFS-2 for each testbed OSB considered herein and for $\rho_{trans} = 0.5\rho_{long}$ are shown in Figure 5.14.

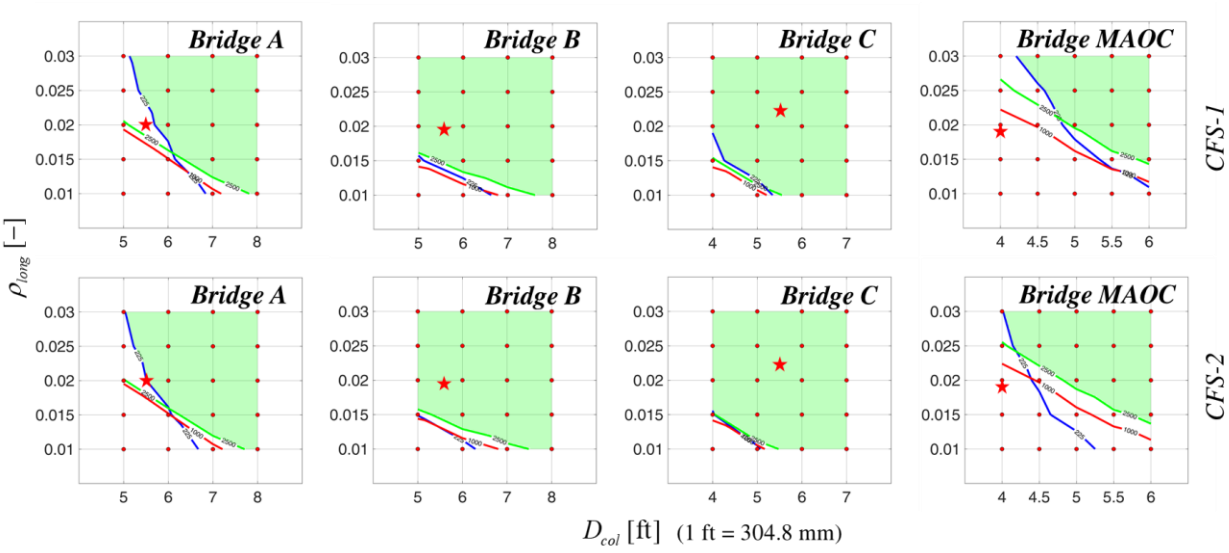

Figure 5.14 Feasible design domains obtained using CFS-1 (1st row) and CFS-2 (2nd row)

As observed by comparing Figure 5.14, the feasible design domains for the testbed OSBs obtained using CFS-2 match the corresponding numerically obtained feasible design domains

better than those obtained using CFS-1. This is attributed to the fact that CFS-2 approximates the seismic hazard curve more accurately as compared to CFS-1. However, both CFSs-1 and -2 can lead to considerable errors in the estimation of the feasible design domains and the identification of the governing *LS*s along the boundary of the feasible design domains. It is also noted that the use of CFSs does not alleviate the computational expense associated with the most expensive step of running ensemble NLTHAs for a bridge, albeit circumventing the rather inexpensive numerical evaluation of the demand and damage hazard integrals. Moreover, the results obtained using such simplified CFSs, that require going through almost the same rigmarole as that in the numerical full-fledged method, are often inaccurate by a significant margin.

5.6 Conclusions

Erratic levels of safety exhibited by a set of distinct as-designed representative California OSB testbeds illustrates the need for a PBSD framework for OSBs such that explicitly stated risk-targeted performance objectives are consistently satisfied by the population of OSBs in California. The formulation (assembly) and software implementation of a rigorous framework for risk-targeted PBSD of OSBs is presented in this paper. The proposed design methodology is a two-stage procedure with the first-stage involving the design of the bridge columns and the second-stage the determination of other design variables (e.g., the ones not restricted by the geometry of the bridge, available real estate, traffic flow requirements, etc.) so as to meet code-based requirements of capacity design (to limit the number and locations of damage and failure mechanisms), minimum ductility limitations, reinforcement ratio restrictions, etc. The end-product of this design framework are regions of safety and/or feasibility, referred to as feasible design domains, over a two-dimensional design space of primary design variables pertaining to the

seismic design of bridge columns. Knowledge of the feasible design domain of an OSB in its design space emerges as an extremely valuable resource in the context of a design process to be carried out in stages as it can be utilized to make risk-informed adjustments, if and when required, of the primary design variables while ensuring the satisfaction of multiple risk-based performance objectives, and thus leading to safe and economic design of OSBs.

The PBSD framework presented in this paper is currently being extended via incorporation of finite element model parameter uncertainty and probability distribution parameter estimation uncertainty as additional pertinent sources of aleatoric and epistemic uncertainty. A comprehensive evaluation of the significance of these commonly neglected sources of uncertainty in the seismic performance assessment and PBSD of OSBs will be the subject of an upcoming paper.

The set of three *LS*s defined and considered herein for the development of the proposed PBSD methodology for OSBs is neither exhaustive nor definitive. The proposed methodology and the supporting software/computational framework are developed with *LS* definitions as mere placeholders and is readily able to accommodate more refined (e.g., more mechanics-based) definitions and/or a larger number of *LS*s.

The seismic performance measure selected in this study is the MRP of *LS* exceedance. This can be taken one step further by defining performance measures in terms of the hazard associated with the exceedance of specific values of decision variables, e.g., monetary loss, downtime, deaths, etc., which are more meaningful to stakeholders and/or decision makers (e.g., government officials).

The proposed PBSD methodology is formulated by retaining the inherent rigor of the PEER PBEE framework lying at its crux. The implementation of this framework in a practical design

environment may seem computationally overpriced. In this regard, efforts can be channeled to distill out of this comprehensive study, without significantly compromising its rigor, a simplified, computationally economical, and sufficiently accurate PBSD methodology for OSBs following either a more traditional design format requiring LRFD-like checks of structural demand-to-capacity ratios or a new unconventional design format.

The proposed PBSD method recommends determining most secondary design variables, upon sizing of the primary design variables, to meet code-based requirements of capacity design, minimum ductility limitations, reinforcement ratio restrictions, etc. These requirements typically involve the use of prescriptive measures and/or safety factors such that undesirable consequences are prevented with some level of confidence. Empirical observations, experience and/or engineering judgment have dictated the prescription of such measures and safety factors in codes of practice. Future research can be directed towards developing a more transparent and more probabilistically explicit determination of these secondary design variables. Finally, extension of the proposed framework for PBSD of OSBs to accommodate larger and more complicated bridge structures involving a higher-dimensional primary design parameter space can be the subject of future research.

5.7 Acknowledgements

Support of this research by the California Department of Transportation under Grand No. 65A0594, Task No. 2880 is gratefully acknowledged. The authors wish to thank the following individuals for their help and insightful discussions related to the work presented in this paper: Messrs. M. Mahan, T. Ostrom, A. Shamsabadi, T. Shantz, and C. Sikorsky from the Engineering Division at Caltrans, along with Dr. Frank McKenna at UC Berkeley for help with HPC and

OpenSees. The authors also acknowledge the Texas Advanced Computing Center (TACC) at The University of Texas at Austin (http://www.tacc.utexas.edu) for providing HPC resources that have contributed to the research results reported within this paper. Chapter 5, in full, has been submitted for publication of the material as it may appear in the following paper (the dissertation author is the first author of this paper):

Deb, A., Zha, A. L., Caamaño-Withall, Z. A., Conte, J. P., Restrepo, J. I. (2021). "Framework for risk-targeted performance-based seismic design of ordinary standard bridges." Submitted to *Journal of Structural Engineering*

6 Simplified Risk-targeted Performance-based Seismic Design Method for Ordinary Standard Bridges

6.1 Abstract

This paper presents the formulation of a comprehensive risk-targeted performance-based seismic design (PBSD) framework involving the seismic design of bridge piers for California Ordinary Standard Bridges (OSBs) facilitating risk-informed design and decision making in the face of uncertainty. A full-fledged implementation of this all-inclusive design method formulated by retaining the inherent rigor of the underlying seismic performance assessment methodology might impose a seemingly prohibitive computational cost for the available resources in the current scenario of seismic bridge design practice. For reasons of practicability, the findings of the full-fledged design framework are inventively utilized to distill out a computationally more economical and simplified PBSD procedure and its efficacy is validated using four real-world California testbed OSBs as cases in point. The proposed simplified design methodology is able to (1) find a design point in the primary design parameter space of a bridge being designed for multiple risk-targeted performance objectives, and (2) delineate an approximate, yet sufficiently accurate, feasible design domain and identify the limit-states controlling its boundary in the primary design parameter space of the bridge, at a computational cost significantly lower than that of the original method.

6.2 Introduction

Current practice of seismic design for ordinary or conventional reinforced concrete (RC) bridges primarily includes two design methodologies. The first is a force-based approach incorporated into the American Association of State Highway and Transportation Officials (AASHTO) LRFD Bridge Design Specifications (AASHTO 2012), while the second is a displacement-based approach on which the AASHTO Guide Specifications for Seismic Bridge Design (AASHTO 2011) is predicated. The force-based approach, with capacity design as its underlying philosophy, relies on designing specific structural components of the bridge to dissipate energy by way of yielding when subjected to an earthquake. The imposed seismic force demands are calculated corresponding to a design ground motion (with a probability of exceedance of 5% in 50 years or 1000-year mean return period (MRP)). While adequate detailing is provided at the locations of yielding to get desired inelastic action through ductility, all other structural members are capacity-protected to ensure linear elastic behavior. The displacement-based approach differs from its force-based counterpart in that it involves a direct check of the displacement capacity of the primary lateral load resisting system (i.e., bridge column bents). Still rooted in capacity design philosophy, this approach first involves the selection of a trial design for a column bent that is detailed for suitable inelastic action and ductility. This is followed by a direct check of the displacement capacity of the trial design via nonlinear static pushover analysis of the column bent. The system displacement capacity is controlled by material fibers reaching or exceeding prescribed strain limits corresponding to different damage limit-states (*LS*s). The inelastic displacement capacity is then compared to the displacement demand (determined either from equivalent static analysis or from elastic dynamic analysis) generated due to the action of the design earthquake (with a probability of exceedance of 5% in 50 years or 1000-year return period).

In addition to an inaccurate account of pertinent uncertainties by merely considering an incomplete probabilistic description of the input seismic hazard in both design approaches, the force-based approach has the added disadvantage of assuming that the satisfaction of prescriptive code-based requirements will ensure desired bridge performance without any direct check of system level seismic response/behavior. The displacement-based approach has the merit of a quantitative check of displacement capacity and is welcoming of the definition of displacement-based *LS*s of interest and their intended satisfaction, thus bringing in the notion of explicit statements of structural performance objectives. However, structural performance evaluation in the displacement-based approach is assumed to be void of uncertainties and the satisfaction of prescriptive measures based on laboratory tests, simplified analytical models, and engineering judgment are subjectively assumed to translate to satisfactory system behavior. Moreover, metrics of structural performance being specific to the profession and not risk-targeted, do not allow the public/stakeholders to participate in risk-informed decision making

Risk-targeted performance-based seismic design (PBSD) therefore emerges as the most scientific and promising design methodology and is expected to provide the foundation for future design codes (Cornell 2000; Ellingwood 2008; NCHRP 2013). It involves designing a structure to meet more refined and non-traditional performance objectives explicitly stated in terms of the risk (or the probability in a specified exposure time) associated with the exceedance of critical *LS*s or certain tolerable thresholds of monetary loss, downtime, etc. The recent advent of performance-based earthquake engineering (PBEE) and its culmination in the form of the fully probabilistic, rigorous and advanced assessment framework (Moehle and Deierlein 2004; Porter 2003) developed under the auspices of the Pacific Earthquake Engineering Research (PEER) Center, not only provides technical support for this intended shift of design philosophy, but also brings about

a novel way to tailor structural design to meet the societal risk tolerance. Although not in its all-inclusive and rigorous form, PBEE has already started to find its footing in both spheres of seismic design of buildings and bridges (Buckle et al. 2006; Cornell et al. 2002; Franchin et al. 2018; Hamburger 2006; Mackie and Stojadinović 2007; Saini and Saiidi 2014), albeit the latter has seen relatively less advancement as compared to the former (NCHRP 2013).

Building on this comprehensive probabilistic framework integrating site-specific seismic hazard analysis, structural demand analysis and damage analysis, while keeping loss analysis outside the scope of this study, a PBSD framework involving the design of the bridge columns, the primary lateral load resisting component of Ordinary Standard Bridges (OSBs) (Caltrans 2013), was recently proposed by the authors (Deb et al. 2021b). According to this framework, a primary design space is first defined for an OSB in terms of column design parameters to which the sought metrics of structural performance, i.e., the MRPs of exceedances of a selected set of *LS*s, are believed to be most sensitive. Probabilistic performance-based assessments of parametrically redesigned versions of an OSB are then carried out to obtain regions of safety and/or feasibility with respect to multiple risk-targeted performance objectives, referred to as feasible design domains, delineated over the primary design space of the bridge. Upon selection of a physically realizable DP (subject to practical constraints reflecting design/construction practice) in the primary design parameter space either lying on the boundary of, or inside and in the vicinity of the boundary of, the feasible design domain, other bridge design variables are to be determined and adjusted to meet requirements of capacity design, code-based minimum ductility capacity and minimum reinforcement, etc., and/or other restrictions imposed by the real estate available, traffic flow, etc. In this regard, knowledge of the feasible design domain of an OSB in its design space emerges as an extremely valuable resource in the context of a design process to be carried out in

stages as it can be utilized to make risk-informed adjustments, if required, of the primary design variables.

The full-fledged PBSD framework can be very well used for the seismic design of OSBs unless, owing to its all-inclusive nature and pressing computational requirements, it imposes a computational cost that is prohibitive for the computational resources available. For reasons of practicability, the findings of the full-fledged design framework are inventively utilized to distill out a computationally more economical and simplified risk-targeted PBSD procedure and its efficacy is validated using four real-world California testbed OSBs as cases in point. The proposed simplified design methodology is able to: (i) find a DP in the primary design parameter space of a bridge being designed for multiple risk-targeted performance objectives; and (ii) delineate an approximate, yet sufficiently accurate, feasible design domain and identify the *LS*s controlling its boundary in the primary design parameter space of the bridge, at a computational cost significantly lower than that of the full-fledged method.

6.3 Testbed Bridges and Computational Models

OSBs are conventional, multiple-span, short (span length less than 91.4 m or 300 ft) and, in general, skewed reinforced concrete (RC) bridges with single superstructures emulating a cast-in-place continuous structure and supported on soils which may or may not be susceptible to liquefaction and/or scour (Caltrans 2013). These are the most common bridges in California designed in-house by the California Department of Transportation. Several testbed OSBs located in regions with disparate levels of seismicity in California are selected for this study in order to cover a range of realistic design situations for OSBs and ensure that the parametric probabilistic performance-based assessment framework formulated herein is general within its scope and is

applicable to the gamut of design situations representative of the population of OSBs in California. Four existing California OSBs (Figure 5.1), namely Bridge A, Bridge B, Bridge C and Bridge MAOC, are chosen for this purpose. These OSBs have been studied extensively in recent research projects (Kaviani et al. 2012; Omrani et al. 2015) and are representative of modern OSBs in California constructed between late 90's and early 2000s.

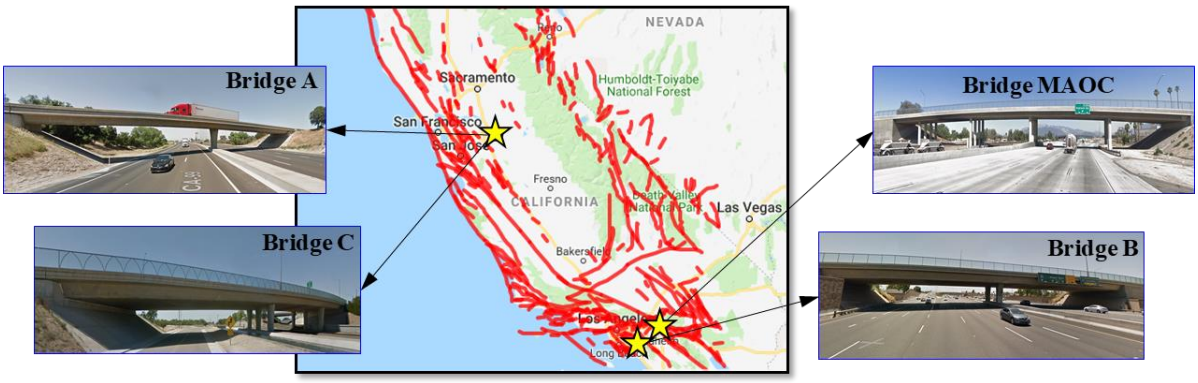

Figure 6.1 Location of testbed OSBs

Bridge A is the Jack Tone Road Overcrossing in Ripon, California consisting of two spans with a single column bent. Bridge B is the La Veta Avenue Overcrossing in Tustin, California also consisting of two spans but supported on a two-column bent. Bridge C is the Jack Tone Road Overhead in Ripon, California (located adjacent to Bridge A) consisting of three spans supported on two bents with three columns in each. Bridge MAOC, the Massachusetts Avenue Overcrossing located in San Bernardino, California consists of five spans supported on four bents each consisting of four columns. These bridges primarily consist of prestressed concrete box-girder decks supported by column-bent(s) on pile foundations and seat-type abutments also on pile foundations.

Three-dimensional nonlinear finite element (FE) models (consisting of nonlinear fiber-section beam-column elements and nonlinear springs) of these bridges are constructed (Deb et al. 2018, 2021a) in OpenSees (Mazzoni et al. 2006), the open-source FE analysis software framework

developed at PEER. A schematic representation of the computational model of one of the four testbed OSBs (Bridge C) is shown in Figure 5.2.

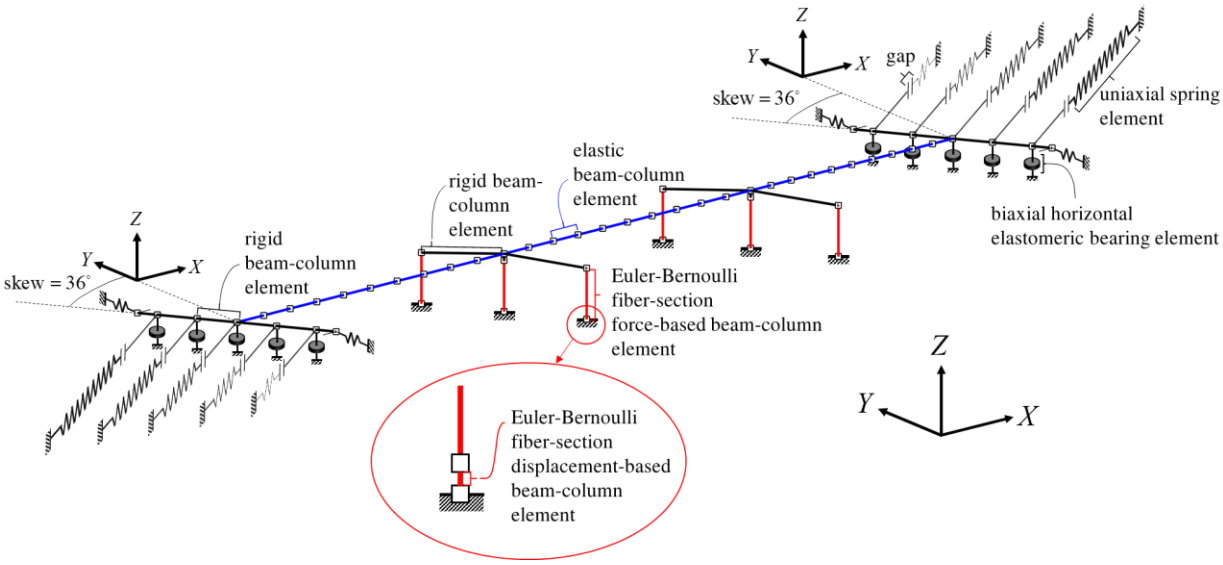

Figure 6.2 Schematic representation of the FE model of Bridge C

6.4 Forward Probabilistic Performance Assessment

6.4.1 PEER PBEE Framework Integral

Metrics of structural performance considered in this study are the mean annual rates (MARs), or equivalently the MRPs, of exceedances for a selected set of practical *LS*s, which according to the PEER PBEE methodology are given by:

$$\nu_{LS_k} = \int_{IM} \int_{EDP_k} P\left[Z_k < 0 \,|\, EDP_k = \delta\right] \cdot f_{EDP_k|IM}\left(\delta \,|\, x\right) \cdot d\delta \cdot \left|d\nu_{IM}(x)\right| \tag{6.1}$$

where $P[Z_k < 0 \,|\, EDP_k = \delta]$ is the fragility function expressing the conditional probability of exceedance of *LS k* (i.e., safety margin $Z_k = C_k - EDP_k < 0$ where C_k is the structural capacity associated with LS_k and EDP_k is the associated engineering demand parameter) given a specific

value δ of EDP_k, $f_{EDP_k|IM}(\delta \mid x)$ is the conditional probability distribution of EDP_k given a specific value *x* of the intensity measure (*IM*), and $\nu_{IM}(x)$ is the MAR of *IM* exceeding the specific value *x*.

6.4.2 Improvement of PEER PBEE Assessment Framework

Novelties and improvements from state-of-the-art literature related to the individual steps of the PEER PBEE assessment methodology are incorporated in this study (Deb et al. 2021a). These improvements/updates include:

(i) inclusion of an improved *IM*, i.e., average spectral acceleration over a period range (Baker and Cornell 2006; Kohrangi et al. 2016),

(ii) conditional mean spectrum (CMS)-based site-specific risk-consistent ground motion selection (Jayaram et al. 2011; Kohrangi et al. 2017) (100 ground motions per hazard level for six seismic hazard levels corresponding to MRPs of *IM* exceedances equal to 72, 224, 475, 975, 2475, and 4975 years, respectively) for ensemble nonlinear response-history analyses

(iii) introduction of material strain-based EDPs (see Table 5.1) associated with practical material strain-based *LS*s related to the desirable (targeted) failure mode concerning RC bridge columns (i.e., flexural hinging of columns), namely (1) concrete cover spalling, (2) initiation (onset) of longitudinal bar buckling, and (3) initiation (onset) of longitudinal bar fracture post-buckling

(iv) identification of experimental test programs and numerical studies (Duck et al. 2018; Goodnight et al. 2015; Murcia-Delso et al. 2013; Schoettler et al. 2015; Trejo et al. 2014) providing reliable data for the development of strain-based normalized fragility functions

for the considered *LS*s. Fragility functions for *LS*s 1 through 3, are normalized using appropriate deterministic capacity prediction equations (Duck et al. 2018; Goodnight et al. 2016) (listed in Table 5.2). Normalized fragility functions for *LS*s 1 through 3 are shown in Figure 5.8.

Table 6.1 *LS*s and associated strain-based *EDP*s

LS #	***Associated Engineering Demand Parameter (EDP)***	
1	Maximum absolute compressive strain of any longitudinal bar in any column.	$\max_{col}\left(\max_{bar}\left(\max_{t}\left\|\varepsilon_{comp}^{bar}(t)\right\|\right)\right)$
2	Maximum tensile strain of any longitudinal bar in any column.	$\max_{col}\left(\max_{bar}\left(\max_{t}\varepsilon_{tensile}^{bar}(t)\right)\right)$
3	Maximum strain range/excursion (i.e., difference of maximum tensile and minimum compressive strain, the latter following the former) of any longitudinal bar in any column	$\max_{col}\left(\max_{bar}\left(\max_{t}\varepsilon_{tensile}^{bar}(t)-\min_{t'>t}\varepsilon_{comp}^{bar}(t')\right)\right)$

Table 6.2 Deterministic predictive capacity models for the considered *LS*s

LS #	***Predictive Capacity Model***	
1	$EDP_{C_1}^{\text{PRED}} = 0.004$	(6.2)
2	$EDP_{C_2}^{\text{PRED}} = 0.03 + 700\rho_{trans}\frac{f_{yhe}}{E_s} - 0.1\frac{P}{f'_{ce}A_g}$	(6.3)
3	$EPD_{C_3}^{\text{PRED}} = 0.11 + \min(0.054,\ 3.2\rho_{trans}) - 0.0175\left\|\left(\sqrt[3]{n_{bar}} - 2.93\right)\right\| - 0.054\frac{T}{Y}$	(6.4)

In Eqs. (4.13) and (4.14), ρ_{trans} is the volumetric transverse reinforcement ratio, f_{yhe} is the expected yield stress of the transverse reinforcement, E_s is the elastic modulus of the transverse reinforcement, P is the axial load on the column (taken as the axial load due to gravity loads), f'_{ce} is the expected compressive yield stress of the unconfined concrete, A_g is the gross cross-sectional area of the column, n_{bar} is the number of bundles of longitudinal bars in a column, and $\frac{T}{Y}$, taken as 1.4 (Duck et al. 2018), is the ratio of the ultimate stress to the yield stress of the longitudinal steel reinforcement.

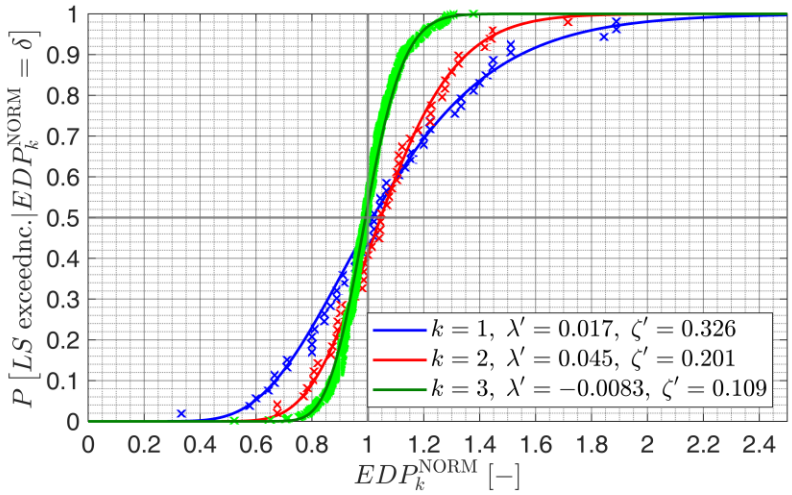

Figure 6.3 Normalized fragility curves (fitted experimental/numerical data shown as crosses)

6.5 Risk-targeted PBSD Methodology

In a recent study by the authors (Deb et al. 2021b), a two-stage design procedure was proposed with the first-stage involving the design of RC bridge columns, the primary lateral load resisting structural components of OSBs, followed by the determination of other design variables (e.g., the ones not restricted by the geometry of the bridge, available real estate, traffic flow requirements, etc.) so as to meet code-based requirements of capacity design (to limit the number

and locations of damage and failure mechanisms to be considered), minimum ductility limitations, reinforcement ratio restrictions, etc. This framework allows delineation of regions of safety and/or feasibility, referred to as feasible design domains, over a two-dimensional design space of primary design variables.

6.5.1 Primary and Secondary Design Variables

Design variables/parameters to which the exceedances of the selected set of *LS*s are believed to be most sensitive are referred to as primary design variables. These variables, revolving around the design of RC bridge columns and with readily alterable values from a design perspective, are: (i) the column diameter, D_{col}, and (ii) the column longitudinal reinforcement ratio, ρ_{long}. In defining an OSB's primary design space, practical constraints applicable to the values of the chosen primary design variables are considered. According to practicing engineers in Caltrans, admissible values of the diameter of a bridge column, with regard to the availability of existing prefabricated formwork used in bridge construction, range from 1.2 m (4 ft) to 2.4 m (8 ft) in increments of 15.24 cm (6 in) depending on the bridge span and/or number of columns per bent in an OSB. Practical values of the longitudinal steel reinforcement ratio, although a continuous variable, range from 0.01 (1.0 %) to 0.03 (3.0 %) in increments of 0.005 (0.5 %). The primary design space of each testbed OSB considered is hence defined as a two-dimensional regular grid of possible DPs (see Figure 5.9). It is noted that in defining the primary design space for each testbed OSB, the minimum value of D_{col} is selected such that localization or softening behavior (leading to loss of objectivity in strain prediction) is not observed for RC column sections with low expected axial load ratios (typically less than 15% under combined gravity and earthquake loading) which are characteristic of OSBs in California (Coleman and Spacone 2001).

All other bridge design parameters, viz., (i) parameters whose values are chosen after determining the values of primary design variables, to meet the requirements of capacity design, minimum ductility capacity, code-based reinforcement ratio restrictions, etc., and/or (ii) those restricted by the geometry of the bridge, available real estate, traffic requirements, etc., are grouped into the category of secondary design variables. A non-exhaustive list of such variables include column transverse reinforcement ratio (ρ_{trans}), spacing of transverse hoops in a column, diameter and distribution of longitudinal bars in a column, height of a column, number of columns in a bent, skew of column bent(s), number of bents, variables involving the design of bridge deck, bent cap, abutment shear keys, backwall, foundations, etc. In the parametric study of the four testbed OSBs, values of the respective secondary design variables are taken as per the original designs of the testbed OSBs, except for ρ_{trans}. The value of ρ_{trans} is expressed as a practical fraction of ρ_{long}, i.e., $\rho_{trans} = 0.5\rho_{long}$, which has been found to ensure stable post-peak response of longitudinal reinforcement bars (Duck et al. 2018)

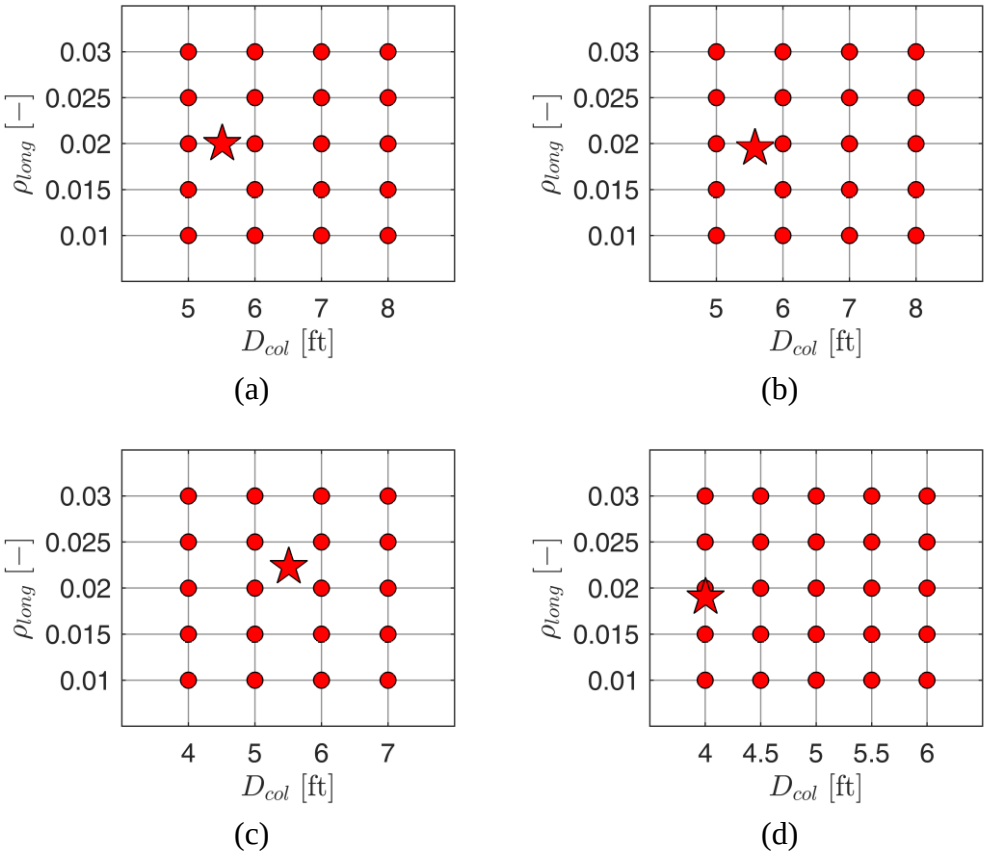

Figure 6.4 Primary design space for (a) Bridge A, (b) Bridge B, (c) Bridge C, and (d) Bridge MAOC (red stars indicate the as-designed testbed OSBs, red circles indicate considered re-designs of the testbed OSBs)

6.5.2 Overall Workflow for Full-fledged Parametric Forward PBEE Assessment

For each design point (DP) in the primary design space of an OSB, a full-fledged seismic performance assessment, involving probabilistic seismic hazard analysis (PSHA), ground motion selection (GMS), nonlinear time-history analyses (NLTHA), probabilistic seismic demand hazard analysis (PSDemHA), and probabilistic seismic damage hazard analysis (PSDamHA), is carried out (see Figure 5.10) using a fully-automated, open-source, object-oriented, cross-platform compatible Python package, named PyPBEE (PBEE for Python) (Deb et al. 2021a) to arrive at

estimates of the MRP of exceedances of the selected set of *LS*s. The exceedingly large number of NLTHA to be performed necessitates the extensive use of high-performance computing (HPC) resources made available through Stampede2, the flagship supercomputer at the University of Texas at Austin's Texas Advanced Computing Center (TACC). This is easily achieved using the cross-platform capabilities of PyPBEE which allows for an equally efficient execution of the workflow in both desktop computing and supercomputing environment.

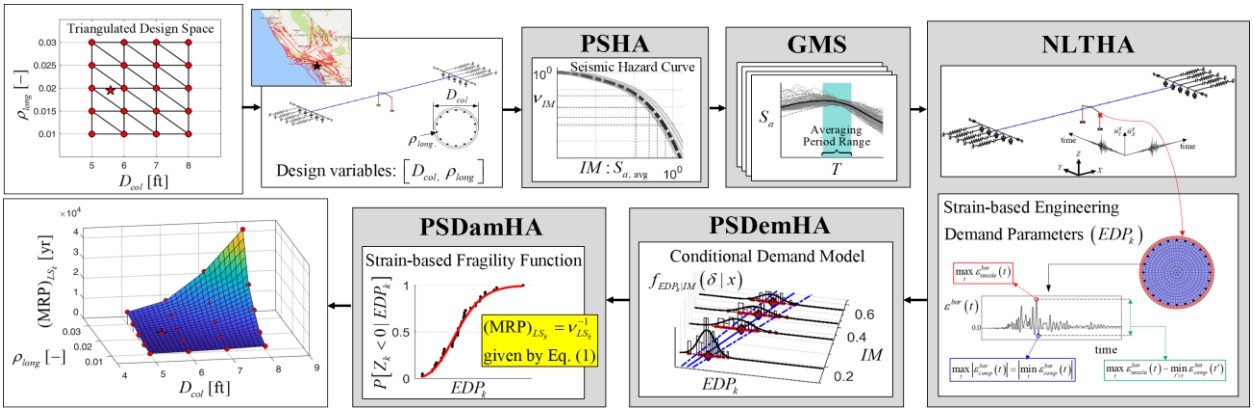

Figure 6.5 Overall workflow for parametric probabilistic seismic performance assessment

6.5.3 Feasible Design Domains and Risk-targeted PBSD

The MRPs of exceedances for the considered *LS*s computed for all the re-designs of an OSB are used to construct three (one for each *LS*) piecewise-linear MRP interpolation surfaces over a triangulation of the regular grid of DPs (see Figure 5.10) defining the OSB's primary design space. A feasible design domain consisting of DPs in the primary design space of each OSB with MRPs of exceedances of the considered *LS*s higher than or equal to respectively specified target MRPs (see Table 5.3) is delineated and *LS*s controlling its boundary are identified (see Figure 5.12). The target values of MRPs of *LS* exceedances are based on discussions with and feedback from expert Caltrans engineers thereby reflecting the current risk tolerance of the bridge engineering community in general. The as-designed OSBs, originally designed following a more

traditional (prescriptive) seismic design philosophy rather than an explicitly performance-based one, are found to exhibit erratic levels of conservativeness. While some of the as-designed testbed bridges are found to be conservative (Bridges B and C), sometimes too much, with respect to the selected *LS*s and corresponding target MRPs, others are found to lie near the borderline of safety (e.g., Bridge A), or clearly in the unsafe domain (e.g., Bridge MAOC). This illustrates the need for a PBSD framework for OSBs such that explicitly stated risk-targeted performance objectives are consistently satisfied by the population of OSBs in California.

Table 6.3 Target MRPs of LS exceedance

LS	***Target MRP of exceedance (years)***
4. Concrete cover spalling	225
5. Longitudinal bar buckling	1000
6. Longitudinal bar fracture	2500

The concept of a feasible design domain in the design parameter space can be utilized to make risk-informed design decisions while trying to satisfy multiple risk-targeted objectives. Values of primary design variables are first selected such that multiple risk-targeted performance objectives are met. This involves selection of a physically realizable DP (subject to practical constraints reflecting design/construction practice) in the primary design parameter space either lying on the boundary of, or inside and in the vicinity of the boundary of, the feasible design domain. Upon selection of primary design variables, secondary design variables are to be determined and adjusted to meet requirements of capacity design, code-based minimum ductility capacity and minimum reinforcement, etc., and/or other restrictions imposed by the real estate

available, traffic flow, etc. In this regard, knowledge of the feasible design domain of an OSB in its design space emerges as an extremely valuable resource in the context of a design process to be carried out in stages as it can be utilized to make risk-informed adjustments, if required, of the primary design variables. After all primary and secondary design variables have been determined, a final check of structural performance is required to ensure that the final design still satisfies the specified risk-targeted performance objectives.

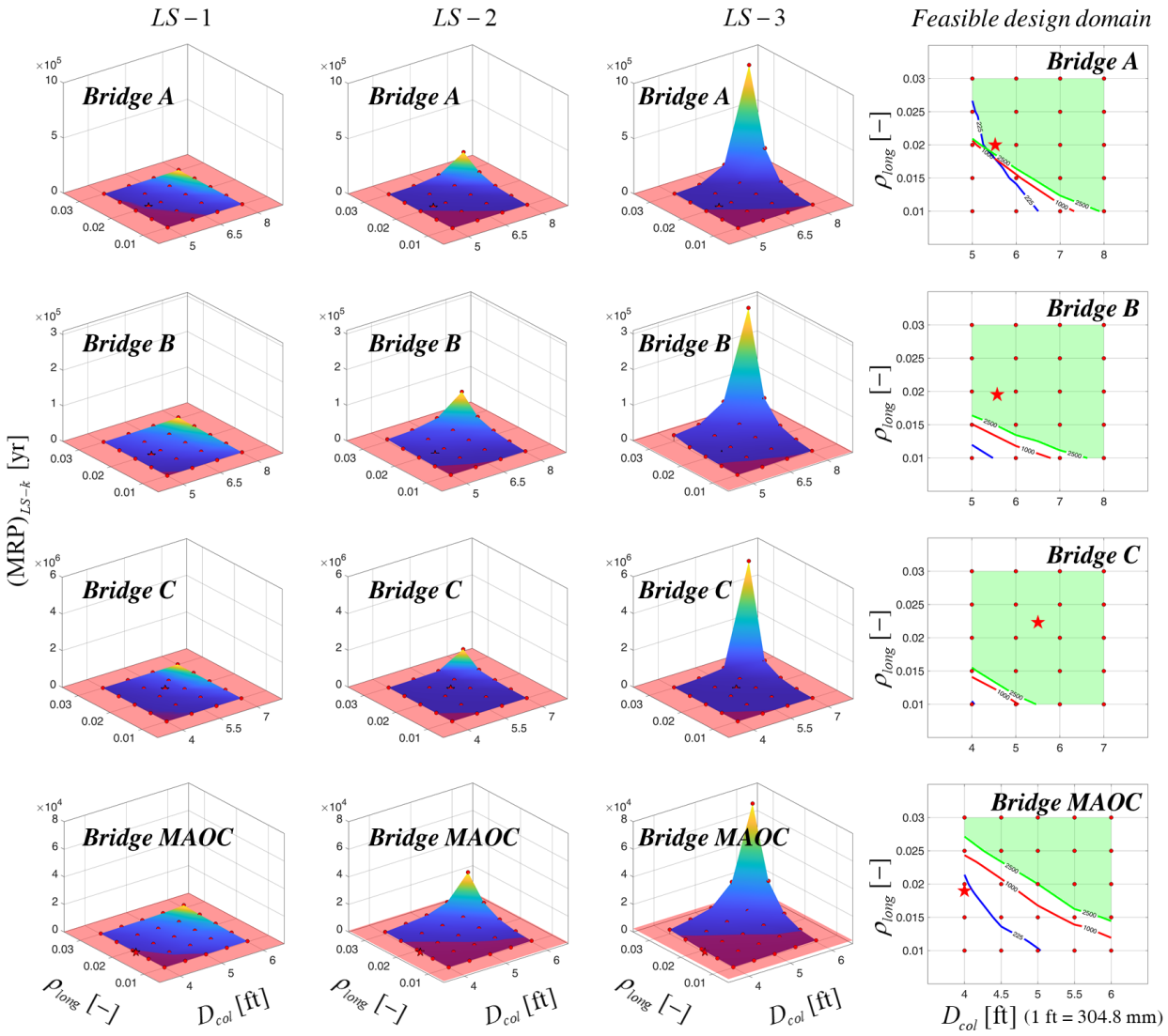

Figure 6.6 MRP interpolation surfaces and feasible design domains (green shaded region) for the considered testbed OSBs. Target MRP contour line for *LSs* 1, 2, and 3 shown in blue, red,

and green respectively. As-designed testbed OSB shown as a red star**Simplified Risk-Targeted PBSD Methodology**

The full-fledged PBSD methodology involving parametric probabilistic seismic performance assessments can be used for the design of a new OSB unless its computational cost is prohibitive for the computational resources available. For reasons of practicability in current bridge design practice, findings of the full-fledged method are inventively utilized to distill out a computationally more economical, simplified, non-traditional, risk-targeted PBSD procedure. The simplified PBSD methodology proposed herein is intended to:

(i) primarily find a DP in the primary design parameter space of a bridge being designed for multiple risk-targeted performance objectives, and

(ii) optionally delineate an approximate, yet sufficiently accurate, feasible design domain and identify the *LS*s controlling its boundary in the primary design parameter space of the bridge

at a computational cost significantly lower than that of the full-fledged method.

6.6.1 Finding a DP Satisfying Multiple Risk-targeted Performance Objectives

It is noted from the results of the parametric study that along any line $\overrightarrow{\mathbf{D}_1\mathbf{D}_p}$ connecting p (≥ 2) DPs $(\mathbf{D}_1,\cdots,\mathbf{D}_p)$ in the primary design parameter space with a positive gradient, i.e., along any direction with increasing values of D_{col} and ρ_{long}, the MRP surfaces corresponding to the *LS*s of interest can be well-approximated using a piecewise power law (see Figure 6.7 (a) and (b)). The equation of such a line is given by:

$$\rho_{long}\left[-\right] = m\left[\text{ft}^{-1}\right] \cdot D_{col}\left[\text{ft}\right] + \alpha\left[-\right] \tag{6.5}$$

where m denotes the slope of the line, and α is the intercept of the line along the ρ_{long} axis. Having selected such a line with a positive slope equal to m ft^{-1}, in the design space, a unitless non-physical quantity, *X*, with the role of continuously increasing values of D_{col} and ρ_{long} along that line is defined as follows:

$$X\left[-\right] = \rho_{long}\left[-\right] + \frac{1}{m}\left[\text{ft}^{-1}\right] D_{col}\left[\text{ft}\right] \tag{6.6}$$

Mathematically, Eq. (6.6) represents a family of lines with slopes equal to $-1/m$ ft^{-1} which are perpendicular to the original line $\overrightarrow{\mathbf{D}_1\mathbf{D}_p}$ (of slope equal to m ft^{-1}) with different values of X representing the intercepts of these lines along the ρ_{long} axis as shown in Figure 6.7 (c). Comparisons of observed versus assumed (piecewise power law) variation of MRP of *LS* exceedance (for *LS*-2 for Bridge A as an example) with respect to *X* for three possible choices of the line $\overrightarrow{\mathbf{D}_1\mathbf{D}_p}$ (shown in Figure 6.7 (a)) are shown in Figure 6.7 (d) through (f).

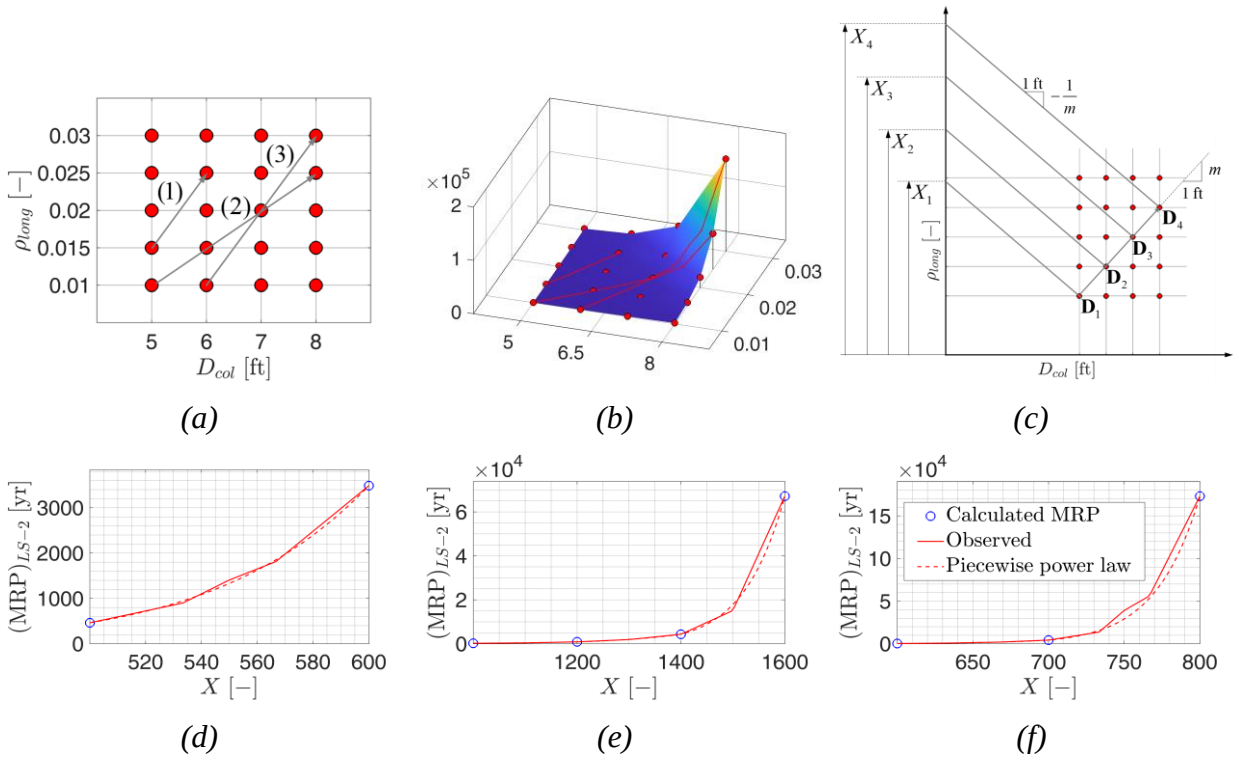

Figure 6.7 (a) Three possible definitions of $\overrightarrow{\mathbf{D}_1\mathbf{D}_p}$, (b) observed variation of MRP surface (for Bridge A, *LS*-2) along considered $\overrightarrow{\mathbf{D}_1\mathbf{D}_p}$'s, (c) graphical interpretation of X; (d) through (f): variation of MRP with X (observes vs assumed) for lines (1) through (3), respectively

To reasonably capture the variation of MRP of *LS* exceedance versus X using the proposed piecewise power law, it is recommended to use three (i.e., $p=3$) DPs in defining $\overrightarrow{\mathbf{D}_1\mathbf{D}_p}$. These three DPs ($\mathbf{D}_1$, $\mathbf{D}_2$, and $\mathbf{D}_3$) are numbered in order of increasing D_{col} and ρ_{long}, i.e., corresponding to increasingly stronger designs along the positive gradient line $\overrightarrow{\mathbf{D}_1\mathbf{D}_3}$. The choice of these three DPs, however, is not completely arbitrary. The procedure for choosing these DPs is illustrated in the flowchart in Figure 6.8.

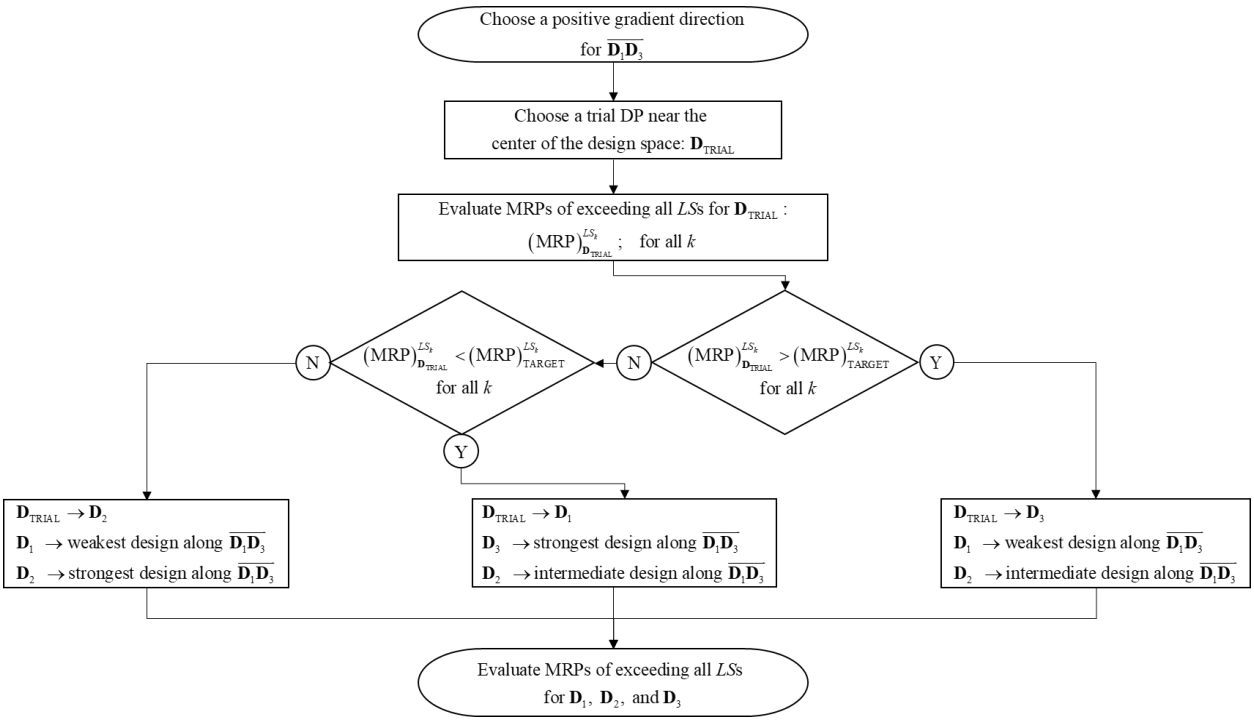

Figure 6.8 Procedure for selection of the three DPs to be assessed in the simplified PBSD methodology

Having carried out full-fledged probabilistic seismic performance assessments for the three DPs along $\overrightarrow{\mathbf{D}_1\mathbf{D}_3}$, one can interpolate a final DP, $\mathbf{D}^*$, satisfying multiple risk-targeted performance objectives (i.e., exactly satisfying the target MRP of exceedance for one *LS* while being on the safer side for the other *LS*s) with reasonable accuracy using the assumed piecewise power law variation of MRP of *LS* exceedance versus *X*. As per this assumption which is shown to hold well along $\overrightarrow{\mathbf{D}_1\mathbf{D}_3}$, the value of X, i.e., $(X^*)^{LS_k}$, satisfying a target value of MRP of exceedance, i.e., $(\text{MRP})_{\text{TARGET}}^{LS_k}$, for the k^{th} *LS* such that $(\text{MRP})_i^{LS_k} < (\text{MRP})_{\text{TARGET}}^{LS_k} < (\text{MRP})_{i+1}^{LS_k}$ is given by:

$$\left(X^*\right)^{LS_k} = \exp\left(\ln X_i + \frac{\ln X_{i+1} - \ln X_i}{\ln\left(\text{MRP}\right)_{i+1}^{LS_k} - \ln\left(\text{MRP}\right)_i^{LS_k}} \times \left(\ln\left(\text{MRP}\right)_{\text{TARGET}}^{LS_k} - \ln\left(\text{MRP}\right)_i^{LS_k}\right)\right) \quad (6.7)$$

where X_i corresponds to the DP $\mathbf{D}_i$ for which the MRP of *LS-k* exceedance is evaluated (via full-fledged seismic performance assessment) to be $(\text{MRP})_i^{LS_k}$. X^*, representing the final DP, $\mathbf{D}^*$, is given by:

$$X^* = \max\left((X^*)^{LS_1}, \cdots, (X^*)^{LS_n}\right) \tag{6.8}$$

where n is the number of *LS*s considered, in this case, equal to 3. Once a value of X^* is obtained, Eq. (6.6) can be invoked to write:

$$X^* = \rho^*_{long}\left[-\right] + \frac{1}{m}\left[\text{ft}^{-1}\right] D^*_{col}\left[\text{ft}\right] \tag{6.9}$$

where, D^*_{col} and ρ^*_{long} are the primary design parameters of the DP $\mathbf{D}^*$. Eq. (6.9) represents the equation of a line passing through the DP $\mathbf{D}^*$ and perpendicular to $\overrightarrow{\mathbf{D}_1\mathbf{D}_3}$. The coordinates of $\mathbf{D}^*$, the point of intersection between the two lines given by Eq. (6.5) and Eq. (6.9), can henceforth be obtained as follows:

$$\mathbf{D}^* = \begin{bmatrix} D^*_{col}\left[\text{ft}\right] \\ \rho^*_{long}\left[-\right] \end{bmatrix} = \begin{bmatrix} \frac{1}{m}\left[\text{ft}^{-1}\right] & 1\left[-\right] \\ -m\left[\text{ft}^{-1}\right] & 1\left[-\right] \end{bmatrix}^{-1} \begin{bmatrix} X^*\left[-\right] \\ \alpha\left[-\right] \end{bmatrix} \tag{6.10}$$

Final DPs, $\mathbf{D}^*$s, obtained for the considered testbed OSBs are shown in Figure 6.9. DPs, $\mathbf{D}_1$, $\mathbf{D}_2$, and $\mathbf{D}_3$, considered in each case are shown as yellow circles, the positive gradient line $\overrightarrow{\mathbf{D}_1\mathbf{D}_3}$ is shown as an arrow, and the DP $\mathbf{D}^*$ is marked as a yellow star. The close proximity of $\mathbf{D}^*$, in each case, with respect to the boundary of the originally delineated feasible design domain is suggestive of the validity of the assumed piecewise power law form for capturing the variation of MRP of *LS* exceedance versus *X*.

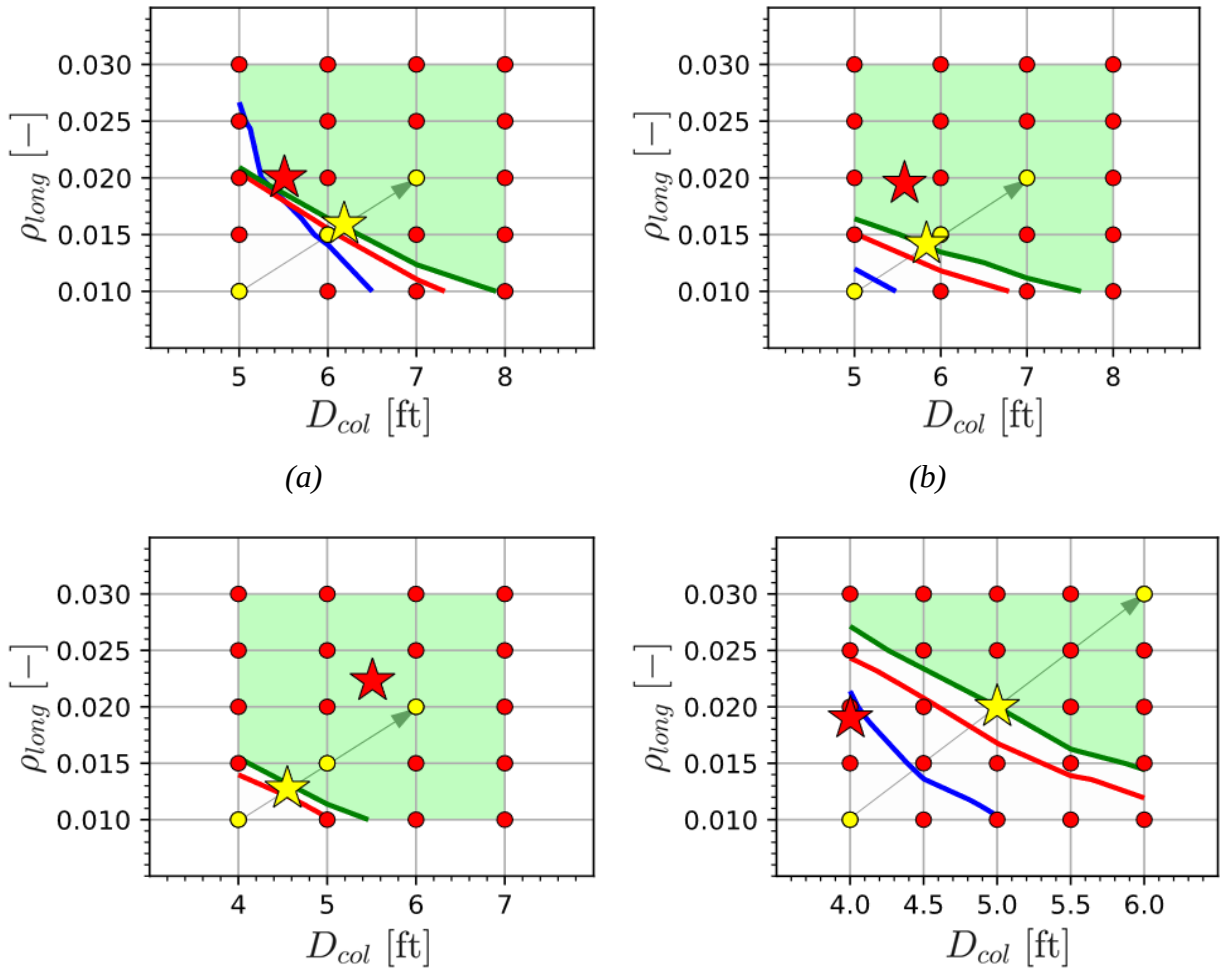

Figure 6.9 Final DPs, $\mathbf{D}^*$ s, satisfying multiple risk-targeted performance objectives shown along with the originally delineated feasible design domains, for (a) Bridge A, (b) Bridge B, (c) Bridge C, and (d) Bridge MAOC.

It is to be noted that, in practice, values of D_{col} and ρ_{long} are constrained by various factors such as the availability of existing prefabricated formwork, restrictions on rebar sizes, etc. In case the exact values of D_{col}^* and ρ_{long}^* obtained are not practically realizable, a viable DP nearest to $\mathbf{D}^*$ along $\overrightarrow{\mathbf{D}_1\mathbf{D}_3}$ and on the safer side is chosen as the final design. However, it is possible that some other DP in the design space of an OSB near $\overline{\mathbf{D}_1\mathbf{D}_3}$, and not exactly on it, can be more

economical, practicable, and hence more desirable than the next viable safe DP lying along $\overrightarrow{\mathbf{D}_1\mathbf{D}_3}$. This, along with the need to make risk-informed design adjustments in the context of a design process to be carried out in stages (i.e., determining secondary design variables upon an initial selection of the primary design variables), highlights the importance of knowing the feasible design domain in the design parameter space of an OSB, an approximate delineation of which is discussed next.

6.6.2 Approximate Delineation of a Feasible Design Domain

From observations of the topology of the MRP interpolation surfaces for the selected set of *LS*s, contour lines of these surfaces can be reasonably assumed as bilinear about the chosen positive gradient line $\overrightarrow{\mathbf{D}_1\mathbf{D}_3}$ and also approximately parallel to each other over the primary design space. The next step in the simplified PBSD methodology towards delineating an approximate feasible design domain is, therefore, to obtain an approximate MRP interpolation surface over the primary design space of an OSB for *LS-k* with bilinear (about $\overrightarrow{\mathbf{D}_1\mathbf{D}_3}$) and parallel contours.

The proposed procedure requires full-fledged seismic performance assessments of two additional DPs, $\mathbf{D}_r^a$ with $r \in [1, 2]$, that form a rectangle in the design space with $\overrightarrow{\mathbf{D}_1\mathbf{D}_3}$ as the diagonal. Bilinear contour lines are split into two segments, each corresponding to region *r* (see Figure 6.10) defined as the region in the design space with respect to the line $\overrightarrow{\mathbf{D}_1\mathbf{D}_3}$ containing $\mathbf{D}_r^a$. The DP $(\mathbf{D}_r^{a'})^{LS_k}$ (yellow diamonds in Figure 6.10) along $\overrightarrow{\mathbf{D}_1\mathbf{D}_3}$ having the same MRP of exceeding *LS-k* as that of $\mathbf{D}_r^a$, i.e., $(\text{MRP})_{\mathbf{D}_r^a}^{LS_k}$, is found, as follows:

$$(\mathbf{D}_r^{a\prime})^{LS_k} = \begin{bmatrix} \frac{1}{m}\left[\text{ft}^{-1}\right] & 1[-] \\ -m\left[\text{ft}^{-1}\right] & 1[-] \end{bmatrix}^{-1} \begin{bmatrix} (X_r^{a\prime})^{LS_k}[-] \\ \alpha[-] \end{bmatrix} \tag{6.11}$$

where $(X_r^{a\prime})^{LS_k}$, as per Eq. (6.7), is given by:

$$(X_r^{a\prime})^{LS_k} = \exp\left(\ln X_i + \frac{\ln X_{i+1} - \ln X_i}{\ln\left(\text{MRP}\right)_{i+1}^{LS_k} - \ln\left(\text{MRP}\right)_i^{LS_k}} \times \left(\ln\left(\text{MRP}\right)_{\mathbf{D}_r^a}^{LS_k} - \ln\left(\text{MRP}\right)_i^{LS_k} \right) \right) \tag{6.12}$$

The orientation of the bilinear contours of the MRP surface for *LS-k* in region *r* is hence given by m_r^k which is equal to the gradient of the line $\overrightarrow{\mathbf{D}_r^a (\mathbf{D}_r^{a\prime})^{LS_k}}$. The above procedure is graphically shown in Figure 6.10.

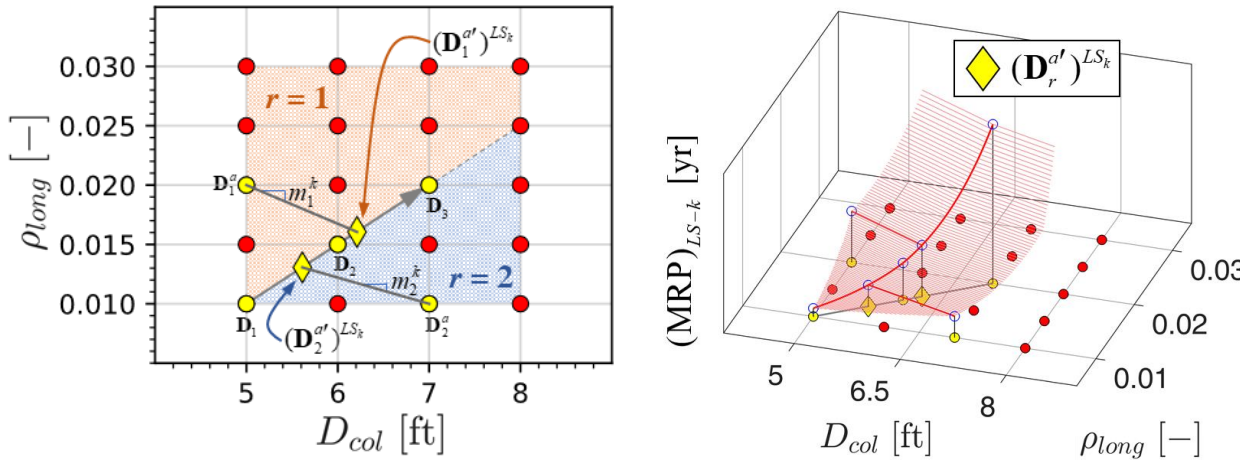

(a) *(b)*

Figure 6.10 (a) Illustrative definitions of $\mathbf{D}_r^a$, $(\mathbf{D}_r^{a\prime})^{LS_k}$, and m_r^k for *LS-k*, (b) illustration of the procedure to determine m_r^k for *LS-k*

To obtain an approximate value of MRP of *LS-k* exceedance for an arbitrary DP, $\mathbf{D} = [D_{col}, \rho_{long}]^{\mathrm{T}}$, lying in region *r* over the primary design space of an OSB, $(X')^{LS_k}$

corresponding to $(\mathbf{D}')^{LS_k} = [D'^{k}_{col}, \rho'^{k}_{long}]^{\mathrm{T}}$, the point of intersection of $\overrightarrow{\mathbf{D}_1\mathbf{D}_3}$ with a line passing through **D** and having gradient m_r^k is first calculated as:

$$(X')^{LS_k} = \rho'^{k}_{long}\left[-\right] + \frac{1}{m}\left[\mathrm{ft}^{-1}\right] D'^{k}_{col}\left[\mathrm{ft}\right] \tag{6.13}$$

where

$$\begin{bmatrix} D'^{k}_{col}\left[\mathrm{ft}\right] \\ \rho'^{k}_{long}\left[-\right] \end{bmatrix} = \begin{bmatrix} m\left[\mathrm{ft}^{-1}\right] & -1\left[-\right] \\ m_r^k\left[\mathrm{ft}^{-1}\right] & -1\left[-\right] \end{bmatrix}^{-1} \begin{bmatrix} -\alpha\left[-\right] \\ \left(m_r^k D_{col} - \rho_{long}\right)\left[-\right] \end{bmatrix} \tag{6.14}$$

This value of X' is used to determine $(\mathrm{MRP})_{\mathbf{D}}^{LS_k}$, the MRP of *LS-k* exceedance for the DP **D**, using the piecewise power law for MRP versus *X* assumed to hold along $\overrightarrow{\mathbf{D}_1\mathbf{D}_3}$ as follows:

$$(\mathrm{MRP})_{\mathbf{D}}^{LS_k} = \exp\left(\ln\left(\mathrm{MRP}\right)_i^{LS_k} + \frac{\ln\left(\mathrm{MRP}\right)_{i+1}^{LS_k} - \ln\left(\mathrm{MRP}\right)_i^{LS_k}}{\ln X_{i+1} - \ln X_i} \times \left(\ln\left(X'\right)^{LS_k} - \ln X_i\right) \right) \tag{6.15}$$

where $X_i < X' < X_{i+1}$.

Eq. (6.15) represents an approximate MRP interpolation surface over the primary design space (i.e., the $D_{col} - \rho_{long}$ space) of an OSB for *LS-k* with bilinear (about $\overrightarrow{\mathbf{D}_1\mathbf{D}_3}$) and parallel contours. Approximate feasible design domains delineated for the four testbed OSBs using such approximate MRP interpolation surfaces are shown in Figure 6.11.

As observed from Figure 6.11, the approximate feasible design domains for all four testbed OSBs tally reasonably well with the feasible design domains previously outlined using the full-fledged parametric PBSD methodology, hence validating the simplified PBSD methodology. It is to be noted that benefit (i.e., the gain in ability to make risk-informed design adjustments in the primary design space of an OSB which could potentially lead to safe and more economic design of OSBs) derived from this optional step of approximately delineating the feasible design domain

greatly outweigh the computational cost involved in the seismic performance assessments of two additional DPs.

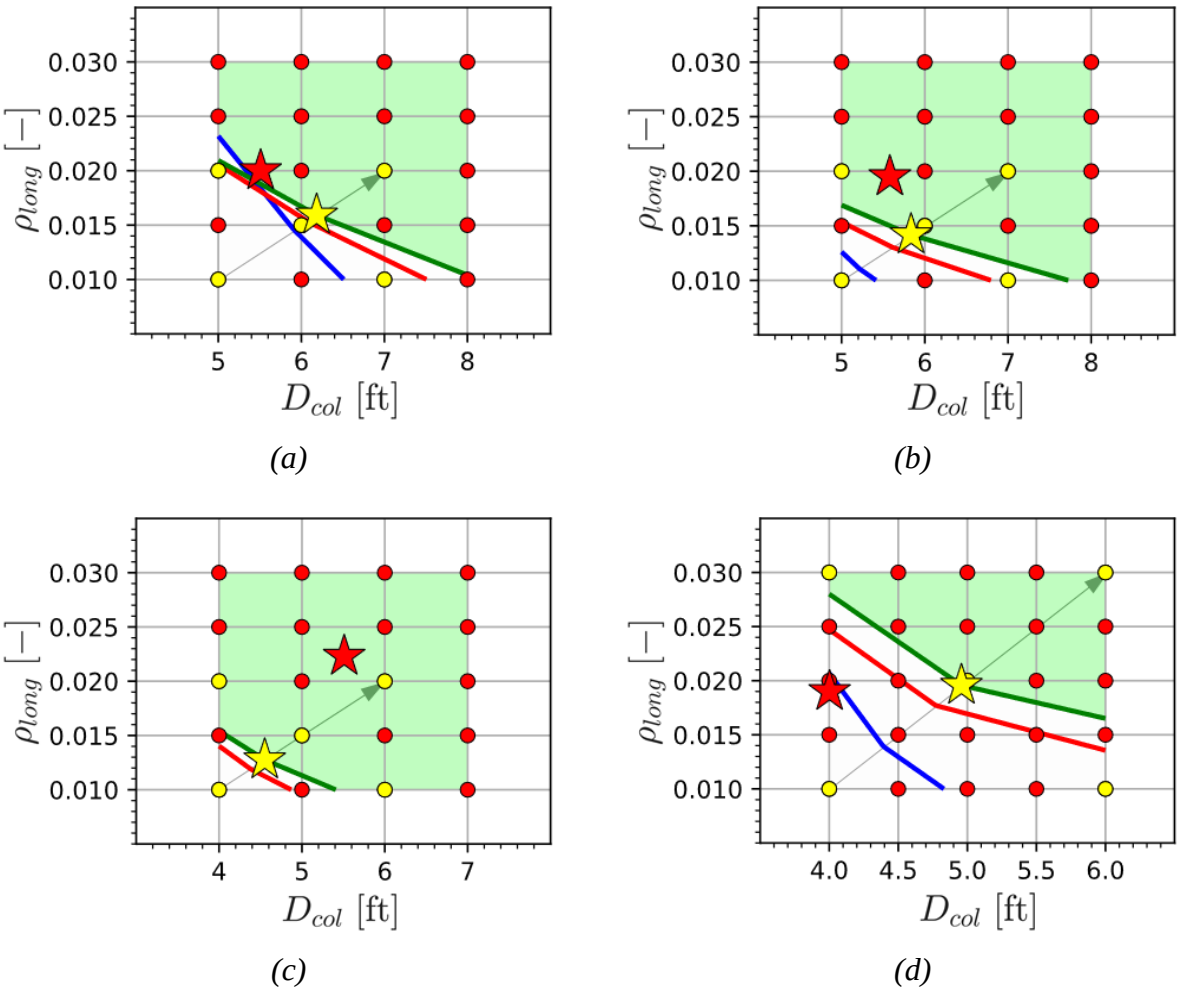

Figure 6.11 Approximate feasible design domains, for (a) Bridge A, (b) Bridge B, (c) Bridge C, and (d) Bridge MAOC

6.6.3 Further Reduction in Computational Workload

The simplified PBSD methodology, formulated thus far, significantly reduces the computational workload, as compared to the full-fledged method, in terms of the number of DPs to be assessed towards achieving the goal of finding a DP satisfying multiple risk-targeted performance objectives and obtaining a feasible design domain in the design space of an OSB.

While maintaining reasonable levels of accuracy of results, it is found that further reduction in computational cost is possible in terms of the number of seismic hazard levels considered (from 6 to 3) and the number of nonlinear time-history analyses performed per hazard level (from 100 to as low as 20) in the performance assessment for a single DP. The set of three seismic hazard levels to be considered for the performance evaluation of a DP are recommended to be well-spaced in terms of MRPs of *IM* exceedance (e.g., 72 yrs., 975 yrs., and 4975 yrs.). Final DPs, $\mathbf{D}^*$ s, satisfying multiple risk-targeted performance objectives and approximate feasible design domains hence obtained for the considered testbed OSBs are shown in Figure 6.12. The results of this reduced-workload simplified PBSD method are found to be in reasonable agreement with the previously obtained results corresponding to both the full-fledged PBSD method and the simplified PBSD method.

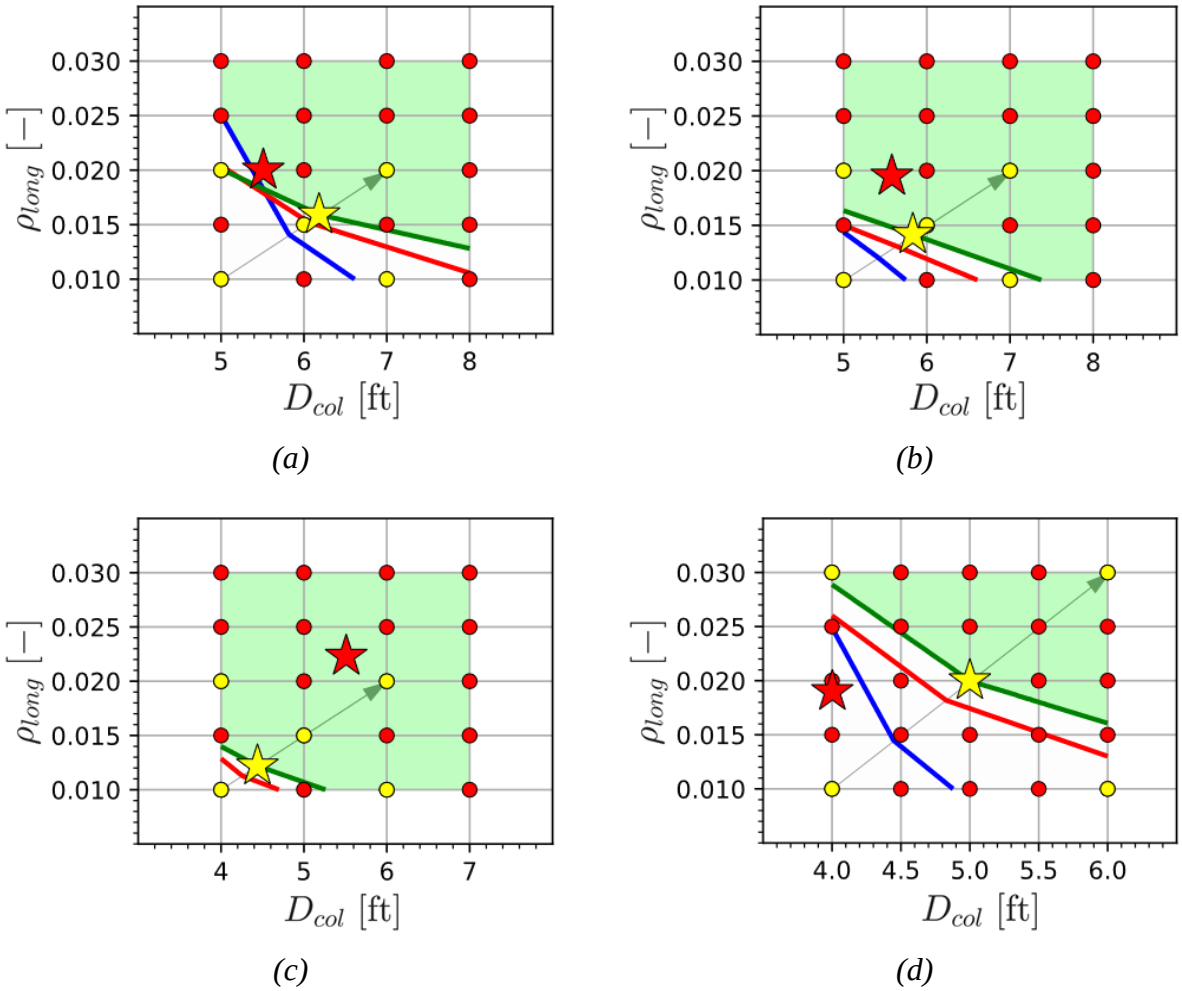

Figure 6.12 Approximate feasible design domains obtained using reduced computational workload, for (a) Bridge A, (b) Bridge B, (c) Bridge C, and (d) Bridge MAOC

6.7 Conclusions

A simplified PBSD methodology for OSBs is distilled out of a full-fledged parametric PBSD methodology previously forwarded by the authors. The full-fledged method is used to calibrate and validate the proposed simplified procedure with four real-world testbed OSBs as cases in point. With this, a step forward in the direction of a rigorously implemented practicable risk-targeted PBSD framework for bridges is taken. The need for such a framework is illustrated by the telltale irregularities in the seismic performance (gauged by the MRP of exceeding a

practical set of pertinent *LS*s) of the as-designed testbed OSBs which are designed using traditional prescriptive design methods.

The proposed simplified PBSD method preserves the original idea (of the full-fledged parametric PBSD method) of a two-stage design procedure with the first-stage involving the design of the bridge columns and the second-stage the determination of other design variables (e.g., the ones not restricted by the geometry of the bridge, available real estate, traffic flow requirements, etc.) so as to meet code-based requirements of capacity design (to limit the number and locations of damage and failure mechanisms to be considered), minimum ductility limitations, reinforcement ratio restrictions, etc. A significant bottleneck in the full-fledged method inhibiting its practical implementation is the computationally prohibitive step of carrying out extensive ensemble NLTHA for the seismic performance assessments of multiple DPs. The purpose of the simplified method is therefore to provide, without any compromise in rigor, a computationally more frugal alternative to the full-fledged method.

The reduction in the computational load for the simplified method primarily comes from (i) reduction in the number of DPs to be assessed, (ii) reduction in the number of seismic hazard levels at which ensemble NLTHA are performed, and (iii) reduction in the size of the ensemble, i.e., the number of NLTHA, per seismic hazard level. By implementing a smart combination of the above, the desired design objectives of (i) finding a DP in the primary design space of a bridge being designed for multiple risk-targeted performance objectives, and (ii) delineating an approximate, yet accurate, feasible design domain facilitating risk-informed design adjustments in the face of uncertainty, are systematically achieved while striking the right balance between computational cost, practicability, and rigor. In addition, the distinguishing features of the proposed PBSD methodology are:

(i) explicit account of pertinent sources of uncertainty

(ii) comprehensive seismic damage hazard assessments of OSBs

(iii) state-of-the-art strain-based criteria for damage assessment

(iv) ability to accommodate any number of pertinent LSs

(v) reliance on rigorous probabilistic performance assessments of design iterations (or DPs) to arrive at a final DP

It is believed that the adoption of the proposed PBSD methodology will be extremely beneficial in the medium and long-term. An immediate implementation of this rather non-traditional design method in current bridge design practice might still seem overly optimistic. However, such an initial venture will prove crucial in supporting and fostering future research work and innovative technological developments in bridge infrastructure engineering.

6.8 Preview to Chapter 7

The PBSD framework proposed thus far explicitly considers: (1) the uncertainty in the seismic input, and (2) the uncertainty in the capacity of the various *LS*s. This framework is enhanced in the next chapter to account for the following additional sources of uncertainty: (i) the aleatory uncertainty associated with FE model parameters, and (ii) the epistemic parameter estimation uncertainty associated with using finite datasets to estimate the parameters of the probability distributions characterizing FE model parameters and *LS* fragilities.

6.9 Acknowledgements

Support of this research by the California Department of Transportation under Grand No. 65A0594, Task No. 2880 is gratefully acknowledged. The authors wish to thank the following

individuals for their help and insightful discussions related to the work presented in this paper: Messrs. M. Mahan, T. Ostrom, A. Shamsabadi, T. Shantz, and C. Sikorsky from the Engineering Division at Caltrans, along with Dr. Frank McKenna at UC Berkeley for help with HPC and OpenSees. The authors also acknowledge the Texas Advanced Computing Center (TACC) at The University of Texas at Austin (http://www.tacc.utexas.edu) for providing HPC resources that have contributed to the research results reported within this paper. Chapter 6, in full, is currently being prepared for submission for publication of the material as it may appear in the following paper (the dissertation author is the first author of this paper):

Deb, A., Zha, A. L., Caamaño-Withall, Z. A., Conte, J. P., Restrepo, J. I. (2021). "Simplified risk-targeted performance-based seismic design method for ordinary standard bridges." Under preparation for submission to *Journal of Bridge Engineering*.

7 Comprehensive Treatment of Uncertainties in Risk-targeted Performance-based Seismic Design and Assessment of Bridges

7.1 Abstract

This study complements and extends a recent work on the development of a rigorous framework for risk-targeted performance-based seismic design/assessment of ordinary standard bridges (OSBs) in California. Rooted in the formulation of this framework is an updated fully probabilistic performance-based earthquake engineering (PBEE) assessment methodology wherein metrics of structural performance are formulated in terms of the mean return periods of exceedances for several strain-based limit-states (*LS*s). The originally proposed framework explicitly considering: (1) the uncertainty in the seismic input, and (2) the uncertainty in the capacity of the various *LS*s, is extended in this study to account for the following additional pertinent sources of uncertainty: (i) the aleatory uncertainty associated with finite element (FE) model parameters, and (ii) the epistemic parameter estimation uncertainty associated with using finite datasets to estimate the parameters of the probability distributions characterizing the FE model parameters and *LS* fragilities. These additional sources of uncertainty are commonly omitted or neglected in PBEE often by invoking that the earthquake ground motion uncertainty is the predominant source of uncertainty. However, their inclusion and consistent propagation in seismic performance-based assessment of OSBs is imperative to obtain a more complete picture of seismic performance, thereby leading to more comprehensive, transparent, and reliable design of these simple, yet essential bridges which represent an integral part of lifeline infrastructure systems

especially in earthquake-prone regions. The analytical and computational framework previously assembled is extended via modular incorporation of these additional sources of uncertainty. Four OSB testbeds and their risk-targeted re-designed versions are analyzed with and without these additional sources of uncertainty to evaluate their significance.

7.2 Introduction

Several studies (Cornell et al. 2002; Ellingwood 2008; Franchin et al. 2018; Hamburger 2006; Mackie and Stojadinović 2007; Saini and Saiidi 2014) have focused on the applicability of the probabilistic performance-based earthquake engineering (PBEE) assessment framework (Moehle and Deierlein 2004; Porter 2003), developed under the auspices of the Pacific Earthquake Engineering Research (PEER) Center, in the performance-based seismic design (PBSD) of structures. Notwithstanding, the seismic design of bridge structures remains a relatively less trodden area than for building systems in terms of rigorous/comprehensive PBEE applications. Recent studies on PBSD of bridges either rely on simplified closed-form solutions (Mackie and Stojadinović 2007), or lack comprehensiveness by estimating the probabilities of damage/limit-state (*LS*) exceedances conditioned on earthquakes at discrete seismic hazard levels only (Saini and Saiidi 2014), thereby neglecting the contributions of the continuum of seismic hazard levels to the total probability of *LS* exceedance (*LSE*).

The somewhat hindered implementation of PBEE in bridge seismic design is addressed in Deb et al. (Deb et al. 2021b), wherein a full-fledged risk-targeted PBSD framework, and a simplification thereof (Deb et al. 2021c), are proposed for ordinary standard bridges (OSBs), which represent the most common reinforced concrete (RC) bridges in California and are designed in-house by the California Department of Transportation (Caltrans). The PBSD methods proposed

by Deb et al. (Deb et al. 2021b; c) explicitly consider the following basic sources of uncertainty: (i) the uncertainty associated with the seismic intensity measure (*IM*) at the bridge site (Boore and Atkinson 2008), (ii) the record-to-record variability of earthquake ground motions given a seismic hazard level (a specific value of *IM*) by using ensembles of ground motions consistent with the natural conditional variability of earthquake ground motions given *IM* (Kohrangi et al. 2017; Lin et al. 2013a), and (iii) the uncertainty in the capacity of the various strain-based *LS*s (Duck et al. 2018; Goodnight et al. 2016) as represented by the corresponding fragility curves; while ignoring the following additional pertinent sources of uncertainty: (i) the aleatory uncertainty associated with finite element (FE) model parameters (e.g., constitutive material model parameters, damping model parameters), and (ii) the epistemic parameter estimation uncertainty associated with using finite datasets to estimate the parameters of the probability distributions characterizing FE model parameters and *LS* fragilities. However, recent studies (Bradley 2010, 2013b; Gokkaya et al. 2016; Iervolino 2017; Lee and Mosalam 2005; Li et al. 2020; Liel et al. 2009; Padgett et al. 2013; Pang et al. 2014) have shown that these additional sources of uncertainty can be significant and must be included for a comprehensive seismic performance assessment of structures.

Despite being traditionally overlooked, the importance of the inclusion of FE model parameter uncertainty in the seismic performance assessment of structures (Gokkaya et al. 2016; Lee and Mosalam 2005; Liel et al. 2009) in general, and bridges (Li et al. 2020; Padgett et al. 2013; Pang et al. 2014) in particular, has been recently studied, although not extensively. Factors contributing to this conventional disregard range from misconceptions about the relative importance of this source of uncertainty when compared to the uncertainty in the seismic input, to the high computational cost incurred due to the inclusion of this additional source of uncertainty. To address the latter concern, some researchers have proposed a preliminary screening of random

variables (RVs) based on sensitivity studies to allow for savings in the computational effort required (Padgett and DesRoches 2007; Porter et al. 2002; Tubaldi et al. 2012). Some researchers have used traditional simplified approaches based on the first-order second-moment (FOSM) method (Barbato et al. 2010; Lee and Mosalam 2005) to account for this source of uncertainty, while others have looked into the use of more advanced response surface/regression-based techniques (Liel et al. 2009; Mangalathu et al. 2018). However, such methods are found to yield inaccurate results in the case of highly nonlinear structural systems and/or high dimensionality of the vector of RVs describing the FE model parameters (Gokkaya et al. 2016). With the surging advent of high-performance computing (HPC) resources and the ready availability of ample computational power, Monte-Carlo (MC) simulation emerges as one of the most reliable approaches for incorporating and propagating the FE model parameter uncertainty in nonlinear time history analyses. MC simulation is also the approach adopted in this paper.

Most studies [e.g., 18,20] on the effects of parameter estimation uncertainty have primarily focused on the use of a finite number of ground motion records in the estimation of the seismic demand, and not on the use of finite datasets to estimate the parameters of the probability distributions characterizing FE model parameters and *LS* fragilities. To the authors' knowledge, a comprehensive analytical and computational framework explicitly accounting for all the above-mentioned sources of uncertainty is not currently available for the seismic performance evaluation and PBSD of bridge structures. Available are only studies [e.g., 16–24] that include one or the other of these targeted additional sources of uncertainty in addition to the uncertainties associated to the earthquake ground motion input and *LS* capacities. The current study augments the full-fledged PBSD methodology proposed by Deb et al. (Deb et al. 2021b) via the inclusion, quantification, and propagation of the targeted additional sources of uncertainty in the underlying

PBEE assessment framework. The analytical and computational framework previously assembled is extended via the modular incorporation of these additional sources of uncertainty. Four testbed OSBs and their risk-targeted re-designed versions are analyzed with and without these additional sources of uncertainty to evaluate their significance.

7.3 Description of Testbed Bridges

OSBs are conventional, multiple-span, short (span length less than 91.4 m or 300 ft) and, in general, skewed RC bridges with monolithic or monolithic-equivalent superstructure supported on soils that may or may not be susceptible to liquefaction and/or scour (Caltrans 2013). The current study focuses on the as-designed and risk-targeted re-designed (as per Deb et al. (Deb et al. 2021b; c)) versions of four existing California OSBs (see Figure 7.1), namely Bridge A, Bridge B, Bridge C, and Bridge MAOC. Bridge A is the Jack Tone Road Overcrossing in Ripon, California, which has two spans and one single column bent. Bridge B is the La Veta Avenue Overcrossing in Tustin, California, consisting of two spans but supported on a two-column bent. Bridge C is the Jack Tone Road Overhead in Ripon, California (located adjacent to Bridge A), which consists of three spans supported on two bents with three columns each. Bridge MAOC, the Massachusetts Avenue Overcrossing located in San Bernardino, California has five spans supported on four bents with four columns each. These bridges primarily consist of prestressed concrete box-girder decks supported by column bent(s) on pile foundations and seat-type abutments also on pile foundations.

Three-dimensional nonlinear FE models (consisting of nonlinear fiber-section beam-column elements and nonlinear springs) of these bridges developed (detailed description provided in Deb et al. (Deb et al. 2018, 2021a)) in OpenSees (Mazzoni et al. 2006), the open-source FE

analysis software framework developed at PEER, are employed in this study. A schematic representation of the computational model of one of the four testbed OSBs (Bridge C) is shown in Figure 7.2. Figure 7.3 shows the hysteretic constitutive models used for concrete and reinforcing steel as well as different structural components of Bridge C.

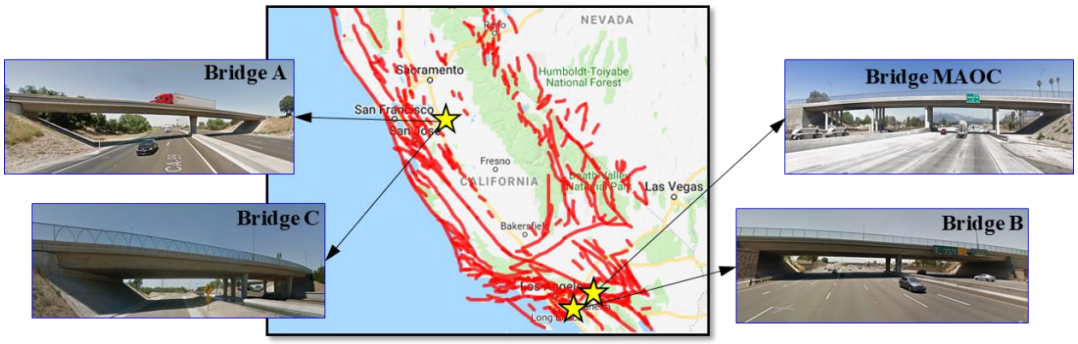

Figure 7.1 Locations of testbed OSBs

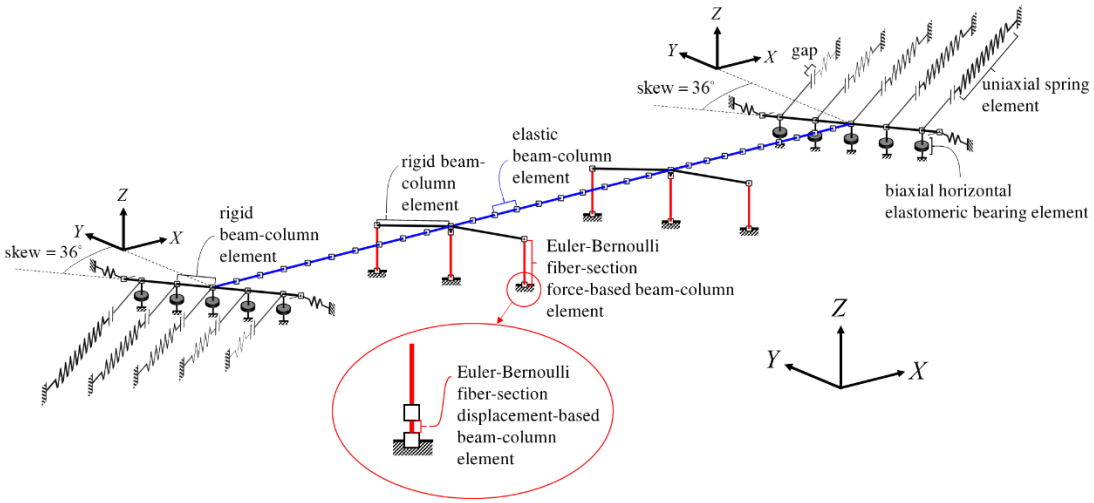

Figure 7.2 Schematic representation of FE model of Bridge C

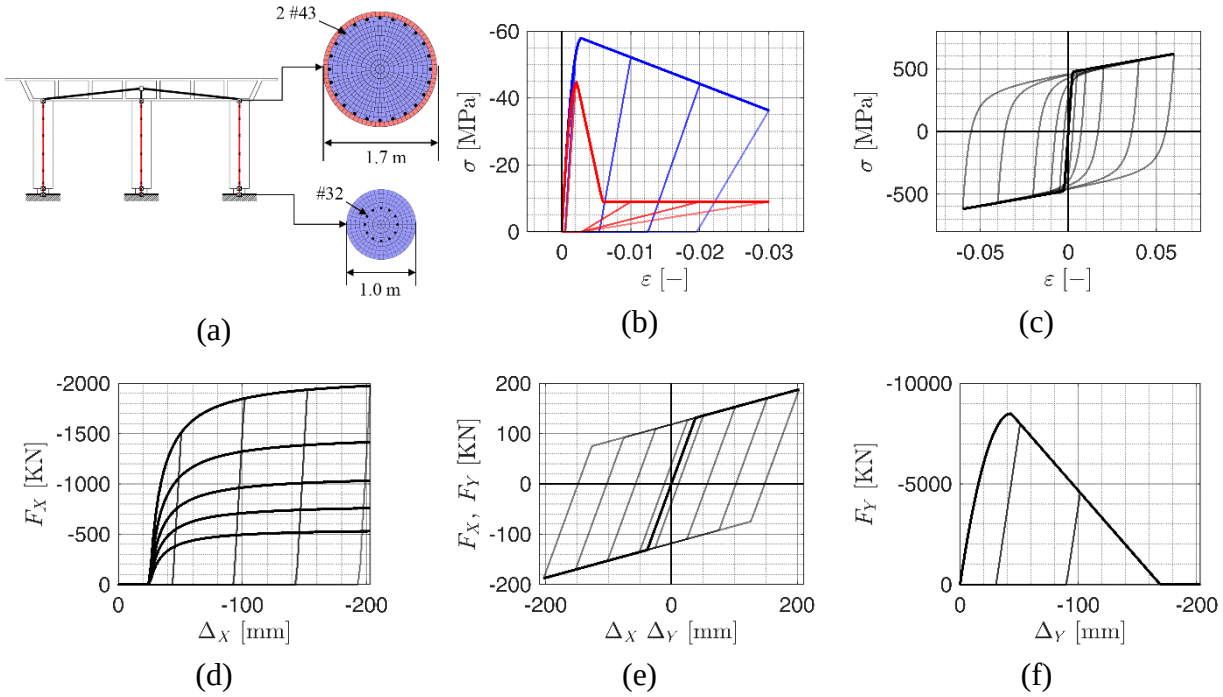

Figure 7.3 FE modeling details for Bridge C: (a) Column and base-hinge fiber-section definition; Material hysteretic stress-strain relations for (b) unconfined (red) and confined (blue) concrete fibers (Kent and Park 1971; Mander et al. 1988; Scott et al. 1982) using *Concrete01* in OpenSees, and (c) reinforcing steel (black) fibers (Filippou et al. 1983; Menegotto and Pinto 1973) using *SteelMPF* in OpenSees; Nonlinear hysteretic force-deformation relations assigned to: (d) backfill distributed spring model (Shamsabadi et al. 2020) using *HyperbolicGapMaterial* in OpenSees, (e) each bearing pad element using *elastomericBearingPlasticity* in OpenSees, and (f) each non-isolated exterior shear key spring (Megally et al. 2002) using *Concrete01* in OpenSees

7.4 Framework for Risk-targeted PSBD of OSBs

7.4.1 Computational Framework for Forward PBEE Assessment

The four-step PEER PBEE assessment methodology involves (i) site-specific probabilistic seismic hazard analysis (PSHA) in terms of a ground motion *IM*, (ii) probabilistic seismic demand hazard analysis (PSDemHA) in terms of engineering demand parameters (*EDP*s), (iii) probabilistic seismic damage hazard analysis (PSDamHA) in terms of practical *LS*s of interest, and (iv) probabilistic seismic loss hazard analysis (PSLHA) in terms of pertinent decision variables (*DV*s)

(e.g., downtime, monetary loss, deaths). With performance measures defined as the mean annual rate (MAR), or equivalently its reciprocal, the mean return period (MRP), of *LSE* for a selected set of *LS*s, and keeping the fourth step of PSLHA outside the scope of this study, the PEER PBEE integral quantifying structural performance of a bridge in terms of the MAR of exceedance for *LS-k* ($\nu_{LS,k}$) takes the following form:

$$\begin{aligned}\nu_{LS,k} &= \int_{IM}\int_{EDP_k} P\left[EDP_{C,k}^{bridge} < EDP_k \mid EDP_k = \delta\right]\cdot f_{EDP_k|IM}\left(\delta \mid x\right)\cdot d\delta\cdot\left|d\nu_{IM}\left(x\right)\right| \\ &= \int_{EDP_k} F_{EDP_{C,k}^{bridge}}\left(\delta\right)\cdot\left|d\nu_{EDP_k}\left(\delta\right)\right|\end{aligned} \tag{7.1}$$

where $P[EDP_{C,k}^{bridge} < EDP_k \mid EDP_k = \delta]$ is the conditional probability of exceedance of *LS-k* given a specified value δ of the associated *EDP* (EDP_k), $EDP_{C,k}^{bridge}$ denotes the structural capacity against the exceedance of *LS-k* in the bridge being analyzed, $f_{EDP_k|IM}(\delta \mid x)$ is the conditional probability distribution function (PDF) of EDP_k given $IM = x$, $\nu_{IM}(x)$ is the MAR of *IM* exceeding the specified value *x*, $F_{EDP_{C,k}^{bridge}}(\delta)$ is the cumulative distribution function (CDF) of $EDP_{C,k}^{bridge}$ evaluated at δ (this is commonly referred to as the fragility function for *LS-k*), and $\nu_{EDP_k}(\delta)$ is the MAR of EDP_k exceeding the specified value δ. $EDP_{C,k}^{bridge}$ in Eq. (7.1) can be written as

$$EDP_{C,k}^{bridge} = \frac{EDP_{C,k}^{\mathrm{MEAS}}}{EDP_{C,k}^{\mathrm{PRED}}} \times EDP_{C,k}^{\mathrm{PRED},\,bridge} \tag{7.2}$$

where $EDP_{C,k}^{\mathrm{MEAS}} / EDP_{C,k}^{\mathrm{PRED}}$ is the ratio of the experimentally measured to deterministically predicted (using a predictive capacity model) values of *EDP-k* at which *LS-k* exceedance is encountered for different experimentally (or numerically) tested specimens, and $EDP_{C,k}^{\mathrm{PRED},\,bridge}$

denotes the predicted (using the same predictive capacity model) value of capacity against the exceedance of *LS-k* in the bridge being analyzed.

Deb et al. (Deb et al. 2021a) recently developed a modular computational implementation, in the form of a Python package named PyPBEE (PBEE for Python), of an updated version of the PEER PBEE framework assembling different state-of-the-art improved ingredients of the multidisciplinary PEER PBEE framework, particularly suited to bridge structures These improvements include: (i) introduction of an improved *IM*, i.e., average spectral acceleration over a period range, (ii) conditional mean spectrum-based hazard-consistent and site-specific ground motion selection, (iii) use of practical *LS*s pertinent to seismic damage evaluation of bridge columns: concrete cover spalling (*LS*-1), the onset of longitudinal bar buckling (*LS*-2), and a precursor stage to bar fracture (*LS*-3), (iii) introduction of material strain-based *EDP*s (see Table 7.1) associated with the considered *LS*s, and (v) identification of reliable experimental/analytical studies and predictive capacity models (see Table 7.2) for the development of strain-based fragility functions for the considered *LS*s. Such an effort is of paramount importance and is the first step required towards the development of any comprehensive, scientific, and rational PBSD method/procedure. It not only equips bridge engineers with a handy analytical tool enabling them to rigorously carry out the inevitable step of forward structural performance assessment in solving a PBSD problem (which is an inverse assessment problem), but also allows them to readily incorporate alternative and more refined ingredients reflecting future improvements and progress made in the various aspects of the field.

Table 7.1 Definition of *LS*s and associated *EDP*s

#	*LS*	Associated *EDP*
1	Concrete cover spalling	Maximum absolute compressive strain in any longitudinal bar of any column, $EDP_1 = \max_{col}\left(\max_{bar}\left(\max_{t}\left\|\varepsilon_{comp}^{bar}(t)\right\|\right)\right)$
2	Onset of longitudinal rebar buckling	Maximum tensile strain in any longitudinal bar of any column $EDP_2 = \max_{col}\left(\max_{bar}\left(\max_{t}\varepsilon_{tensile}^{bar}(t)\right)\right)$
3	Precursor to longitudinal rebar fracture	Maximum difference of tensile (positive) and compressive (negative) strain, with the latter following the former, in any longitudinal bar of any column, $EDP_3 = \max_{col}\left(\max_{bar}\left(\max_{t}\varepsilon_{tensile}^{bar}(t) - \min_{t'>t}\varepsilon_{comp}^{bar}(t')\right)\right)$

Table 7.2 Deterministic predictive capacity models for the considered *LS*s

LS #	*Predictive Capacity Model*	
1	$EDP_{C,1}^{\text{PRED}} = 0.004$ (Goodnight et al. 2016)	*(7.3)*
2	$EDP_{C,2}^{\text{PRED}} = 0.03 + 700\rho_{trans}\frac{f_y}{E_s} - 0.1\frac{P}{f_c' A_g}$ (Goodnight et al. 2016)	*(7.4)*
3	$EDP_{C,3}^{\text{PRED}} = 0.11 + \min(0.054,\ 3.2\rho_{trans}) - 0.0175\left\|\left(\sqrt[3]{n_{bar}} - 2.93\right)\right\| - 0.054\frac{f_u}{f_y}$ (Duck et al. 2018)	*(7.5)*

Remarks:

(i) In Eq. (7.4), ρ_{trans} is the column transverse reinforcement ratio (taken as 0.5 times the column longitudinal reinforcement ratio (Duck et al. 2018)), f_y is the yield stress of the transverse reinforcement, E_s is the elastic modulus of the transverse reinforcement, P is the axial load on the column due to gravity loads, f_c' is the compressive strength of the unconfined concrete, and A_g is the gross cross-sectional area of the column.

(ii) In Eq. (7.5), n_{bar} is the number of bundles of longitudinal bars in a column, and f_u / f_y is the ratio of the ultimate to the yield stress of the longitudinal steel reinforcement (taken as 1.4 (Duck et al. 2018)).

7.4.2 Risk-targeted PBSD Methodology

Deb et al. (Deb et al. 2021b) demonstrated the capabilities of PyPBEE by extensively utilizing this tool for comprehensive parametric performance assessment studies of four California testbed OSBs. The parametric study was carried out over a two-dimensional regular grid representing the primary design space of an OSB comprising of values of the column diameter (D_{col}) and column longitudinal reinforcement ratio (ρ_{long}) subjected to practical constraints reflecting design/construction practice. This study was aimed to investigate the effects of varying key/primary structural design parameters on the sought performance measures, i.e., the MRPs of exceedance of a set of strain-based *LS*s pertaining to RC bridge columns, the primary lateral load resisting structural components of OSBs. Based on this parametric study, Deb et al. (Deb et al. 2021b) proposed a full-fledged PBSD framework for OSBs being designed for multiple risk-targeted performance objectives. This procedure requires a full-blown parametric performance assessment of a preliminary design (based on traditional prescriptive measures) of the OSB over its primary design space and delineation of a risk-based feasible design domain defined as the collection of design points (DPs) in the two-dimensional primary design parameter space of the OSB with MRPs of exceeding the considered set of *LS*s higher than or equal to the respective specified target MRPs (225 years for *LS*-1, 1000 years for *LS*-2, and 2500 years for *LS*-3). Upon selection of a physically realizable DP in the primary design parameter space (either lying on the boundary of, or inside and in the vicinity of the boundary of the feasible design domain), other

(secondary) bridge design variables are determined/adjusted and finalized to meet requirements of capacity design, code-based minimum ductility capacity and minimum reinforcement, etc., and/or other restrictions imposed by the real estate available, traffic flow, etc. Knowledge of the risk-based feasible design domain of an OSB in its design space provides an extremely valuable resource in the context of a design process to be carried out in stages as it can be utilized to make risk-informed adjustments in the face of uncertainty, if required, of the primary design variables. Figure 7.4 shows the feasible design domain obtained for each of the four testbed OSBs considered along with the as-designed version (red star) and one possible redesigned version (yellow star) satisfying the three risk-targeted performance objectives of interest. The telltale irregularity in the seismic performance of the as-designed testbed OSBs (gauged by the difference in the calculated vs expert opinion-based target MRPs of *LSE*s) observed in this study is indicative of the inconsistency and opacity of current design principles and methods that do not explicitly state, analyze, and design for risk-targeted performance objectives, but implicitly expect them to be satisfied.

For reasons of practicability, Deb et al. (Deb et al. 2021c) distilled out a computationally more economical and simplified PBSD procedure from the findings obtained using the full-fledged risk-targeted design framework. The simplified PBSD method, while significantly alleviating the computational burden of the full-fledged method, inventively utilizes the findings of the latter to: (i) determine accurately the DP at the intersection of a chosen line in the primary design parameter space and the boundary of the feasible design domain of a bridge being designed for multiple risk-targeted performance objectives, and (ii) delineate an approximate, yet sufficiently accurate, feasible design domain and identify the *LS*s controlling its boundary in the primary design parameter space of the bridge.

For the purpose of this study, the as-designed and redesigned versions (DPs indicated by the red and yellow stars, respectively, in Figure 7.4) of the four testbed OSBs are re-evaluated after incorporation of the targeted additional sources of uncertainty that were neglected in the original study, i.e., (i) the aleatory uncertainty associated with FE model parameters, and (ii) the epistemic parameter estimation uncertainty (in addition to (i)) associated with the probability distributions characterizing the FE model parameters and *LS* fragilities. The systematic approach taken to this end along with the necessary modifications/upgrades to the originally updated and assembled PBEE assessment framework are outlined in the subsequent sections. It is to be noted that the choice of the redesigned versions of the testbed OSBs considered in this study is arbitrary, and the following discussion would hold equally well for the redesigns of these bridges obtained using the simplified PBSD method (Deb et al. 2021c), or any other viable redesigns for that matter.

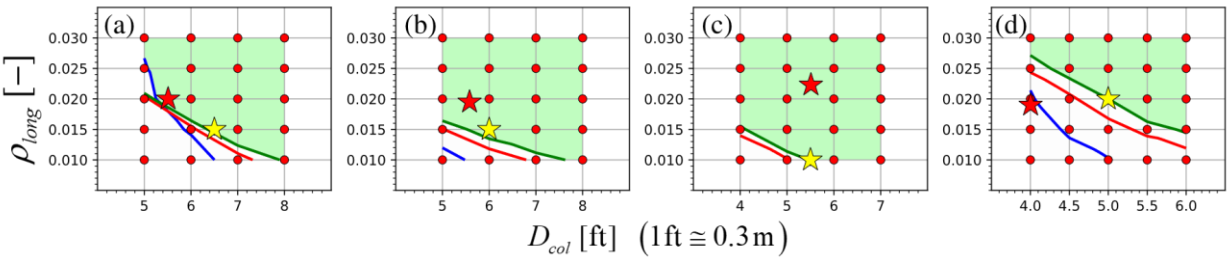

Figure 7.4 Risk-based feasible design domain, as-designed version (red star), and one possible redesigned version (yellow star) for (a) Bridge A, (b) Bridge B, (c) Bridge C, and (d) Bridge MAOC. Target MRP contour line for *LSs* 1, 2, and 3 shown in blue, red, and green, respectively

7.5 Incorporation of FE Model Parameter Uncertainty

The PEER PBEE framework integral in Eq. (7.1) can be rewritten as follows showing its explicit dependance on the vector $(\boldsymbol{\Theta})$ (denoted in bold font) of RVs describing random/uncertain FE model parameters:

$$\nu_{LS,k}\left(\boldsymbol{\Theta}=\boldsymbol{\theta}\right)=\int_{EDP_k} F_{EDP_{C,k}^{bridge}\,|\,\boldsymbol{\Theta}}\left(\delta\,|\,\boldsymbol{\theta}\right)\cdot\left|d\nu_{EDP_k|\boldsymbol{\Theta}}\left(\delta\,|\,\boldsymbol{\theta}\right)\right| \tag{7.6}$$

where $\boldsymbol{\theta}$ (in lower case) represents a specific realization (random variate) of $\boldsymbol{\Theta}$. The above form of the damage hazard integral clearly shows the dependence of the structural demand and capacity on the FE model parameter vector $\boldsymbol{\Theta}$. It is important to note that, for the results shown in Figure 7.4 where FE model parameter uncertainty is not accounted for, $\boldsymbol{\theta}$ corresponds to the expected value of each of the FE model parameters.

From the standpoint of basic MC simulation, as shown schematically in Figure 7.5, each simulated variate ($\boldsymbol{\theta}^{(i)},\ i \in [1, \ldots, N_S^{\boldsymbol{\Theta}}]$) of $\boldsymbol{\Theta}$, sampled from its joint probability distribution $f_{\boldsymbol{\Theta}}(\boldsymbol{\theta})$ representing the aleatory uncertainty of $\boldsymbol{\Theta}$, corresponds to a randomly realized bridge FE model. For each such FE model, a full-fledged probabilistic seismic performance assessment is carried out to obtain $\nu_{LS,k}(\boldsymbol{\theta}^{(i)})$, the conditional MAR of *LSE*, given $\boldsymbol{\Theta} = \boldsymbol{\theta}^{(i)}$, for *LS-k* as per Eq. (7.6). The unconditional MAR of exceedance of *LS-k* is theoretically defined as the expectation, with respect to (w.r.t) the joint PDF of $\boldsymbol{\Theta}$, of the conditional MAR of *LSE*, given $\boldsymbol{\Theta}$. This can be approximated in a MC sense by computing the sample mean estimate of $\nu_{LS,k}(\boldsymbol{\theta}^{(i)})$ for $i = 1, \ldots, N_S^{\boldsymbol{\Theta}}$ as shown below (note that, for any RV *X*, its PDF and the expectation operator w.r.t its PDF are denoted by $f_X(x)$ and $E_X[\cdot]$, respectively):

$$\begin{aligned} \nu_{LS,k} &= \int_{\boldsymbol{\Theta}} \nu_{LS,k}(\boldsymbol{\theta}) \cdot f_{\boldsymbol{\Theta}}(\boldsymbol{\theta}) \cdot d\boldsymbol{\theta} = E_{\boldsymbol{\Theta}}\left[\nu_{LS,k}(\boldsymbol{\Theta})\right] \\ &\cong \frac{1}{N_S^{\boldsymbol{\Theta}}} \sum_{i=1}^{N_S^{\boldsymbol{\Theta}}} \nu_{LS,k}\left(\boldsymbol{\theta}^{(i)}\right) \end{aligned} \tag{7.7}$$

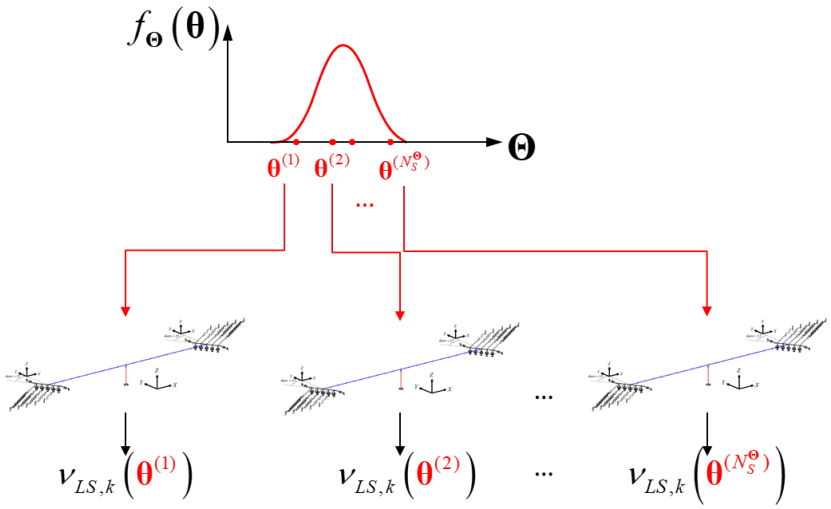

Figure 7.5 Schematic representation of the incorporation of FE model parameter uncertainty

An important quantity of interest to practicing engineers is the probability of *LSE* during a specified exposure time/period T_E. Assuming that – (i) the homogenous Poisson process describes the random earthquake temporal occurrences, (ii) the bridge in question (characterized by the FE model with $\boldsymbol{\Theta} = \boldsymbol{\theta}^{(i)}$) does not deteriorate in time and is restored to its initial undamaged state after each damaging earthquake, and (iii) the uncertainty in *IM*, record-to-record variability given *IM*, and the uncertainty in the normalized part (explained in the next line) of *LS* capacities (especially for load path/history dependent *LS*s such as rebar buckling/fracture) renew with each earthquake occurrence, the temporal exceedances of a specific *LS*, conditioned on $\boldsymbol{\Theta} = \boldsymbol{\theta}^{(i)}$, also follow a Poisson (censored-Poisson) random counting process. Note that an *LS* capacity is given by the product of a normalized part $EDP_{C,k}^{\text{MEAS}} / EDP_{C,k}^{\text{PRED}}$ and a predictive capacity part $EDP_{C,k}^{\text{PRED},\,bridge}(\boldsymbol{\theta}^{(i)})$; the former is assumed to renew with each earthquake occurrence while the $\boldsymbol{\Theta}$-dependent latter part remains invariant in time as the values of parameters $\boldsymbol{\Theta}$ (i.e., $\boldsymbol{\theta}^{(i)}$) do not renew at each earthquake occurrence (in stochastic process theory, the RVs in $\boldsymbol{\Theta}$ are said to be non-ergodic in time (Kiureghian 2005)). Thus, the Poisson probability of exceedance of *LS-k* at

least once during the exposure time T_E, conditioned on $\boldsymbol{\Theta} = \boldsymbol{\theta}^{(i)}$ (i.e., for the bridge characterized by the FE model with $\boldsymbol{\Theta} = \boldsymbol{\theta}^{(i)}$) is given by:

$$P\left[LSE \text{ during exposure time } T_E \mid \boldsymbol{\Theta} = \boldsymbol{\theta}^{(i)} \right] = 1 - \exp\left(-\nu_{LS,k}\left(\boldsymbol{\theta}^{(i)} \right) \times T_E \right) \tag{7.8}$$

Note that $\nu_{LS,k}$, the unconditional MAR of *LS-k* exceedance (given by Eq. (7.7) as the expected value of Poisson-MARs of *LSE*s conditioned on specific variates of $\boldsymbol{\Theta}$) is not the MAR of a Poisson process and one cannot just invoke Eq. (7.8) with $\nu_{LS,k}$ in the right-hand-side to determine the unconditional probability of *LS-k* exceedance during the exposure time T_E. The unconditional probability of exceedance of *LS-k* during the exposure time T_E is correctly estimated as:

$$\begin{aligned} P\left[LSE \text{ in time } T_E \right] &= \int_{\boldsymbol{\Theta}} 1 - \exp\left(-\nu_{LS,k}\left(\boldsymbol{\theta}^{(i)} \right) \times T_E \right) \cdot f_{\boldsymbol{\Theta}}\left(\boldsymbol{\theta} \right) \cdot d\boldsymbol{\theta} \\ &\cong \frac{1}{N_S^{\boldsymbol{\Theta}}} \sum_{i=1}^{N_S^{\boldsymbol{\Theta}}} 1 - \exp\left(-\nu_{LS,k}\left(\boldsymbol{\theta}^{(i)} \right) \times T_E \right) \end{aligned} \tag{7.9}$$

7.5.1 Random Variables

A total of 10 parameters influencing different aspects of FE modeling, e.g., material constitutive laws, soil-structure interaction, structural geometry, mass, and viscous damping, are modeled as basic RVs. These parameters include (note that a FE model parameter modeled as a RV is marked with a tilde):

- the compressive strength $(\tilde{f}_c')$ and the modulus of elasticity $(\tilde{E}_c)$ of unconfined concrete,
- the yield strength $(\tilde{f}_y)$, the ultimate strength $(\tilde{f}_u)$, the uniform strain $(\tilde{\varepsilon}_u)$, and the modulus of elasticity $(\tilde{E}_s)$, of steel rebars,

- the total ultimate strength ($\tilde{F}_{ult}$) and the total secant stiffness ($\tilde{K}_{50}$) (secant stiffness corresponding to $0.5\tilde{F}_{ult}$) of the embankment backfill on each side of a bridge,
- the RC weight density ($\tilde{w}_{conc}$), and
- the damping ratio ($\tilde{\xi}_{1,trans}$) assigned to the first mode of an OSB in the supposedly more critical transverse direction.

Table 7.3 provides the marginal probability distributions, expected values, and coefficients of variation (COVs) of each of these parameters as obtained from the available literature, experimental observations, and/or engineering judgment.

Table 7.3 Marginal distributions of RVs

RV (unit)	Marginal distribution	Expected value	COV (%)
$\tilde{f}_c'$ (MPa)	Normal (Mirza et al. 1979)	$1.3\,f_{c,nom}'$ (Caltrans 2013)	16
$\tilde{E}_c$ (MPa)	Normal (Mirza et al. 1979)	$3320\sqrt{1.3\,f_{c,nom}'}+6900$ (Carrasquillo et al. 1981)	10
$\tilde{f}_y$ (MPa)	Beta (Bournonville et al. 2004; Mirza and MacGregor 1979)	475.7 (Bournonville et al. 2004; Caltrans 2013)	4 (Carreño et al. 2020)
$\tilde{f}_u$ (MPa)	Beta (Bournonville et al. 2004; Mirza and MacGregor 1979)	656.4 (Bournonville et al. 2004)	3 (Carreño et al. 2020)
$\tilde{\varepsilon}_u$ (-)	Normal (Lee and Mosalam 2006; Mirza and Skrabek 1991)	0.15 (Lee and Mosalam 2006; Mirza and Skrabek 1991)	20 (Lee and Mosalam 2006; Mirza and Skrabek 1991)
$\tilde{E}_s$ (MPa)	Normal (Lee and Mosalam 2006; Mirza and MacGregor 1979)	2×10^5 (Lee and Mosalam 2006; Mirza and MacGregor 1979)	3.3 (Lee and Mosalam 2006; Mirza and MacGregor 1979)
$\tilde{K}_{50}$ (kN/mm)	Lognormal (Xie et al. 2019)	see Table 7.4	20
$\tilde{F}_{ult}$ (kN)	Lognormal (Xie et al. 2019)	see Table 7.4	20
$\tilde{w}_{conc}$ (kN/m^3)	Normal (Ellingwood et al. 1982)	22.6 (Caltrans 2013)	4
$\tilde{\xi}_{1,trans}$ (-)	Shifted lognormal	0.01	50 (Astroza et al. 2013)

Table 7.4 Expected values ($E[\cdot]$) of $\tilde{K}_{50}$ and $\tilde{F}_{ult}$ (Shamsabadi et al. 2020)

Bridge	**Skew** (degree)	**Backwall dim. (h × w)** (m)	$E[\tilde{K}_{50}]$ (kN/mm)	$E[\tilde{F}_{ult}]$ (kN)
A	33.0	1.4 × 6.5	81.5	967.5
B	0.0	1.9 × 19.2	598.7	9.5×10^3
C	36.0	1.9 × 24.3	342.3	5.5×10^3
MAOC	8.0	1.4 × 12.2	263.1	3.0×10^3

Remarks

(i) The Pearson's correlation coefficient between the following hyphen (-) separated pairs, viz., $\tilde{f}_c'$ - $\tilde{E}_c$, $\tilde{f}_y$ - $\tilde{f}_u$, $\tilde{f}_y$ - $\tilde{\varepsilon}_u$, $\tilde{f}_u$ - $\tilde{\varepsilon}_u$, and $\tilde{K}_{50}$ - $\tilde{F}_{ult}$ are assumed to be 0.40, 0.85 (JCSS 2001; Lee and Mosalam 2006; Mirza and MacGregor 1979), -0.50 (JCSS 2001; Lee and Mosalam

2006), -0.55 (JCSS 2001; Lee and Mosalam 2006), and 0.50, respectively. All other possible pairs of RVs are assumed to be statistically independent.

(ii) The respective COVs of $\tilde{f}_c'$ and $\tilde{E}_c$, and their correlation coefficient, are estimated using experimental data (corresponding to $\tilde{f}_c'$ lying between 34.5 MPa to 69 MPa) obtained from some recently conducted uniaxial compression tests on concrete cylinders (see Figure 7.6).

(iii) For ASTM (American Society for Testing and Materials) A 706 Grade 60 rebars (used in the testbed OSBs considered), the minimum and maximum values of $\tilde{f}_y$ are 413.7 MPa and 588.8 MPa, respectively (Bournonville et al. 2004), while those of $\tilde{f}_u$ are 551.6 MPa and 799.8 MPa, respectively (Bournonville et al. 2004).

(iv) Expected values and COVs of $\tilde{K}_{50}$ and $\tilde{F}_{ult}$ for the four testbed OSBs considered are calculated using the skew-log-spiral-hyperbolic model (Shamsabadi et al. 2020) assuming highly engineered embankment backfills with 95% compaction. The respective COVs of $\tilde{K}_{50}$ and $\tilde{F}_{ult}$, and their assumed (based on engineering judgment) correlation coefficient are in reasonable agreement with Xie et al. (Xie et al. 2019).

(v) In addition to capturing the natural variability of RC weight density, the assumed COV of $\tilde{w}_{conc}$ serves as a proxy for other sources of uncertainty in structural mass/gravity-loads such as geometric imperfections of formwork, and design versus built geometric characteristics.

(vi) $\tilde{\xi}_{1,trans}$ is assumed to follow the shifted lognormal distribution with a minimum value (shift) of 0.0025 to avoid impractically small damping ratios. The expected value of $\tilde{\xi}_{1,trans}$ is assumed to be 0.01 (small) to prevent double-counting of damping in a nonlinear FE model

wherein nonlinear material hysteresis is already explicitly accounted for. To damp out the effect of spurious higher modes, a high damping ratio of 0.05 is deterministically assigned to a sufficiently large frequency (e.g., 20 Hz).

(vii) Material parameters defining the stress-strain behavior of confined concrete (Mander et al. 1988) in bridge columns are modeled as derived RVs (depending on $\tilde{f}_c'$ and $\tilde{E}_c$ of column concrete, and $\tilde{f}_y$ and $\tilde{E}_s$ of transverse rebars). The strain hardening ratio parameter ($\tilde{b}$) of longitudinal rebars required in the *SteelMPF* material definition is modeled as a derived RV given by $(\tilde{f}_u - \tilde{f}_y) \times (0.5\tilde{\varepsilon}_u - \tilde{f}_y / \tilde{E}_s)^{-1} \times \tilde{E}_s^{-1}$. The force-deformation relationship of abutment exterior shear keys (Megally et al. 2002) depends on $\tilde{f}_c'$ of concrete in the abutment, and $\tilde{f}_y$ and $\tilde{E}_s$ of the shear key/stemwall reinforcement. The predictive capacity model for *LS*-2 (Eq. (7.4)) depends on $\tilde{f}_c'$ of column concrete, and $\tilde{f}_y$ and $\tilde{E}_s$ of column transverse rebars, while that for *LS*-3 (Eq. (7.5)) depends on $\tilde{f}_y$ and $\tilde{f}_u$ of column longitudinal rebars.

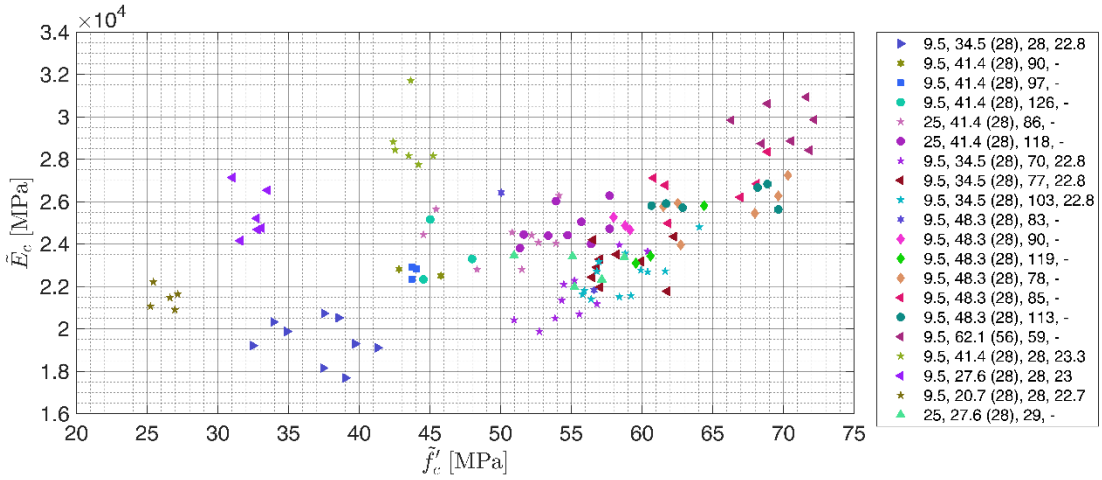

Figure 7.6 Experimentally measured values of $\tilde{f}_c'$ and $\tilde{E}_c$ for concrete cylinders tested in uniaxial compression. Values in the legend indicate maximum aggregate size (in mm), target compressive strength (in MPa) at day (in parentheses), age of specimen in days, and concrete unit weight (in kN/m^3) of the different batches of specimens tested.

7.5.2 Complete Vector and Correlation Matrix (Accounting for Random Spatial Variability) of FE Model Parameters

The complete vector $\boldsymbol{\Theta}$ of random FE model parameters and the corresponding matrix $\mathbf{R}$ of correlation coefficients between pairs of these parameters, approximately accounting for their spatial variability in the FE model of an OSB, are defined in this section. Incorporation of random spatial variability of FE model parameters can be rigorously achieved via stochastic FE modeling requiring a random field representation in terms of the considered RVs. However, for practical purposes, a simplified, yet reasonably accurate, approach is adopted in this paper.

Each plastic hinge region h ($h \in [1,2]$), of column c ($c \in [1,...,N_{col}]$, where N_{col} is the number of columns in a bridge) is characterized by a vector $\boldsymbol{\Theta}^{hinge\ h,col\ c}$ and a correlation matrix $\mathbf{R}^{hinge\ h,col\ c}$ given by:

$$\boldsymbol{\Theta}^{hinge\,h,\,col\,c} = \left[\underbrace{\tilde{f}_c'}_{\substack{\text{unconfined}\\\text{concrete}}},\ \underbrace{\tilde{E}_c}_{\substack{\text{unconfined}\\\text{concrete}}},\ \underbrace{\tilde{f}_y,\ \tilde{f}_u,\ \tilde{\varepsilon}_u,\ \tilde{E}_s}_{\substack{\text{longitudinal}\\\text{rebars}}},\ \underbrace{\tilde{f}_y,\ \tilde{E}_s}_{\substack{\text{transverse}\\\text{rebars}}} \right], \quad \mathbf{R}^{hinge\,h,\,col\,c} = \begin{bmatrix} 1.0 & & & & & & & \\ 0.40 & 1.0 & & & & & & \\ 0.0 & 0.0 & 1.0 & & & \textit{sym} & & \\ 0.0 & 0.0 & 0.85 & 1.0 & & & & \\ 0.0 & 0.0 & -0.5 & -0.55 & 1.0 & & & \\ 0.0 & 0.0 & 0.0 & 0.0 & 0.0 & 1.0 & & \\ 0.0 & 0.0 & 0.0 & 0.0 & 0.0 & 0.0 & 1.0 & \\ 0.0 & 0.0 & 0.0 & 0.0 & 0.0 & 0.0 & 0.0 & 1.0 \end{bmatrix} \tag{7.10}$$

Each abutment a $(a \in [1,2])$ is characterized by a vector $\boldsymbol{\Theta}^{abut\,a}$ and a correlation matrix $\mathbf{R}^{abut\,a}$ given by

$$\boldsymbol{\Theta}^{abut\,a} = \left[\underbrace{\tilde{f}_c',\ \tilde{f}_y,\ \tilde{E}_s}_{\substack{\text{shear key concrete}\\\text{and reinforcement}}},\ \underbrace{\tilde{K}_{50},\ \tilde{F}_{ult}}_{\substack{\text{embankment}\\\text{backfill}}} \right], \quad \mathbf{R}^{abut\,a} = \begin{bmatrix} 1.0 & & & & \\ 0.0 & 1.0 & & \textit{sym} & \\ 0.0 & 0.0 & 1.0 & & \\ 0.0 & 0.0 & 0.0 & 1.0 & \\ 0.0 & 0.0 & 0.0 & 0.5 & 1.0 \end{bmatrix} \tag{7.11}$$

Finally, the vector $\boldsymbol{\Theta}$ and the correlation matrix $\mathbf{R}$ of random FE model parameters are defined as follows:

$$\boldsymbol{\Theta} = \left[...,\ \boldsymbol{\Theta}^{hinge\,h,\,col\,c},\ ...,\ \boldsymbol{\Theta}^{abut\,a},\ ...,\ \tilde{w}_{conc},\ \tilde{\xi}_{1,trans} \right]^T, \quad \mathbf{R} = \begin{bmatrix} \ddots & & & & & \\ & \mathbf{R}^{hinge\,h,\,col\,c} & & & \mathbf{0} & \\ & & \ddots & & & \\ & & & \mathbf{R}^{abut\,a} & & \\ & & & & \ddots & \\ & \mathbf{0} & & & & 1 \\ & & & & & & 1 \end{bmatrix} \tag{7.12}$$

7.5.3 Latin Hypercube Sampling

Latin hypercube (LH) sampling is a variance reduction technique that is widely used in seismic response assessment of structures. This method has been shown to effectively reduce the variance of the class of estimators of the form given by Eq.s (7.7) and (7.9) (i.e., the sample mean estimator) (McKay et al. 2000), especially for small to moderate sample size, by drawing variates of the considered RVs from equiprobable disjoint strata covering the entire range of possible values of these RVs. Under incomplete probability information of prescribed marginal distributions of the RVs in $\boldsymbol{\Theta}$ and their correlation matrix $\mathbf{R}$, $N_S^{\boldsymbol{\Theta}}$ variates of $\boldsymbol{\Theta}$, preserving the desired correlation structure, are generated according to the following algorithm (Chang et al. 1994) (demonstrated in Figure 7.7 (a) through (d) for a special case of correlated RVs $\boldsymbol{\Theta} = [\tilde{K}_{50}, \tilde{F}_{ult}]^T$ for Bridge A, and $N_S^{\boldsymbol{\Theta}}$ = 30.):

- Generate $N_S^{\boldsymbol{\Theta}}$ LH variates $(\mathbf{u}^{(i)},\ i = 1, \ldots, N_S^{\boldsymbol{\Theta}})$ of a vector $\mathbf{U}$ (of dimension equal to that of $\boldsymbol{\Theta}$) of independent uniformly distributed (between 0 and 1) RVs (see Figure 7.7 (a)).
- Transform $\mathbf{u}^{(i)}$ to independent standard normal variates $\mathbf{z}^{(i)}$ by $\mathbf{z}^{(i)} = \Phi^{-1}(\mathbf{u}^{(i)})$, where $\Phi^{-1}(\cdot)$ is the standard normal inverse cumulative distribution function (CDF) (see Figure 7.7 (b)).
- Transform $\mathbf{z}^{(i)}$ to correlated standard normal variates $\mathbf{y}^{(i)}$ by inverse orthogonal transformation, i.e., $\mathbf{y}^{(i)} = \boldsymbol{\Psi}_{\mathbf{R}'} \cdot \boldsymbol{\Lambda}_{\mathbf{R}'} \cdot \mathbf{z}^{(i)}$, where $\boldsymbol{\Psi}_{\mathbf{R}'}$ and $\boldsymbol{\Lambda}_{\mathbf{R}'}$ are the matrix of eigenvectors and the diagonal matrix of eigenvalues of $\mathbf{R}'$, the equivalent correlation matrix of $\mathbf{R}$ in the standard normal space as per the Nataf model (Liu and Der Kiureghian 1986), respectively (see Figure 7.7 (c))

- Transform $\mathbf{y}^{(i)}$ to the targeted variates $\boldsymbol{\theta}^{(i)}$ by the following one-to-one nonlinear transformation $\theta_m^{(i)} = F_{\Theta_m}^{-1}(\Phi(y_m^{(i)}))$, where $\theta_m^{(i)} \in \boldsymbol{\theta}^{(i)}$, $y_m^{(i)} \in \mathbf{y}^{(i)}$, $F_{\Theta_m}^{-1}(\cdot)$ is the marginal inverse CDF of Θ_m, and $\Phi(\cdot)$ is the standard normal CDF (see Figure 7.7 (d)).

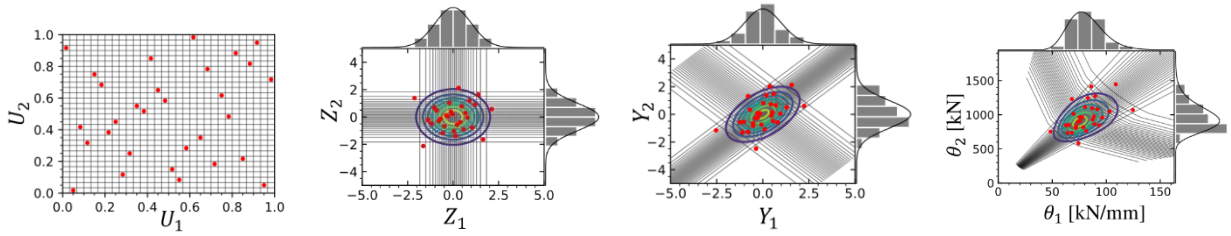

(a) (b) (c) (d)

Figure 7.7 LH sampling of correlated RVs $\boldsymbol{\Theta} = [\tilde{K}_{50}, \tilde{F}_{ult}]^T$ for Bridge A (contour lines represent the Nataf joint PDF of $\boldsymbol{\Theta}$ and the regions between grid lines represent equiprobable strata)

7.5.4 Probabilistic Seismic Damage Hazard Analysis with Revised Definition of *LS*s and Associated *EDP*s

The considered set of *LS*s and their associated *EDP*s, previously defined at the system level (i.e., extremum over all plastic hinge regions and columns of a bridge) (Deb et al. 2021b), are now redefined at the component level for each plastic hinge region h $(h \in [1,2])$ of column c $(c \in [1,..., N_{col}])$ in the FE model realization corresponding to $\boldsymbol{\Theta} = \boldsymbol{\theta}^{(i)}$ $(i \in [1,..., N_S^{\boldsymbol{\Theta}}])$ as shown in Table 7.5.

Table 7.5 Revised definitions of *LS*s and associated *EDP*s for FE model corresponding to a single FE model realization

#	***LS* (for hinge *h* of column *c*)**	**Associated *EDP* (for hinge *h* of column *c*)**
1	Concrete cover spalling	Maximum absolute compressive strain of any longitudinal rebar $EDP_1^{h,c} = \max_{bar}\left(\max_t \left\lvert \varepsilon_{comp}^{bar}(t)\right\rvert\right)$
2	Onset of longitudinal rebar buckling	Maximum tensile strain of any longitudinal rebar $EDP_2^{h,c} = \max_{bar}\left(\max_t \varepsilon_{tensile}^{bar}(t)\right)$
3	Precursor to longitudinal rebar fracture	Maximum difference of tensile (positive) and compressive (negative) strain, the latter following the former, of any longitudinal rebar $EDP_3^{h,c} = \max_{bar}\left(\max_t \varepsilon_{tensile}^{bar}(t) - \min_{t'>t} \varepsilon_{comp}^{bar}(t')\right)$

The damage hazard integral (Eq. (7.6)) is rewritten as follows in terms of the revised definition of the k^{th} *LS* and its associated *EDP*:

$$\nu_{LS,k}^{h,c}\left(\boldsymbol{\theta}^{(i)}\right) = \int_{EDP_k^{h,c}} F_{EDP_{C,k}^{h,c}|\boldsymbol{\Theta}}\left(\delta \mid \boldsymbol{\theta}^{(i)}\right) \cdot \left| d\nu_{EDP_k^{h,c}|\boldsymbol{\Theta}}\left(\delta \mid \boldsymbol{\theta}^{(i)}\right)\right| \tag{7.13}$$

where $\nu_{LS,k}^{h,c}(\boldsymbol{\theta}^{(i)})$ is the MAR of exceedance of *LS-k*, $\nu_{EDP_k^{h,c}|\boldsymbol{\Theta}}\left(\delta \mid \boldsymbol{\theta}^{(i)}\right)$ is the demand hazard curve in terms of $EDP_k^{h,c}$, and $EDP_{C,k}^{h,c}$ is the structural capacity against the exceedance of *LS-k*, all corresponding to plastic hinge region *h* of column *c* in the bridge FE model realization given by $\boldsymbol{\Theta} = \boldsymbol{\theta}^{(i)}$. $EDP_{C,k}^{h,c}$ given $\boldsymbol{\Theta} = \boldsymbol{\theta}^{(i)}$ in Eq. (7.13) can be written (in a way similar to Eq. (7.2)) as:

$$EDP_{C,k}^{h,c} \mid \boldsymbol{\Theta} = \boldsymbol{\theta}^{(i)} = \frac{EDP_{C,k}^{\text{MEAS}}}{EDP_{C,k}^{\text{PRED}}} \times EDP_{C,k}^{\text{PRED},h,c}\left(\boldsymbol{\theta}^{(i)}\right) \tag{7.14}$$

where $EDP_{C,k}^{\text{PRED},h,c}\left(\boldsymbol{\theta}^{(i)}\right)$ is the predicted (using the predictive capacity model for *LS-k*) value of capacity against the exceedance of *LS-k* in plastic hinge region *h* of column *c* in the bridge model realization corresponding to $\boldsymbol{\Theta}=\boldsymbol{\theta}^{(i)}$. Note that under a lognormal distribution assumption for the normalized RV $EDP_{C,k}^{\text{MEAS}} / EDP_{C,k}^{\text{PRED}}$ with parameters $\lambda_{C,k}$ and $\zeta_{C,k}$ (which are the mean and the standard deviation of the natural logarithm of $EDP_{C,k}^{\text{MEAS}} / EDP_{C,k}^{\text{PRED}}$, respectively), the RV $EDP_{C,k}^{h,c}$ given $\boldsymbol{\Theta}=\boldsymbol{\theta}^{(i)}$ also follows a lognormal distribution with parameters given by $\lambda_{C,k}+\log EDP_{C,k}^{\text{PRED},h,c}\left(\boldsymbol{\theta}^{(i)}\right)$ and $\zeta_{C,k}$, respectively.

PSDamHA thus entails the convolution (as per Eq. (7.13)) of the fragility curve for each plastic hinge region of each column in each bridge model realization (the first term of the integrand in Eq. (7.13)) with the corresponding absolute differential of the demand hazard curve (the second term of the integrand in Eq. (7.13)). The MAR of exceedance of *LS-k* at the system level for a particular bridge model realization characterized by $\boldsymbol{\Theta}=\boldsymbol{\theta}^{(i)}$ is then defined as the most frequent (over all plastic hinge regions in different columns of the bridge) rate of *LS-k* exceedance and computed as follows:

$$\nu_{LS,k}\left(\boldsymbol{\theta}^{(i)}\right)=\max_{h,c}\left(...,\ \nu_{LS,k}^{h,c}\left(\boldsymbol{\theta}^{(i)}\right),\ ...\right) \tag{7.15}$$

It is noted that, for simplicity, a single component-level performance metric (i.e., the MAR of *LS-k* exceedance in a single plastic hinge region) is evaluated independently/irrespective of the performance of other plastic hinge regions in the bridge, thus not requiring the statistical correlation between *EDP-k*'s corresponding to different plastic hinge regions in different columns of an OSB. This correlation can be accounted for in future research to rigorously explore the joint statistical behavior of *LSE*s in different regions/parts of a bridge. Finally, Eq.s (7.7) and (7.9) are

invoked to determine the unconditional (or expected value of), w.r.t the joint PDF of $\boldsymbol{\Theta}$, MAR and probability (in some exposure period), respectively, of exceedance of *LS-k* for a bridge.

7.6 Incorporation of Probability Distribution Parameter Estimation Uncertainty

The damage hazard integral, giving the MAR of exceedance of *LS-k* at the system level for a specific bridge model realization, explicitly conditioned on the probability distribution parameters (also referred to as probabilistic model parameters) of the RVs at play is rewritten as follows:

$$\nu_{LS,k}\left(\boldsymbol{\theta},\boldsymbol{\lambda}_{L,k}\right)=\max_{h,c}\left(...,\int_{EDP_k^{h,c}} F_{EDP_{C,k}^{h,c}|\boldsymbol{\Theta},\boldsymbol{\Lambda}_{L,k}}\left(\delta\,|\,\boldsymbol{\theta},\boldsymbol{\lambda}_{L,k}\right)\cdot\left|d\nu_{EDP_k^{h,c}|\boldsymbol{\Theta}}\left(\delta\,|\,\boldsymbol{\theta}\right)\right|,\ ...\right) \tag{7.16}$$

where $\boldsymbol{\theta}$ is a specific variate of $\boldsymbol{\Theta}$ drawn from $f_{\boldsymbol{\Theta}|\boldsymbol{\Lambda}_{\boldsymbol{\Theta}}}(\boldsymbol{\theta}\,|\,\boldsymbol{\lambda}_{\boldsymbol{\Theta}})$, the joint PDF of $\boldsymbol{\Theta}$ conditioned on a specific variate $(\boldsymbol{\lambda}_{\boldsymbol{\Theta}})$ of the vector $(\boldsymbol{\Lambda}_{\boldsymbol{\Theta}})$ of parameters (e.g., means, COVs, and correlation coefficients) characterizing the probability structure of $\boldsymbol{\Theta}$, and $\boldsymbol{\lambda}_{L,k}$ is a specific variate of the vector $(\boldsymbol{\Lambda}_{L,k})$ of probabilistic model parameters characterizing the normalized fragility function corresponding to *LS-k*. Parameters in $\boldsymbol{\Lambda}_{\boldsymbol{\Theta}}$ and $\boldsymbol{\Lambda}_{L,k}$ are modeled as RVs owing to finite-sample estimation (say with n_s samples) of these parameters in practice. The unconditional (w.r.t the joint PDF of $\boldsymbol{\Theta}$, $\boldsymbol{\Lambda}_{\boldsymbol{\Theta}}$, and $\boldsymbol{\Lambda}_{L,k}$) MAR of exceedance of *LS-k* is hence given by:

$$
\begin{aligned}
\nu_{LS,k} &= E_{\boldsymbol{\Lambda}_{L,k}\boldsymbol{\Lambda}_{\boldsymbol{\Theta}}\boldsymbol{\Theta}}\left[\nu_{LS,k}\left(\boldsymbol{\Theta},\boldsymbol{\Lambda}_{L,k}\right)\right] = \\
&= \int_{\boldsymbol{\Lambda}_{L,k}}\int_{\boldsymbol{\Lambda}_{\boldsymbol{\Theta}}}\int_{\boldsymbol{\Theta}} \nu_{LS,k}\left(\boldsymbol{\theta},\boldsymbol{\lambda}_{L,k}\right)\cdot f_{\boldsymbol{\Theta}|\boldsymbol{\Lambda}_{\boldsymbol{\Theta}}}\left(\boldsymbol{\theta}\,|\,\boldsymbol{\lambda}_{\boldsymbol{\Theta}}\right)\cdot f_{\boldsymbol{\Lambda}_{\boldsymbol{\Theta}}}\left(\boldsymbol{\lambda}_{\boldsymbol{\Theta}}\right)\cdot f_{\boldsymbol{\Lambda}_{L,k}}\left(\boldsymbol{\lambda}_{L,k}\right)\cdot d\boldsymbol{\theta}\cdot d\boldsymbol{\lambda}_{\boldsymbol{\Theta}}\cdot d\boldsymbol{\lambda}_{L,k} \\
&= \int_{\boldsymbol{\Lambda}_{L,k}}\int_{\boldsymbol{\Theta}} \nu_{LS,k}\left(\boldsymbol{\theta},\boldsymbol{\lambda}_{L,k}\right)\cdot \overline{f}_{\boldsymbol{\Theta}}\left(\boldsymbol{\theta}\right)\cdot f_{\boldsymbol{\Lambda}_{L,k}}\left(\boldsymbol{\lambda}_{L,k}\right)\cdot d\boldsymbol{\theta}\cdot d\boldsymbol{\lambda}_{L,k} \\
&\cong \frac{1}{N_S^{\boldsymbol{\Theta}}}\sum_{i=1}^{N_S^{\boldsymbol{\Theta}}}\frac{1}{N_S^{\boldsymbol{\Lambda}_{L,k}}}\sum_{l=1}^{N_S^{\boldsymbol{\Lambda}_{L,k}}} \nu_{LS,k}\left(\boldsymbol{\theta}^{(i)},\boldsymbol{\lambda}_{L,k}^{(l)}\right)
\end{aligned}
\tag{7.17}
$$

where $\boldsymbol{\lambda}_{L,k}^{(l)}$ $(l=1,\ldots,N_S^{\boldsymbol{\Lambda}_{L,k}})$ in Eq. (7.17) are specific variates of $\boldsymbol{\Lambda}_{L,k}$, drawn from its joint PDF $f_{\boldsymbol{\Lambda}_{L,k}}\left(\boldsymbol{\lambda}_{L,k}\right)$ for a given n_s (also known as the sampling distribution of $\boldsymbol{\Lambda}_{L,k}$ given n_s; the procedure to draw these variates is discussed in the next section), and $\boldsymbol{\theta}^{(i)}$ $(i=1,\ldots,N_S^{\boldsymbol{\Theta}})$ are variates of $\boldsymbol{\Theta}$ drawn from $\overline{f}_{\boldsymbol{\Theta}}\left(\boldsymbol{\theta}\right)$, the predictive (marked with a bar) joint PDF of $\boldsymbol{\Theta}$ defined as follows:

$$
\begin{aligned}
\overline{f}_{\boldsymbol{\Theta}}\left(\boldsymbol{\theta}\right) &= \int_{\boldsymbol{\Lambda}_{\boldsymbol{\Theta}}} f_{\boldsymbol{\Theta}|\boldsymbol{\Lambda}_{\boldsymbol{\Theta}}}\left(\boldsymbol{\theta}\,|\,\boldsymbol{\lambda}_{\boldsymbol{\Theta}}\right)\cdot f_{\boldsymbol{\Lambda}_{\boldsymbol{\Theta}}}\left(\boldsymbol{\lambda}_{\boldsymbol{\Theta}}\right)\cdot d\boldsymbol{\lambda}_{\boldsymbol{\Theta}} \\
&\cong \frac{1}{N_S^{\boldsymbol{\Lambda}_{\boldsymbol{\Theta}}}}\sum_{j=1}^{N_S^{\boldsymbol{\Lambda}_{\boldsymbol{\Theta}}}} f_{\boldsymbol{\Theta}|\boldsymbol{\Lambda}_{\boldsymbol{\Theta}}}\left(\boldsymbol{\theta}\,|\,\boldsymbol{\lambda}_{\boldsymbol{\Theta}}^{(j)}\right)
\end{aligned}
\tag{7.18}
$$

where $\boldsymbol{\lambda}_{\boldsymbol{\Theta}}^{(j)}$ $(j=1,\ldots,N_S^{\boldsymbol{\Lambda}_{\boldsymbol{\Theta}}})$ in Eq. (7.18) are specific variates of $\boldsymbol{\Lambda}_{\boldsymbol{\Theta}}$, drawn from its joint PDF $f_{\boldsymbol{\Lambda}_{\boldsymbol{\Theta}}}\left(\boldsymbol{\lambda}_{\Theta}\right)$ for a given n_s (i.e., the sampling distribution of $\boldsymbol{\Lambda}_{\boldsymbol{\Theta}}$ given n_s; the procedure to draw theses variates is discussed next). The above discussion is schematically described in Figure 7.8

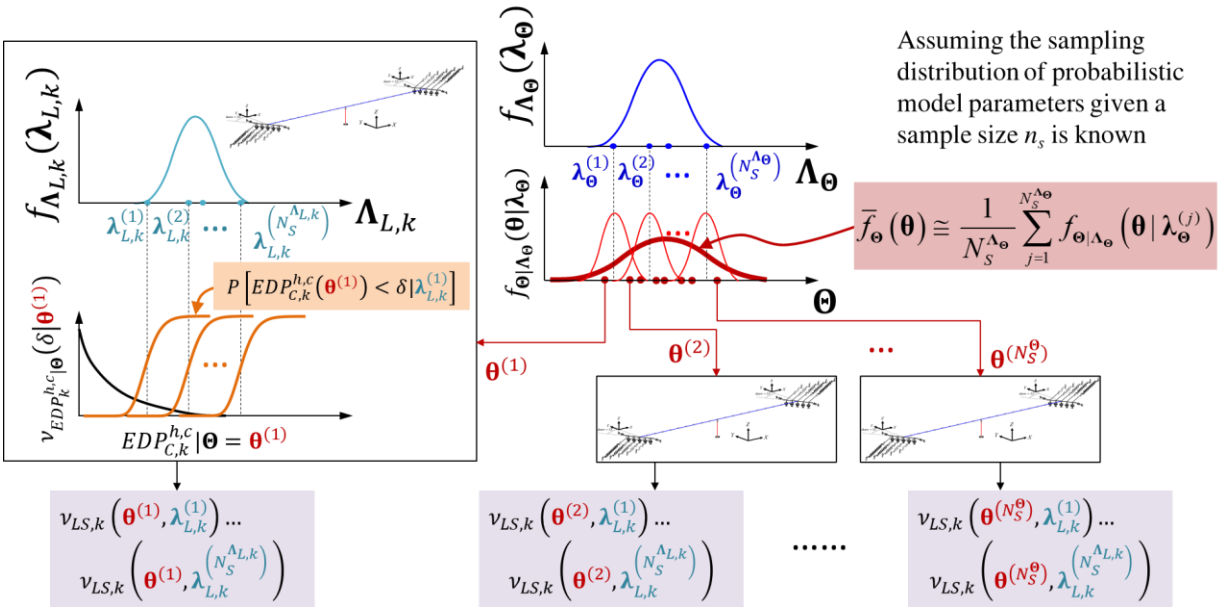

Figure 7.8 Schematic representation of the incorporation of probabilistic model parameter estimation uncertainty using MCS

7.6.1 Drawing Variates from the Sampling Distribution of Probabilistic Model Parameters

It is noted that the predictive distribution of FE model parameters, i.e., $\bar{f}_{\boldsymbol{\Theta}}(\boldsymbol{\theta})$, as per Eq. (7.18), follows a mixture distribution defined as the sample mean of $f_{\boldsymbol{\Theta}|\boldsymbol{\Lambda}_{\boldsymbol{\Theta}}}(\boldsymbol{\theta}\,|\,\boldsymbol{\lambda}_{\boldsymbol{\Theta}}^{(j)})$ $(j=1,\ldots,N_S^{\boldsymbol{\Lambda}_{\boldsymbol{\Theta}}})$ in an MC sense. Thus, $\bar{f}_{\boldsymbol{\Theta}}(\boldsymbol{\theta})$ can be very accurately and inexpensively approximated (schematically shown in Figure 7.8 (b)) using massive MC simulation of an arbitrarily large number (say 50,000) of variates ($\boldsymbol{\lambda}_{\boldsymbol{\Theta}}^{(j)}$, $j=1,\ldots,N_S^{\boldsymbol{\Lambda}_{\boldsymbol{\Theta}}}$) of $\boldsymbol{\Lambda}_{\boldsymbol{\Theta}}$, provided the joint distribution of $\boldsymbol{\Lambda}_{\boldsymbol{\Theta}}$ (for a given n_s) is known. It is to be noted that the uncertainty in $\boldsymbol{\Lambda}_{\boldsymbol{\Theta}}$ is purely epistemic in nature with $f_{\boldsymbol{\Lambda}_{\boldsymbol{\Theta}}}(\boldsymbol{\lambda}_{\boldsymbol{\Theta}})$ approaching the Dirac delta function $\delta(\boldsymbol{\lambda}_{\boldsymbol{\Theta}}-\boldsymbol{\lambda}_{\boldsymbol{\Theta}}^{\mathrm{TRUE}})$ and $\bar{f}_{\boldsymbol{\Theta}}(\boldsymbol{\theta})$ approaching the true distribution $f_{\boldsymbol{\Theta}}(\boldsymbol{\theta})$ as n_s approaches ∞.

A complete knowledge of the joint distribution of $\boldsymbol{\Lambda}_{\boldsymbol{\Theta}}$ for a given n_s requires deriving joint distributions of sample statistics which are functions of the underlying RVs in $\boldsymbol{\Theta}$. Closed-form solutions of such distributions are available in the literature only for a few special cases when the underlying RVs are distributed according to some specific distributions. Deriving the joint distribution $f_{\boldsymbol{\Lambda}_{\boldsymbol{\Theta}}}(\boldsymbol{\lambda}_{\boldsymbol{\Theta}})$ in closed-form for the general case of correlated RVs (listed in Table 7.3) is extremely challenging, if not impossible. Therefore, a MC simulation-based algorithmic expedient (described below) is incorporated in this study to generate $N_S^{\boldsymbol{\Lambda}_{\boldsymbol{\Theta}}}$ variates of $\boldsymbol{\Lambda}_{\boldsymbol{\Theta}}$ without knowing the form of $f_{\boldsymbol{\Lambda}_{\boldsymbol{\Theta}}}(\boldsymbol{\lambda}_{\boldsymbol{\Theta}})$ for a given n_s.

- Assume that the known parameters (e.g., means, COVs, and correlation coefficients) characterizing the probability structure of $\boldsymbol{\Theta}$ are the true parameters, given by $\boldsymbol{\lambda}_{\boldsymbol{\Theta}}^{\text{TRUE}}$
- Repeat the following steps for $j = 1, \ldots, N_S^{\boldsymbol{\Lambda}_{\boldsymbol{\Theta}}}$
    - Generate n_s random (not LH) variates of $\boldsymbol{\Theta}$ drawn from $f_{\boldsymbol{\Theta}|\boldsymbol{\Lambda}_{\boldsymbol{\Theta}}}(\boldsymbol{\theta} \mid \boldsymbol{\lambda}_{\boldsymbol{\Theta}}^{\text{TRUE}})$ (Note that for this purpose, the algorithm described under section 7.5.3 can be used by modifying just the first step to generate n_s (and not $N_S^{\boldsymbol{\Theta}}$) random (and not LH) variates of independent uniformly distributed (between 0 and 1) RVs).
    - With n_s variates of $\boldsymbol{\Theta}$ generated in the previous step, estimate the j^{th} variate of the sample mean vector and sample covariance matrix of $\boldsymbol{\Theta}$
    - Compute $\boldsymbol{\lambda}_{\boldsymbol{\Theta}}^{(j)}$, i.e., the j^{th} variate of parameters characterizing the probability structure of $\boldsymbol{\Theta}$ using the quantities estimated (using n_s samples) in the previous step.

The algorithm described above holds equally well for generating $N_S^{\boldsymbol{\Lambda}_{L,k}}$ variates of $\boldsymbol{\Lambda}_{L,k}$ to be used in Eq. (7.17) without knowing the form of $f_{\boldsymbol{\Lambda}_{L,k}}(\boldsymbol{\lambda}_{L,k})$ for a given n_s. For *LS-k*, replace

$\boldsymbol{\Theta}$ in the above algorithm with the RV $EDP_{C,k}^{\text{MEAS}} / EDP_{C,k}^{\text{PRED}}$ which is assumed to follow a lognormal distribution with the probabilistic model parameter vector $\boldsymbol{\Lambda}_{L,k}$ defined as $[\tilde{\lambda}_{C,k}, \tilde{\zeta}_{C,k}]$, where $\tilde{\lambda}_{C,k}$ and $\tilde{\zeta}_{C,k}$ (note the tilde on each parameter representing a RV) are the mean and the standard deviation of $\ln(EDP_{C,k}^{\text{MEAS}} / EDP_{C,k}^{\text{PRED}})$, respectively.

7.6.2 Predictive Distribution of FE Model Parameters

Having generated $N_S^{\boldsymbol{\Lambda}_\Theta}$ variates of $\boldsymbol{\Lambda}_{\boldsymbol{\Theta}}$, a Nataf model of the predictive joint distribution of $\boldsymbol{\Theta}$ corresponding to a specific value of n_s can now be constructed wherein each RV in $\boldsymbol{\Theta}$ can be assumed to marginally follow a mixture distribution with a PDF and a CDF given by

$$\begin{aligned} \bar{f}_{\Theta_m}(\theta_m) &\cong \frac{1}{N_S^{\boldsymbol{\Lambda}_\Theta}} \sum_{j=1}^{N_S^{\boldsymbol{\Lambda}_\Theta}} f_{\Theta_m \mid \boldsymbol{\Lambda}_{\Theta_m}}\left(\theta_m \mid \boldsymbol{\lambda}_{\Theta_m}^{(j)}\right) \\ \bar{F}_{\Theta_m}(\theta_m) &\cong \frac{1}{N_S^{\boldsymbol{\Lambda}_\Theta}} \sum_{j=1}^{N_S^{\boldsymbol{\Lambda}_\Theta}} F_{\Theta_m \mid \boldsymbol{\Lambda}_{\Theta_m}}\left(\theta_m \mid \boldsymbol{\lambda}_{\Theta_m}^{(j)}\right) \end{aligned} \qquad \Theta_m \in \boldsymbol{\Theta},\ \boldsymbol{\Lambda}_{\Theta_m} \subset \boldsymbol{\Lambda}_{\boldsymbol{\Theta}} \tag{7.19}$$

The total mean vector (denoted by $\bar{\boldsymbol{\mu}}_{\boldsymbol{\Theta}}$) and the total covariance matrix (denoted by $\bar{\boldsymbol{\Sigma}}_{\boldsymbol{\Theta}\boldsymbol{\Theta}}$) of $\boldsymbol{\Theta}$ to be used in defining the Nataf model of the predictive joint distribution can be determined as follows (note that a subscripted expectation ($E[\cdot]$) or covariance ($\text{cov}[\cdot]$) operator indicates the operation w.r.t the joint PDF of the vector in the subscript):

$$\bar{\boldsymbol{\mu}}_{\boldsymbol{\Theta}} = E_{\boldsymbol{\Lambda}_\Theta}\left[E_{\boldsymbol{\Theta}|\boldsymbol{\Lambda}_\Theta}\left[\boldsymbol{\Theta}|\boldsymbol{\Lambda}_\Theta\right]\right] \cong \frac{1}{N_S^{\boldsymbol{\Lambda}_\Theta}} \sum_{j=1}^{N_S^{\boldsymbol{\Lambda}_\Theta}} \underbrace{\frac{1}{n_s} \sum_{s=1}^{n_s} \boldsymbol{\theta}^{(s)} \mid \boldsymbol{\lambda}_{\boldsymbol{\Theta}}^{(j)}}_{\boldsymbol{\mu}_{\boldsymbol{\Theta}|\boldsymbol{\Lambda}_\Theta}^{(j)}} \tag{7.20}$$

$$\begin{aligned}\bar{\boldsymbol{\Sigma}}_{\boldsymbol{\Theta}\boldsymbol{\Theta}} &= E_{\boldsymbol{\Lambda}_{\boldsymbol{\Theta}}}\left[\mathrm{cov}_{\boldsymbol{\Theta}|\boldsymbol{\Lambda}_{\boldsymbol{\Theta}}}\left[\boldsymbol{\Theta},\boldsymbol{\Theta}\,|\,\boldsymbol{\Lambda}_{\boldsymbol{\Theta}}\right]\right]+\mathrm{cov}_{\boldsymbol{\Lambda}_{\boldsymbol{\Theta}}}\left[E_{\boldsymbol{\Theta}|\boldsymbol{\Lambda}_{\boldsymbol{\Theta}}}\left[\boldsymbol{\Theta}\,|\,\boldsymbol{\Lambda}_{\boldsymbol{\Theta}}\right],E_{\boldsymbol{\Theta}|\boldsymbol{\Lambda}_{\boldsymbol{\Theta}}}\left[\boldsymbol{\Theta}\,|\,\boldsymbol{\Lambda}_{\boldsymbol{\Theta}}\right]\right] \\ &\cong \frac{1}{N_S^{\boldsymbol{\Lambda}_{\boldsymbol{\Theta}}}}\sum_{j=1}^{N_S^{\boldsymbol{\Lambda}_{\boldsymbol{\Theta}}}}\frac{1}{n_s-1}\sum_{s=1}^{n_s}\left[\left(\boldsymbol{\theta}^{(s)}\,|\,\boldsymbol{\lambda}_{\boldsymbol{\Theta}}^{(j)}\right)-\boldsymbol{\mu}_{\boldsymbol{\Theta}|\boldsymbol{\Lambda}_{\boldsymbol{\Theta}}}^{(j)}\right]\left[\left(\boldsymbol{\theta}^{(s)}\,|\,\boldsymbol{\lambda}_{\boldsymbol{\Theta}}^{(j)}\right)-\boldsymbol{\mu}_{\boldsymbol{\Theta}|\boldsymbol{\Lambda}_{\boldsymbol{\Theta}}}^{(j)}\right]^T+\ldots \\ &\quad \ldots+\frac{1}{N_S^{\boldsymbol{\Lambda}_{\boldsymbol{\Theta}}}-1}\sum_{j=1}^{N_S^{\boldsymbol{\Lambda}_{\boldsymbol{\Theta}}}}\left(\boldsymbol{\mu}_{\boldsymbol{\Theta}|\boldsymbol{\Lambda}_{\boldsymbol{\Theta}}}^{(j)}-\bar{\boldsymbol{\mu}}_{\boldsymbol{\Theta}}\right)\left(\boldsymbol{\mu}_{\boldsymbol{\Theta}|\boldsymbol{\Lambda}_{\boldsymbol{\Theta}}}^{(j)}-\bar{\boldsymbol{\mu}}_{\boldsymbol{\Theta}}\right)^T\end{aligned} \tag{7.21}$$

The algorithm described under section 7.5.3 can now be invoked to generate LH variates of $\boldsymbol{\Theta}$ drawn from its predictive joint distribution. Note that the marginal inverse predictive CDF, $\bar{F}_{\Theta_m}^{-1}(\cdot)$, required in the algorithm can be obtained numerically.

7.7 Case Studies and Discussion of Results

Three analysis cases are considered to evaluate the impact of the inclusion of the targeted additional sources of uncertainty in the seismic performance assessment of the considered OSBs. These cases include:

- Case 1: As-designed testbed OSBs (red stars in Figure 7.4) with FE model parameter uncertainty only,
- Case 2: As-designed testbed OSBs (red stars in Figure 7.4) with both FE model parameter uncertainty and probability distribution parameter estimation uncertainty, and
- Case 3: Redesigned testbed OSBs (yellow stars in Figure 7.4) with both FE model parameter uncertainty and probability distribution parameter estimation uncertainty.

For each testbed OSB analyzed under each analysis case, 50 variates of the FE model parameter vector $\boldsymbol{\Theta}$ are generated. Seismic performance evaluation of each FE model realization is carried out using 300 ground motion records (50 ground motion records at six different seismic hazard levels with MRP of *IM* exceedance ranging from 72 years to 4975 years) selected for that specific FE model realization. For analyses cases 2 and 3, 50,000 variates of $\boldsymbol{\Lambda}_{\boldsymbol{\Theta}}$, the vector of probabilistic

model parameters characterizing the distributions of FE model parameters, are generated to accurately approximate the predictive distributions (corresponding to a finite dataset size $n_s = 5$) of FE model parameters. However, the number of variates of $\boldsymbol{\Lambda}_{L,k}$, the vector of probabilistic model parameters characterizing the normalized fragility function for *LS-k*, is intentionally kept equal to the number of variates generated for the FE model parameter vector $\boldsymbol{\Theta}$ (i.e., $N_S^{\boldsymbol{\Theta}} = N_S^{\boldsymbol{\Lambda}_{L,k}}$). This is done to induce the same level of estimation error due to the finite sampling of both $\boldsymbol{\Lambda}_{L,k}$ and $\boldsymbol{\Theta}$, the two vectors of RVs w.r.t which the unconditional MAR of *LS-k* exceedance is estimated using Monte Carlo simulation (see Eq. (7.17)).

Table 7.6, shows the following quantities of interest computed for the selected set of *LS*s as comma-separated ordered lists of three values corresponding to the three analyses cases mentioned above:

- the COV of MRP of *LSE*,
- the ratio of *E*[MRP] (the expected value of MRP of *LSE* estimated by the sample mean of MRP of *LSE* values obtained for each FE model realization) to MRP^{Det} (the respective MRP of *LSE* evaluated for the deterministic FE model without accounting for any of the additional uncertainties)
- the probability of MRP of *LSE* being less than $\text{MRP}^{\text{Target}}$ (the respective specified target MRP of LSE, i.e., 225 years for *LS*-1, 1000 years for *LS*-2, and 2500 years for *LS*-3),
- the probability of MRP of *LSE* being less than MRP^{Det},
- the non-Poisson probability of *LSE* in an exposure period equal to 50 years and how it compares (in terms of % change) to the corresponding Poisson probability evaluated for the deterministic FE model case.

Table 7.6 Results of seismic performance assessment corresponding to analyses cases 1, 2, and 3 shown as comma-separated ordered lists of values; (all values in %)

OSB	*LS*	COV of MRP	$\underline{E}$[MRP] / MRP^{Det}	P[MRP < MRP^{Target}]	P[MRP < MRP^{Det}]	P[*LSE* in 50 years]	
						Case: 1, 2, 3	Change w.r.t Det. case
A	1	36.8, 48.7, 41.4	92.5, 98.2, 101.0	40.0, 49.5, 14.4	62.0, 64.0, 55.5	20.4, 20.1, 14.0	19.3, 17.6, 13.8
	2	42.7, 51.9, 46.1	98.1, 97.8, 107.0	24.0, 31.5, 22.8	60.0, 68.4, 54.6	4.09, 4.2, 3.86	18.1, 21.3, 11.9
	3	48.2, 54.9, 43.4	100.0, 99.4, 101.0	36.0, 45.1, 50.8	68.0, 68.3, 59.3	1.8, 1.84, 2.06	17.2, 19.5, 16.4
B	1	37.0, 38.0, 39.6	83.7, 83.3, 87.6	6.0, 10.6, 19.2	78.0, 73.9, 69.7	13.6, 13.8, 15.4	31.6, 33.6, 28.2
	2	55.1, 49.4, 43.8	75.7, 73.9, 83.4	8.0, 8.52, 32.5	80.0, 82.8, 75.4	2.98, 2.97, 4.34	63.4, 62.8, 40.3
	3	75.2, 58.8, 51.6	73.1, 68.8, 74.2	30.0, 28.2, 68.4	82.0, 83.7, 83.8	1.59, 1.56, 2.57	88.9, 85.8, 63.4
C	1	37.0, 48.7, 49.9	64.8, 63.9, 78.6	0.0, 0.0, 15.4	92.0, 89.1, 77.7	4.95, 5.47, 13.5	71.7, 89.6, 53.8
	2	42.1, 49.7, 42.2	58.5, 62.6, 67.9	0.0, 0.0, 53.6	92.0, 90.4, 88.6	0.733, 0.724, 5.69	94.6, 92.2, 73.1
	3	45.0, 57.5, 40.3	51.9, 59.0, 64.9	0.0, 0.0, 90.0	94.0, 90.6, 91.2	0.326, 0.309, 3.43	123.0, 111.0, 78.5
MAOC	1	17.6, 27.9, 31.1	78.4, 77.5, 77.6	94.0, 91.2, 22.3	90.0, 84.7, 83.0	26.9, 28.1, 16.6	26.2, 31.9, 37.1
	2	20.8, 28.5, 28.7	72.6, 72.3, 71.6	100.0, 99.8, 58.8	94.0, 91.0, 90.3	10.8, 11.2, 5.39	40.7, 45.6, 49.3
	3	23.7, 28.4, 30.2	66.2, 64.5, 65.9	100.0, 100.0, 93.8	96.0, 95.8, 93.8	7.09, 7.4, 3.25	56.9, 63.7, 64.0

Based on the results of analysis case 1 (first of the three comma-separated values in Table 7.6), it can be concluded that the inclusion of FE model parameter uncertainty induces significant variability (indicated by large COVs ranging from 18 – 75 %) in the computed MRPs of *LSE*s. The estimates of the unconditional (expected value of) MRPs of *LSE*s are found to be lower than the respective MRPs computed for the deterministic FE models of the considered OSBs by as much as 48%, barring the case of Bridge A where these quantities are found to be almost equal (note that MRP of *LSE* is directly proportional to the reliability/safety of an OSB against the exceedance of the considered *LS*). The probabilities that MRPs of *LSE*s for the as-designed testbed OSBs are less than the respective specified target MRP values are found to be moderate to high (up to 40 %) for Bridges A and B lying on the conservative side of their respective feasible

domains, extremely low (~ 0 %) for Bridge C lying too conservatively inside the feasible domain, and exceedingly high (~ 100 %) for the as-designed Bridge MAOC lying clearly in the unsafe domain. More interestingly, the probabilities that MRPs of *LSE*s for these OSBs are less than the respective MRPs of *LSE*s evaluated for deterministic FE models (in other words, the probabilities that the actual performance of these bridges are worse than that assessed without accounting for FE model parameter uncertainty) are consistently found to be very high (60 – 96 %). Finally, the probabilities of *LSE*s in 50 years are also found to be consistently higher (by even more than 100 %) than the corresponding probabilities evaluated for the deterministic FE models.

The inclusion of probability distribution parameter estimation uncertainty on top of FE model parameter uncertainty is found to moderately influence the results of seismic performance assessment. The results of analysis case 2 (second of the three comma-separated values in Table 7.6) are sometimes found to be even counter-intuitive with smaller values of COVs than those computed in analysis case. This additional source of uncertainty is also found to somewhat increase (sometimes even decrease), when compared to the results of analysis case 1, the amount by which the probabilities of *LSE*s in 50 years are more than these probabilities evaluated for the deterministic FE models. This is attributed to the fact these quantities are themselves estimated using a finite number of ground motion records and FE model realizations. Hence, the effect of the inclusion of probability distribution parameter estimation uncertainty is seemingly buried in the noise associated with the finite-sample estimation (w.r.t the number of ground motion records and FE model realizations) of the quantities of interest shown here.

Although found to be not significantly influential, the incorporation of probability distribution parameter estimation uncertainty on top of FE model parameter uncertainty requires minimal additional computational overhead. The performance assessment of the redesigned

versions of the testbed OSBs, under analysis case 3, is therefore carried out accounting for both sources of uncertainty. Figure 7.9 shows the resulting probability density normalized histograms and empirical CDFs of MRPs of *LSE* obtained for the four testbed OSBs analyzed. As expected, analysis case 3 not only results in high COVs (ranging from 29 – 52 %) of the MRPs of *LSE*s, but also leads to increase (w.r.t the deterministic FE model case) in probabilities of *LSE*s in 50 years exposure period. It is important to note that the redesigned version of each testbed OSB analyzed under analysis case 3 is a DP satisfying all risk-targeted performance objectives. However, in the PBSD procedure used to arrive at these DPs, the targeted additional sources of uncertainty are not accounted for. Inclusion of these sources of uncertainty (more importantly, FE model parameter uncertainty) in the seismic performance assessments of these presumably ideal design situations now reveals a more transparent and complete picture. The probabilities that the MRPs of *LSE*s for these DPs are smaller than the respective previously assessed target-achieving values (using deterministic FE models) are found to be remarkably high (59 % for Bridge A, 84 % for Bridge B, 91 % for Bridge C, and 94 % for Bridge MAOC), thereby deeming these DPs to be of questionable reliability.

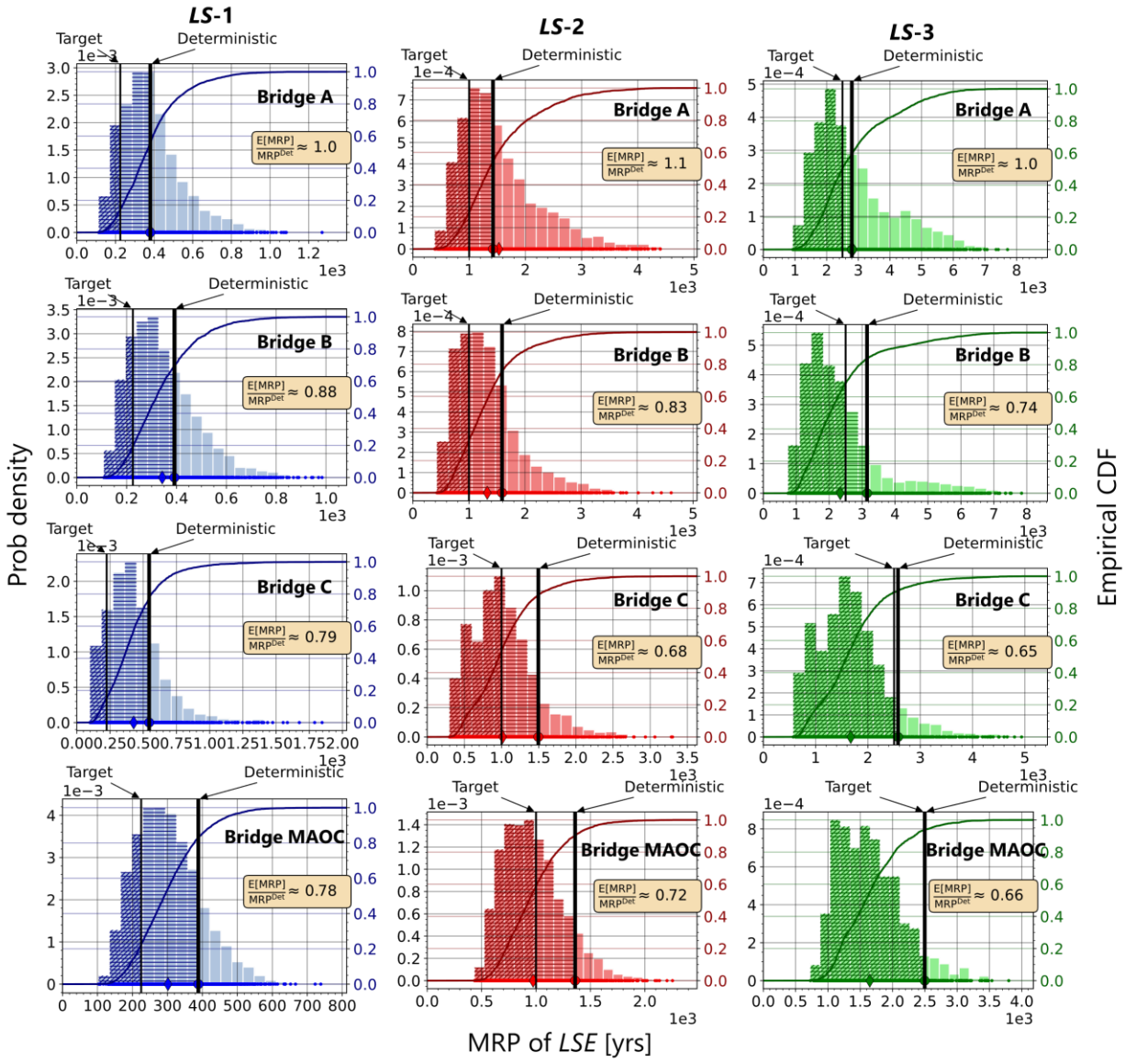

Figure 7.9 Probability density normalized histograms and empirical CDFs of MRPs of *LSE* for the redesigned versions of the testbed OSBs considered; note that the diamond represents E[MRP], while the circle represents MRP^{Det}; also note that the horizontally hatched region represents $P[MRP < MRP^{Target}]$ while the angled hatched region represents $P[MRP < MRP^{Det}]$

7.8 Conclusions

This paper presents the analytical and computational extension of a risk-targeted PBSD framework by incorporating the following sources of uncertainty into the underlying performance assessment methodology – (i) the aleatory uncertainty associated with FE model parameters, and

(ii) the epistemic finite-sample uncertainty in the estimated parameters of the probability distributions characterizing the FE model parameters and *LS* fragilities. These uncertainties are meticulously quantified via RV modeling of FE model parameters recognizing their random spatial variability in a bridge, characterization of their joint probability structure, and determination of the predictive distribution of FE model parameters and *LS* fragilities in the presence of finite-sample estimation uncertainty. The targeted uncertainties are then propagated using MC simulation with LH sampling in the seismic performance assessment of the as-designed and redesigned (using the original PBSD methodology) versions of four representative testbed California OSBs.

Incorporation of FE model parameter uncertainty induces significant variability in bridge seismic performance assessed in terms of the MRPs of exceedance of a set of three practical strain-based *LS*s that are pertinent to the seismic evaluation of bridge structures and physically meaningful to practicing bridge engineers. The MRP of *LSE*, which is a function of random FE model parameters, can be viewed as a derived RV. Random MRPs of *LSE*s are generally found to exhibit high COVs with expected values smaller than their deterministic counterparts (i.e., those evaluated for a deterministic FE model) thereby indicating worse reliability/safety against the exceedances of the considered *LS*s. The probability of MRP of *LSE* being less than its deterministic counterpart (i.e., the probability of actual bridge performance being worse than that assessed for a deterministic FE model) is also found to be high in general. Furthermore, the inclusion of this source of uncertainty systematically leads to higher (w.r.t the deterministic FE model case) probabilities of *LSE*s in specified target exposure periods. Accounting for probability distribution parameter estimation uncertainty on top of FE model parameter uncertainty is found to moderately impact these results. Notwithstanding, a rigorous procedure is outlined that inventively achieves this optional inclusion with minimal additional computational overhead.

The importance of a comprehensive treatment of uncertainties in the context of PBSD is established by re-evaluating the seismic performance of risk-targeted redesigns of the considered bridges initially chosen such that multiple performance objectives are deterministically satisfied without accounting for the targeted sources of uncertainty. The redesigned OSBs are now found to violate the targeted performance objectives with high probabilities thus revealing the true (probabilistic) picture of their seismic performance. This brings in transparency in design/decision-making in the face of uncertainty, one of the key promises of PBSD.

Bolstered by a modular computational seismic performance assessment framework developed by the authors along with the availability of high-performance computing resources, this study provided the unique opportunity of investigating the effect of pertinent sources of uncertainty that are typically ignored in seismic performance-based assessment/design of ordinary bridges. The modular design of the underlying computational framework can be further leveraged to study the effect of structural model discrepancy or model form uncertainty (the subject of an upcoming paper), which is another major, yet seldom accounted for, source of uncertainty.

7.9 Acknowledgments

Support of this research by the Pacific Earthquake Engineering Research Center under Transportation Systems Research Program, Project # 1147-NCTRTE, is gratefully acknowledged. The authors wish to thank the following individuals for their help in insightful discussions related to the work presented in this paper: Messrs. M. Mahan, T. Ostrom, A. Shamsabadi, T. Shantz, and C. Sikorsky from the Engineering Division at Caltrans, along with Dr. Frank McKenna at UC Berkeley for help with HPC and OpenSees. The authors also acknowledge the Texas Advanced Computing Center (TACC) at The University of Texas at Austin (http://www.tacc.utexas.edu) for

providing HPC resources that have contributed to the research results reported within this paper.

Chapter 7, in full, is currently being prepared for submission for publication of the material as it may appear in the following paper (the dissertation author is the first author of this paper):

Deb, A., Conte, J. P., Restrepo, J. I. (2021). "Comprehensive treatment of uncertainties in risk-targeted performance-based seismic design and assessment of bridges." Under preparation for submission to *Earthquake Engineering & Structural Dynamics*.

8 Conclusions

8.1 Summary of Research Work

Probability-based design provides the most scientific and rational solution to an earthquake-resistant structural design problem wherein an inherently uncertain structural system needs to be designed such that its performance entails, not only resisting highly uncertain seismic demands, but also meeting reliably societal demands of life safety, economy, and resiliency. The classification of structural performance should therefore be predicated on an acceptable risk, defined by the risk tolerance of society as a whole. Fueled by such needs, the structural engineering community, over the last few decades, has moved on towards implementing the philosophy of probabilistic performance-based earthquake engineering (PBEE) in the realm of structural seismic design. Probabilistic performance-based seismic design (PBSD) involves designing a structure to meet more refined and non-traditional performance objectives explicitly stated in terms of the risk associated with the exceedance of critical damage limit-states (*LS*s) or certain tolerable thresholds of monetary loss, downtime, etc. (i.e., probability of *LS* or threshold exceedance in a specified exposure time). The recent advent of PBEE in seismic design practice of buildings motivated this research wherein a simplified risk-targeted PBSD methodology, building on the comprehensive probabilistic PEER PBEE framework, is developed for Ordinary Standard Bridges (OSBs) in California. The overarching goal of this project is to address, without any compromise in rigor, the somewhat hindered implementation of the PEER PBEE framework in seismic bridge design practice owing to its all-inclusive nature, pressing computational requirements and inherent theoretical complexity.

A summary of the overall approach taken to arrive at a solution to the formulated problem can be best presented by classifying the entire bulk of the conducted research into three distinct phases:

I. Implementation of the PEER PBEE assessment framework
II. Full-fledged parametric probabilistic performance assessment
III. Development of simplified risk-targeted PBSD methodology
IV. Comprehensive treatment of uncertainties in PBSD

The following sections provide a general idea of the work entailed in each of these three phases.

8.1.1 Phase I: Implementation of the PEER PBEE Assessment Framework

At the very outset, the road taken involves a meticulous implementation of the PEER PBEE assessment framework for OSBs which lies at the heart of the proposed PBSD methodology. The performance measure sought for in this study is the MAR of *LS* exceedance or, equivalently its reciprocal, the mean return period (MRP) of *LS* exceedance. The task of probabilistically predicting the future seismic performance of a bridge, in terms of the MRPs of exceeding a selected set of *LS*s, is broken down into three analytical steps, namely: probabilistic seismic hazard analysis (PSHA), probabilistic seismic demand hazard analysis (PSDemHA), and probabilistic seismic damage hazard analysis (PSDamHA). Improvements from state-of-the-art literature relating to various steps of the PEER PBEE analytical framework are also incorporated.

PSHA is formulated in terms of an improved (in terms of "efficiency" and "sufficiency") earthquake *IM*, i.e., average spectral acceleration over a specified period range. Owing to the novelty of the chosen *IM*, standard PSHA tools do not include seismic hazard assessments in terms

of this *IM*. Hence, a convenient, yet rigorous, workaround is adopted based on the results of standard PSHA for spectral accelerations at single periods such that the seismic hazard in terms of the average spectral acceleration can be reasonably approximated.

A state-of-the-art ground motion selection algorithm is implemented for the selection of site-specific risk-consistent ensembles of ground motion records. The algorithm employs a conditional mean spectrum-based ground motion selection to pick earthquake records from a strong motion database that, as an ensemble, follow the complete probability structure of the target conditional spectrum defined for a given seismic hazard level.

PSDemHA and PSDamHA are formulated in terms of a set of novel strain-based engineering demand parameters (*EDP*s) and *LS*s. Three *LS*s mainly concerning reinforced concrete bridge columns, the primary lateral load resisting component of an OSB, are defined. These *LS*s are selected as: *LS* 1: concrete cover spalling, *LS* 2: a precursor stage to longitudinal rebar buckling, and *LS* 3: the onset of longitudinal rebar fracture. These *LS*s are pertinent to the seismic evaluation of bridge structures and meaningful to practicing engineers. A fourth *LS* corresponding to an abutment exterior shear key reaching its shear strength capacity is also considered. Material strain-based *EDP*s associated with the *LS*s related to the desired failure mode involving bridge columns (i.e., hinging of columns) are defined. Strain-based *EDP*s correlate better to damage than traditionally used displacement based *EDP*s (e.g., column drift, plastic hinge rotation).

Strain-based fragility functions based on reliable experimental data or high-fidelity numerical data are developed or inherited for the considered *LS*s through proper identification of relevant test and research programs previously conducted. Fragility functions, typically constructed using experimental or numerical data pertaining to specimens or models with different geometric, material and mechanical characteristics, need to be normalized such that they can be

used for structural components of any specified characteristics. Appropriate normalizing deterministic capacity prediction equations are identified and used for this purpose.

The proposed PBEE assessment framework is computationally implemented as a Python library, named PyPBEE (PBEE for Python). PyPBEE admits modular class definitions of analysis steps (i.e., PSHA, ground motion selection (GMS), nonlinear time-history analysis (NLTHA), PSDemHA, and PSDamHA) and the interface variables (i.e., OSB, *IM*s, *EDP*s, and *LS*s). PyPBEE is designed to readily accommodate alternative and more refined/effective definitions of its components reflecting future improvements made in the various steps of the multidisciplinary PBEE methodology.

The improved version of the PEER PBEE framework is utilized for the seismic performance assessment of four real-world California testbed OSBs located in regions with disparate levels of seismicity. The selected testbed bridges also cover a wide range of geometrical parameters such as number of spans, span lengths, number of columns per bent, skew angle, etc. It is noted that caution is exercised in the mitigation of non-collapse related convergence issues in the iterative scheme used to integrate the nonlinear equations of motion. This helps avoid the common practice of "throwing away" non-converged analyses results, which can lead to the introduction of significant biases in the results of probabilistic analyses.

8.1.2 Phase II: Full-fledged Parametric Probabilistic Performance Assessment

A two-dimensional design space is defined in terms of the primary design variables, viz., column diameter (D_{col}) and column longitudinal reinforcement ratio (ρ_{long}), to which the exceedances of the selected set of *LS*s are believed to be most sensitive. The chosen design variables pertain to the reinforced concrete bridge columns because they constitute the primary

lateral load resisting structural components of an OSB. Moreover, column plastic hinge regions are also meant in a seismic event to act as structural fuses and thereby dissipate energy through inelastic material behavior. All other bridge design parameters to be determined by meeting the requirements of capacity design, minimum ductility capacity, reinforcement ratio restrictions, etc., and/or restricted by the geometry of the bridge, available real estate, traffic requirements, etc. are referred to as secondary design variables. In the parametric study of the four testbed OSBs, values of the respective secondary design variables are taken as per the original designs of the testbed OSBs, except for the column transverse reinforcement ratio (ρ_{trans}), the value of which is expressed as a practical fraction of ρ_{long}, i.e., $\rho_{trans} = 0.5\rho_{long}$.

A fully automated workflow incorporating an efficient utilization of available computing resources is developed for a smooth and seamless execution of the full-fledged parametric probabilistic seismic performance assessment of the considered bridges. The seismic performance of re-designs of the considered testbed OSBs generated by varying the primary design parameters, subject to practical constraints, are evaluated using the improved PEER PBEE framework described. This involved the extensive parallelization of computationally independent jobs, which was made possible through Stampede2, the flagship supercomputer at the University of Texas at Austin's Texas Advanced Computing Center (TACC). It is noteworthy to mention here that for the sizable number of nonlinear time-history analyses performed for each of the re-designs of the considered testbed bridges, convergence of the numerical integration of the equations of motion over the entire duration of the seismic input is also ensured in an automated fashion.

Finally, for each considered *LS*, a piecewise-linear interpolation surface for MRP of exceedance is constructed using the computed MRPs over a triangulated regular grid representing the primary design space of an OSB. Topologies and contours of these surfaces are explored.

Feasible design domains, i.e., collection of design points in the two-dimensional design parameter space with MRPs of *LS* exceedances higher than or equal to the respective specified targets, are identified. Safety of the as-designed bridges and feasibility of their re-designs are examined.

8.1.3 Phase III: Development of Simplified Risk-targeted PBSD Methodology

The concept of a feasible design domain in the design parameter space can be utilized to make risk-informed design decisions while trying to satisfy multiple risk-based performance objectives. The full-fledged parametric probabilistic seismic performance assessment framework can therefore be very well used for the design of a new OSB unless its computational cost is prohibitive for the computational resources available. For reasons of practicability in current bridge design practice, a computationally more economical, simplified, non-traditional, risk-targeted PBSD procedure is distilled out of this study by inventively utilizing the findings of the full-fledged parametric probabilistic seismic performance assessment carried out for the testbed bridges. The proposed simplified design methodology is able to:

(i) find a design point in the primary design parameter space of a bridge being designed for multiple risk-based performance objectives; and

(ii) delineate an approximate, yet sufficiently accurate, feasible design domain and identify the *LS*s controlling its boundary in the primary design parameter space of the bridge,

at a computational cost significantly lower than that of the full-fledged parametric method.

Upon selection of primary design variables, secondary design variables are to be determined and adjusted to meet requirements of capacity design, code-based minimum ductility capacity and minimum reinforcement, etc., and/or other restrictions imposed by the real estate available, traffic flow, etc. After all primary and secondary design variables have been determined,

a final check of structural performance is required to ensure that the final design still satisfies the specified risk-based performance objectives.

8.1.4 Phase IV: Comprehensive treatment of uncertainties in PBSD

The underlying PBEE assessment methodology of the PBSD framework proposed thus far explicitly considers only the following basic sources of uncertainty: (i) the uncertainty associated with the seismic *IM*, (ii) the record-to-record variability of earthquake ground motions given a seismic hazard level (a specific value of *IM*) by using ensembles of ground motions consistent with the natural conditional variability of earthquake ground motions given *IM*, and (iii) the uncertainty in the capacity of the various strain-based *LS*s as represented by the corresponding fragility curves. The PBEE assessment methodology is now significantly enhanced by the inclusion of the following additional sources of uncertainty: (i) the aleatory uncertainty associated with FE model parameters (e.g., constitutive material model parameters, damping model parameters), and (ii) the epistemic parameter estimation uncertainty associated with using finite datasets to estimate the parameters of the probability distributions characterizing FE model parameters and *LS* fragilities.

These uncertainties are meticulously quantified via random variable modeling of FE model parameters recognizing their random spatial variability in a bridge, characterization of their joint probability structure, and determination of the predictive distribution of FE model parameters and *LS* fragilities in the presence of finite-sample estimation uncertainty. The targeted uncertainties are then propagated using Monte-Carlo simulation with Latin Hypercube sampling in the seismic performance assessment of the as-designed and redesigned (using the original PBSD methodology) versions of four representative testbed California OSBs.

8.2 Highlight of Findings

Findings of the present research related to the phases of work described above are grouped accordingly and presented next.

8.2.1 Findings of Phase I

As expected, the results of PSDamHA of the testbed bridges show that exceedances of increasingly severe *LS*s, i.e., *LS*s 1 through 3, concerning the reinforced concrete bridge columns for OSBs have increasing values of MRPs. The as-designed testbed bridges considered, as assessed using the implemented PEER PBEE framework, exhibit a wide range of seismic performance as measured by the MRPs of exceeding the selected set of *LS*s. The MRPs of exceeding *LS*s 1 through 3 are found to cover a wide range of values from 208 to 1,709 years for *LS* 1, 626 to 13,245 years for *LS* 2, and 1,080 to 34,185 years for *LS* 3. The MRP of exceeding the 4th *LS*, namely that of an abutment exterior shear key reaching its shear strength capacity, is found to range between 85 and 5,844 years depending on the type of shear key used in the bridge. Bridges A, B and C, having monolithic non-isolated type abutment shear keys, show high MRPs of exceeding *LS* 4, while the MRP of exceedance associated with this *LS* is found to be relatively small (compared to those of Bridges A, B, and C) for Bridge MAOC with sacrificial isolated type shear keys specified in its design. It is also found that the MRP of abutment shear key *LS* exceedance is almost the same as that of exceeding the critical *LS* of rebar fracture for Bridges A and B. Shear keys of Bridges C and MAOC, on the other hand, are found to exceed this *LS* with MRPs smaller than the respective MRPs of exceeding the *LS* of concrete cover spalling.

The implementation of the present improved version of the PEER PBEE framework, developed with painstaking details, is highly advantageous. A design method based on or distilled

out of this rigorous assessment framework will be fittingly risk-informed, rational, and scientific. The MAR or MRP of a damage *LS* exceedance for an OSB, according to the PEER PBEE framework, is computed by aggregating or accounting for the contributions from all seismic hazard levels. As shown by the disaggregation with respect to *IM* of the MRP of exceedance of (or the hazard level associated with) any of the damage *LS*s considered, different levels of *IM* (both corresponding to higher and lower MRPs of exceedance as compared to the specific MRP of the damage *LS* exceedance) contribute to the damage *LS* hazard. This provides a scientific basis to disapprove an incomplete method according to which, for the sake of computational and/or theoretical convenience, one chooses to design a bridge such that specified *LS*s are not exceeded (with a specified confidence levels) at specified discrete seismic hazard levels (e.g., earthquake ground motions with an MRP of *IM* exceedance of 975 years, 2475 years, etc.).

8.2.2 Findings of Phase II

For each of the three *LS*s pertaining to bridge columns (i.e., *LS*s 1 through 3), a piecewise-linear interpolation surface for MRP of exceedance is constructed using the computed MRPs over a triangulated regular grid representing the primary design space of an OSB. Although the overall topologies of the MRP surfaces over the design space are accurate, some topology details are by-products of the type of interpolation assumed (here piecewise linear). It is important to notice that the MRP of *LS* exceedance results obtained for the as-designed bridges, in each case, are in excellent agreement with the topology of the MRP surfaces despite being excluded from the data used for constructing these surfaces.

Increasing values of the two primary design variables (both related to the design of the bridge columns) result in stronger, and thereby translating to safer designs characterized by lower

MARs or higher MRPs of *LS* exceedances. The MRPs of exceeding these *LS*s, pertaining to seismic design of OSBs, are found to be indeed sensitive to the chosen primary design variables thereby justifying their choice.

Contour lines of the MRP surfaces for *LS*s 1, 2, and 3, corresponding to respectively specified target MRPs selected based on discussions with and feedback from expert Caltrans engineers, are superimposed in the primary design space to delineate the overall feasible design domains. This also helps identify the governing *LS*s along the boundaries of the feasible design domains. The seismic performance of the as-designed version of a testbed bridge is gauged by the location of the corresponding design point in the design parameter space relative to the overall feasible design domain of the bridge (i.e., does the as-designed bridge belong to the feasible design domain and how close is it from its boundary?). While some of the as-designed testbed bridges are found to be conservative, sometimes too much, with respect to the selected *LS*s and corresponding target MRPs, others are found to lie near the borderline of safety, or clearly in the unsafe domain. This telltale irregularity in the seismic performance of the as-designed testbed OSBs (gauged by the difference in the estimated vs expert opinion-based target MRPs of *LSE*s) observed in this study is indicative of the inconsistency and opacity of current design principles that do not explicitly state, analyze, and design for risk-targeted performance objectives, but implicitly expect them to be satisfied.

The idea of a full-fledged parametric probabilistic seismic performance assessment framework lends itself to the formulation of PBSD of OSBs as an inverse assessment problem. A two-stage design procedure is thus proposed. The first-stage involves the design of the bridge columns, the primary lateral load resisting component of OSBs. Values of primary design variables are first selected such that multiple risk-targeted performance objectives are met. This involves

selection of a physically realizable design point in the primary design parameter space either lying on the boundary of, or inside and in the vicinity of the boundary of, the feasible design domain. The second-stage involves the determination of secondary design variables (the ones not restricted by the geometry of the bridge, available real estate, traffic flow requirements, etc.) to meet code-based requirements of capacity design (to limit the number and locations of damage and failure mechanisms to be considered), minimum ductility limitations, reinforcement ratio restrictions, etc.

The categorization of an important column design parameter, the transverse reinforcement ratio (ρ_{trans}), for columns with low expected axial load ratios (typically less than 15% under combined gravity and earthquake loading) which is typical of OSBs, as a secondary design variable is investigated. A non-negligible impact of ρ_{trans} on the results of seismic performance assessment of OSBs brings out the importance of ρ_{trans} in the context of seismic design of bridge columns. Hence, a smart and practical initial choice of this, rather critical, secondary design variable (e.g., $\rho_{trans} = 0.5\rho_{long}$) is essential as the primary design variables are being determined.

A comparative study is conducted between feasible design domains obtained using closed-form solutions to the MRP of *LS* exceedances, available in the literature, and the one obtained numerically via the full-fledged probabilistic performance assessment method. This is done to assess the potential viability of LRFD-like design formats based on such closed-form solutions to be used as the sought PBSD methodology. These closed-form solutions still require the computationally most demanding step of running ensemble nonlinear time-history analyses for a bridge, while circumventing the rather inexpensive numerical evaluation of the demand and damage hazard integrals. Moreover, the results obtained from such simplified closed-form solutions, that require going through almost the same rigmarole as that in the numerical full-fledged method, are often inaccurate by a significant margin.

8.2.3 Findings of Phase III

The topologies of the MRP surfaces for *LS*s 1, 2, and 3, in the primary design parameter space are explored. These topologies are found to be well-captured by piecewise power functions. Based on this observation, a step-by-step strategy requiring the performance evaluation of only 3 design points is devised that allows locating a design point, which satisfies multiple risk-based performance objectives, in the primary design parameter space of a bridge under design. An approximate delineation of the feasible design domain is systematically achieved with the performance evaluation of 2 additional design points. This approach is based on the observation that contours of the MRP surfaces for the *LS*s considered can be approximated by parallel bilinear lines in the primary design space.

The computational requirement of the full-fledged parametric method is therefore significantly reduced by requiring the performance evaluation of only 3 (or 5) design points to realize the risk-targeted design objectives. The computational workload is further reduced by drastically curtailing the total number of nonlinear time-history analyses to be run for the performance evaluation of a single design point while still maintaining reasonable levels of accuracy.

Results of the reduced-workload, simplified, non-traditional, risk-targeted, performance-based seismic design procedure applied to the considered testbed bridges are found to tally well with the results of the full-fledged parametric method, thereby validating the proposed PBSD methodology.

8.2.4 Findings of Phase IV

Incorporation of FE model parameter uncertainty induces significant variability in bridge seismic performance assessed in terms of the MRPs of exceedance of the considered set of *LS*s. MRPs of *LS* exceedances are generally found to exhibit high coefficient of variations with expected values smaller than their deterministic counterparts (i.e., those evaluated for a deterministic FE model) thereby indicating worse reliability/safety against the exceedances of the considered *LS*s. The probability of actual bridge performance being worse than that assessed for a deterministic FE model is also found to be high in general. Accounting for probability distribution parameter estimation uncertainty on top of FE model parameter uncertainty is found to moderately impact these results. Notwithstanding, a rigorous procedure is outlined that inventively achieves this optional inclusion with minimal additional computational overhead.

The importance of a comprehensive treatment of uncertainties in the context of PBSD is established by re-evaluating the seismic performance of risk-targeted redesigns of the considered bridges initially chosen such that multiple performance objectives are deterministically satisfied without accounting for the targeted sources of uncertainty. These redesigned bridges when assessed via consistent quantification and propagation of pertinent uncertainties, are found to have high probabilities of violating the targeted performance objectives. The reliability of these presumably ideal design points is found to be questionable in light of the true (probabilistic) picture of their seismic performance. Comprehensive treatment of uncertainties in seismic performance assessment thus brings in transparency in design/decision-making in the face of uncertainty, one of the key promises of PBSD.

8.3 Recommendations for Future Research

The completed research work is neither exhaustive nor fully devoid of limitations. A brief account of identified issues, possible solutions, and relevant avenues for further research is presented in this section.

At the heart of performance-based earthquake engineering is the explicit quantification of relevant uncertainties and their consistent propagation through the performance assessment framework. Bolstered by a modular computational seismic performance assessment framework developed herein, along with the availability of high-performance computing resources, this study provided the unique opportunity of investigating the effect of pertinent sources of uncertainty that are typically ignored in seismic performance-based assessment/design of ordinary bridges. The modular design of the underlying computational framework can be further leveraged to study the effect of structural model discrepancy or model form uncertainty, which is another major (Terzic et al. 2015), yet seldom accounted for, source of uncertainty. Some avenues that can be explored in this regard are listed below:

(i) improvement of computational models of OSBs to account for the effect of complicated yet realistic phenomena, e.g., flexure-shear interaction in bridge piers, and bar bond-slip in the column-foundation and/or column/bent-cap interface due to strain penetration, the soil-structure interaction effects at the column foundations and/or at the abutments, response of structures to the vertical and/or rotational component of ground motions, etc.;

(ii) use of more elaborate hysteretic material stress-strain laws and force-deformation relationships for different structural components;

(iii) improvement of the modeling of skewed bridge abutment components by calibrating and validating such models with experimental data from reliable sources and/or numerical data from analyses conducted using full-fledged physics-based high-fidelity FE models;

(iv) use of different/improved damping models in the nonlinear response history analyses of OSBs

Future research can focus towards alleviating the computational cost involved in the uncertainty quantification/propagation phase of the proposed seismic performance assessment/design framework via the use of advanced response surface/regression-based techniques. However, such methods are found to yield inaccurate results in the case of highly nonlinear structural systems coupled with high dimensionality of the vector of random variables describing the FE model parameters. In this regard, a screening of random variables based on global sensitivity studies would help rigorously, accurately, and efficiently propagate the uncertainty in FE model parameters using response surface/regression-based techniques, thus bringing about savings in the required computational effort.

This work quantifies the seismic performance of an OSB in terms of the most frequent (over all plastic hinge regions in different columns of the bridge) rate of *LS* exceedance. The statistical correlation between performance metrics (i.e., the joint statistical behavior of the performance metrics) computed for different plastic hinge regions in a bridge can be studied to better quantify system-level bridge performance. Also, for simplicity, a single component-level performance metric (i.e., the MAR of *LS-k* exceedance in a single plastic hinge region) is evaluated independently/irrespective of the performance of other plastic hinge regions in the bridge, thus not requiring the statistical correlation between *EDP-k*'s corresponding to different plastic hinge

regions in different columns of an OSB. This correlation can be accounted for in future research to rigorously explore the joint statistical behavior of *LSE*s in different regions/parts of a bridge.

Both a scalar *IM* for PSHA and a scalar *EDP* associated with each damage *LS* of interest for both PSDemHA and PSDamHA are considered in this study. Vector-valued *IM*s are found to characterize/predict more accurately, by exhibiting higher levels of "efficiency" and "sufficiency", the seismic demand on structural systems. A single predictive demand parameter can be insufficient to perfectly predict whether an *LS* is reached or exceeded (i.e., other demand parameters may also play a role). A vector of statistically correlated *EDP*s can therefore be used to more accurately predict the exceedance of damage *LS*s of interest.

Explicit consideration of near fault effects in PSHA and a risk-consistent incorporation of velocity pulses in the selected ensembles of ground motion records are kept beyond the scope of this project. This can lead to an underestimated seismic risk to OSBs as evaluated using the current implementation of the PEER PBEE framework.

The set of *LS*s considered in this paper for the evaluation of seismic performance of OSBs is neither exhaustive nor definitive. The proposed framework is developed with such *LS* definitions as mere placeholders and is readily able to accommodate more refined (e.g., more mechanics-based) definitions of *LS*s and/or a larger number of *LS*s. Moreover, the influence of the exceedances of other *LS*s (e.g., full development of the shear key damage mechanism) on the exceedances of critical *LS*s related to column damage/failure should be investigated.

The seismic performance measure selected in this study is the MAR of *LS* exceedance or, equivalently, the MRP of *LS* exceedance. This can be taken one step further by defining performance measures in terms of the hazard associated with the exceedance of specific values of

decision variables, e.g., monetary loss, downtime, deaths, etc., which are more meaningful to stakeholders and/or decision makers (e.g., government officials).

The proposed simplified PBSD methodology is formulated by retaining the inherent rigor of the PEER PBEE framework lying at its crux. As a result, a rather non-traditional design method is proposed requiring complete probabilistic performance assessments of design iterations (i.e., design points). In this regard, efforts can be channeled to convert the non-traditional method distilled out of this project, without significantly compromising its rigor, into a more traditional design format requiring LRFD-like checks of structural demand-to-capacity ratios. Furthermore, different techniques (e.g., uncertainty aggregation methods) can be explored to reorganize/simplify the nested approach (taken herein) for the inclusion and treatment of different sources of uncertainty considered in this work. Future research can also be directed towards reproducing, in a consistent but simpler way, the effects of the nested inclusion of these uncertainties. Care should be exercised, however, so that the achievement of a middle ground between rigor and practicability does not involve any over-simplification.

Having identified the combined values of primary design variables satisfying multiple risk-based performance objectives, the proposed PBSD method recommends determining most secondary design variables (e.g., the ones not restricted by the geometry of the bridge, available real estate, traffic flow requirements, etc.) so as to meet code-based requirements of capacity design, minimum ductility limitations, reinforcement ratio restrictions, etc. These requirements typically involve the use of prescriptive measures and/or safety factors such that undesirable consequences are prevented with some level of confidence. Empirical observations, experience and/or engineering judgment have dictated the prescription of such measures and safety factors in

codes of practice. Future research can be directed towards developing a more transparent and more probabilistically explicit determination of these secondary design variables.

Finally, the viability of the proposed simplified PBSD methodology currently relies on a two-dimensional primary design parameter space for OSBs. The possibility of extending the proposed simplified method to accommodate more than two primary design variables, especially for non-ordinary, larger, and more complicated bridge structures, should be investigated.

References

AASHTO. (2011). “Guide specifications for LRFD seismic bridge design.” *American Association of State Highway and Transportation Officials (AASHTO), Washington, D. C.*

AASHTO. (2012). “LRFD Bridge Design Specifications, 6th ed.,.” *American Association of State Highway and Transportation Officials (AASHTO), Washington, D. C.*

ASCE/COPRI. (2014). “Seismic design of piers and wharves.” American Society of Civil Engineers.

ASCE. (2005). “ASCE 7-05: Minimum design loads for buildings and other structures.” American Society of Civil Engineers.

ASCE. (2010). *ASCE 7-10: Minimum Design Loads for Buildings and Other Structures*. American Society of Civil Engineers.

ASCE. (2013). “Report card for America’s infrastructure.” American Society of Civil Engineers.

Aslani, H., and Miranda, E. (2005). “Probability-based seismic response analysis.” *Engineering Structures*, Elsevier, 27(8), 1151–1163.

Astroza, R., Ebrahimian, H., Conte, J. P., Restrepo, J. I., and Hutchinson, T. C. (2013). “Statistical analysis of the identified modal properties of a 5-story RC seismically damaged building specimen.” *Proceedings of the 11th International Conference on Structural Safety and Reliability (ICOSSAR’13)*, 16–20.

ATC 3-06. (1978). *Tentative provisions for the development of seismic regulations for buildings: a cooperative effort with the design professions, building code interests, and the research community*. US Department of Commerce, National Bureau of Standards.

Augusti, G., and Ciampoli, M. (2008). “Performance-based design in risk assessment and reduction.” *Probabilistic Engineering Mechanics*, Elsevier, 23(4), 496–508.

Baker, J. W., and Cornell, C. A. (2003). *Uncertainty specification and propagation for loss estimation using FOSM methods*. Pacific Earthquake Engineering Research Center, College of Engineering ….

Baker, J. W., and Cornell, C. A. (2006). “Spectral shape, epsilon and record selection.” *Earthquake Engineering & Structural Dynamics*, Wiley Online Library, 35(9), 1077–1095.

Baker, J. W., and Jayaram, N. (2008). “Correlation of spectral acceleration values from NGA

ground motion models." *Earthquake Spectra*, 24(1), 299–317.

Barbato, M., Gu, Q., and Conte, J. P. (2010). "Probabilistic push-over analysis of structural and soil-structure systems." *Journal of structural engineering*, American Society of Civil Engineers, 136(11), 1330–1341.

Barbato, M., Petrini, F., Unnikrishnan, V. U., and Ciampoli, M. (2013). "Performance-based hurricane engineering (PBHE) framework." *Structural Safety*, Elsevier, 45, 24–35.

Beckwith, F., Restrepo, J. I., and Shing, P.-S. (2015). *Nonlinear Time-History Analysis of Bridges with Varying Skew Angle to Determine the Sesimic Demand on Abutment Shear Keys*.

Berry, M., and Eberhard, M. (2004). *Performance Models for Flexural Damage in Reinforced Concrete Columns*. Berkeley, Pacific Earthquake Engineering Research Center.

Berry, M. P., and Eberhard, M. O. (2005). "Practical performance model for bar buckling." *Journal of Structural Engineering*, American Society of Civil Engineers, 131(7), 1060–1070.

Boore, D. M., and Atkinson, G. M. (2008). "Ground-motion prediction equations for the average horizontal component of PGA, PGV, and 5%-damped PSA at spectral periods between 0.01 s and 10.0 s." *Earthquake Spectra*, 24(1), 99–138.

Bournonville, M., Dahnke, J., and Darwin, D. (2004). *Statistical analysis of the mechanical properties and weight of reinforcing bars*. University of Kansas Center for Research, Inc.

Bradley, B. A. (2010). "Epistemic uncertainties in component fragility functions." *Earthquake Spectra*, SAGE Publications Sage UK: London, England, 26(1), 41–62.

Bradley, B. A. (2013a). "Practice-oriented estimation of the seismic demand hazard using ground motions at few intensity levels." *Earthquake Engineering & Structural Dynamics*, Wiley Online Library, 42(14), 2167–2185.

Bradley, B. A. (2013b). "A critical examination of seismic response uncertainty analysis in earthquake engineering." *Earthquake Engineering & Structural Dynamics*, Wiley Online Library, 42(11), 1717–1729.

Bradley, B. A., and Dhakal, R. P. (2008). "Error estimation of closed-form solution for annual rate of structural collapse." *Earthquake Engineering & Structural Dynamics*, Wiley Online Library, 37(15), 1721–1737.

Buckle, I. G., Friedland, I., Mander, J., Martin, G., Nutt, R., and Power, M. (2006). *Seismic retrofitting manual for highway structures. Part 1, Bridges*. Turner-Fairbank Highway Research Center.

Caltrans. (1999). “Seismic Design Criteria, v. 1.4.” California Department of Transportation (Caltrans).

Caltrans. (2013). “Seismic Design Criteria, v. 1.7.” California Department of Transportation (Caltrans).

Caltrans. (2019). “Seismic Design Criteria, v. 2.0.” California Department of Transportation (Caltrans).

Carrasquillo, R. L., Nilson, A. H., and Slate, F. O. (1981). “Properties of High Strength Concrete Subjectto Short-Term Loads.” *Journal Proceedings*, 171–178.

Carreño, R., Lotfizadeh, K. H., Conte, J. P., and Restrepo, J. I. (2020). “Material Model Parameters for the Giuffrè-Menegotto-Pinto Uniaxial Steel Stress-Strain Model.” *Journal of Structural Engineering*, American Society of Civil Engineers, 146(2), 4019205.

Chang, C.-H., Tung, Y.-K., and Yang, J.-C. (1994). “Monte Carlo simulation for correlated variables with marginal distributions.” *Journal of Hydraulic Engineering*, American Society of Civil Engineers, 120(3), 313–331.

Chiou, B., Darragh, R., Gregor, N., and Silva, W. (2008). “NGA project strong-motion database.” *Earthquake Spectra*, SAGE Publications Sage UK: London, England, 24(1), 23–44.

Ciampoli, M., and Petrini, F. (2012). “Performance-based Aeolian risk assessment and reduction for tall buildings.” *Probabilistic Engineering Mechanics*, Elsevier, 28, 75–84.

Ciampoli, M., Petrini, F., and Augusti, G. (2011). “Performance-based wind engineering: towards a general procedure.” *Structural Safety*, Elsevier, 33(6), 367–378.

Coleman, J., and Spacone, E. (2001). “Localization issues in force-based frame elements.” *Journal of Structural Engineering*, American Society of Civil Engineers, 127(11), 1257–1265.

Conte, J. P., and Zhang, Y. (2007). “Performance based earthquake engineering: Application to an actual bridge-foundation-ground system.” *Proceedings of the 12th Italian national conference on earthquake engineering, Pisa, Italy*, 1–18.

Cornell, C. A. (1968). “Engineering seismic risk analysis.” *Bulletin of the seismological society of America*, The Seismological Society of America, 58(5), 1583–1606.

Cornell, C. A. (2000). “Progress and challenges in seismic performance assessment.” *PEER newsletter*.

Cornell, C. A., Jalayer, F., Hamburger, R. O., and Foutch, D. A. (2002). "Probabilistic basis for 2000 SAC federal emergency management agency steel moment frame guidelines." *Journal of structural engineering*, American Society of Civil Engineers, 128(4), 526–533.

Cornell, C. A., and Newmark, N. M. (1978). "Seismic reliability of nuclear power plants." *Probabilistic analysis of nuclear reactor safety*.

De, R. S. (1990). "Offshore structural system reliability: wave-load modeling, system behavior, and analysis."

Deb, A., Zha, A. L., Caamaño-Withall, Z. A., Conte, J. P., and Restrepo, J. I. (2018). *Performance-based Seismic Design of Ordinary Standard Bridges*.

Deb, A., Zha, A. L., Caamaño-Withall, Z. A., Conte, J. P., and Restrepo, J. I. (2021a). "Updated Probabilistic Seismic Performance Assessment Framework for Ordinary Standard Bridges in California." *Earthquake Engineering & Structural Dynamics*, 1– 20.

Deb, A., Zha, A. L., Caamaño-Withall, Z. A., Conte, J. P., and Restrepo, J. I. (2021b). "Framework for Risk-targeted Performance-based Seismic Design of Ordinary Standard Bridges." *Journal of Structural Engineering*.

Deb, A., Zha, A. L., Caamaño-Withall, Z. A., Conte, J. P., and Restrepo, J. I. (2021c). "Simplified Risk-targeted Performance-based Seismic Design Method for Ordinary Standard Bridges." *Journal of Bridge Engineering*.

Duck, D. E., Carreno, R., and Restrepo, J. I. (2018). "Plastic Buckling-Straightening Fatigue of Large Diameter Reinforcing Steel Bars." *La Jolla, California, University of California, San Diego*.

Eads, L., Miranda, E., and Lignos, D. G. (2015). "Average spectral acceleration as an intensity measure for collapse risk assessment." *Earthquake Engineering & Structural Dynamics*, Wiley Online Library, 44(12), 2057–2073.

Ellingwood, B., MacGregor, J. G., Galambos, T. V, and Cornell, C. A. (1982). "Probability based load criteria: load factors and load combinations." *Journal of the Structural Division*, ASCE, 108(5), 978–997.

Ellingwood, B. R. (2001). "Earthquake risk assessment of building structures." *Reliability Engineering & System Safety*, Elsevier, 74(3), 251–262.

Ellingwood, B. R. (2008). "Structural reliability and performance-based engineering." *Proceedings of the Institution of Civil Engineers-Structures and Buildings*, Thomas Telford Ltd, 161(4), 199–207.

Ellingwood, B. R., and Ang, A. H. S. (1974). "Risk-based evaluation of design criteria." *Journal of the Structural Division*, 100(Proc. Paper 10778).

FEMA-273. (1997). *NEHRP Guidelines for the Seismic Rehabilitation of Buildings*. FEDERAL EMERGENCY MANAGEMENT AGENCY Washington, D.C.

FEMA-356. (2000). *Prestandard and Commentary for the Seismic Rehabilitation of Buildings*. Federal Emergency Management Agency Washington, D.C.

FEMA-368. (2001). *NEHRP Recommended Provisions for Seismic Regulations for New Buildings and Other Structures*. FEDERAL EMERGENCY MANAGEMENT AGENCY Washington, D.C.

FEMA-445. (2006). *Next-Generation Performance-based Seismic Design Guidelines: Program Plan for New and Existing Buildings*. FEDERAL EMERGENCY MANAGEMENT AGENCY Washington, D.C.

Field, E. H., Jordan, T. H., and Cornell, C. A. (2003). "OpenSHA: A developing community-modeling environment for seismic hazard analysis." *Seismological Research Letters*, Seismological Society of America, 74(4), 406–419.

Filippou, F. C., Popov, E. P., and Bertero, V. V. (1983). "Effects of bond deterioration on hysteretic behavior of reinforced concrete joints." Earthquake Engineering Research Center, University of California Berkeley.

Franchin, P., Petrini, F., and Mollaioli, F. (2018). "Improved risk-targeted performance-based seismic design of reinforced concrete frame structures." *Earthquake Engineering & Structural Dynamics*, Wiley Online Library, 47(1), 49–67.

Ghosh, J., and Padgett, J. E. (2011). "Probabilistic seismic loss assessment of aging bridges using a component-level cost estimation approach." *Earthquake Engineering & Structural Dynamics*, Wiley Online Library, 40(15), 1743–1761.

Gobbato, M., Conte, J. P., Kosmatka, J. B., and Farrar, C. R. (2012). "A reliability-based framework for fatigue damage prognosis of composite aircraft structures." *Probabilistic Engineering Mechanics*, Elsevier, 29, 176–188.

Gobbato, M., Kosmatka, J. B., and Conte, J. P. (2014). "A recursive Bayesian approach for fatigue damage prognosis: An experimental validation at the reliability component level." *Mechanical Systems and Signal Processing*, Elsevier, 45(2), 448–467.

Gokkaya, B. U., Baker, J. W., and Deierlein, G. G. (2016). "Quantifying the impacts of modeling uncertainties on the seismic drift demands and collapse risk of buildings with implications on

seismic design checks." *Earthquake Engineering & Structural Dynamics*, Wiley Online Library, 45(10), 1661–1683.

Goodnight, J. C., Feng, Y., Kowalsky, M. J., and Nau, J. M. (2015). *The effects of load history and design variables on performance limit states of circular bridge columns-volume 2: experimental observations.* Alaska. Dept. of Transportation and Public Facilities. Research, Development ….

Goodnight, J. C., Kowalsky, M. J., and Nau, J. M. (2016). "Strain limit states for circular RC bridge columns." *Earthquake Spectra*, Earthquake Engineering Research Institute, 32(3), 1627–1652.

Guenard, Y. F. (1984). *Application of system reliability analysis to offshore structures*. John A. Blume Earthquake Engineering Center Stanford, Calif, USA.

Günay, S., and Mosalam, K. M. (2013). "PEER performance-based earthquake engineering methodology, revisited." *Journal of Earthquake Engineering*, Taylor & Francis, 17(6), 829–858.

Hamburger, R. O. (2006). "The ATC-58 project: development of next-generation performance-based earthquake engineering design criteria for buildings." *Structures Congress 2006: Structural Engineering and Public Safety*, 1–8.

Iervolino, I. (2017). "Assessing uncertainty in estimation of seismic response for PBEE." *Earthquake Engineering & Structural Dynamics*, Wiley Online Library, 46(10), 1711–1723.

Jayaram, N., and Baker, J. W. (2008). "Statistical tests of the joint distribution of spectral acceleration values." *Bulletin of the Seismological Society of America*, Seismological Society of America, 98(5), 2231–2243.

Jayaram, N., Lin, T., and Baker, J. W. (2011). "A computationally efficient ground-motion selection algorithm for matching a target response spectrum mean and variance." *Earthquake Spectra*, SAGE Publications Sage UK: London, England, 27(3), 797–815.

JCSS. (2001). "JCSS Probabilistic Model Code Part 3: Resistance Models." Joint Committee on Structural Safety.

Johnson, G. S., Harn, R., Lai, C., and Jaradat, O. (2013). "The new ASCE standard for seismic design of piers and wharves." *Ports 2013: Success through Diversification*, 1345–1354.

Kaviani, P., Zareian, F., and Taciroglu, E. (2012). "Seismic behavior of reinforced concrete bridges with skew-angled seat-type abutments." *Engineering Structures*, Elsevier, 45, 137–150.

Kaviani, P., Zareian, F., and Taciroglu, E. (2014). *Performance-based seismic assessment of skewed bridges*. Pacific Earthquake Engineering Research Center.

Kennedy, R. P., Cornell, C. A., Campbell, R. D., Kaplan, S., and Perla, H. F. (1980). "Probabilistic seismic safety study of an existing nuclear power plant." *Nuclear engineering and design*, Elsevier, 59(2), 315–338.

Kennedy, R. P., and Ravindra, M. K. (1984). "Seismic fragilities for nuclear power plant risk studies." *Nuclear Engineering and Design*, Elsevier, 79(1), 47–68.

Kent, D. C., and Park, R. (1971). "Flexural members with confined concrete." *Journal of the Structural Division*.

Keon, D., Pancake, C. M., Steinberg, B., and Yeh, H. (2016). "Performance-Based Tsunami Engineering via a Web-Based GIS Data Explorer." *Journal of Disaster Research*, Fuji Technology Press Ltd., 11(4), 624–633.

Kiureghian, A. Der. (2005). "Non-ergodicity and PEER's framework formula." *Earthquake engineering & structural dynamics*, Wiley Online Library, 34(13), 1643–1652.

Kohrangi, M., Bazzurro, P., and Vamvatsikos, D. (2016). "Vector and scalar IMs in structural response estimation, Part I: Hazard analysis." *Earthquake Spectra*, SAGE Publications Sage UK: London, England, 32(3), 1507–1524.

Kohrangi, M., Bazzurro, P., Vamvatsikos, D., and Spillatura, A. (2017). "Conditional spectrum-based ground motion record selection using average spectral acceleration." *Earthquake Engineering & Structural Dynamics*, Wiley Online Library, 46(10), 1667–1685.

Lee, T.-H., and Mosalam, K. M. (2006). *Probabilistic seismic evaluation of reinforced concrete structural components and systems*. Pacific Earthquake Engineering Research Center.

Lee, T., and Mosalam, K. M. (2005). "Seismic demand sensitivity of reinforced concrete shear-wall building using FOSM method." *Earthquake engineering & structural dynamics*, Wiley Online Library, 34(14), 1719–1736.

Li, H., Li, L., Zhou, G., and Xu, L. (2020). "Effects of various modeling uncertainty parameters on the seismic response and seismic fragility estimates of the aging highway bridges." *Bulletin of Earthquake Engineering*, Springer, 18(14), 6337–6373.

Liel, A. B., Haselton, C. B., Deierlein, G. G., and Baker, J. W. (2009). "Incorporating modeling uncertainties in the assessment of seismic collapse risk of buildings." *Structural Safety*, Elsevier, 31(2), 197–211.

Lin, T., Harmsen, S. C., Baker, J. W., and Luco, N. (2013a). "Conditional spectrum computation incorporating multiple causal earthquakes and ground-motion prediction models." *Bulletin of the Seismological Society of America*, Seismological Society of America, 103(2A), 1103–1116.

Lin, T., Haselton, C. B., and Baker, J. W. (2013b). "Conditional spectrum-based ground motion selection. Part I: hazard consistency for risk-based assessments." *Earthquake engineering & structural dynamics*, Wiley Online Library, 42(12), 1847–1865.

van de Lindt, J. W., and Dao, T. N. (2009). "Performance-based wind engineering for wood-frame buildings." *Journal of Structural Engineering*, American Society of Civil Engineers, 135(2), 169–177.

Liu, P.-L., and Der Kiureghian, A. (1986). "Multivariate distribution models with prescribed marginals and covariances." *Probabilistic Engineering Mechanics*, Elsevier, 1(2), 105–112.

Mackie, K. R., and Stojadinović, B. (2007). "Performance-based seismic bridge design for damage and loss limit states." *Earthquake engineering & structural dynamics*, Wiley Online Library, 36(13), 1953–1971.

Mackie, K., and Stojadinovic, B. (2004). "Fragility curves for reinforced concrete highway overpass bridges." *13th World conference on earthquake engineering*, Vancouver BC, Canada, 1–6.

Mander, J. B., Priestley, M. J. N., and Park, R. (1988). "Theoretical stress-strain model for confined concrete." *Journal of structural engineering*, American Society of Civil Engineers, 114(8), 1804–1826.

Mander, J. B., Sircar, J., and Damnjanovic, I. (2012). "Direct loss model for seismically damaged structures." *Earthquake engineering & structural dynamics*, Wiley Online Library, 41(3), 571–586.

Mangalathu, S., Jeon, J., and DesRoches, R. (2018). "Critical uncertainty parameters influencing seismic performance of bridges using Lasso regression." *Earthquake Engineering & Structural Dynamics*, Wiley Online Library, 47(3), 784–801.

Marasco, S., and Cimellaro, G. P. (2018). "A new energy-based ground motion selection and modification method limiting the dynamic response dispersion and preserving the median demand." *Bulletin of Earthquake Engineering*, Springer, 16(2), 561–581.

Marshall, P. W. (1969). "Rick Evaluations for Offshore Structures." *Journal of the Structural Division*, ASCE, 95(12), 2907–2930.

Masters, F. J., Gurley, K. R., Shah, N., and Fernandez, G. (2010). "The vulnerability of residential window glass to lightweight windborne debris." *Engineering Structures*, Elsevier, 32(4), 911–921.

May, P. J. (2001). *Organizational and societal considerations for performance-based earthquake engineering*. Pacific Earthquake Engineering Research Center.

Mazzoni, S., McKenna, F., Scott, M. H., and Fenves, G. L. (2006). "OpenSees command language manual." *Pacific Earthquake Engineering Research (PEER) Center*, Berkeley, California, United States, 264.

McKay, M. D., Beckman, R. J., and Conover, W. J. (2000). "A comparison of three methods for selecting values of input variables in the analysis of output from a computer code." *Technometrics*, Taylor & Francis Group, 42(1), 55–61.

McKenna, F. (2011). "OpenSees: a framework for earthquake engineering simulation." *Computing in Science & Engineering*, IEEE, 13(4), 58–66.

Megally, S. H., Silva, P. F., and Seible, F. (2002). *Seismic response of sacrificial shear keys in bridge abutments*.

Menegotto, M., and Pinto, P. E. (1973). "Method of analysis for cyclically loaded RC plane frames including changes in geometry and non-elastic behavior of elements under combined normal force and bending." *Proc. of IABSE symposium on resistance and ultimate deformability of structures acted on by well defined repeated loads*, 15–22.

Miranda, E., Aslani, H., and Taghavi, S. (2004). "Assessment of seismic performance in terms of economic losses." *Proceedings, International Workshop on Performance-Based Seismic Design: Concepts and Implementation*, Pacific Earthquake Engineering Research (PEER) Center, University of …, 149–160.

Mirza, S. A., and MacGregor, J. G. (1979). "Variability of mechanical properties of reinforcing bars." *Journal of the Structural Division*, 105(ASCE 14590 Proceeding).

Mirza, S. A., MacGregor, J. G., and Hatzinikolas, M. (1979). "Statistical descriptions of strength of concrete." *Journal of the Structural Division*, ASCE, 105(6), 1021–1037.

Mirza, S. A., and Skrabek, B. W. (1991). "Reliability of short composite beam-column strength interaction." *Journal of Structural Engineering*, American Society of Civil Engineers, 117(8), 2320–2339.

Moan, T. (1981). "Risk Assessment of Offshore Structures Experience and Principles."

Moan, T. (1994). “Reliability and risk analysis for design and operations planning of offshore structures.” *ICOSSAR’93 (Innsbruck) Balkema*, 21–43.

Moehle, J., and Deierlein, G. G. (2004). “A framework methodology for performance-based earthquake engineering.” *13th world conference on earthquake engineering*.

Murcia-Delso, J., Pui-shum, B. S., Stavridis, A., and Liu, Y. (2013). *Required embedment length of column reinforcement extended into type II shafts*. Citeseer.

NCHRP. (2013). *Performance-Based Seismic Bridge Design*. *National Cooperative Highway Research Program (NCHRP) Synthesis 440*.

Nezamian, A., and Morgan, P. M. (2014). “Performance-based Seismic Design of Fixed Offshore Platforms and Comparison with ISO and API Seismic Design Guidelines.” *The Twenty-fourth International Ocean and Polar Engineering Conference*, International Society of Offshore and Polar Engineers.

Nielson, B. G. (2005). “Analytical fragility curves for highway bridges in moderate seismic zones.” Georgia Institute of Technology.

Omrani, R., Mobasher, B., Liang, X., Gunay, S., Mosalam, K. M., Zareian, F., and Taciroglu, E. (2015). “Guidelines for nonlinear seismic analysis of ordinary bridges: Version 2.0.” *Caltrans Final Report*.

Padgett, J. E., and DesRoches, R. (2007). “Sensitivity of seismic response and fragility to parameter uncertainty.” *Journal of Structural Engineering*, American Society of Civil Engineers, 133(12), 1710–1718.

Padgett, J. E., Ghosh, J., and Dueñas-Osorio, L. (2013). “Effects of liquefiable soil and bridge modelling parameters on the seismic reliability of critical structural components.” *Structure and Infrastructure Engineering*, Taylor & Francis, 9(1), 59–77.

Pang, Y., Wu, X., Shen, G., and Yuan, W. (2014). “Seismic fragility analysis of cable-stayed bridges considering different sources of uncertainties.” *Journal of Bridge Engineering*, American Society of Civil Engineers, 19(4), 4013015.

PIANC. (2001). *Seismic Design Guidelines for Port Structures*. A.A. Balkema Publishers.

POLA. (2010). “Port of Los Angeles Code for Seismic Design, Upgrade and Repair of Container Wharves.” City of Los Angeles Harbor Department Los Angeles, CA.

Poland, C. D., Hill, J., Sharpe, R. L., Soulages, J., California., S. E. A. of, California., and Services., O. of E. (1995). “Vision 2000 : performance based seismic engineering of

buildings." Structural Engineers Association of California, Sacramento, CA.

POLB. (2009). *Port of Long Beach Wharf Design Criteria, Version 2.0*.

Porter, K. A. (2003). "An overview of PEER's performance-based earthquake engineering methodology." *Proceedings of ninth international conference on applications of statistics and probability in civil engineering*, 1–8.

Porter, K. A., Beck, J. L., and Shaikhutdinov, R. V. (2002). "Sensitivity of building loss estimates to major uncertain variables." *Earthquake Spectra*, 18(4), 719–743.

Priestley, M. J. N., Calvi, G. M., and Kowalsky, M. J. (2007). *Displacement-based seismic design of structures*. IUSS Press, Pavia, Italy.

Rezaei, H., Moayyedi, S. A., and Jankowski, R. (2020). "Probabilistic seismic assessment of RC box-girder highway bridges with unequal-height piers subjected to earthquake-induced pounding." *Bulletin of Earthquake Engineering*, Springer, 18(4), 1547–1578.

Riggs, H. R., Robertson, I. N., Cheung, K. F., Pawlak, G., Young, Y. L., and Yim, S. C. S. (2008). "Experimental simulation of tsunami hazards to buildings and bridges." *Proceedings of 2008 NSF Engineering Research and Innovation Conference, Knoxville, Tennessee*, 1056–1064.

Rini, D., and Lamont, S. (2008). "Performance based structural fire engineering for modern building design." *Structures Congress 2008: Crossing Borders*, 1–12.

Saini, A., and Saiidi, M. (2014). *Probabilistic damage control approach for seismic design of bridge columns*. California Department of Transportation Research, Rep. No. 65A0419.

Schoettler, M. J., Restrepo, J. I., Guerrini, G., Duck, D. E., and Carrea, F. (2015). "A full-scale, single-column bridge bent tested by shake-table excitation. PEER report 2015/02. Pacific Earthquake Engineering Research Center (PEER)." *University of California, Berkeley, CA*.

Scott, B. D., Park, R., and Priestley, M. J. N. (1982). "Stress-strain behavior of concrete confined by overlapping hoops at low and high strain rates." *Journal Proceedings*, 13–27.

Scott, M. H., and Hamutçuoğlu, O. M. (2008). "Numerically consistent regularization of force-based frame elements." *International journal for numerical methods in engineering*, Wiley Online Library, 76(10), 1612–1631.

Shamsabadi, A., Dasmeh, A., Nojoumi, A., Rollins, K. M., and Taciroglu, E. (2020). "Lateral Capacity Model for Backfills Reacting against Skew-Angled Abutments under Seismic Loading." *Journal of Geotechnical and Geoenvironmental Engineering*, American Society of Civil Engineers, 146(2), 04019129.

Shi, Y., and Stafford, P. J. (2018). “Markov chain Monte Carlo ground-motion selection algorithms for conditional intensity measure targets.” *Earthquake Engineering & Structural Dynamics*, Wiley Online Library, 47(12), 2468–2489.

Shinozuka, M., Hwang, H., and Reich, M. (1984). “Reliability assessment of reinforced concrete containment structures.” *Nuclear Engineering and Design*, Elsevier, 80(2), 247–267.

Terzic, V., Schoettler, M. J., Restrepo, J. I., and Mahin, S. A. (2015). “Concrete column blind prediction contest 2010: outcomes and observations.” *PEER Report*, 1, 1–145.

Trejo, D., Barbosa, A. R., and Link, T. (2014). *Seismic performance of circular reinforced concrete bridge columns constructed with grade 80 reinforcement.* Pacific Northwest Transportation Consortium.

Tubaldi, E., Barbato, M., and Dall’Asta, A. (2012). “Influence of model parameter uncertainty on seismic transverse response and vulnerability of steel–concrete composite bridges with dual load path.” *Journal of Structural Engineering*, American Society of Civil Engineers, 138(3), 363–374.

Vamvatsikos, D. (2013). “Derivation of new SAC/FEMA performance evaluation solutions with second-order hazard approximation.” *Earthquake Engineering & Structural Dynamics*, Wiley Online Library, 42(8), 1171–1188.

Veletzos, M. J., Panagiotou, M., Van Den Einde, Y., Restrepo, J. I., and Sahs, S. (2008). “Post-Earthquake Assessment of Bridge Columns.” *Concrete International*, 30(3).

Vosooghi, A., and Saiidi, M. S. (2012). “Experimental Fragility Curves for Seismic Response of Reinforced Concrete Bridge Columns.” *ACI Structural Journal*, 109(6).

Wen, Y.-K. (2004). “Probabilistic aspects of earthquake engineering.” *Earthquake Engineering*, CRC Press, 411–467.

Whittaker, A., Hamburger, R. O., and Mahoney, M. (2003). “Performance-based engineering of buildings and infrastructure for extreme loadings.” *Proceedings, AISC-SINY Symposium on Resisting Blast and Progressive Collapse, American Institute of Steel Construction, New York*.

Xie, Y., Zheng, Q., Yang, C.-S. W., Zhang, W., DesRoches, R., Padgett, J. E., and Taciroglu, E. (2019). “Probabilistic models of abutment backfills for regional seismic assessment of highway bridges in California.” *Engineering Structures*, Elsevier, 180, 452–467.

Zhang, Y. (2006). “Probabilistic structural seismic performance assessment methodology and application to an actual bridge-foundation-ground system.” UC San Diego.